UNIVERSITÀ
DI TRENTO

Doctoral School in Mathematics

Theoretical and numerical aspects of advection-pressure splitting for 1D blood flow models

Alessandra Spilimbergo

UNIVERSITÀ DI TRENTO | Dipartimento di Matematica

Doctoral School in Mathematics

XXXVI cycle

Doctoral Thesis in Mathematics

Author: **Alessandra Spilimbergo**

Supervisors: Prof. **Lucas O. Müller**, *University of Trento*

Prof. **Eleuterio F. Toro**, *University of Trento*

In fulfillment of the requirements for the Degree of:

Doctor of Philosophy

Dottore di Ricerca in Matematica

PhD Defense Date: 19th April 2024

Univeristy of Trento

Trento, Italy

April 2024

Aa me tèra ae me raìxe aa me xénte

Abstract

In this Thesis we explore, both theoretically and numerically, splitting strategies for a hyperbolic system of one-dimensional (1D) blood flow equations with a passive scalar transport equation. Our analysis involves a two-step framework that includes splitting at the level of partial differential equations (PDEs) and numerical methods for discretizing the ensuing problems. This study is inspired by the original flux splitting approach of Toro and Vázquez-Cendón (2012) originally developed for the conservative Euler equations of compressible gas dynamics. In this approach the flux vector in the conservative case, and the system matrix in the non-conservative one, are split into advection and pressure terms: in this way, two systems of partial differential equations are obtained, the advection system and the pressure system.

From the mathematical as well as numerical point of view, a basic problem to be solved is the special Cauchy problem called the Riemann problem. This latter provides an analytical solution to evaluate the performance of the numerical methods and, in our approach, it is of primary importance to build the presented numerical schemes.

In the first part of the Thesis a detailed theoretical analysis is presented, involving the exact solution of the Riemann problem for the 1D blood flow equations, depicted for a general constant momentum correction coefficient and a tube law that allows to describe both arteries and veins with continuous or discontinuous mechanical and geometrical properties and an advection equation for a passive scalar transport. In literature, this topic has been already studied only for a momentum correction coefficient equal to one, that is related to the prescribed velocity profile and in this case corresponds to a flat one, i.e. an inviscid fluid. In the case of discontinuous properties, only the subsonic regime is considered. In addition we propose a procedure to compute the obtained exact solution and finally we validate it numerically, by comparing exact solutions to those obtained with well-known, numerical schemes on a carefully designed set of test problems. Furthermore, an analogous theoretical analysis and resolution algorithm are presented for the advection system and the pressure system arising from the splitting at the level of PDEs of the complete system of 1D blood flow equations. It is worth noting that the pressure system, in case of veins, presents a loss of genuine non-linearity resulting in the formation of rarefactions, shocks and compound waves, these latter being a composition of rarefactions and shocks.

In the second part of the Thesis we present novel finite volume-type, flux splitting-based, numerical schemes for the conservative 1D blood flow equations and splitting-based numerical schemes for the non-conservative 1D blood flow equations that incorporate an advection equation for a passive scalar transport, considering tube laws that allow to model blood flow in arteries and veins and take into account a general constant momentum correction coefficient. A detailed efficiency analysis is performed in order to showcase the advantages of the proposed methodologies in comparison to standard approaches.

ACKNOWLEDGMENTS

First and foremost, I am profoundly grateful to my supervisors, Prof. Lucas O. Müller and Prof. Eleuterio F. Toro, for believing in me and assessing my progress throughout these years of my Ph.D. Their expertise, experience, patience and dedication to science have consistently served as a source of inspiration and encouragement, guiding me through the entirety of my academic research.

I would also like to thank Prof. Annunziato Siviglia for his contribution to a relevant part of my Ph.D. project, which has culminated in two scientific publications.

I also thank the University of Trento, and in particular the Department of Mathematics, for providing the financial and academic support to carry out this Ph.D. research project in terms of scholarship and allowances for participating in relevant conferences and advanced courses and workshops.

I conclude this section expressing my profound gratitude to my parents Alessandro and Anna Rosa. Without their continuous emotional and material support, I would never have completed this journey.

CONTENTS

Scientific Publications

This Thesis is presented in the following articles (published or in preparation):

- Eleuterio F. Toro, Annunziato Siviglia, **Alessandra Spilimbergo** and Lucas O. Müller. Advection-pressure splitting schemes for the equations of blood flow. Conservative and non-conservative forms. In: *East Asian J. Appl. Math.*, 14.2, (2024). DOI: 10.4208/eajam.2023-045.090523

- **Alessandra Spilimbergo**, Eleuterio F. Toro, Annunziato Siviglia and Lucas O. Müller. Flux vector splitting schemes applied to a conservative 1D blood flow model with transport for arteries and veins. In: *Comput. Fluids*, 271, (2024). DOI: 10.1016/j.compfluid.2023.106165

- **Alessandra Spilimbergo**, Eleuterio F. Toro and Lucas O. Müller. Exact solution of the Riemann problem for the one-dimensional blood flow equations with general constant momentum correction coefficient. In: *Commun. Comput. Phys.*, (2024). In press.

- **Alessandra Spilimbergo**, Eleuterio F. Toro, Annunziato Siviglia and Lucas O. Müller. Advection-pressure splitting schemes applied to a non-conservative 1D blood flow model with transport for arteries and veins. In preparation.

- **Alessandra Spilimbergo**, Eleuterio F. Toro and Lucas O. Müller. Exact solution of the Riemann problem for the pressure system in the framework of advection-pressure splitting for a conservative 1D blood flow model with transport. In preparation.

- **Alessandra Spilimbergo**, Eleuterio F. Toro and Lucas O. Müller. Exact solution of the Riemann problem for the advection system in the framework of advection-pressure splitting for 1D blood flow models. In preparation.

NTRODUCTION

I Motivations and goals

Blood circulation is fundamental to human physiology, having as main functions the transport of substances and the regulation of temperature. Modelling such processes in single vessels or in networks of vessels allows to study the effect of different stimuli on blood flow from a systemic point of view. In turn, these effects are related to changes in the geometry and mechanical properties of vessels. Arterial circulation has been the focus of attention in the past decades for researchers looking at pathological states of the cardiovascular system and its role played in other diseases. However, nowadays clinical research is looking into the potential role played by the venous system in the development and clinical course of neurodegenerative diseases such as *Idiophatic Parkinson's disease* [48], *Ménière disease* [2, 14, 25], *multiple sclerosis* [74, 95, 99, 37].

Blood flow models are essential tools used in medical research and healthcare to study and understand the complex dynamics of blood circulation in the human body. These models are designed to simulate the flow of blood through various parts of the body and can be used to study diseases, develop new treatments, and improve medical technologies. The three-dimensional (3D) incompressible Navier-Stokes equations are commonly utilized as a preferred model to examine the blood flow in a specific region of the cardiovascular system. The main goal of these models is to improve our understanding of the complex processes that take place within the cardiovascular system. It is imperative to consider the mechanical reaction of vessel or organ walls when simulating the cardiovascular system. 3D fluids models combined with a description of the interation between fluid and vessel walls result in 3D fluid-structure-interaction (FSI) solvers. These models take into account the 3D geometry of blood vessels, and thus provide 3D description of pressure and velocity fields [19]. While 3D blood flow models provide a high level of detail and accuracy, they are computationally expensive and often require high-performance computing resources to run simulations. Consequentially these models can be time-consuming and expensive to implement, making them less practical for routine clinical use.

One-dimensional (1D) blood flow models [40] are simplified models derived from the 3D FSI models. For certain applications, they are more computationally efficient than the 3D Fluid Structure Interaction (FSI) models [94], making them more suitable for clinical applications [36]. These schemes use simplified representations of blood vessels as interconnected 1D segments, and they focus on modeling blood flow in a more macroscopic manner. While 1D blood flow models may lack the fine-grained detail of their 3D counterparts, they can be readily integrated into clinical workflow and can provide rapid assessments of hemodynamic parameters, making them valuable for diagnostic and treatment planning purposes. Moreover, these models can be used to study large-scale physiological phenomena and simulate the effects of various cardiovascular pathologies on blood circulation. They are in fact valuable for studying various aspects of blood flow, including pressure and flow waveforms [72].

This Thesis focuses on the construction of new efficient first-order, finite-volume numerical schemes, to model 1D blood flow in arteries and veins with a passive scalar transport equation

added, for different constant velocity profiles. Not inferior in significance an extensive theoretical analysis and the exact solutions of the considered mathematical problems is presented, providing also reference solutions along with building blocks for the numerical schemes under study.

II State of the art

The one-dimensional blood flow equations are a non-linear system of two partial differential equations with source term. These equations represent conservation of mass and balance of momentum and are obtained by cross-sectional averaging the 3D Navier-Stokes equations, and including a tube law describing the interaction between vessel wall and fluid [28]. The space- and time-dependent unknowns are the cross-sectional area, flow rate and pressure. To close the system, elastic tube laws have been proposed, which distinguish between arteries and veins. In Bernard et al. [4], 1D blood flow equations were derived for the first time from the 3D incompressible Navier-Stokes equations. During the derivation of the 1D blood flow equations the velocity profile of the axial component of velocity has to be prescribed. This in turn determines a couple of coefficients appearing in the momentum balance equation, one related to dissipation due to friction between blood and the vessel wall and a second one, called momentum correction coefficient, which is related to the convective term of the equation.

One-dimensional blood flow models have been extensively used to study wave propagation phenomena in arteries [27, 73, 6, 60, 8, 51]. More recently, their use has been extended to the venous circulation [57, 58, 61]. Main aspects of the venous system posing modelling challenges are collapsibility of veins and the relevance of external forces such as gravity and external pressure to venous flow. Nevertheless, the effectiveness of 1D blood flow models for various applications has been verified through in-silico analysis, where the predictions of these models were compared with those of more complex models [36, 94, 10], in-vitro by assessing 1D blood flow model output with respect to highly controlled experiments [52, 5] and in-vivo by assessing the capacity of these models to reproduce pressure and flow waveforms observed in the clinical context [62, 69]. Moreover, when combined with zero-dimensional (0D) models, 1D blood flow models have enabled the development of comprehensive models of the entire human circulation [1, 46, 57, 9, 61, 31]. Additionally, 1D models have proven to be valuable in their ability to be coupled with 3D models, thereby providing realistic boundary conditions necessary for the analysis of detailed 3D problems that focus on the investigation of spatially localized pathological conditions [26, 7, 29, 68].

1D blood flow models with discontinuous mechanical and geometrical properties are representative of physical situations of medical interest in which certain properties that characterize compliant vessels change rapidly in space, for example due to the insertion of stents in arteries or in veins after a surgical procedure with the purpose of returning the vessel lumen to approximately its original shape. A common pathology in the human circulatory system is the presence of atherosclerotic plaques that can cause restrictions of the arterial lumen called stenoses. In the most severe cases stenoses may hinder, or even stop, the flow of blood. One of the available techniques to treat this problem is the implantation of a stent (an expandable metal mesh) into the affected region which has the purpose of returning the artery lumen to approximately its original shape. Whenever possible, this procedure is preferred to more invasive ones, such as surgical by-pass. Nevertheless, besides other effects, the presence of a stent causes an abrupt variation in the elastic properties of the vessel wall, since the stent is usually different from the soft arterial tissue [15, 72]. This may cause a disturbance in the blood flow pattern and wall displacement with the appearance of reflected waves and abrupt jumps in mechanical and geometrical properties may arise. As a consequence of the spatial variation of parameters, the one-dimensional mathematical model will include additional source terms involving parameter

derivatives. These source terms are called *geometric source terms* and must be treated carefully while discretizing the equations. Otherwise, spurious oscillations may arise in approximated solutions and numerical schemes will be unable to correctly resolve steady or stationary solutions (see for example [3, 35]). Numerical schemes able to appropriately solve steady state solutions are said to be well-balanced [64]. While in this Thesis we deal with an extreme case of discontinuous parameters (see next paragraph), it is worth noting that many have addressed the smooth case. The impact of varying mechanical properties due to stent placement was addressed in [72], where smooth variations where considered and no considerations on the well-balanced properties of the resulting schemes were made. Well-balanced schemes for smooth variation of parameters were designed in [22, 59, 93, 30, 45].

From the mathematical as well as numerical point of view, a basic problem to be solved is the special Cauchy problem called the Riemann problem [44, 87, 33]. In particular, comprehending the behavior when dealing with discontinuous parameters enables us to effectively apply coupling conditions at vessel junctions [11, 53, 18]. Toro and Siviglia [90] formulated a complete one-dimensional blood flow model with discontinuous properties and passive scalar transport equation added. They presented the complete exact solution for the Riemann problem for initial conditions resulting in sub-critical flow regimes. This topic was completed in Spilimbergo et al. [81] with a novel approach to calculate superimposed contact waves relations. The complete solution of the Riemann problem was addressed in [38, 39], evidencing the existence of multiple solutions. More recently, an entropy-based criteria was proposed to identify the physically relevant solution [71]. It is worth noting that these last contributions about complete solutions to the Riemann problem regard blood flow in arteries, while the venous counterpart (highly non-linear and exhibiting large deformations, including collapse) remains to be studied. All these available exact solutions were obtained for a momentum correction coefficient equal to one (i.e. corresponding to a flat blood velocity profile and consequently to an inviscid fluid).

The model presented in Toro and Siviglia [90] can not be cast in conservative form for conserved variables. Numerical approximation of this type of problems are found resorting in generalizations of well-known results for conservative problems [21], and numerical approximations are obtained with so-called path-conservative numerical schemes [64]. In particular, Dumbser and Toro [23, 24] extended the Osher-Solomon Riemann solver [63] to non-conservative systems, presenting a path-conservative, finite-volume type, first order scheme and a high-order extension. Subsequently Müller and Toro [56] improved it, constructing well-balanced fluctuations for a first order non-oscillatory scheme, and extending it to higher order of accuracy in both space and time. Moreover, a different approach based on the Generalized Hydrostatic Reconstruction [16] was followed in [55, 67], where an exactly well-balanced scheme for non-stationary steady state solutions was designed.

It is worth noting that the specific waveforms arising in the aforementioned Riemann problems are smooth waves (rarefactions), discontinuous jumps (shocks) and contact discontinuities, due to the particular nature of the related characteristic fields. In fact, for these models, the aforementioned fields are normally genuinely non-linear (rarefactions and shocks) and linearly degenerate (contact discontinuities) [80]. In [42], Lax introduced the notion of genuine non-linearity and solved the Riemann problem with initial data sufficiently close to each other, with the discontinuous solutions satisfying the so-called Lax-Entropy criterion. Smoller [78, 79] solved the Riemann Problem in the class of shock and rarefaction waves, for arbitrary initial states, under certain conditions and the assumption that the characteristic fields are genuinely non-linear and the discontinuous solutions satisfy the Lax-Entropy criterion. Liu [49] proved the existence and uniqueness of the solution of the Riemann Problem for general 2x2 hyperbolic conservation laws, with particular conditions for fluxes, in the class of shocks, rarefaction waves and contact discontinuities, when the genuine non-linearity condition is lost on a disjoint union of 1-manifolds in the phase-plane, introducing a new entropy criterion for the discontinuous jumps, the so-called *Oleinik-Liu* condition. The characteristic fields with this peculiarity are called

nongenuinely non-linear. Afterwards Liu [50] extended this theory to general systems of $n \times n$ hyperbolic conservation laws. The consequences of the loss of the genuine non-linearity include the formation of a new type of wave, composed by a mix of rarefactions and shocks [49, 50].

III Contributions of the Thesis

Computational cost plays a crucial role when describing the flow of blood in complex networks of vessels. Hence, it is imperative to prioritize the investigation of numerical techniques that exhibit growing efficiency. In this regard, a particular approach involves the utilization of splitting techniques, which partition the initial system into two subsystems. These subsystems possess a simpler eigenstructure compared to the entire system, thereby contributing to improve the computational efficiency [85, 43, 47, 97, 92]. Our analysis involves a two-step framework that includes flux splitting at the level of partial differential equations (PDEs) and numerical methods for discretizing the ensuing problems. We build upon the flux splitting approach of Toro and Vázquez [92], hereafter called the TV splitting, originally developed for the conservative Euler equations of compressible gas dynamics. In this approach the flux vector is split into advection and pressure terms: in this way, two systems of partial differential equations are obtained, one advection system and one pressure system. The TV-splitting approach exhibits several properties that are potentially valuable for simulating blood flow in complex vessel networks. By separating the original problem into an advection and a pressure system, the wave relations that need to be enforced when employing a Riemann solver are simplified. In more general blood flow models, wave relations can be highly complex and require the solution of non-linear ordinary differential equations for evaluation, of which a closed form is not always available (Chapter 2). The simplification of wave relations will also yield positive effects not only on the numerical method utilized to solve the blood flow equations within vessels but also on the determination of coupling conditions between one-dimensional domains, which are in turn determined by wave relations [27, 73].

Regarding the conservative 1D blood flow model, we introduce two main modifications with respect to the approach presented in [92]. The first change is at PDEs level and regards the flux of the continuity equation: in the TV splitting approach this flux is assigned to the advection system, here it is assigned to the pressure system. This particular feature is consistent with zero-dimensional models that are based on neglecting the inertial term in the momentum equation, followed by spatial integration. Furthermore, straightforward calculations show that applying the splitting methodology as presented in [92] to the 1D blood flow equations, leads to a loss of hyperbolicity of the two resulting subsystems of PDEs. The second modification is at the numerical level: the numerical fluxes for the advection and the pressure system are obtained from exact or approximate Riemann problem solvers for each system, being the Riemann problem a special Cauchy problem [44, 87, 33]. The difference lies in the way the solution of the cited Riemann solvers is used to construct the advection numerical flux. An advection equation for the concentration of a passive scalar is added, at PDEs level its conservative flux is assigned to the advection system for simplicity. In this study we consider a general tube law that can accurately describe relations between pressure and area [13, 27, 75]. This general setting has a a significant impact on the complexity of the various elements that characterize the underlying hyperbolic PDEs system. At the numerical level, on the other hand, we propose simple finite volume, first order, numerical schemes of the Godunov type, evaluated on a suite of test problems with exact solution. This research study has been carried out in collaboration with with Prof. Toro, Prof. Siviglia and Prof. Müller and has been published in [83, 91].

Regarding the non-conservative case, our analysis involves the same two-step framework that considers a first split at the level of PDEs in which the initial complete system is divided

into two subsystems of PDEs, with a simpler eigenstructure with respect to the complete one. Again we add an advection equation for a passive scalar and consider a general tube law that can accurately describe blood flow in arteries and veins. Furtermore we take into account a momentum correction coefficient that describes flat and parabolic velocity profiles. The complete system of non-conservative 1D blood flow equations is again split into the advection subsystem in conservative form, and the pressure one in non-conservative form. At PDEs level the modification with respect to the original TV-splitting approach in [92] is maintaned: the flux of the continuity equation is assigned to the pressure system instead to the advection one as for the conservative case, this choice is determined by both the consistency with zero-dimensional models and the loss of the hyperbolicity of the resulting subsystems of PDEs, otherwise. Regarding the advection equation for a passive scalar transport, at PDEs level its conservative flux is assigned to the advection system for simplicity. At the numerical level, on the other hand, we propose simple, finite volume-type, first order, numerical schemes derived from a conservative form of the path-conservative schemes [64] applied to the pressure system, evaluated on a set of test problems with exact solution. This topic is a joint work with Prof. Toro, Prof. Siviglia and Prof. Müller and is in preparation.

The proposed numerical schemes are first order accurate, they can be integrated into higher-order methods. For more details see [76].

Concerning the theoretical analysis of the exact solution of the Riemann problems, the complete knowledge of the model eigenstructure and wave relations for a momentum correction coefficient different from one (i.e. for different velocity profiles) is highly desirable, since these relations play a fundamental role in the determination of coupling and boundary conditions when 1D blood flow models are applied to networks of vessels [73, 54]. In the most general setting, the momentum correction coefficient, which depends on the assumed velocity profile, can be space and/or time dependent [69]. In this study, we consider the momentum correction coefficient as a constant, ranging values that result from velocity profiles frequently used to describe friction terms in the momentum balance equation [77, 10]. While in this Thesis friction terms are omitted since we focus our attention on the analysis of Riemann problems, which, as is well-established, considers only the homogeneous part of the system, we emphasize that our results are also relevant for blood flow simulations where the friction terms are actually considered, since the discretization of this model often relies on having to solve classical Riemann problems to compute numerical fluxes or coupling conditions. Noteworthy, the derivation of the exact Riemann problem solution for the non-linear hyperbolic 1D blood flow equations with continuous and discontinuous parameters for the cases of arteries and veins and for a constant momentum correction coefficient $\alpha \in [1, 2]$, turns out to be significantly more challenging than the one employed for previously presented results, due in part to the lack of closed-form wave relations for rarefaction waves. This research study has been carried out in collaboration with Prof. Toro and Prof. Müller and is in press in [82].

A complete analysis of the exact solutions of the Riemann problem for the advection and pressure subsystems resulting from the aforementioned splitting is also presented, both being hyperbolic systems of PDEs, giving further reference solutions and building blocks for the numerical schemes under study. The advection system, in particular, can be traced back to the more well-known class of *pressureless* systems of PDEs, generally developed for the Euler equations, which have been deprived of the pressure-related parts of the system. Such a model has been proposed by Zeldovich [96] as a simplified model for the early stages of the formation of galaxies, when a dust of particles moving without pressure should start to collide and aggregate into bigger and bigger clusters. In our approach, the modified TV-splitting we apply to the complete system of 1D blood flow equations leaves the resulting conservative advection subsystem without both the pressure terms and the flux of the continuity equation. We propose a complete mathematical analysis of the wave relations and the construction of the exact solution of the Riemann problem. The pressure system, on the other hand, is a hyperbolic system of PDEs whose

characteristic fields present a loss of genuine non-linearity in a isolated point of the domain in case of veins. Solving this problem requires a different entropy criterion for the discontinuous jumps with respect to the ones that occur in the more common genuinely non-linear fields, i.e. the *Oleinik-Liu* entropy condition [49, 50]. Its solution depicts a waveform not included in the genuinely non-linear case: the *compound wave* i.e. a wave composed by rarefactions and semi-characteristic shocks [70, 98]. This topic has not been extensively explored for the 1D blood flow equations and in this work we propose a complete mathematical analysis and a numerical procedure to compute the resulting exact solution for the case of continuous parameters and transport, for both arteries and veins. It is worth noting that no momentum correction coefficient is present, being assigned to the advection system after the aforementioned splitting at the level of PDEs. These latter research works are in preparation.

IV Structure of the Thesis

This Thesis is divided into two parts.

- **Part 1: Theoretical Analysis**
  This part is devoted to the theoretical discussion of the hyperbolic systems of PDEs under study, and their related Riemann problems. In Chapter 1 we introduce the 1D blood flow equations deriving them from the 3D Navier-Storkes equations. In Chapter 2 we present the theoretical analysis and the numerical construction of the exact solution of the Riemann problem for the complete 1D blood flow equations with continuous and discontinuous parameters and transport added, with a constant momentum correction coefficient different from one and tube laws that describes both arteries and veins. In Chapter 3 we propose the actual advection-pressure splitting at the level of PDEs we apply in this study. Subsequently in Chapter 4 the exact solution of the Riemann problem for the advection system derived from the splitting of the 1D blood flow equations with continuous and discontinuous parameters and a constant momentum correction coefficient different from one, arising from the aforementioned splitting is detailed theoretically and constructed numerically. Finally the same theoretical and numerical description regarding the exact solution of the Riemann problem for the pressure system for both arteries and veins and transport added, limited to the case af continuous mechanical and geometrical properties (conservative case) is depicted (Chapter 5).

- **Part 2: Numerical Schemes**
  This part is devoted to the presentation of novel finite volume-type, advection-pressure splitting, numerical schemes, to solve the complete 1D blood flow model with continuous and discontinuous properties and a passive scalar transport equation added, with a general constant momentum correction coefficient, presented in Chapter 2. In particular we present two novel first-order, finite volume-type, flux splitting numerical schemes for the 1D blood flow equations with continuous mechanical and geometrical parameters and an advection equation for a passive scalar transport added (Chapter 6). In addition two novel first-order, finite volume, advection-pressure splitting numerical schemes for the 1D blood flow equations with discontinuous mechanical and geometrical parameters and a passive scalar transport equation added, are also presented (Chapter 7).

Part I

THEORETICAL ANALYSIS

Chapter 1

Derivation of the mathematical model

In this Chapter, following [28], starting from the 3D Navier-Stokes equations, considering an incompressible Newtonian fluid and from the Reynolds Theorem applied to a 3D blood vessel, we derive the 1D blood flow equations, which are constituted by mass conservation and momentum balance laws, with the addition of the 1D advection equation for a passive scalar transport.

1.1 The incompressible Navier-Stokes equations

The incompressible Navier-Stokes equations in Cartesian coordinates are

$$\begin{cases} \partial_x u + \partial_y v + \partial_z w = 0, \\ \partial_t u + u\partial_x u + v\partial_y u + w\partial_z u + \dfrac{1}{\rho}\partial_x p = g_x + \dfrac{\mu}{\rho}\left(\partial_x^2 u + \partial_y^2 u + \partial_z^2 u\right), \\ \partial_t v + u\partial_x v + v\partial_y v + w\partial_z v + \dfrac{1}{\rho}\partial_y p = g_y + \dfrac{\mu}{\rho}\left(\partial_x^2 v + \partial_y^2 v + \partial_z^2 v\right), \\ \partial_t w + u\partial_x w + v\partial_y w + w\partial_z w + \dfrac{1}{\rho}\partial_z p = g_z + \dfrac{\mu}{\rho}\left(\partial_x^2 w + \partial_y^2 w + \partial_z^2 w\right), \end{cases} \tag{1.1}$$

where the unknowns are

$$\begin{array}{ll} \mathbf{U}(x,y,z,t) = (u,v,w) & \text{Velocity vector,} \\ p(x,y,z,t) & \text{pressure,} \end{array} \tag{1.2}$$

while

$$\begin{array}{ll} \mathbf{G}(x,y,z) = (g_x, g_y, g_z) & \text{external force vector,} \\ \rho & \text{constant density of blood,} \\ \mu & \text{constant viscosity of blood} \end{array} \tag{1.3}$$

are known values. The equations (1.1) can also be written more succinctly as

$$\begin{cases} \nabla \cdot \mathbf{U} = 0 & \text{continuity,} \\ \partial_t \mathbf{U} + (\mathbf{U}\cdot\nabla)\mathbf{U} + \dfrac{1}{\rho}\nabla p = \dfrac{\mu}{\rho}\Delta\mathbf{U} + \mathbf{G} & \text{momentum,} \end{cases} \tag{1.4}$$

where ∇ is the gradient operator and Δ is the Laplacian operator.

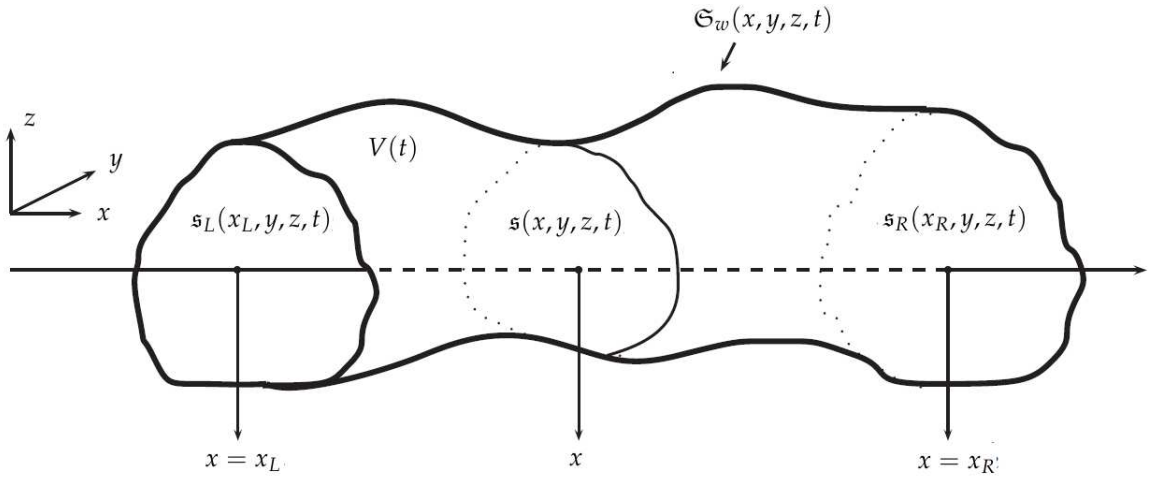

Figure 1.1: Sketch of section of blood vessel in three dimensions defining control volume $V = V(t)$ with boundary $\mathfrak{S} = \mathfrak{S}(t)$. Courtesy of E. F. Toro.

1.2 Derivation of the one-dimensional equations

Consider a generic blood vessel with axial coordinate x as shown in Fig.1.1:

- $\mathfrak{s} = \mathfrak{s}(x,y,z,t)$: generic cross section at x,
- $\mathfrak{s}_L$: left cross section at $x = x_L$, fixed, normal to direction x,
- $\mathfrak{s}_R$: right cross section at $x = x_R$ fixed, normal to direction x,
- V=$V(t)$ is the vessel control volume,
- boundary $\mathfrak{S} = \mathfrak{S}(t)$ is decomposed as

$$\mathfrak{S} = \mathfrak{S}_w \cup \{\mathfrak{s}_L, \mathfrak{s}_R\}, \tag{1.5}$$

- $\mathfrak{S}_w = \mathfrak{S}_w(x,y,z,t)$: vessel wall.

Theorem 1.2.1 (Reynolds transport theorem)**.** *Being* $\mathbf{U}_b$*: velocity of boundary* $\mathfrak{S}$*,* $\mathcal{F}(\mathbf{x},t)$*: a continuous function,* $\boldsymbol{x}$=(x,y,z)*,* $\boldsymbol{n}$*: outward unit normal vector to* $\mathfrak{S}$*; the Reynolds transport theorem states:*

$$\frac{d}{dt}\int_V \mathcal{F}(\mathbf{x},t)dV = \int_V \partial_t \mathcal{F}(\mathbf{x},t)dV + \int_{\mathfrak{S}} \mathcal{F}\mathbf{U}_b \cdot \mathbf{n}d\sigma. \tag{1.6}$$

Proof. Omitted (see [28]). □

For our problem the Reynolds theorem becomes

$$\frac{d}{dt}\int_V \mathcal{F}(\mathbf{x},t)dV = \int_V \partial_t \mathcal{F}(\mathbf{x},t)dV + \int_{\mathfrak{S}_w} \mathcal{F}\mathbf{U}_w \cdot \mathbf{n}d\sigma, \tag{1.7}$$

with $\mathbf{U}_w$ the velocity of the vessel wall $\mathfrak{S}_w$. Note that $\mathbf{U}_b \cdot \mathbf{n} = 0$ at $x = x_L$ and $x = x_R$ (i.e. here the normal component of $\mathbf{U}_b$ is 0).

Assume the general case in which there may be fluid filtration across the vessel wall (permeable wall). Then the *relative velocity* is

$$\mathbf{U}_r = \mathbf{U}_w - \mathbf{U}. \tag{1.8}$$

Definition 1.2.1 (Cross-sectional average). *The cross-sectional average of a quantity $a(\mathbf{x},t)$ at section $\mathfrak{s}$ of area A is*

$$\bar{a} = \frac{1}{A}\int_{\mathfrak{s}} a(\mathbf{x},t)d\sigma, \tag{1.9}$$

where: $A = A(x,t) = \int_{\mathfrak{s}} d\sigma$.

Note that

$$\int_V a(\mathbf{x},t)dV = \int_{x_L}^{x_R}\left[\int_{\mathfrak{s}} a(\mathbf{x},t)d\sigma\right]dx. \tag{1.10}$$

By (1.9) we have

$$\int_V a(\mathbf{x},t)dV = \int_{x_L}^{x_R} A\bar{a}(\mathbf{x},t)dx. \tag{1.11}$$

Being x_L and x_R independent of time, we have

$$\frac{d}{dt}\int_V \mathcal{F}(\mathbf{x},t)dV = \frac{d}{dt}\int_{x_L}^{x_R} A\overline{\mathcal{F}}(\mathbf{x},t)dx = \int_{x_L}^{x_R}\partial_t\left(A\overline{\mathcal{F}}(\mathbf{x},t)\right)dx. \tag{1.12}$$

The second term of the right hand side of (1.7), considering (1.8), becomes

$$\int_{\mathfrak{S}_w}\mathcal{F}\mathbf{U}_w\cdot\mathbf{n}d\sigma = \int_{\mathfrak{S}_w}\mathcal{F}\mathbf{U}_r\cdot\mathbf{n}d\sigma + \int_{\mathfrak{S}_w}\mathcal{F}\mathbf{U}\cdot\mathbf{n}d\sigma. \tag{1.13}$$

For an impermeable wall, the first term of the right hand side of (1.13) is zero. Noting that $\mathfrak{S}$ can be decomposed as in (1.5), the second term of the right hand side of (1.13) becomes

$$\int_{\mathfrak{S}_w}\mathcal{F}\mathbf{U}\cdot\mathbf{n}d\sigma = \int_{\mathfrak{S}}\mathcal{F}\mathbf{U}\cdot\mathbf{n}d\sigma - \int_{\mathfrak{s}_L}\mathcal{F}\mathbf{U}\cdot\mathbf{n}d\sigma - \int_{\mathfrak{s}_R}\mathcal{F}\mathbf{U}\cdot\mathbf{n}d\sigma. \tag{1.14}$$

Since u is the x component of velocity $\mathbf{U}$, then (1.14) becomes

$$\int_{\mathfrak{S}_w}\mathcal{F}\mathbf{U}\cdot\mathbf{n}d\sigma = \int_{\mathfrak{S}}\mathcal{F}\mathbf{U}\cdot\mathbf{n}d\sigma + \int_{\mathfrak{s}_L}\mathcal{F}ud\sigma - \int_{\mathfrak{s}_R}\mathcal{F}ud\sigma. \tag{1.15}$$

The first term on the right hand side of (1.15), in view of Gauss' theorem, becomes

$$\int_{\mathfrak{S}}\mathcal{F}\mathbf{U}\cdot\mathbf{n}d\sigma = \int_V \nabla\cdot(\mathcal{F}\mathbf{U})dV, \tag{1.16}$$

and thus (1.15) becomes

$$\int_{\mathfrak{S}_w}\mathcal{F}\mathbf{U}\cdot\mathbf{n}d\sigma = \int_V \nabla\cdot(\mathcal{F}\mathbf{U})dV + \int_{\mathfrak{s}_L}\mathcal{F}ud\sigma - \int_{\mathfrak{s}_R}\mathcal{F}ud\sigma. \tag{1.17}$$

From (1.9) we may write the last two terms in (1.17) as

$$\int_{\mathfrak{s}_L}\mathcal{F}ud\sigma - \int_{\mathfrak{s}_R}\mathcal{F}ud\sigma = -\int_{x_L}^{x_R}\partial_x(A\overline{\mathcal{F}u})dx, \tag{1.18}$$

and thus (1.17) becomes

$$\int_{\mathfrak{S}_w}\mathcal{F}\mathbf{U}_w\cdot\mathbf{n}d\sigma = \int_{\mathfrak{S}_w}\mathcal{F}\mathbf{U}_r\cdot\mathbf{n}d\sigma + \int_V \nabla\cdot(\mathcal{F}\mathbf{U})dV - \int_{x_L}^{x_R}\partial_x(A\overline{\mathcal{F}u})dx. \tag{1.19}$$

Inserting (1.12) and (1.19) in (1.7) and using (1.10) yields

$$\int_{x_L}^{x_R} \partial_t(A\overline{\mathcal{F}})dx = \int_V \partial_t \mathcal{F} dV + \int_V \nabla\cdot(\mathcal{F}\mathbf{U})dV + \int_{\mathfrak{S}_w} \mathcal{F}\mathbf{U}_r\cdot\mathbf{n}d\sigma - \int_{x_L}^{x_R}\partial_x(A\overline{\mathcal{F}u})dx. \tag{1.20}$$

That is

$$\begin{aligned}\int_{x_L}^{x_R} \partial_t(A\overline{\mathcal{F}})dx = \int_{x_L}^{x_R}\left(\int_{\mathfrak{s}}\partial_t\mathcal{F}d\sigma\right)dx + \int_{x_L}^{x_R}\left(\int_{\mathfrak{s}}\nabla\cdot(\mathcal{F}\mathbf{U})d\sigma\right)dx + \\ + \int_{x_L}^{x_R}\left(\int_{\partial\mathfrak{s}}\mathcal{F}\mathbf{U}_r\cdot\mathbf{n}d\epsilon\right)dx - \int_{x_L}^{x_R}\partial_x(A\overline{\mathcal{F}u})dx,\end{aligned} \tag{1.21}$$

which after rearranging becomes

$$\partial_t(A\overline{\mathcal{F}}) + \partial_x(A\overline{\mathcal{F}u}) = \int_{\mathfrak{s}}\left(\partial_t\mathcal{F} + \nabla\cdot(\mathcal{F}\mathbf{U})\right)d\sigma + \int_{\partial\mathfrak{s}}\mathcal{F}\mathbf{U}_r\cdot\mathbf{n}d\epsilon. \tag{1.22}$$

The function $\mathcal{F}$ is open to choice, and appropriate choices of it will give the governing blood flow equations. For an impermeable wall the last term on the right hand side vanishes.

1.2.1 Conservation of mass

Using (1.22), setting $\mathcal{F}$=1 and noting that for an incompressible fluid

$$\nabla\cdot\mathbf{U} = 0, \tag{1.23}$$

equation (1.22) gives the *equation of continuity* or *mass conservation equation*

$$\partial_t A + \partial_x(A\bar{u}) = \int_{\partial\mathfrak{s}}\mathbf{U}_r\cdot\mathbf{n}d\epsilon, \tag{1.24}$$

which for an impermeable wall

$$\partial_t A + \partial_x(A\bar{u}) = 0, \tag{1.25}$$

where

- $A(x,t)$ is the unknown cross-sectional area,
- $\bar{u}(x,t)$ is the unknown cross-section averaged velocity across x.

1.2.2 Balance of momentum

Setting $\mathcal{F} = u$, noting that

$$\nabla\cdot(u\mathbf{U}) = u\nabla\cdot\mathbf{U} + \mathbf{U}\cdot\nabla u, \tag{1.26}$$

that for an incompressible fluid

$$\nabla\cdot\mathbf{U} = 0, \tag{1.27}$$

and that

$$\partial_t u + \mathbf{U}\cdot\nabla u = \frac{Du}{Dt}, \tag{1.28}$$

equation (1.22) becomes

$$\partial_t(A\bar{u}) + \partial_x(A\overline{u^2}) = \int_{\mathfrak{s}}\frac{Du}{Dt}d\sigma + \int_{\partial\mathfrak{s}}u\mathbf{U}_r\cdot\mathbf{n}d\epsilon. \tag{1.29}$$

Now imposing the equation for momentum balance

$$\int_V \frac{D(\rho \mathbf{U})}{Dt} dV = \int_V \rho \mathbf{B} dV + \int_{\mathfrak{S}} \mathbf{T}\mathbf{n} d\sigma, \tag{1.30}$$

where

- ρ is density (constant),
- $\mathbf{B}$: body forces,
- $\mathbf{T}$: Cauchy stress tensor.

Applying the divergence theorem to last term in the right hand side of (1.30), we obtain

$$\int_V \frac{D\mathbf{U}}{Dt} dV = \int_V \mathbf{B} dV + \frac{1}{\rho} \int_V \nabla \cdot \mathbf{T} dV. \tag{1.31}$$

From the constitutive law for a fluid

$$\mathbf{T} = -p\mathbf{I} + \mathbf{D}, \tag{1.32}$$

where

- p is pressure,
- $\mathbf{I}$ is the identity tensor,
- $\mathbf{D}$ is tensor of deviatoric stresses.

Equation (1.31) can now be written thus

$$\int_{x_L}^{x_R} \left(\int_{\mathfrak{s}} \frac{D\mathbf{U}}{Dt} d\mathfrak{S} \right) dx = \int_{x_L}^{x_R} \left(\int_{\mathfrak{s}} \left[\mathbf{B} + \frac{1}{\rho}(-\nabla p + \nabla \cdot \mathbf{D}) \right] d\sigma \right) dx. \tag{1.33}$$

For the x-component, equation (1.33), with obvious notation for b and d, becomes

$$\int_{\mathfrak{s}} \frac{Du}{Dt} d\sigma = \int_{\mathfrak{s}} \left[b + \frac{1}{\rho}(-\frac{\partial}{\partial x} p + d) \right] d\sigma. \tag{1.34}$$

Returning to (1.29), we have

$$\partial_t(A\bar{u}) + \partial_x(A\overline{u^2}) = \int_s \left[b + \frac{1}{\rho}(-\partial_x p + d) \right] d\sigma + \int_{\partial \mathfrak{s}} u \mathbf{U}_r \cdot \mathbf{n} d\epsilon. \tag{1.35}$$

In terms of area-averages, and considering p constant over the cross-sectional area we have

$$\partial_t(A\bar{u}) + \partial_x(A\overline{u^2}) = \frac{A}{\rho} \left[\rho \bar{b} - \partial_x \bar{p} + \bar{d}) \right] + \int_{\partial \mathfrak{s}} u \mathbf{U}_r \cdot \mathbf{n} d\epsilon. \tag{1.36}$$

Defining

$$u(x, y, z, t) = s(y, z, t)\bar{u}(x, t), \tag{1.37}$$

where s is the prescribed velocity profile, we have

$$\overline{u^2} = \frac{1}{A} \int_{\mathfrak{s}} u^2 d\sigma = \frac{1}{A} \int_{\mathfrak{s}} s^2 \bar{u}^2 d\sigma = \alpha \bar{u}^2, \tag{1.38}$$

with

$$\alpha = \frac{1}{A} \int_{\mathfrak{s}} s^2 d\sigma \tag{1.39}$$

the momentum correction coefficient. It depends on the assumed velocity profile: $\alpha = 1$ for a flat profile and $\alpha = \frac{4}{3}$ for a parabolic velocity profile. Viscous forces are represented by $\bar{d}$ and here we assume the linear relation

$$\frac{A}{\rho}\bar{d} = -R\bar{u}, \tag{1.40}$$

$R > 0$ represents *viscous resistance* per unit length of tube and depends on the assumed velocity profile. Finally, the *momentum equation* becomes

$$\partial_t(A\bar{u}) + \partial_x(\alpha A\bar{u}^2) + \frac{A}{\rho}\partial_x\bar{p} = A\bar{b} - R\bar{u} + \int_{\partial s} u\mathbf{U}_r \cdot \mathbf{n}d\epsilon. \tag{1.41}$$

Assuming an impermeable wall and zero body forces, we obtain

$$\partial_t(A\bar{u}) + \partial_x(\alpha A\bar{u}^2) + \frac{A}{\rho}\partial_x\bar{p} = -R\bar{u}. \tag{1.42}$$

The unknowns are

- $A(x,t)$: cross-sectional area,
- $\bar{u}(x,t)$: area-averaged velocity,
- $\bar{p}(x,t)$: area-averaged pressure.

To close the system a *tube law* is needed, such law can be constructed from mechanical considerations. Tube laws can be algebraic relations (normally for vessel walls with elastic behaviour) or differential, if viscoelasticity and/or inertia and/or longitudinal tension of vessel walls is accounted for ([27]).

1.2.3 Equation for a passive scalar transport

For what concerns the passive scalar we use (1.22), setting $\mathcal{F}$=ϕ, with $\phi(x,y,z,t)$ the concentration of the passive scalar, equation (1.22) becomes

$$\partial_t(A\bar{\phi}) + \partial_x(A\overline{u\phi}) = \int_s (\partial_t\phi + \nabla\cdot(\phi\mathbf{U}))\, d\sigma + \int_{\partial s} \phi\mathbf{U}_r \cdot \mathbf{n}d\epsilon, \tag{1.43}$$

with $\bar{\phi}$: average concentration of the passive scalar in the considered cross-sectional area. Eq. (1.43) for an impermeable wall becomes

$$\partial_t(A\bar{\phi}) + \partial_x(A\overline{u\phi}) = \int_s (\partial_t\phi + \nabla\cdot(\phi\mathbf{U}))\, d\sigma. \tag{1.44}$$

Noting that being for an incompressible fluid

$$\nabla\cdot\mathbf{U} = 0, \tag{1.45}$$

Eq. (1.44) becomes

$$\partial_t(A\bar{\phi}) + \partial_x(A\overline{u\phi}) = \int_s (\partial_t\phi + \mathbf{U}\nabla\cdot\phi)\, d\sigma. \tag{1.46}$$

The advection equation for a passive scalar is

$$\partial_t\phi + \mathbf{U}\nabla\cdot\phi = 0, \tag{1.47}$$

so (1.46) becomes

$$\partial_t(A\bar{\phi}) + \partial_x(A\overline{u\phi}) = 0. \tag{1.48}$$

Introducing

$$\phi(x,y,z,t) = h(y,z,t)\bar{\phi}(x,t), \tag{1.49}$$

where h is a function that describes the distribution of ϕ over the cross section, we have

$$\overline{u\phi} = \frac{\int_s u\phi}{A} = \frac{\int_s hs\bar{u}\bar{\phi}d\sigma}{A} = \bar{u}\bar{\phi}\omega, \tag{1.50}$$

with

$$\omega = \frac{\int_s shd\sigma}{A}, \tag{1.51}$$

considering by hypothesis that ϕ is uniformly distributed over the cross section, we have that $h = 1$ and by (1.37)

$$\bar{u} = \frac{\int_s sd\sigma}{A}\bar{u} \Longrightarrow \frac{\int_s sd\sigma}{A} = 1, \tag{1.52}$$

i.e $\omega = 1$, so (1.48) becomes

$$\partial_t(A\bar{\phi}) + \partial_x(A\bar{u}\bar{\phi}) = 0, \tag{1.53}$$

the advection equation for a passive scalar in conservative form.

1.3 The complete mathematical model

Dropping bars (standing for cross-section averaged quantities) from the unknowns, equations (1.25), (1.42) and (1.48) become

$$\begin{cases} \partial_t A + \partial_x(Au) = 0, \\ \partial_t(Au) + \partial_x(\alpha Au^2) + \dfrac{A}{\rho}\partial_x p = -Ru, \\ \partial_t(A\phi) + \partial_x(Au\phi) = 0, \end{cases} \tag{1.54}$$

where

- $A(x,t)$ is the cross-sectional area of the vessel or tube at position x and time t assumed $A \in \mathbb{R}^+$,
- $u(x,t) \in \mathbb{R}$ is the averaged velocity of blood at a cross section,
- $p(x,t) \in \mathbb{R}$ is the pressure,
- $R \in \mathbb{R}^+$ is the viscous resistance of the flow per unit lenght of the tube, assumed to be a known function,
- $\rho \in \mathbb{R}^+$ is the density of blood, assumed constant,
- α is the momentum correction coefficient assumed constant,
- $\phi(x,t) \in \mathbb{R}_0^+$ is the concentration of the passive scalar.

The first equation in (1.54) represents the mass conservation, the second the momentum balance, while the third is the advection equation for the passive scalar transport. To close the system, we adopt a *tube law* of the form

$$p = p_e + \psi, \tag{1.55}$$

where

- $p_e(x) \in \mathbb{R}$ is the external pressure,
- $\psi(x,t) \in \mathbb{R}$ is the *transmural pressure*.

This model will be described in detail and analyzed in Chapter 2, for both continuous and discontinuous parameters.

Chapter 2

Exact solution of the Riemann problem for the 1D blood flow equations with general constant momentum correction coefficient and transport

In this Chapter we present the exact solution of the Riemann problem for the 1D blood flow equations describing both arteries and veins with continuous and discontinuous mechanical and geometrical parameters, with a general constant momentum correction coefficient and an advection equation for the passive scalar transport.

The governing equations are well known and widely treated in literature ([40, 28, 90, 84, 71, 81] and others). In particular for their derivation we refer the reader to Chapter 1. In the theoretical discussion we examine both subsonic and transonic flow regimes in the case of continuous parameters, while we consider only the subcritical flow regime when studying the case of discontinuous parameters (for a complete discussion of the Riemann problem for blood flow in arteries with $\alpha = 1$ please see [71]) and we provide new propositions regarding the physical admissibility of rarefactions and shocks in waves associated with genuinely non-linear fields. Finally we compare numerically these results with FORCE, a centred, monotone, numerical scheme, suitable for conservative systems [88], and DOT, a Riemann solver suitable for non-conservative systems [23], in order to further validate the theoretical analysis since the two selected numerical methods use minimal information from the PDEs.

In detail, in Section 2.1 we discuss the 1D blood flow model with continuous properties: in Section 2.1.1 we present the mathematical model, in Section 2.1.2 we give a theoretical presentation of the exact solution of the Riemann problem while in Section 2.1.3 we describe our solution strategy, which follows the methodology presented in [87]. In Section 2.1.4 we show and comment the numerical results. The same structure is adopted for the 1D blood flow model with discontinuous properties in Section 2.2. In Section 2.2.1 we present the mathematical model. Then, in Section 2.2.2 we give a theoretical presentation of the exact solution of the Riemann problem, while in Section 2.2.3 we describe the practical approach adopted to obtain it, following the methodology presented in [90, 81]. Finally, in Section 2.2.4 we present and discuss the numerical results. In Section 2.3 the conclusions are drawn.

Part of the of the content of this Chapter has been published in Spilimbergo et al. [82].

2.1 THE 1D BLOOD FLOW MODEL WITH CONTINUOUS PROPERTIES AND TRANSPORT

2.1.1 GOVERNING EQUATIONS

Assuming an axially symmetric vessel configuration in three space dimensions at time t, and a one-dimensional flow in the axial direction x, the 1D blood flow model with continuous properties reads

$$\begin{cases} \partial_t A + \partial_x(Au) = 0, \\ \partial_t(Au) + \partial_x(\alpha A u^2) + \dfrac{A}{\rho}\partial_x p = 0, \\ \partial_t(A\phi) + \partial_x(Au\phi) = 0, \end{cases} \tag{2.1}$$

where $A(x,t)$ is the cross-sectional area of the vessel at position x and time t, assumed to be $A \in \mathbb{R}^+$, $u(x,t) \in \mathbb{R}$ is the averaged velocity of blood at a cross section, $p(x,t) \in \mathbb{R}$ is the pressure, $\rho \in \mathbb{R}^+$ is the density of blood, assumed constant, $\phi(x,t) \in \mathbb{R}_0^+$ is the concentration of a passive scalar, α is the momentum correction coefficient.

The momentum correction coefficient in the 1D blood flow equations is related to the assumed velocity profile. Here we consider the velocity profile function proposed in [77] and given by

$$s(r) = \frac{\xi + 2}{\xi}\left[1 - \left(\frac{r}{R}\right)^{\xi}\right], \tag{2.2}$$

where $r = [0, R]$ is the radial coordinate and $\xi \in \mathbb{R}^+$ determines the shape of the velocity profile. Then, the momentum correction coefficient α can be defined as in Chapter 1, i.e.

$$\alpha = \frac{\int_{\mathfrak{s}} s^2 d\sigma}{A}, \tag{2.3}$$

where $\mathfrak{s}$ is the cross section of the vessel and $A = \int_{\mathfrak{s}} d\sigma$ is the cross-sectional area of the vessel. Inserting (2.2) in (2.3), we obtain

$$\alpha = \alpha(\xi) = \frac{2 + \xi}{1 + \xi}, \tag{2.4}$$

that has the following property

$$\frac{d\alpha}{d\xi} < 0, \quad \forall \xi > 0. \tag{2.5}$$

Clearly

$$\lim_{\xi \to +\infty} \alpha(\xi) = 1, \qquad \lim_{\xi \to 0^+} \alpha(\xi) = 2, \tag{2.6}$$

consequently in this Thesis we consider $\alpha \in [1, 2]$. In particular $\xi = 2$ $\left(\text{i.e. } \alpha = \dfrac{4}{3}\right)$ is related to a parabolic velocity profile, and $\xi \to +\infty$ (i.e. $\alpha \to 1$) to an inviscid fluid (Fig. 2.1).

The first equation in (2.1) represents the mass conservation, the second describes the momentum conservation, the third equation is the advection equation for a passive scalar transport. To close the system, we adopt the following tube law

$$p = p_e + \psi(A), \tag{2.7}$$

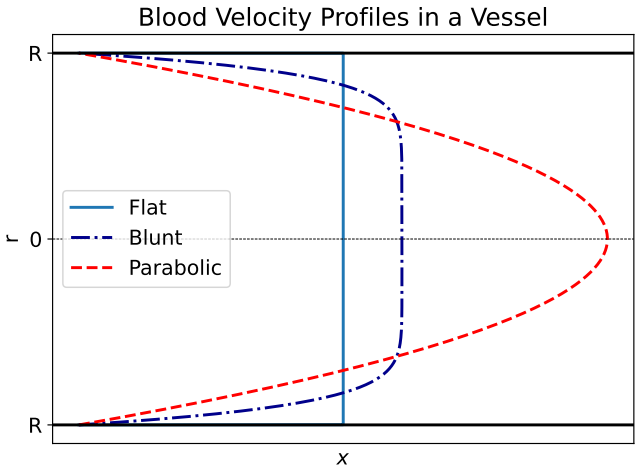

Figure 2.1: Velocity profiles obtained with (2.2). The flat velocity profile is the limiting value for $\xi \to +\infty$ (i.e. $\alpha \to 1$) and is related to an inviscid fluid. The blunt velocity profile observed in canine large vessels by [41] and widely adopted in the one-dimensional blood flow literature, is obtained with $\xi = 9$ ($\alpha = 1.1$). The parabolic velocity profile corresponds to $\xi = 2$ ($\alpha = \frac{4}{3}$). The two black thick horizontal continuous lines represent the vessel walls.

where p_e is the external pressure and $\psi(A)$ is the *transmural pressure*, assumed of the form

$$\psi(A) = K\left[\left(\frac{A}{A_0}\right)^m - \left(\frac{A}{A_0}\right)^n\right], \tag{2.8}$$

with

$$K = \begin{cases} \dfrac{E}{(1-\nu^2)}\left(\dfrac{h_0}{R_0}\right) & \text{for arteries,} \\ \dfrac{E}{12(1-\nu^2)}\left(\dfrac{h_0}{R_0}\right)^3 & \text{for veins,} \end{cases} \tag{2.9}$$

$$m = \begin{cases} 1/2 & \text{for arteries,} \\ 10 & \text{for veins,} \end{cases} \qquad n = \begin{cases} 0 & \text{for arteries,} \\ -3/2 & \text{for veins.} \end{cases} \tag{2.10}$$

h_0 is the vessel wall thickness, A_0 and R_0 are the cross-sectional area of the vessel and the radius at equilibrium, i.e. $\psi(A) = 0$, E is the Young's modulus, ν is the Poisson ratio taken as $\nu = 0.5$, m, $n \in \mathbb{R}$ and in general are taken $m > 0$ and $-2 \leq n \leq 0$. $K \in \mathbb{R}^+$, $A_0 \in \mathbb{R}^+$, $p_e \in \mathbb{R}$, $R_0 \in \mathbb{R}^+$, $E \in \mathbb{R}^+$, $h_0 \in \mathbb{R}^+$ are constants.

System (2.1) is conservative, in fact it can be written as

$$\begin{cases} \partial_t A + \partial_x(Au) = 0, \\ \partial_t(Au) + \partial_x\left(\alpha A u^2 + \displaystyle\int c^2(A)dA\right) = 0, \\ \partial_t(A\phi) + \partial_x(Au\phi) = 0, \end{cases} \tag{2.11}$$

i.e. in the form

$$\partial_t \mathbf{Q} + \partial_x \mathbf{F}(\mathbf{Q}) = \mathbf{0}, \tag{2.12}$$

with

$$\mathbf{Q} = \begin{bmatrix} A(x,t) \\ Au(x,t) \\ A\phi(x,t) \end{bmatrix},$$

$$\mathbf{F}(\mathbf{Q}) = \begin{bmatrix} Au \\ \alpha Au^2 + \int c^2(A)\, dA \\ Au\phi \end{bmatrix} = \begin{bmatrix} Au \\ \alpha Au^2 + \dfrac{KA}{\rho}\left(\dfrac{m}{m+1}\left(\dfrac{A}{A_0}\right)^m - \dfrac{n}{n+1}\left(\dfrac{A}{A_0}\right)^n\right) \\ Au\phi \end{bmatrix}, \tag{2.13}$$

where c is the *wave speed*

$$c(A) = \sqrt{\frac{A}{\rho}\frac{\partial p}{\partial A}} = \sqrt{\frac{K}{\rho}\left[m\left(\frac{A}{A_0}\right)^m - n\left(\frac{A}{A_0}\right)^n\right]}, \tag{2.14}$$

which is always real, for the choices of m and n given in (2.10). The Jacobian matrix of system (2.11) is

$$\mathbf{J}(\mathbf{Q}) = \begin{bmatrix} 0 & 1 & 0 \\ c^2 - \alpha u^2 & 2\alpha u & 0 \\ -u\phi & \phi & u \end{bmatrix}. \tag{2.15}$$

The eigenvalues of $\mathbf{J}(\mathbf{Q})$ are given by

$$\lambda_1 = \alpha u - c_\alpha, \qquad \lambda_2 = u, \qquad \lambda_3 = \alpha u + c_\alpha, \tag{2.16}$$

with

$$c_\alpha(\mathbf{Q}) = \sqrt{c^2 + \alpha(\alpha - 1)u^2}, \tag{2.17}$$

a possible choice of right eigenvectors of $\mathbf{J}(\mathbf{Q})$ corresponding to eigenvalues (2.16) is

$$\mathbf{R}_1(\mathbf{Q}) = \begin{bmatrix} 1 \\ \alpha u - c_\alpha \\ \phi \end{bmatrix}, \qquad \mathbf{R}_2(\mathbf{Q}) = \begin{bmatrix} 0 \\ 0 \\ 1 \end{bmatrix}, \qquad \mathbf{R}_3(\mathbf{Q}) = \begin{bmatrix} 1 \\ \alpha u + c_\alpha \\ \phi \end{bmatrix}. \tag{2.18}$$

Remark 2.1.1. Please note that in this Section we denote flow rate as Au or $q = Au$ interchangeably (and obviously $u = \dfrac{q}{A}$).

Proposition 2.1.1 (Hyperbolicity)**.** *The system of conservation laws defined in* (2.11) *is strictly hyperbolic under the following hypotheses:*

1. *the set of admissible solutions is restricted to* $\mathbf{Q} \in \Omega = [\mathbb{R}^+ \times \mathbb{R} \times \mathbb{R}_0^+] \subset \mathbb{R}^3$;
2. $\alpha \in [1, 2]$;
3. *the tube law is a monotonically increasing function of the cross-sectional area* A*, i.e.* $\dfrac{\partial p}{\partial A} > 0$, $\forall A \in \mathbb{R}^+$.

Proof. It is straightforward to prove that under the specified hypotheses and parameters $c_\alpha \in \mathbb{R}^+$ and thus eigenvalues (2.16) will always be real and distinct $\forall \mathbf{Q} \in \Omega$. In particular this is true for parameters in (2.9), (2.10). □

Proposition 2.1.2 (Nature of the λ_1-characteristic field)**.** *Under the hypotheses of Proposition 2.1.1, the λ_1-characteristic field is genuinely non-linear with*

$$\nabla\lambda_1(\mathbf{Q})\cdot\mathbf{R}_1(\mathbf{Q})<0,\quad \forall\mathbf{Q}\in\Omega, \tag{2.19}$$

provided $m>0$, $-2\leq n\leq 0$.

Proof. From (2.16)

$$\nabla\lambda_1(\mathbf{Q})=\left[\frac{\partial\lambda_1(\mathbf{Q})}{\partial A},\frac{\partial\lambda_1(\mathbf{Q})}{\partial q},\frac{\partial\lambda_1(\mathbf{Q})}{\partial(A\phi)}\right]=\left[-\alpha\frac{u}{A}-\frac{\partial c_\alpha}{\partial A},\frac{\alpha}{A}-\frac{\partial c_\alpha}{\partial q},0\right]. \tag{2.20}$$

Then, inserting (2.18) and (2.20) in (2.19), and recalling that $q=Au$, after manipulations one obtains

$$\nabla\lambda_1(\mathbf{Q})\cdot\mathbf{R}_1(\mathbf{Q})=-\frac{2\alpha(Ac_\alpha+q-\alpha q)^2+A^3\dfrac{\partial c}{\partial A}2c}{2A^3c_\alpha}. \tag{2.21}$$

The denominator is always positive. To check the genuine non-linearity the numerator must be different from zero. In particular we will prove that

$$2\alpha(Ac_\alpha+q-\alpha q)^2+A^3\frac{\partial c}{\partial A}2c>0. \tag{2.22}$$

(2.22) can be written as

$$-\frac{\partial c}{\partial A}-\frac{c}{A}g_1(A,\alpha)<0, \tag{2.23}$$

with

$$g_1(A,\alpha)=\frac{\alpha}{c^2}[c_\alpha+(1-\alpha)u]^2; \tag{2.24}$$

that can be proved to be

$$g_1(A,\alpha)\geq 1,\qquad g_1(A,1)=1,\quad \forall\mathbf{Q}\in\Omega. \tag{2.25}$$

For $\alpha=1$ (2.23) is satisfied if parameters m and n are in the range we consider, i.e. $m>0$, $-2\leq n\leq 0$. It follows that for this same range of the parameters, for $\alpha\in[1,2]$ (2.23) holds too, consequently we have proved the statement. □

Proposition 2.1.3 (Nature of the λ_3-characteristic field)**.** *Under the hypotheses of Proposition 2.1.1 and Proposition 2.1.2 the λ_3-characteristic field is genuinely non-linear with*

$$\nabla\lambda_3(\mathbf{Q})\cdot\mathbf{R}_3(\mathbf{Q})>0,\quad \forall\mathbf{Q}\in\Omega. \tag{2.26}$$

Proof. From (2.16)

$$\nabla\lambda_3(\mathbf{Q})=\left[\frac{\partial\lambda_3(\mathbf{Q})}{\partial A},\frac{\partial\lambda_3(\mathbf{Q})}{\partial q},\frac{\partial\lambda_3(\mathbf{Q})}{\partial(A\phi)}\right]=\left[-\alpha\frac{u}{A}+\frac{\partial c_\alpha}{\partial A},\frac{\alpha}{A}+\frac{\partial c_\alpha}{\partial q},0\right]. \tag{2.27}$$

Then, inserting (2.18) and (2.27) in (2.26), and recalling that $q=Au$, after some manipulations one obtains

$$\nabla\lambda_3(\mathbf{Q})\cdot\mathbf{R}_3(\mathbf{Q})=\frac{2\alpha(Ac_\alpha-q+\alpha q)^2+A^3\dfrac{\partial c}{\partial A}2c}{2A^3c_\alpha}. \tag{2.28}$$

The denominator is always positive. To check the genuine non-linearity the numerator must be different from zero. In particular we will prove that

$$2\alpha(Ac_\alpha - q + \alpha q)^2 + A^3\frac{\partial c}{\partial A}2c > 0. \tag{2.29}$$

(2.29) can be written as

$$\frac{\partial c}{\partial A} + \frac{c}{A}g_2(A,\alpha) > 0, \tag{2.30}$$

with

$$g_2(A,\alpha) = \frac{\alpha}{c^2}[(\alpha-1)u + c_\alpha]^2; \tag{2.31}$$

that can be proved to be

$$g_2(A,\alpha) \geq 1, \qquad g_2(A,1) = 1, \quad \forall \mathbf{Q} \in \Omega. \tag{2.32}$$

For $\alpha = 1$ (2.30) is satisfied if parameters m and n are in the range we consider, i.e. $m > 0$, $-2 \leq n \leq 0$. It follows that for this same range of the parameters, for $\alpha \in [1,2]$, (2.30) holds too, consequently we have the statement. □

Proposition 2.1.4 (Nature of the λ_2-characteristic field)**.** *Under the hypotheses of Proposition 2.1.1 the λ_2-characteristic field is linearly degenerate.*

Proof. It is straightforward to prove that

$$\nabla\lambda_2(\mathbf{Q}) \cdot \mathbf{R}_2(\mathbf{Q}) = 0, \quad \forall \mathbf{Q} \in \Omega. \tag{2.33}$$

□

2.1.2 Exact solution of the Riemann problem - Theoretical study

In this Section we generalize the results provided in [90, 81], to a generic coefficient $\alpha \in [1,2]$.

The Riemann problem for system (2.12) is the initial-value problem

$$\begin{cases} \partial_t \mathbf{Q} + \partial_x \mathbf{F}(\mathbf{Q}) = \mathbf{0}, & x \in \mathbb{R}, \quad t > 0, \\ \mathbf{Q}(x,0) = \begin{cases} \mathbf{Q}_L, & \text{if} \quad x < x_d \\ \mathbf{Q}_R, & \text{if} \quad x > x_d \end{cases} & \text{with } x_d \in \mathbb{R}, \end{cases} \tag{2.34}$$

being x_d the spatial coordinate of the discontinuity at $t = 0$. The initial conditions are given by the two constant states

$$\mathbf{Q}_L = \begin{bmatrix} A_L \\ A_L u_L \\ A_L \phi_L \end{bmatrix}, \qquad \mathbf{Q}_R = \begin{bmatrix} A_R \\ A_R u_R \\ A_R \phi_R \end{bmatrix}. \tag{2.35}$$

The unknown is $\mathbf{Q}^*$ defined as

$$\mathbf{Q}^* = \begin{bmatrix} A^* \\ A^* u^* \\ A^* \phi^* \end{bmatrix}. \tag{2.36}$$

Fig. 2.2 depicts the structure of the exact solution of the Riemann problem (2.34) for the homogeneous blood flow equations (2.12). There are two wave families associated with the two real eigenvalues $\lambda_1 = \alpha u - c_\alpha$, $\lambda_3 = \alpha u + c_\alpha$, these are associated with genuinely non-linear fields

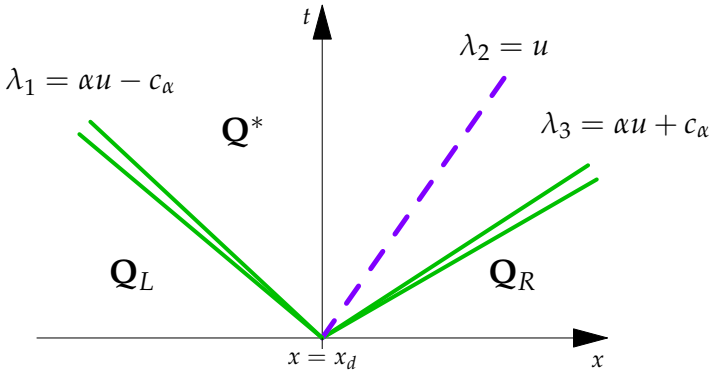

Figure 2.2: The configuration of the solution of Riemann problem (2.34) within the subsonic regime. The green solid lines represent waves associated with genuinely non-linear fields, that can be either shocks or rarefactions. In this Section the λ_1-wave will be sometimes called *left wave*, while the λ_3-wave, *right wave*. It follows that the related wave patterns will be called *left rarefaction/left shock* or *right rarefaction/right shock*. The dashed purple line depicts a wave associated with a linearly degenerate field and is a contact discontinuity.

and can be either shocks (elastic jumps) or rarefactions [80]. The λ_2-characteristic field is a contact discontinuity.

We say that we are in *subsonic regime* if

$$\lambda_1(\mathbf{Q}) < 0 \quad \text{and} \quad \lambda_3(\mathbf{Q}) > 0, \quad \text{i.e.} \quad \alpha|u| < c_\alpha \quad \forall\, \mathbf{Q} \in \Omega. \tag{2.37}$$

In this Section we will present test problems that fulfill this property and a test that does not, i.e. a test in which the associated left eigenvalue $\lambda_1(\mathbf{Q})$ goes monotonically from negative values to positive ones, passing through a critical point where $\alpha u = c_\alpha$.

Remark 2.1.2. In this Thesis we do not focus our attention on proving the existence and uniqueness of the solution of the Riemann problem for the 1D blood flow equations. The existence and uniqueness of the solution of the Riemann problem has already been proved for strictly hyperbolic systems of conservation laws defined in a open set $\Omega \in \mathbb{R}^n$, with smooth coefficients, provided the initial data are *sufficiently close* and each characteristic field is either genuinely non-linerar or linearly degenerate [12].

Proposition 2.1.5 (Generalized Riemann invariants for the λ_1- and λ_3-characteristic fields)**.** *A not complete list of Riemann invariants is*

$$\phi = const. \tag{2.38}$$

for the λ_1 and λ_3-characteristic fields. Regarding the relations between variables A and u no closed form is present for $\alpha > 1$.

Proof. The problem can be solved applying the generalized Riemann invariants method (see for example [90]), i.e for a given hyperbolic system of n unknowns $[w_1, w_2, \dots, w_n]^T$, for any λ_k-characteristic field with right eigenvector $\mathbf{R}_k = [r_{1,k}, r_{2,k}, \dots, r_{n,k}]^T$ the generalized Riemann invariants are solutions of the following $n-1$ ordinary differential equations in phase-plane

$$\frac{dw_1}{r_{1,k}} = \frac{dw_2}{r_{2,k}} = \cdots = \frac{dw_n}{r_{n,k}}. \tag{2.39}$$

For the λ_1-characteristic field we have

$$\frac{dA}{1} = \frac{d(Au)}{\alpha u - c_\alpha} = \frac{d(A\phi)}{\phi}. \tag{2.40}$$

From the first and the second term results

$$\frac{dq}{dA} = \alpha u - c_\alpha, \tag{2.41}$$

that can not be solved in closed form and will be treated later. From the first and the third

$$\frac{dA}{1} = \frac{d(A\phi)}{\phi} \Longrightarrow d\phi = 0 \Longrightarrow \phi = const. \tag{2.42}$$

For the λ_3-characteristic field instead

$$\frac{dA}{1} = \frac{d(Au)}{\alpha u + c_\alpha} = \frac{d(A\phi)}{\phi}. \tag{2.43}$$

From the first and the second term results

$$\frac{dq}{dA} = \alpha u + c_\alpha, \tag{2.44}$$

that again will be treated later. From the first and the third

$$\frac{dA}{1} = \frac{d(A\phi)}{\phi} \Longrightarrow \phi = 0 \Longrightarrow \phi = const. \tag{2.45}$$

□

2.1.2.1 WAVE RELATIONS ACROSS THE CONTACT DISCONTINUITY

Proposition 2.1.6 (Generalized Riemann invariants for the λ_2-characteristic field)**.** *The generalized Riemann invariants are*

$$A = const, \qquad Au = const. \tag{2.46}$$

for the λ_2 characteristic field.

Proof. Applying again the generalized Riemann invariants method [90], for the λ_2-characteristic field we have

$$\frac{dA}{0} = \frac{d(Au)}{0} = \frac{d(A\phi)}{1}, \tag{2.47}$$

from which we obtain the statement. □

Considering Propositions 2.1.5 and 2.1.6, across the waves associated with the genuinely non-linear fields the variable ϕ remains constant. In addition, the contact wave λ_2 is the only discontinuity for the passive scalar ϕ, while the other variables remain constant. It follows that in the entire Star Region (the region between the two waves associated with the genuinely non-linear fields in Fig. 2.2), the unknowns A^* and q^* remain constant. Furthermore the third equation in (2.1) is not affecting the others, consequentially to study the relations across the waves associated with the genuinely non-linear fields we focus only on the first two variables, referring to the unknown as

$$\mathbf{Q}^* = \begin{bmatrix} A^* \\ q^* \end{bmatrix}, \tag{2.48}$$

and addressing ϕ^* at a later point.

2.1.2.2 Wave relations across rarefactions

An integral curve for $\mathbf{R}_k(\mathbf{Q})$, $k = 1, 3$ in (2.18) is a curve in the phase plane (A, q) which has the property that the tangent to the curve at any point $\mathbf{Q} \in \Omega$ lies in the direction of the vector field $\mathbf{R}_k(\mathbf{Q})$ [44]. A rarefaction is a smooth wave whose states belong to that integral curve in the phase-plane (A, q), this latter defined as the solution of an initial-value problem involving the following Ordinary Differential Equations (ODEs)

$$\begin{cases} \dfrac{dA}{d\xi} = 1 \\ \dfrac{d(Au)}{d\xi} = \alpha u - c_\alpha \end{cases} \quad \text{for the } \lambda_1\text{-wave,} \tag{2.49}$$

$$\begin{cases} \dfrac{dA}{d\xi} = 1 \\ \dfrac{d(Au)}{d\xi} = \alpha u + c_\alpha \end{cases} \quad \text{for the } \lambda_3\text{-wave.} \tag{2.50}$$

Substituting $q = Au$, carrying out some algebraic calculations and adding the initial conditions, systems (2.49), (2.50) become

$$\left.\begin{aligned} \text{ODE:} \quad & \frac{dq}{dA} = \alpha \frac{q}{A} - c_\alpha, \\ \text{IC:} \quad & q(A_L) = q_L, \end{aligned}\right\} \quad \text{for the } \lambda_1\text{-wave,} \tag{2.51}$$

$$\left.\begin{aligned} \text{ODE:} \quad & \frac{dq}{dA} = \alpha \frac{q}{A} + c_\alpha \\ \text{IC:} \quad & q(A_R) = q_R, \end{aligned}\right\} \quad \text{for the } \lambda_3\text{-wave,} \tag{2.52}$$

where c_α is defined in (2.17). Solving (2.51) and (2.52) for $A \in \mathbb{R}^+$, results in the construction of the two integral curves, one for each wave (the association of the λ_1-wave with $\mathbf{Q}_L$ in (2.35) is straightforward: this latter is the initial data that is connected to the unknown $\mathbf{Q}^*$ by the considered wave, the same for the right wave) that are actually functions of variable A (see Fig. 2.3c)

$$q_{rarL}(A) \quad \text{and} \quad q_{rarR}(A) \quad \text{with} \quad A \in \mathbb{R}^+. \tag{2.53}$$

Remark 2.1.3. In literature usually both the rarefaction and shock curves $f = (A, q)$ are represented depending on a parameter ξ in this way [42, 44]:

$$f(\xi) = (A(\xi), q(\xi)). \tag{2.54}$$

In our case the parameter is the variable A. This choice is justified by (2.49) and (2.50): from the first equations of the two systems we have in fact that $dA = d\xi$. Thus the resulting curves are

$$\mathbf{Q}(A) = (A, q(A)). \tag{2.55}$$

Being q a function of A we will usually refer to these curves simply as $q(A)$. Additionally, with an abuse of notation, we sometimes refer to $\mathbf{Q}(A) = [A, q(A)]^T$ as a generic state belonging to that curve.

Remark 2.1.4. It is straightforward to see that the solutions of the ODEs (2.51) and (2.52) are the generalized Riemann invariants respectively for the λ_1- and λ_3-characteristic fields [90, 81]

Proposition 2.1.7 (Physically admissible rarefaction curves)**.**
If the λ_1-wave, associated with a genuinely non-linear field, is a smooth wave (i.e. is a physically admissible rarefaction), the related admissible rarefaction curve in the (A, q) phase-plane is

$$q^a_{rarL}(A) = \{[A, q_{rarL}(A)]^T, \text{ s.t. } A \in \mathbb{R}^+ \text{ and } A \leq A_L\}, \tag{2.56}$$

with $q_{rarL}(A)$ in (2.53). In particular $A^* \leq A_L$.

If the λ_3-wave, associated with a genuinely non-linear field, is a smooth wave (i.e. is a physically admissible rarefaction), the related admissible rarefaction curve in the (A, q) phase-plane is

$$q^a_{rarR}(A) = \{[A, q_{rarR}(A)]^T, \text{ s.t. } A \in \mathbb{R}^+ \text{ and } A \leq A_R\}, \tag{2.57}$$

with $q_{rarR}(A)$ in (2.53). In particular $A^* \leq A_R$.

Proof. In a k-th genuinely non-linear characteristic field, $\lambda_k(A)$ is monotonically varying along the entire integral curve. Given the left state $\mathbf{Q}_{\hat{L}}$ belonging to the aforementioned integral curve $\mathbf{Q}_{rar}(A) = (A, q_{rar}(A))$, the admissible rarefaction curve is the part of that integral curve s.t

$$\lambda_k(\mathbf{Q}_{\hat{L}}) \leq \lambda_k(\mathbf{Q}_{rar}). \tag{2.58}$$

For the case of the λ_1-wave, having a physically admissible rarefaction with left value $\mathbf{Q}_L$, the admissible rarefaction curve is the set of generic states $\mathbf{Q}_{rarL}(A) = [A, q_{rarL}(A)]^T$ in the phase-plane (A, q), lying on the left integral curve $q_{rarL}(A)$ built in (2.51), for $A \in \mathbb{R}^+$, such that

$$\lambda_1(\mathbf{Q}_L) \leq \lambda_1(\mathbf{Q}_{rarL}(A)). \tag{2.59}$$

Considering now the curve $\mathbf{Q}_{rarL}(A) = (A, q_{rarL}(A))$ we want to calculate

$$\frac{d\lambda_1(\mathbf{Q}_{rarL}(A))}{dA} = \nabla\lambda_1(\mathbf{Q}_{rarL}(A)) \cdot \frac{d\mathbf{Q}_{rarL}(A)}{dA}. \tag{2.60}$$

We have that

$$\frac{d\mathbf{Q}_{rarL}(A)}{dA} = \begin{bmatrix} 1 \\ \dfrac{dq_{rarL}(A)}{dA} \end{bmatrix}, \tag{2.61}$$

but by construction of (2.51)

$$\frac{dq_{rarL}(A)}{dA} = \alpha\frac{q_{rarL}(A)}{A} - c_\alpha(\mathbf{Q}_{rarL}(A)), \tag{2.62}$$

consequently

$$\frac{d\mathbf{Q}_{rarL}(A)}{dA} = \begin{bmatrix} 1 \\ \alpha\dfrac{q_{rarL}(A)}{A} - c_\alpha(\mathbf{Q}_{rarL}(A)) \end{bmatrix} = \mathbf{R}_1(\mathbf{Q}_{rarL}(A)), \tag{2.63}$$

where $\mathbf{R}_1$ is the right eigenvector in (2.18). So

$$\frac{d\lambda_1(\mathbf{Q}_{rarL}(A))}{dA} = \nabla\lambda_1(\mathbf{Q}_{rarL}(A)) \cdot \mathbf{R}_1(\mathbf{Q}_{rarL}(A)) < 0, \tag{2.64}$$

for genuine non-linearity of the λ_1-field, as presented in Proposition 2.1.2. This means that $\lambda_1(\mathbf{Q}_{rarL}(A))$ is strictly decreasing in the domain $A \in \mathbb{R}^+$. In other words from (2.59)

$$\lambda_1(\mathbf{Q}_L) = \lambda_1(\mathbf{Q}_{rarL}(A_L)) \leq \lambda_1(\mathbf{Q}_{rarL}(A)) \qquad \Longrightarrow \qquad A \leq A_L, \tag{2.65}$$

thus we obtain the statement. In particular for a left rarefaction that has as left state $\mathbf{Q}_L$ and right state $\mathbf{Q}^*$, (2.59) becomes

$$\lambda_1(\mathbf{Q}_L) \leq \lambda_1(\mathbf{Q}^*), \tag{2.66}$$

from which

$$A^* \leq A_L. \tag{2.67}$$

On the contrary, given the right state $\mathbf{Q}_{\widehat{R}}$ belonging to the integral curve $\mathbf{Q}_{rar}(A) = (A, q_{rar}(A))$, the admissible rarefaction curve is the part of that integral curve s.t

$$\lambda_k(\mathbf{Q}_{rar}) \leq \lambda_k(\mathbf{Q}_{\widehat{R}}). \tag{2.68}$$

For the case of the λ_3-wave, having a physically admissible rarefaction with right value $\mathbf{Q}_R$, the admissible rarefaction curve is the set of generic states $\mathbf{Q}_{rarR}(A) = [A, q_{rarR}(A)]^T$ in the phase-plane (A, q), lying on the right integral curve $q_{rarR}(A)$ built in (2.52), for $A \in \mathbb{R}^+$, such that

$$\lambda_3(\mathbf{Q}_{rarR}(A)) \leq \lambda_3(\mathbf{Q}_R). \tag{2.69}$$

Considering now the curve $\mathbf{Q}_{rarR}(A) = (A, q_{rarR}(A))$, we want to calculate

$$\frac{d\lambda_3(\mathbf{Q}_{rarR}(A))}{dA} = \nabla\lambda_3(\mathbf{Q}_{rarR}(A)) \cdot \frac{d\mathbf{Q}_{rarR}(A)}{dA}. \tag{2.70}$$

We have that

$$\frac{d\mathbf{Q}_{rarR}(A)}{dA} = \begin{bmatrix} 1 \\ \dfrac{dq_{rarR}(A)}{dA} \end{bmatrix}, \tag{2.71}$$

but by construction of (2.52)

$$\frac{dq_{rarR}(A)}{dA} = \alpha\frac{q_{rarR}(A)}{A} + c_\alpha(\mathbf{Q}_{rarR}(A)), \tag{2.72}$$

consequently

$$\frac{d\mathbf{Q}_{rarR}(A)}{dA} = \begin{bmatrix} 1 \\ \alpha\dfrac{q_{rarR}(A)}{A} + c_\alpha(\mathbf{Q}_{rarR}(A)) \end{bmatrix} = \mathbf{R}_3(\mathbf{Q}_{rarR}(A)), \tag{2.73}$$

where $\mathbf{R}_3$ is the right eigenvector in (2.18). So

$$\frac{d\lambda_3(\mathbf{Q}_{rarR}(A))}{dA} = \nabla\lambda_3(\mathbf{Q}_{rarR}(A)) \cdot \mathbf{R}_3(\mathbf{Q}_{rarR}(A)) > 0 \tag{2.74}$$

for genuine non-linearity of the λ_3-field, as presented in Proposition 2.1.3. This means that $\lambda_3(\mathbf{Q}_{rarR}(A))$ is strictly increasing in the domain $A \in \mathbb{R}^+$. In other words

$$\lambda_3(\mathbf{Q}_{rarR}(A)) \leq \lambda_3(\mathbf{Q}_{rarR}(A_R)) = \lambda_3(\mathbf{Q}_R) \qquad \Longrightarrow \qquad A \leq A_R, \tag{2.75}$$

thus we obtain the result. In particular for a right rarefaction that has as left state $\mathbf{Q}^*$ and right state $\mathbf{Q}_R$ we have

$$\lambda_3(\mathbf{Q}^*) \leq \lambda_3(\mathbf{Q}_R), \tag{2.76}$$

from which

$$A^* \leq A_R. \tag{2.77}$$

□

2.1.2.3 WAVE RELATIONS ACROSS SHOCKS

We start considering that if a discontinuity propagating with speed S has constant values $\mathbf{Q}_{\hat{R}}$, $\mathbf{Q}_{\hat{L}}$, on either side (right and left) of it, then the Rankine-Hugoniot jump condition [44] must hold, namely

$$\mathbf{F}(\mathbf{Q}_{\hat{R}}) - \mathbf{F}(\mathbf{Q}_{\hat{L}}) = S(\mathbf{Q}_{\hat{R}} - \mathbf{Q}_{\hat{L}}). \tag{2.78}$$

Substituting $\mathbf{Q}_{\hat{R}}$ with $\mathbf{Q}^* = [A^*, q^*]^T$, $\mathbf{Q}_{\hat{L}}$ with $\mathbf{Q}_j = [A_j, q_j]^T$, S with S_j, with $j = L, R$ and $q = Au$, we obtain two different systems

$$\begin{cases} q^* - q_j = S_j(A^* - A_j), \\ \alpha \dfrac{q^{*2}}{A^*} - \alpha \dfrac{q_j^2}{A_j} + B_j = S_j(q^* - q_j), \end{cases} \tag{2.79}$$

with

$$B_j(A^*) = \frac{K}{\rho}\left[\frac{m}{m+1}\frac{A^{*m+1} - A_j^{m+1}}{A_0^m} - \frac{n}{n+1}\frac{A^{*n+1} - A_j^{n+1}}{A_0^n}\right], \tag{2.80}$$

one for each $j = L, R$. Solving for q^* we obtain

$$q^* = \frac{A^* q_j}{A_j\alpha + A^* - \alpha A^*} \pm \sqrt{\frac{(A_j - A^*)A^*(-A_j(A_j\alpha + A^* - \alpha A^*)B_j + (\alpha - 1)\alpha(A_j - A^*)q_j^2)}{A_j(A_j\alpha + A^* - \alpha A^*)^2}}, \tag{2.81}$$

with $j = L, R$. We thus obtain two q^* values for each state $j = L, R$ but unfortunately there is actually one and only q^* as the result of the entire Riemann problem (see for example [20]). We must consider the following propositions.

Proposition 2.1.8. *We define one and only admissible, locally at least C^1, shock curve in the phase-plane (A, q), passing through the left state $\mathbf{Q}_L$ and one and only admissible, locally at least C^1, shock curve passing through the right state $\mathbf{Q}_R$ as*

$$q_{shockL}(A) = \begin{cases} q_{HL}^+(A) & \text{for} \quad A \le A_L, \\ q_{HL}^-(A) & \text{for} \quad A > A_L, \end{cases} \quad \text{for the left state,} \tag{2.82}$$

$$q_{shockR}(A) = \begin{cases} q_{HR}^-(A) & \text{for} \quad A \le A_R, \\ q_{HR}^+(A) & \text{for} \quad A > A_R. \end{cases} \quad \text{for the right state,} \tag{2.83}$$

with

$$q_{Hj}^-(A) = \frac{Aq_j}{A_j\alpha + A - \alpha A} - \sqrt{\frac{(A_j - A)A(-A_j(A_j\alpha + A - \alpha A)B_j + (\alpha - 1)\alpha(A_j - A)q_j^2)}{A_j(A_j\alpha + A - \alpha A)^2}}, \tag{2.84}$$

$$q_{Hj}^+(A) = \frac{Aq_j}{A_j\alpha + A - \alpha A} + \sqrt{\frac{(A_j - A)A(-A_j(A_j\alpha + A - \alpha A)B_j + (\alpha - 1)\alpha(A_j - A)q_j^2)}{A_j(A_j\alpha + A - \alpha A)^2}}, \tag{2.85}$$

with $j = L, R$.

Proof. Substituting $\mathbf{Q}_{\hat{R}}$ with $\mathbf{Q}_{Hj}$ and $\mathbf{Q}_{\hat{L}}$ with $\mathbf{Q}_j$, $j = L, R$, the Rankine-Hugoniot condition (2.78) becomes

$$\mathbf{F}(\mathbf{Q}_{Hj}) - \mathbf{F}(\mathbf{Q}_j) = S_j(\mathbf{Q}_{Hj} - \mathbf{Q}_j). \tag{2.86}$$

Attempting to determine the set of all states $\mathbf{Q}_{Hj}(A) = [A, q_{Hj}(A)]^T$ that can be connected to $\mathbf{Q}_j$ by a discontinuity satisfying (2.86) for some S_j, the so-called *Hugoniot Locus* of $\mathbf{Q}_j \in \mathbb{R}^2$, we obtain a system of 2 equations in $2+1$ unknowns: the 2 components of $\mathbf{Q}_{Hj}$ and S_j

$$\begin{cases} q_{Hj}(A) - q_j = S_j(A - A_j), \\ \alpha \dfrac{q_{Hj}^2(A)}{A} - \alpha \dfrac{q_j^2}{A_j} + B_j = S_j(q_{Hj}(A) - q_j), \end{cases} \tag{2.87}$$

with B_j in (2.80). In other words we obtain 2 curves through each state $\mathbf{Q}_j$, $q_{Hj}^-(A)$ and $q_{Hj}^+(A)$, defined in (2.84) and (2.85), for $j = L, R$. $q_{Hj}^-(A)$ and $q_{Hj}^+(A)$ are called *Hugoniot curves*. If $\mathbf{Q}_{Hj}$ lies on the k-th Hugoniot curve passing through $\mathbf{Q}_j$, then we say that $\mathbf{Q}_j$ and $\mathbf{Q}_{Hj}$ are connected by a k-shock (see [44]). These curves can be parametrized in various manners. In this Thesis, as previously done for the rarefaction curves, for computational simplicity we use as parameter the variable A (see Remark (2.1.3)). (2.86) is clearly

$$\mathbf{F}(\mathbf{Q}_{Hj}(A)) - \mathbf{F}(\mathbf{Q}_j) = S_j(A)(\mathbf{Q}_{Hj}(A) - \mathbf{Q}_j), \tag{2.88}$$

differentiating this expression with respect to A and setting $A = A_j$ gives

$$\mathbf{F}_{\mathbf{Q}}(\mathbf{Q}_{Hj}(A_j))\mathbf{Q}'_{Hj}(A_j) = S'_j(A_j)(\mathbf{Q}_{Hj}(A_j) - \mathbf{Q}_j) + S_j(A_j)\mathbf{Q}'_{Hj}(A_j). \tag{2.89}$$

Being $\mathbf{Q}_{Hj}(A_j) = \mathbf{Q}_j$, we have

$$\mathbf{F}_{\mathbf{Q}}(\mathbf{Q}_j)\mathbf{Q}'_{Hj}(A_j) = S_j(A_j)\mathbf{Q}'_{Hj}(A_j), \tag{2.90}$$

that is not-trivially satisfied if and only if $\mathbf{Q}'_{Hj}(A_j)$ is an eigenvector of $\mathbf{F}_{\mathbf{Q}}(\mathbf{Q}_j)$ and $S_j(A_j)$ the correspondent eigenvalue. At this point we must check which curve, or part of it, is really admissible for each state. Clearly the admissible one for each state is $\mathbf{Q}_{shockj}(A) = (A, q_{shockj}(A))$, $j = L, R$ such that,
for $\mathbf{Q}_L$: $\mathbf{Q}_{shockL}(A)$ such that

$$\mathbf{Q}'_{shockL}(A_L) = \mathbf{R}_1(\mathbf{Q}_L), \tag{2.91}$$

and for $\mathbf{Q}_R$: $\mathbf{Q}_{shockR}(A)$ such that

$$\mathbf{Q}'_{shockR}(A_R) = \mathbf{R}_3(\mathbf{Q}_R), \tag{2.92}$$

in fact $\mathbf{R}_1$ is the tangent vector to the left integral curve at the point $\mathbf{Q}_L$, while $\mathbf{R}_3$ is the tangent vector to the right integral curve at the point $\mathbf{Q}_R$. In other words
for $\mathbf{Q}_L$:

$$\frac{dq_{shockL}}{dA}(A_L) = \lambda_1(\mathbf{Q}_L), \tag{2.93}$$

for $\mathbf{Q}_R$:

$$\frac{dq_{shockR}}{dA}(A_R) = \lambda_3(\mathbf{Q}_R). \tag{2.94}$$

As shown in Figs. 2.3a neither $q_{Hj}^-(A)$ nor $q_{Hj}^+(A)$ are differentiable in A_j, so the tangent does not exist in that point. Calculating we obtain that, for $\dfrac{K}{\rho} > 0$, $A_0 > 0$, $m > 0$, $-2 \leq n \leq 0$

$$\lim_{A \to A_L^+} \frac{dq_{HL}^-(A)}{dA} = \lim_{A \to A_L^-} \frac{dq_{HL}^+(A)}{dA} = \alpha u_L - c_\alpha(\mathbf{Q}_L) = \lambda_1(\mathbf{Q}_L), \tag{2.95}$$

and

$$\lim_{A\to A_R^-}\frac{dq_{HR}^-(A)}{dA}=\lim_{A\to A_R^+}\frac{dq_{HR}^+(A)}{dA}=\alpha u_R+c_\alpha(\mathbf{Q}_R)=\lambda_3(\mathbf{Q}_R), \tag{2.96}$$

while this is not valid for the other limits $\left(\lim_{A\to A_L^-}\frac{dq_{HL}^-(A)}{dA},\lim_{A\to A_L^+}\frac{dq_{HL}^+(A)}{dA},\ \lim_{A\to A_R^+}\frac{dq_{HR}^-(A)}{dA}\right.$ and $\left.\lim_{A\to A_R^-}\frac{dq_{HR}^+(A)}{dA}\right)$. It is clear that we have just defined the two unique, locally at least C^1, shock curves (one for each state) as

$$q_{shockL}(A)=\begin{cases}q_{HL}^+(A) & \text{for}\quad A\le A_L,\\ q_{HL}^-(A) & \text{for}\quad A>A_L,\end{cases} \tag{2.97}$$

$$q_{shockR}(A)=\begin{cases}q_{HR}^-(A) & \text{for}\quad A\le A_R,\\ q_{HR}^+(A) & \text{for}\quad A>A_R,\end{cases} \tag{2.98}$$

(See Fig. 2.3b). We have proved the statement. □

Proposition 2.1.9 (Entropy-satisfying shock curves)**.**
If the λ_1-wave, associated with a genuinely non-linear field, is an admissible entropy-satisfying shock, the related admissible shock curve in the (A,q) phase-plane is

$$q_{shockL}^a(A)=\{[A,q_{shockL}(A)]^T \text{ s.t. } A>A_L\}, \tag{2.99}$$

with A sufficiently close to A_L and $q_{shockL}(A)$ in (2.82). In particular $A^*>A_L$.

If the λ_3-wave, associated with a genuinely non-linear field, is an admissible entropy-satisfying shock, the related admissible shock curve in the (A,q) phase-plane is

$$q_{shockR}^a(A)=\{[A,q_{shockR}(A)]^T \text{ s.t. } A>A_R\}, \tag{2.100}$$

with A sufficiently close to A_R and $q_{shockR}(A)$ in (2.83). In particular $A^*>A_R$.

Proof. With Proposition 2.1.8 we have reduced the Hugoniot Locus of each state $\mathbf{Q}_L$ and $\mathbf{Q}_R$ to one, locally at least C^1, shock curve. Now we must check the *physical* admissibility of each of them.

For a non-linear hyperbolic system in $\mathbb{R}^m$ (in our case $\mathbb{R}^2$), for each state $\mathbf{Q}_{Hj}$ belonging to a k-th curve of the Hugoniot Locus of $\mathbf{Q}_j$, exists a parametrization $A\to\mathbf{Q}_k(A)$ with $1\le k\le m$ defined for A sufficiently close to A_j, and s.t

$$\lambda_k(\mathbf{Q}_k(A))=\lambda_k(\mathbf{Q}_j)+(A-A_j)\nabla\lambda_k(\mathbf{Q}_j)\cdot\mathbf{R}_k(\mathbf{Q}_j)+O((A-A_j)^2), \tag{2.101}$$

(see [33]).

In our case, for a left shock, we consider the just built (2.82), locally at least C^1 curve, so we can apply the Taylor expansion

$$\lambda_1(\mathbf{Q}_{shockL}(A))=\lambda_1(\mathbf{Q}_L)+(A-A_L)\nabla\lambda_1(\mathbf{Q}_L)\cdot\mathbf{R}_1(\mathbf{Q}_L)+O((A-A_L)^2), \tag{2.102}$$

$\forall\ A$ sufficiently close to A_L.
Considering that [33] presents also this result: $\forall\ A$ sufficiently close to A_L

$$S_L(\mathbf{Q}_{shockL}(A))=\frac{1}{2}(\lambda_1(\mathbf{Q}_L)+\lambda_1(\mathbf{Q}_{shockL}(A)))+O((A-A_L)^2), \tag{2.103}$$

it is clear that a generic state $\mathbf{Q}_{shockL}(A)$ belonging to the left shock curve $q_{shockL}(A)$ in (2.82), belongs to the left admissible entropy satisfying shock curve $q^a_{shockL}(A)$ if $\lambda_1(\mathbf{Q}_{shockL}(A)) < \lambda_1(\mathbf{Q}_L)$ in (2.102), that implies $\lambda_1(\mathbf{Q}_L) > S_L(\mathbf{Q}_{shockL}(A))$ in (2.103) verifying the Lax-Entropy condition [42]

$$\lambda_1(\mathbf{Q}_L) > S_L(\mathbf{Q}_{shockL}(A)) > \lambda_1(\mathbf{Q}_{shockL}(A)), \tag{2.104}$$

where S_L is the left shock speed. But this is possible only if

$$A > A_L, \tag{2.105}$$

in (2.102) because $\nabla\lambda_1(\mathbf{Q}_L)\cdot\mathbf{R}_1(\mathbf{Q}_L) < 0$ in (2.102), for genuine non-linearity (Proposition 2.1.2). In particular, considering $\mathbf{Q}^*$, which, when admissible, belongs by definition to the entropy-satisfying subset $q^a_{shockL}(A)$ of the Hugoniot Locus of $\mathbf{Q}_L$, (2.104) becomes

$$\lambda_1(\mathbf{Q}_L) > S_L(\mathbf{Q}^*) > \lambda_1(\mathbf{Q}^*), \tag{2.106}$$

with

$$S_L(\mathbf{Q}^*) = \frac{q^* - q_L}{A^* - A_L}, \tag{2.107}$$

according to the first of (2.79), consequently in case of an entropy-satisfying left shock, the admissible A^* is such that

$$A^* > A_L, \tag{2.108}$$

giving the desired result.

A similar proof for the right wave. In case of an entropy-satisfying right shock

$$\lambda_3(\mathbf{Q}_{shockR}(A)) = \lambda_3(\mathbf{Q}_R) + (A - A_R)\nabla\lambda_3(\mathbf{Q}_R)\cdot\mathbf{R}_3(\mathbf{Q}_R) + O((A - A_R)^2), \tag{2.109}$$

$\forall\ A$ sufficiently close to A_R. Under the same conditions

$$S_R(\mathbf{Q}_{shockR}(A)) = \frac{1}{2}(\lambda_3(\mathbf{Q}_R) + \lambda_3(\mathbf{Q}_{shockR}(A))) + O((A - A_R)^2), \tag{2.110}$$

it is clear that a state $\mathbf{Q}_{shockR}(A) = [A, q_{shockR}(A)]^T \in q_{shockR}(A)$ belongs to the right admissible entropy-satisfying shock curve $q^a_{shockR}(A)$ if $\lambda_3(\mathbf{Q}_{shockR}(A)) > \lambda_3(\mathbf{Q}_R)$ in (2.109), that implies $S_R(\mathbf{Q}_{shockR}(A)) > \lambda_3(\mathbf{Q}_R)$ in (2.110) verifying the Lax-Entropy condition [42]

$$\lambda_3(\mathbf{Q}_{shockR}(A)) > S_R(\mathbf{Q}_{shockR}(A)) > \lambda_3(\mathbf{Q}_R), \tag{2.111}$$

where S_R is the right shock speed. But it is possible only if

$$A > A_R, \tag{2.112}$$

in (2.109) because $\nabla\lambda_3(\mathbf{Q}_R)\cdot\mathbf{R}_3(\mathbf{Q}_R) > 0$ in (2.109) for genuine non-linearity (Proposition 2.1.3). In particular, considering $\mathbf{Q}^*$, which, when admissible, belongs by definition to the entropy-satisfying subset $q^a_{shockR}(A)$ of the Hugoniot locus of $\mathbf{Q}_R$, (2.111) becomes

$$\lambda_3(\mathbf{Q}^*) > S_R(\mathbf{Q}^*) > \lambda_3(\mathbf{Q}_R), \tag{2.113}$$

with

$$S_R(\mathbf{Q}^*) = \frac{q^* - q_R}{A^* - A_R}, \tag{2.114}$$

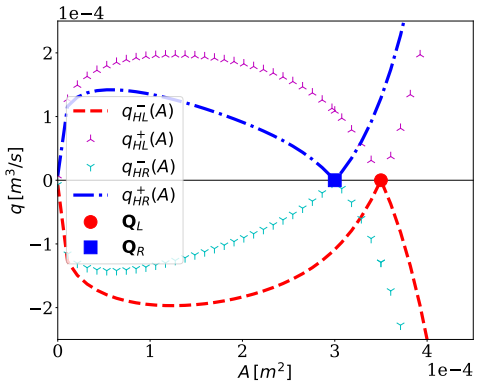

(a) The obtained shock curves for $\mathbf{Q}_L$ and $\mathbf{Q}_R$, for the Test 3 left rarefaction - right shock problem in a vein with $\alpha = 1.1$.

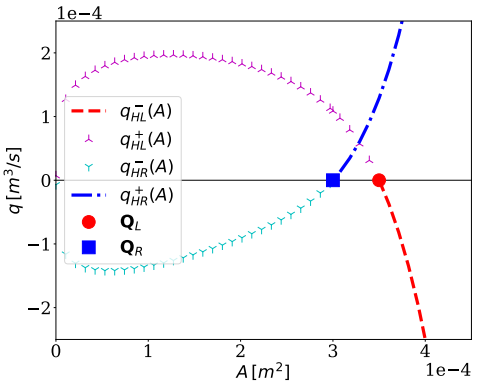

(b) The $q_{shockj}(A)$ $j = L, R$ curves defined in (2.82) and (2.83), for the Test 3 left rarefaction - right shock problem in a vein with $\alpha = 1.1$.

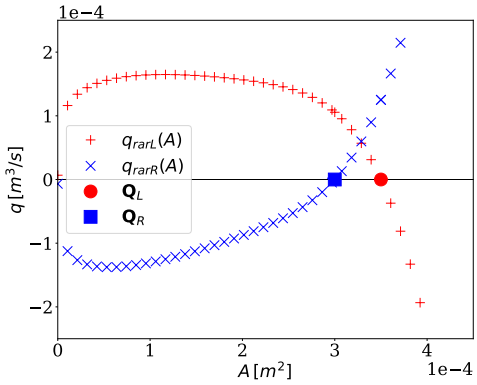

(c) The $q_{rarj}(A)$ $j = L, R$ curves for the Test 3 left rarefaction - right shock problem in a vein with $\alpha = 1.1$.

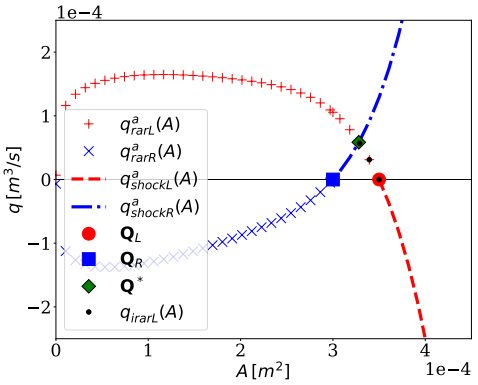

(d) The $q_{left}(A)$ and $q_{right}(A)$ curves for the Test 3 left rarefaction - right shock problem in a vein with $\alpha = 1.1$ as defined in (2.120) and (2.121). The subscript a stands for *admissible*, the curves are explained in Propositions 2.1.7 and 2.1.9. It is clear that this test is a rarefaction - shock problem, due to the nature of the curves at the intersection. In black the part of the left rarefaction curve *inside* the left rarefaction (Section 2.1.2.5).

Figure 2.3: Rarefaction and shock curves in the phase-plane (A, q) for the Test 3 left rarefaction - right shock problem in a vein with $\alpha = 1.1$. Initial data are in Tables 2.3, 2.4.

according to the first of (2.79), consequently in case of an entropy-satisfying right shock, the admissible A^* is such that

$$A^* > A_R, \tag{2.115}$$

giving the desired result. □

2.1.2.4 Solution in the Star Region

Defining the Star Region as the region in the half-plane (x, t) in Fig. 2.2 between the λ_1-wave and the λ_3-wave and considering that a wave associated with a genuinely non-linear field can be either a shock or a rarefaction (see for example [80]) what stated in Sections 2.1.2.2 and 2.1.2.3 leads to the following statements.

Theorem 2.1.1. *Given the Riemann problem (2.34), the λ_1-wave is a physically admissible (left) rarefaction if and only if*

$$A^* \leq A_L. \tag{2.116}$$

The λ_3-wave is a physically admissible (right) rarefaction if and only if

$$A^* \leq A_R. \tag{2.117}$$

Proof.
($\Longrightarrow$)In Proposition 2.1.7 we have proved this part.
($\Longleftarrow$)In Proposition 2.1.9 we have proved this part.

□

Theorem 2.1.2. *Given the Riemann problem (2.34), the λ_1-wave is an entropy-satisfying (left) shock if and only if*

$$A^* > A_L. \tag{2.118}$$

The λ_3-wave is an entropy-satisfying (right) shock if and only if

$$A^* > A_R. \tag{2.119}$$

Proof.
($\Longrightarrow$)In Proposition 2.1.9 we have proved this part.
($\Longleftarrow$)In Proposition 2.1.7 we have proved this part. □

Proposition 2.1.10 (Graphic construction of $\mathbf{Q}^*$)**.** *Given the Riemann problem (2.34), the solution $\mathbf{Q}^*$ is the unique intersection of the two curves in the phase-plane (A, q)*

$$q_{left}(A) = \begin{cases} q^a_{rarL}(A) & \text{for} \quad A \leq A_L, \\ q^a_{shockL}(A) & \text{for} \quad A > A_L, \end{cases} \tag{2.120}$$

$$q_{right}(A) = \begin{cases} q^a_{rarR}(A) & \text{for} \quad A \leq A_R, \\ q^a_{shockR}(A) & \text{for} \quad A > A_R, \end{cases} \tag{2.121}$$

given A "not too far" from A_j, $j = L, R$. The nature of the two curves at the intersection will show the wave pattern (for example see Fig. 2.3d).

Proof. In Propositions 2.1.7 and 2.1.9 we have proved that the physically admissible parts of the left and right rarefaction and shock curves are $q^a_{rarL}(A)$, $q^a_{rarR}(A)$, $q^a_{shockL}(A)$, $q^a_{shockR}(A)$ defined in the statements. The existence of these curves is a necessary condition for the physical admissibility of each type of wave, but not a sufficient one. We can find the unknown $\mathbf{Q}^*$ graphically, without knowing a priori which type of wave is actually present: having constructed all these admissible curves, if the solution of our Riemann problem exists, it is unique (Remark 2.1.2), so by Propositions 2.1.7 and 2.1.9 it must belong to respectively one between $q^a_{rarL}(A)$ and $q^a_{shockL}(A)$ curves and to one between $q^a_{rarR}(A)$ and $q^a_{shockR}(A)$ curves (considering that a wave associated with a genuinely non-linear field can be only a shock or a rarefaction and it is not possible to have both rarefactions and shocks together [80]). In other words the unknown $\mathbf{Q}^*$ is the *unique* intersection of the $q_{left}(A)$ and $q_{right}(A)$ curves in (2.120) and (2.121) thus obtained.

Now we will prove that the intersection of the $q_{left}(A)$ and $q_{right}(A)$ curves (if it exists) is actually unique but only in a small neighbourhood of A_L and A_R, i.e. where the $q^a_{shockj}(A)$, $j = L, R$; curves are built in Proposition 2.1.9. This can be easily proved for any combination of waves. Considering only rarefaction waves, we define

$$h(A) = q_{rarL}(A) - q_{rarR}(A), \tag{2.122}$$

with $q_{rarL}(A)$ and $q_{rarR}(A)$ defined in (2.53). The solution of $h(A) = 0$ is clearly the sought A^*. We want to check

$$\frac{dh}{dA} = \frac{dq_{rarL}}{dA} - \frac{dq_{rarR}}{dA}, \tag{2.123}$$

considering (2.51) and (2.52) we obtain

$$\frac{dh}{dA} = -2c_\alpha < 0, \quad \forall\, A \in \mathbb{R}^+, \tag{2.124}$$

so, in case of two rarefactions, function h in (2.122) is strictly monotonic in $\mathbb{R}^+$, so if a zero exists, it is unique. In case of shocks the discussion is the same, in fact recalling what stated in Proposition 2.1.9, in a small neighbourhood of A_j, $j = L, R$; the behaviour of the two curves is the same. Thus we can conclude that for any admissible wave pattern the intersection of the two $q_{left}(A)$ and $q_{right}(A)$ curves is unique, provided it exists, and a small neighbourhood of the initial data is considered. □

2.1.2.5 Solution inside the rarefactions

If there is a physically admissible left rarefaction, the states $\mathbf{Q}_{irarL} = [A_{irarL}, q_{irarL}]^T$ inside it, are those belonging to the left rarefaction curve $q_{rarL}(A)$ such that $\lambda_1(\mathbf{Q}_L) \leq \lambda_1(\mathbf{Q}_{irarL}) \leq \lambda_1(\mathbf{Q}^*)$, i.e. from Proposition 2.1.7, such that $A^* \leq A_{irarL} \leq A_L$ and consequently $q_{irarL} = q_{rarL}(A_{irarL})$. If there is a physically admissible right rarefaction, the states $\mathbf{Q}_{irarR} = [A_{irarR}, q_{irarR}]^T$ inside it are those belonging to the right rarefaction curve $q_{rarR}(A)$ such that $\lambda_3(\mathbf{Q}^*) \leq \lambda_3(\mathbf{Q}_{irarR}) \leq \lambda_3(\mathbf{Q}_R)$, i.e. from Proposition 2.1.7, such that $A^* \leq A_{irarR} \leq A_R$ and consequently $q_{irarR} = q_{rarR}(A_{irarR})$. In Fig. 2.3d an example for the left rarefaction with data of Test 3.

2.1.2.6 The complete exact solution of the Riemann problem for the 1D blood flow equations with continuous parameters

The complete exact solution of the Riemann problem consists of the states $\mathbf{Q}_L$ and $\mathbf{Q}_R$ (initial data), $\mathbf{Q}^*$ (the unknown), $\mathbf{Q}_{irarL}$ and $\mathbf{Q}_{irarR}$ (solution inside the rarefactions when they exist). In Section 2.1.3 we will describe how we actually obtain these values.

2.1.3 Exact solution of the Riemann problem - Numerical resolution

In this Section we present a practical method to calculate the desired states.

Remark 2.1.5. To compute the exact solution in Section 2.1.2, we must actually approximate numerically the integral curves (2.51) and (2.52) (Section 2.1.3.1), the unknown $\mathbf{Q}^*$ (Section 2.1.3.3) and the solution inside the rarefactions (Section 2.1.3.4). Nevertheless we always refer to the resulting solution as "exact".

We prefer to follow the methodology presented in [87]. We recall that $u = \frac{q}{A}$.

2.1.3.1 Rarefaction curves

Proposition 2.1.11. *Written with respect to variable u, equations (2.51), (2.52) become*

$$\frac{du}{dA} = \frac{(\alpha - 1)u - c_\alpha}{A} \quad \text{for the } \lambda_1\text{-wave}, \tag{2.125}$$

$$\frac{du}{dA} = \frac{(\alpha-1)u + c_\alpha}{A} \quad \text{for the } \lambda_3\text{-wave.} \tag{2.126}$$

Proof. From (2.51)

$$\frac{dq}{dA} = \alpha\frac{q}{A} - c_\alpha \Longrightarrow \frac{d(Au)}{dA} = \alpha u - c_\alpha \Longrightarrow \frac{udA + Adu}{dA} = \alpha u - c_\alpha, \tag{2.127}$$

from which we obtain the result for the λ_1-wave. The proof or the λ_3-wave is similar. □

In case of a generic $\alpha \in [1,2]$ these ODEs have to be computed numerically. We give the procedure for the left part, the right part is equivalent. We first construct a mesh of $E = 100$ equispaced computational cells $A_{rarLdom} = [10^{-10}, A_L]$, where A_L is the left initial condition for A. This is the integration interval for the left side. After we use *scipy.integrate.solve_ivp* Python function, with parameters in order: fun=(2.125), t_span=$[A_{rarLdom}[-1], A_{rarLdom}[0]]$, yo=$u_L$ the left initial condition for u, method='RK45', t_eval=$np.flip(A_{rarLdom})$, rtol=$1e-10$, atol=$1e-13$. We now obtain the $u_{rarLdom} = np.flip(sol.y[0,:])$ values for each state $A_{rarLdom}[i] \in A_{rarLdom}$, and then we construct the required function $u_{rarL}(A)$ with Python *scipy.interpolate.CubicHermiteSpline*, with entries $x = A_{rarLdom}$, $y = u_{rarLdom}$, $dydx$ =(2.125).

The mesh $E = 100$ is chosen after the independence test performed in Section 2.1.4.1.

2.1.3.2 Shock curves

From Propositions 2.1.8 and 2.1.9, we can obtain an analogue formula for $u_{shockj}(A)$ considering Proposition 2.1.9 and simply dividing (2.84), (2.85) by A

$$\begin{aligned} u_{shockL}(A) =& \frac{A_L u_L}{A_L\alpha + A - \alpha A} - \\ & - \sqrt{\frac{(A_L - A)(-A_L(A_L\alpha + A - \alpha A)B_L + (\alpha-1)\alpha(A_L - A)A_L^2u_L^2)}{A_L A(A_L\alpha + A - \alpha A)^2}}, \end{aligned} \tag{2.128}$$

$$\begin{aligned} u_{shockR}(A) =& \frac{A_R u_R}{A_R\alpha + A - \alpha A} + \\ & + \sqrt{\frac{(A_R - A)(-A_R(A_R\alpha + A - \alpha A)B_R + (\alpha-1)\alpha(A_R - A)A_R^2u_R^2)}{A_R A(A_R\alpha + A - \alpha A)^2}}, \end{aligned} \tag{2.129}$$

where B_L and B_R are defined in (2.80).

2.1.3.3 Solution in the Star Region (for variables A and u)

At this point we proceed as indicated, for $\alpha = 1$, for example in [84].

Proposition 2.1.12 (Solution in the Star Region)**.** *The exact solution of the Riemann problem for the 1D blood flow equations with contiuous parameters in the Star Region, is*

$$\mathbf{Q}^* = \begin{bmatrix} A^* \\ A^*u^* \end{bmatrix}, \tag{2.130}$$

and is found as follows: A^* is the root of the non-linear algebraic equation

$$f_L(x) + f_R(x) + u_R - u_L = 0, \tag{2.131}$$

where

$$f_L(x) = \begin{cases} u_L - u_{rarL}(x) & \text{if } x \leq A_L \text{ (left rarefaction)}, \\ u_L - u_{shockL}(x) & \text{if } x > A_L \text{ (left shock)}, \end{cases} \tag{2.132}$$

$$f_R(x) = \begin{cases} -u_R + u_{rarR}(x) & \text{if } x \leq A_R \text{ (right rarefaction)}, \\ -u_R + u_{shockR}(x) & \text{if } x > A_R \text{ (right shock)}. \end{cases} \tag{2.133}$$

Once A^* is known from (2.131) we calculate

$$u^* = \frac{1}{2}(u_L + u_R) + \frac{1}{2}[f_R(A^*) - f_L(A^*)], \tag{2.134}$$

where $u_{rarj}(A)$, $j = L, R$ are defined in Section 2.1.3.1, while $u_{shockj}(A)$, $j = L, R$ are defined in Sec 2.1.3.2.

Proof. As explained in Proposition 2.1.10, if $\mathbf{Q}^*$ exists, it is unique and A^* is the zero of

$$h(A) = q_{left}(A) - q_{right}(A) = 0, \quad A \in \mathcal{N} \subset \mathbb{R}^+, \tag{2.135}$$

with $q_{left}(A)$ and $q_{right}(A)$ in (2.120) and (2.121), and $\mathcal{N}$ a proper neighbourhood of A_L and A_R. A^* is thus the zero of

$$f(A) = \frac{h(A)}{A} = \frac{q_{left}(A)}{A} - \frac{q_{right}(A)}{A} = 0, \quad A \in \mathcal{N} \subset \mathbb{R}^+, \tag{2.136}$$

where

$$\frac{q_{left}(A)}{A} = \begin{cases} \dfrac{q^a_{rar_L}(A)}{A} = u_{rarL}(A) & \text{if} \quad A \leq A_L, \\ \dfrac{q^a_{shock_L}(A)}{A} = u_{shockL}(A) & \text{if} \quad A > A_L, \end{cases} \tag{2.137}$$

$$\frac{q_{right}(A)}{A} = \begin{cases} \dfrac{q^a_{rar_R}(A)}{A} = u_{rarR}(A) & \text{if} \quad A \leq A_R, \\ \dfrac{q^a_{shock_R}(A)}{A} = u_{shockR}(A) & \text{if} \quad A > A_R, \end{cases} \tag{2.138}$$

with $u_{rarj}(A)$, $j = L, R$; defined in Section 2.1.3.1 and $u_{shockj}(A)$, $j = L, R$; defined in Section 2.1.3.2. In [90, 81], for $\alpha = 1$, these formulas hold

$$\begin{aligned} u^*(A^*) &= u_L - f_L(A^*) \quad \text{for a left wave}, \\ u^*(A^*) &= u_R + f_R(A^*) \quad \text{for a right wave}, \end{aligned} \tag{2.139}$$

functions $f_L(A)$ and $f_R(A)$ varying according to the wave pattern (rarefactions or shocks). Considering that $\mathbf{Q}^* = [A^*, A^*u^*]^T$ if it exists, is unique, (2.131) follows. From (2.139) we obtain

$$\begin{aligned} f_L(A^*) &= u_L - u^*(A^*) \quad \text{for a left wave}, \\ f_R(A^*) &= -u_R + u^*(A^*) \quad \text{for a right wave}, \end{aligned} \tag{2.140}$$

from which generalizing and using (2.137) and (2.138) we obtain (2.132) and (2.133). □

Remark 2.1.6. Equation (2.131) is solved for the unknown x, with a globally convergent Newton-Raphson method with initial state $A_I = \min(A_L, A_R)$. For an example see Appendix B.1.

2.1.3.4 Solution inside the rarefactions (for variables A and u)

In this case, too, there are different ways to calculate the sought states. We prefer to continue in the same manner as before.

Proposition 2.1.13 (Solution inside the left rarefaction)**.** *The exact solution of the Riemann problem inside the left rarefaction is*

$$\mathbf{Q}_{irarL} = \begin{bmatrix} A_{irarL} \\ A_{irarL} u_{irarL} \end{bmatrix}, \tag{2.141}$$

where A_{irarL} is obtained solving with respect to the unknown x the following

$$\frac{\mathcal{X}}{t} + c_\alpha(\mathbf{Q}_{rarL}(\mathrm{x})) - \alpha u_{rarL}(\mathrm{x}) = 0, \tag{2.142}$$

with $\mathbf{Q}_{rarL}(\mathrm{x}) = [\mathrm{x}, \mathrm{x}\, u_{rarL}(\mathrm{x})]^T$, being $\mathcal{X} = x - x_d$ where x is the specific place of the domain (vessel) in which we are calculating the desired values, x_d is the vessel spatial coordinate of the initial discontinuity, t is the time, and $u_{rarL}(\mathrm{x})$ defined in Section 2.1.3.1, Afterwards the actual u_{irarL}, corresponding to the found A_{irarL}, is

$$u_{irarL} = u_{rarL}(A_{irarL}). \tag{2.143}$$

Proof. We look for a similarity solution of the type

$$\mathbf{Q}(x,t) = v\left(\frac{\mathcal{X}}{t}\right). \tag{2.144}$$

Being

$$\partial_t \mathbf{Q} = -v'\left(\frac{\mathcal{X}}{t}\right)\frac{\mathcal{X}}{t^2}, \qquad \partial_x \mathbf{Q} = v'\left(\frac{\mathcal{X}}{t}\right)\frac{1}{t}, \tag{2.145}$$

system (2.12) becomes

$$-v'\left(\frac{\mathcal{X}}{t}\right)\frac{\mathcal{X}}{t^2} + \mathbf{J}(\mathbf{Q})v'\left(\frac{\mathcal{X}}{t}\right)\frac{1}{t} = 0, \tag{2.146}$$

with $\mathbf{J}(\mathbf{Q})$ the Jacobian (2.15). (2.146) is

$$\frac{1}{t}\left(\mathbf{J}(\mathbf{Q}) - \frac{\mathcal{X}}{t}\mathbb{I}\right)v'\left(\frac{\mathcal{X}}{t}\right) = 0, \tag{2.147}$$

that is true if and only if

$$v'\left(\frac{\mathcal{X}}{t}\right) = 0, \tag{2.148}$$

trivial solution, or

$$\left(\mathbf{J}(\mathbf{Q}) - \frac{\mathcal{X}}{t}\mathbb{I}\right)v'\left(\frac{\mathcal{X}}{t}\right) = 0, \tag{2.149}$$

i.e if and only if $v'\left(\frac{\mathcal{X}}{t}\right)$ is an eigenvector of $\mathbf{J}(\mathbf{Q})$ and $\frac{\mathcal{X}}{t}$ is the corresponding eigenvalue, i.e.

$$\frac{\mathcal{X}}{t} = \lambda_k, \tag{2.150}$$

with λ_k an eigenvalue in (2.16). This is possible only for eigenvalues and eigenvectors associated with genuinely non-linear fields [33]. Considering (2.150), the unknown state (2.141) must solve

$$\frac{\mathcal{X}}{t} = \lambda_1(\mathbf{Q}_{irarL}) = \alpha u_{irarL} - c_\alpha(\mathbf{Q}_{irarL}), \tag{2.151}$$

in other words we must solve (2.142) with respect to the unknown x. The rest follows. □

Proposition 2.1.14 (Solution inside the right rarefaction)**.** *The exact solution of the Riemann problem inside the right rarefaction is*

$$\mathbf{Q}_{irarR} = \begin{bmatrix} A_{irarR} \\ A_{irarR} u_{irarR} \end{bmatrix}, \tag{2.152}$$

where A_{irarR} is obtained solving with respect the unknown x the following

$$\frac{\mathcal{X}}{t} - c_\alpha(\mathbf{Q}_{rarR}(x)) - \alpha u_{rarR}(x) = 0, \tag{2.153}$$

with $\mathbf{Q}_{rarR}(x) = [x, x\, u_{rarR}(x)]^T$, being $\mathcal{X} = x - x_d$ where x is the specific place of the domain (vessel) in which we are calculating the desired values, x_d is the vessel spatial coordinate of the initial discontinuity, t is the time and $u_{rarR}(x)$ defined in Section 2.1.3.1. Afterwards the actual u_{irarR}, corresponding to the found A_{irarR}, is

$$u_{irarR} = u_{rarR}(A_{irarR}). \tag{2.154}$$

Proof. As in the proof for the left part, looking for a similarity solution as in (2.144) and considering (2.150), the unknown state (2.152) must solve

$$\frac{\mathcal{X}}{t} = \lambda_3(\mathbf{Q}_{irarR}) = \alpha u_{irarR} + c_\alpha(\mathbf{Q}_{irarR}), \tag{2.155}$$

in other words we must solve (2.153) for the unknown x. The rest follows. □

Again (2.142) and (2.153) are solved with a globally convergent Newton-Raphson method with initial points respectively A_L and A_R.

2.1.3.5 The complete exact solution of the Riemann problem for the 1D blood flow equations with continuous parameters

In this Section we present the sampling of the complete exact solution of the Riemann problem for the 1D blood flow equations (2.34). Now we can add the last variable ϕ. Being as before $\mathcal{X} = x - x_d$, x is the specific place of the domain (vessel) in which we are calculating the desired values, x_d is the vessel spatial coordinate of the initial discontinuity, and t is the time, thanks to Theorems. 2.1.1, 2.1.2, on the left side the complete solution is:

- if $A^* \leq A_L$ (left rarefaction):

$$\mathbf{Q}(x,t) = \begin{cases} \mathbf{Q}_L & \text{if} \quad \mathcal{X} < (\alpha u_L - c_\alpha(\mathbf{Q}_L))t, \\ \mathbf{Q}_{irarL} & \text{if} \quad (\alpha u_L - c_\alpha(\mathbf{Q}_L))t \leq \mathcal{X} \leq (\alpha u^* - c_\alpha(\mathbf{Q}^*))t, \\ \mathbf{Q}^* & \text{if} \quad (\alpha u^* - c_\alpha(\mathbf{Q}^*))t < \mathcal{X} \leq \mathcal{R}, \end{cases} \tag{2.156}$$

- if $A^* > A_L$ (left shock):

$$\mathbf{Q}(x,t) = \begin{cases} \mathbf{Q}_L & \text{if} \quad \mathcal{X} \leq S_L t, \\ \mathbf{Q}^* & \text{if} \quad S_L t < \mathcal{X} \leq \mathcal{R}. \end{cases} \tag{2.157}$$

Similarly on the right side the complete solution is

- if $A^* \leq A_R$ (right rarefaction):

$$\mathbf{Q}(x,t) = \begin{cases} \mathbf{Q}^* & \text{if} \quad \mathcal{L} < \mathcal{X} < (\alpha u^* + c_\alpha(\mathbf{Q}^*))t, \\ \mathbf{Q}_{irarR} & \text{if} \quad (\alpha u^* + c_\alpha(\mathbf{Q}^*))t \leq \mathcal{X} \leq (\alpha u_R + c_\alpha(\mathbf{Q}_R))t, \\ \mathbf{Q}_R & \text{if} \quad \mathcal{X} > (\alpha u_R + c_\alpha(\mathbf{Q}_R))t, \end{cases} \tag{2.158}$$

- if $A^* > A_R$ (right shock):

$$\mathbf{Q}(x,t) = \begin{cases} \mathbf{Q}^* & \text{if} \quad \mathcal{L} < \mathcal{X} \leq S_R t, \\ \mathbf{Q}_R & \text{if} \quad \mathcal{X} > S_R t. \end{cases} \tag{2.159}$$

c_α is defined in (2.17), S_L and S_R are the left and the right shock speeds and are defined according to (2.107) and (2.114). $\mathcal{L}$ and $\mathcal{R}$ are the left and the right borders of the Star Region domain and vary according to the presence of shocks or rarefactions, in particular

$$\mathcal{L} = \begin{cases} (\alpha u^* - c_\alpha(\mathbf{Q}^*))t & \text{in case of left rarefaction,} \\ S_L t & \text{in case of left shock,} \end{cases} \tag{2.160}$$

$$\mathcal{R} = \begin{cases} (\alpha u^* + c_\alpha(\mathbf{Q}^*))t & \text{in case of right rarefaction,} \\ S_R t & \text{in case of right shock.} \end{cases} \tag{2.161}$$

Proposition 2.1.15. *The λ_2-discontinuity is always included in the Star Region.*

Proof. It can be proved that

$$\lambda_1(\mathbf{Q}) \leq \lambda_2(\mathbf{Q}), \qquad \forall \quad \mathbf{Q} \in \Omega \tag{2.162}$$

$$\lambda_2(\mathbf{Q}) \leq \lambda_3(\mathbf{Q}), \qquad \forall \quad \mathbf{Q} \in \Omega \tag{2.163}$$

$$S_L \leq \lambda_2(\mathbf{Q}), \qquad \forall \quad \mathbf{Q} \in \Omega \tag{2.164}$$

$$\lambda_2(\mathbf{Q}) \leq S_R, \qquad \forall \quad \mathbf{Q} \in \Omega \tag{2.165}$$

in other words, the discontinuity for the passive scalar $\lambda_2 = u$ is always contained in the Star Region, i.e. the region in the (x,t) plane included between the λ_1 and λ_3 waves. □

Considering Proposition 2.1.15 it follows that the considered quantities described in this Section are

$$\mathbf{Q}_L = \begin{bmatrix} A_L \\ A_L u_L \\ A_L \phi_L \end{bmatrix}, \qquad \mathbf{Q}_R = \begin{bmatrix} A_R \\ A_R u_R \\ A_R \phi_R \end{bmatrix}, \tag{2.166}$$

$$\mathbf{Q}_{irarL} = \begin{bmatrix} A_{irarL} \\ A_{irarL} u_{irarL} \\ A_{irarL} \phi_L \end{bmatrix}, \qquad \mathbf{Q}_R = \begin{bmatrix} A_{irarR} \\ A_{irarR} u_{irarR} \\ A_{irarR} \phi_R \end{bmatrix}, \tag{2.167}$$

$$\mathbf{Q}^* = \begin{bmatrix} A^* \\ A^* u^* \\ A^* \phi \end{bmatrix}. \tag{2.168}$$

All these unknowns have been already treated in the previous Sections, with the exception of ϕ that is defined

$$\phi(x,t) = \begin{cases} \phi_L & \text{if} \quad \mathcal{X} \leq u^* t, \\ \phi_R & \text{if} \quad \mathcal{X} > u^* t. \end{cases} \tag{2.169}$$

2.1.4 Numerical results

Having obtained the exact solution of the Riemann problem as presented in Section 2.1.3, we perform a mesh independence study to justify the choice of the mesh $E = 100$ to build the approximated integral curves in Section 2.1.3.1. After having ensured that our computation of the exact solution is independent of our numerical approach to approximate integral curves, we

evaluate the entire exact solution thus constructed on a suite of test problems involving arteries and veins and different wave patterns, for different momentum correction coefficients α, against FORCE scheme [88] (see Appendix A.1).

2.1.4.1 MESH INDEPENDENCE STUDY

To verify that our exact solution constructed in Section 2.1.3 is mesh independent with respect to the one used to approximate the integral curves (see Section 2.1.3.1), we perform a study with meshes $E_n \in E = [50, 100, 200]$ computational cells choosing tests in which only rarefactions waves are involved. We construct the $u_{rarj}(A)$ curves as presented in Section 2.1.3.1 with each of the prescribed E_n meshes, and then we build the complete solution of the Riemann problem as presented in Section 2.1.3.5 with a mesh of $I = 15000$ computational cells. Then we calculate

$$\begin{aligned} L^1_{err}(t_{End}, \Delta x) &= \Delta x \sum_{i=1}^{I} |q^{t_{End}}_{n+1,k,i} - q^{t_{End}}_{n,k,i}|, \\ L^2_{err}(t_{End}, \Delta x) &= \sqrt{\Delta x \sum_{i=1}^{I} (q^{t_{End}}_{n+1,k,i} - q^{t_{End}}_{n,k,i})^2}, \quad k = 1, 2 \\ L^\infty_{err}(t_{End}, \Delta x) &= \max_{i=1\dots I} |q^{t_{End}}_{n+1,k,i} - q^{t_{End}}_{n,k,i}|, \end{aligned} \tag{2.170}$$

where t_{End} the output time, $q^{t_{End}}_{n,k,i}$ the *k-th* component of the exact solution $\mathbf{Q}^{exact}_{n,i}$ at time t_{End} calculated with mesh E_n with $n = 1, 2, 3$, and $\Delta x = \dfrac{l}{I}$, where l is the length of the vessel. Results are in Tables 2.1, 2.2, the test data are those of Test 2 (left rarefaction - contact discontinuity - right rarefaction in an artery) and Test 5 (left rarefaction - contact discontinuity - right rarefaction in an vein) in Tables 2.3, 2.4. As result of this procedure, we choose the mesh $E = 100$ for the purpose of this Thesis.

2.1.4.2 RESULTS

We plot the exact solution of the Riemann problem for the 1D blood flow equations with continuous parameters presented so far, for test problems that involve both arteries and veins, whose initial data are in Tables 2.3, 2.4, against FORCE method (Appendix A.1) with a Courant–Friedrichs–Lewy number $C_{cfl} = 0.9$, both in a $I = 15000$ computational cells mesh, for different momentum correction coefficents $\alpha = [1,\ 1.1,\ 4/3,\ 2]$, where

Definition 2.1.1 (C_{cfl}). *The Courant Number (C_{cfl}) is defined as*

$$C_{cfl} = \frac{\Delta t}{\Delta x} S^n_{max}, \tag{2.171}$$

where

$$S^n_{max} = max_i \left\{ max_k \left| \lambda^n_{k,i} \right| \right\}, \quad k = 1, \dots N, \quad i = 1, \dots, I; \tag{2.172}$$

with $\lambda^n_{k,i}$ the k-th eigenvalue evaluated in cell i at time t^n, and N is the number of eigenvalues of the considered system.

The numerical results are described in Figs. 2.4, 2.5, 2.6, 2.7, 2.8, 2.9, 2.10, 2.11, 2.12, 2.13. Finally a comparison of the exact solutions for the chosen α is drawn in Fig. 2.14. In Table 2.5 the $\mathbf{Q}^*$ values for each test are presented for the considered α.

Table 2.1: Mesh independence study for artery, left rarefaction - contact discontinuity - right rarefaction, Test 2 problem in Tables 2.3, 2.4.

α	Variable	Mesh	L^1-err	L^2-err	L^∞-err
1	A	50	-	-	-
		100	$1.8913e-13$	$3.2380e-13$	$6.2586e-13$
		200	$8.6133e-15$	$1.4670e-14$	$3.8653e-14$
	Au	50	-	-	-
		100	$8.6353e-15$	$4.4845e-14$	$4.4072e-13$
		200	$5.4880e-16$	$2.8819e-15$	$2.9006e-14$
11/10	A	50	-	-	-
		100	$1.3114e-13$	$2.2222e-13$	$5.8115e-13$
		200	$1.2407e-14$	$2.1242e-14$	$3.7586e-14$
	Au	50	-	-	-
		100	$7.3852e-15$	$3.7584e-14$	$3.7064e-13$
		200	$4.6594e-16$	$2.4094e-15$	$2.5669e-14$
4/3	A	50	-	-	-
		100	$4.0619e-14$	$8.7806e-14$	$5.5381e-13$
		200	$1.1751e-14$	$1.9914e-14$	$3.510e-14$
	Au	50	-	-	-
		100	$5.9117e-15$	$2.9560e-14$	$2.9040e-13$
		200	$3.6012e-16$	$1.7885e-15$	$1.8459e-14$
2	A	50	-	-	-
		100	$1.1844e-13$	$1.9113e-13$	$5.3207e-13$
		200	$1.0169e-14$	$1.6568e-14$	$3.1991e-14$
	Au	50	-	-	-
		100	$4.5326e-15$	$2.0669e-14$	$1.9155e-13$
		200	$2.6224e-16$	$1.1984e-15$	$1.1987e-14$

Table 2.2: Mesh independence study for vein, left rarefaction - contact discontinuity - right rarefaction, Test 5 problem in Tables 2.3, 2.4.

α	Variable	Mesh	L^1-err	L^2-err	L^∞-err
1	A	50	-	-	-
		100	$1.1710e-13$	$4.5173e-13$	$4.7812e-12$
		200	$7.6829e-15$	$2.7388e-14$	$3.0069e-13$
	Au	50	-	-	-
		100	$1.5401e-13$	$4.4924e-13$	$2.4343e-12$
		200	$9.3101e-15$	$2.7259e-14$	$1.5208e-13$
11/10	A	50	-	-	-
		100	$1.4987e-13$	$5.1967e-13$	$5.1267e-12$
		200	$1.0406e-14$	$3.2101e-14$	$3.1329e-13$
	Au	50	-	-	-
		100	$1.3778e-13$	$3.9741e-13$	$2.3985e-12$
		200	$8.3501e-15$	$2.4182e-14$	$1.4707e-13$
4/3	A	50	-	-	-
		100	$2.6502e-13$	$7.2429e-13$	$5.7895e-12$
		200	$8.8624e-15$	$3.8686e-14$	$3.5916e-13$
	Au	50	-	-	-
		100	$1.0290e-13$	$3.1088e-13$	$2.2285e-12$
		200	$6.3128e-15$	$1.9010e-14$	$1.3761e-13$
2	A	50	-	-	-
		100	$2.6884e-13$	$9.3605e-13$	$8.0358e-12$
		200	$6.2201e-14$	$1.4366e-13$	$4.8467e-13$
	Au	50	-	-	-
		100	$1.0144e-13$	$2.8906e-13$	$1.7350e-12$
		200	$6.0544e-15$	$1.7278e-14$	$1.0557e-13$

Test 1 The solution of Test 1 consists of a left transonic rarefaction, a contact discontinuity and a right shock in an artery (R(sonic)CS). In this case the associated left eigenvalue $\lambda_1 = \alpha u - c_\alpha$ goes monotonically from negative values to positive values, passing through a critical point at which $\alpha u = c_\alpha$. We can see how the increasing of α changes noticeably the value of both A^* and u^* in the final result of the exact solution (Fig. 2.14). Also the (A, q) plots describe a remarkable change of the curvature of the $q_{right}(A)$ curve, due to the variation of α, and a lower change of

Table 2.3: Parameters used for Tests from 1 to 5: blood density ρ, vessel wall stiffness K; cross-sectional area A_0; external pressure p_e ; domain length ℓ; location of the initial discontinuity x_d and output time t_{End}. Regarding the resulting wave pattern, R stands for *rarefaction*, S for *shock*, C for *contact discontinuity*.

Test	Vessel	Wave pat.	$\rho[\frac{kg}{m^3}]$	$K[Pa]$	$A_0[m^2]$	$p_e[Pa]$	$\ell[m]$	$x_d[m]$	$t_{End}[s]$
1	Artery	R(sonic)CS	1000	20005.0715	$3.14 \cdot 10^{-4}$	0.0	0.5	0.5ℓ	0.025
2	Artery	RCR	1000	20005.0715	$3.14 \cdot 10^{-4}$	0.0	0.5	0.5ℓ	0.05
3	Vein	RCS	1000	333.0	$3.14 \cdot 10^{-4}$	0.0	0.5	0.5ℓ	0.05
4	Vein	SCS	1000	33.3333	$2.8274 \cdot 10^{-5}$	66.661	0.5	0.5ℓ	0.06
5	Vein	RCR	1000	333.0	$3.14 \cdot 10^{-4}$	0.0	0.5	0.5ℓ	0.07

Table 2.4: Initial conditions for Tests from 1 to 5. The units of measures used for this Thesis are: m, s, kg, Pa.

Test	$A_L[m^2]$	$u_L[m/s]$	ϕ_L	$A_R[m^2]$	$u_R[m/s]$	ϕ_R
1	$10 \cdot 10^{-4}$	0.0	1.0	$1.0 \cdot 10^{-4}$	0.0	0.5
2	$3.14 \cdot 10^{-4}$	-0.5	1.0	$3.14 \cdot 10^{-4}$	0.5	0.5
3	$3.5 \cdot 10^{-4}$	0.0	0.5	$3.0 \cdot 10^{-4}$	0.0	1.0
4	$3.42 \cdot 10^{-5}$	0.5	0.5	$3.34 \cdot 10^{-5}$	-0.1	1.0
5	$3.14 \cdot 10^{-4}$	-0.5	1.0	$3.14 \cdot 10^{-4}$	0.5	0.5

Table 2.5: Exact solution in the Star Region of Tests from 1 to 5.

Test	α	$A^*[m^2]$	$u^*[m/s]$
1	1	$3.5186 \cdot 10^{-4}$	3.8839
	11/10	$3.2357 \cdot 10^{-4}$	4.0178
	4/3	$2.6821 \cdot 10^{-4}$	4.2692
	2	$1.8673 \cdot 10^{-4}$	4.5209
2	1	$2.6722 \cdot 10^{-4}$	0.0
	11/10	$2.6759 \cdot 10^{-4}$	0.0
	4/3	$2.6844 \cdot 10^{-4}$	0.0
	2	$2.7072 \cdot 10^{-4}$	0.0
3	1	$3.2817 \cdot 10^{-4}$	0.1782
	11/10	$3.2807 \cdot 10^{-4}$	0.1783
	4/3	$3.2784 \cdot 10^{-4}$	0.1786
	2	$3.2718 \cdot 10^{-4}$	0.1792
4	1	$3.8944 \cdot 10^{-5}$	0.2187
	11/10	$3.8964 \cdot 10^{-5}$	0.2214
	4/3	$3.9009 \cdot 10^{-5}$	0.2277
	2	$3.9121 \cdot 10^{-5}$	0.2461
5	1	$2.0580 \cdot 10^{-4}$	0.0
	11/10	$2.0791 \cdot 10^{-4}$	0.0
	4/3	$2.1259 \cdot 10^{-4}$	0.0
	2	$2.2418 \cdot 10^{-4}$	0.0

the $q_{left}(A)$ one. (Fig. 2.5). The exact solution regarding the contact discontinuity for the passive scalar ϕ shows instead a minor change (Fig. 2.14).

TEST 2 The solution of Test 2 consists of a left rarefaction a contact discontinuity and a right rarefaction in an artery (RCS) (Fig. 2.7), in this case no transonic rarefactions are depicted. As α increases, the change of the curvature of the $q_{left}(A)$ and $q_{right}(A)$ curves is present but less evident (Fig. 2.6). We face also a change in the value of A^*, instead u^* remains equal to 0; finally the increasing of α produces an elongation of the left and the right rarefactions (Fig. 2.14).

The exact solution regarding the contact discontinuity for the passive scalar ϕ shows instead no remarkable changes (Fig. 2.14).

Test 3 Test 3 presents a left rarefaction a contact discontinuity and a right shock in a vein (RCS) (Fig. 2.8). The difference between the different exact solutions and the different values of A^* and u^* for the given α is the less prominent (Fig. 2.14), but from the (A, q) plots we can appreciate the small variations of the $q_{left}(A)$ and $q_{right}(A)$ curves (Fig. 2.9). Again the exact solution regarding the contact discontinuity for the passive scalar ϕ shows instead no remarkable changes (Fig. 2.14).

Test 4 Test 4 shows a left shock a contact discontinuity and a right shock in a vein (SCS) (Fig. 2.11). The variation of both A^* and u^* is minimal (Fig. 2.14), and thus is the difference between the $q_{left}(A)$ and $q_{right}(A)$ curves shown in the (A, q) plots (Fig. 2.10). For the passive scalar ϕ no visible changes are depicted by the exact solution (Fig. 2.14).

Test 5 Test 5 produces a left rarefaction a contact discontinuity and a right rarefaction in a vein (RCR) (Fig. 2.12). The value of A^* remarkably changes with the increasing of α, while the value of u^* remains 0 (Fig. 2.14). Also in this case we face an elongation of the left and the right rarefaction (Fig. 2.13). Concerning the passive scalar ϕ no visible changes are depicted (Fig. 2.14).

In every case Figs. 2.4, 2.7, 2.8, 2.11, 2.12 show a very good matching between the exact solutions and the approximations obtained with the centered FORCE method.

Test 1. Exact solution of the Riemann problem with $\alpha \in [1, 2]$

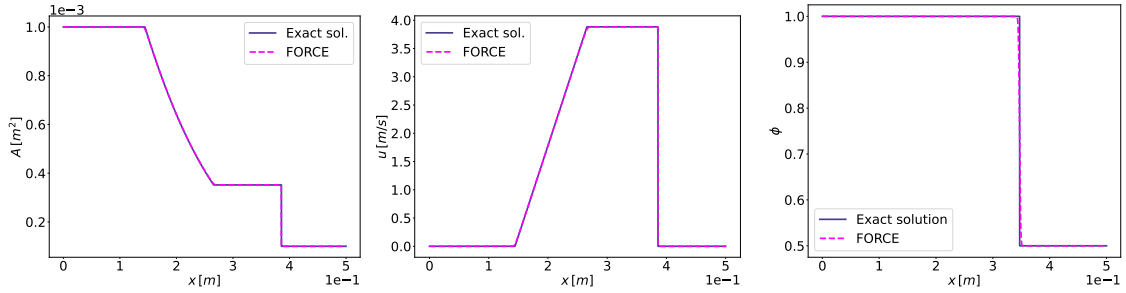

(a) $\alpha = 1$

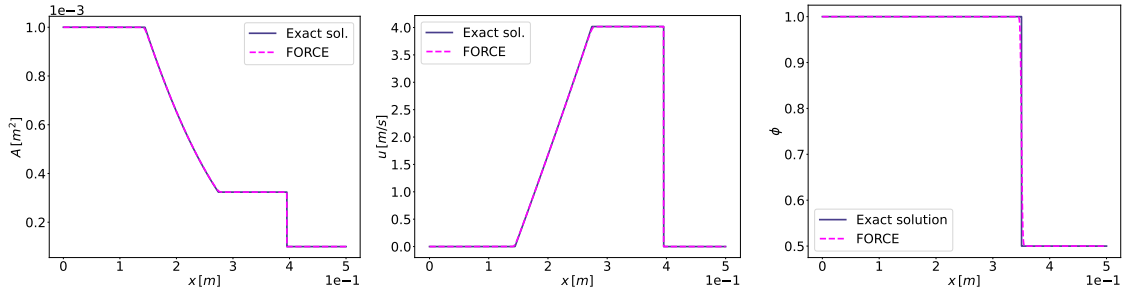

(b) $\alpha = 11/10$

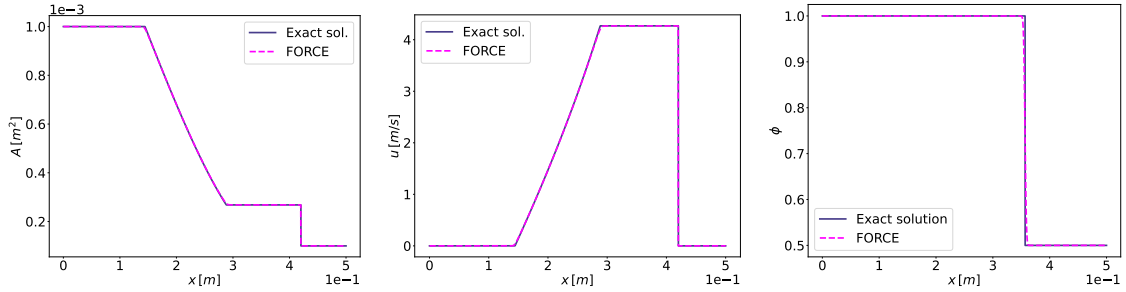

(c) $\alpha = 4/3$

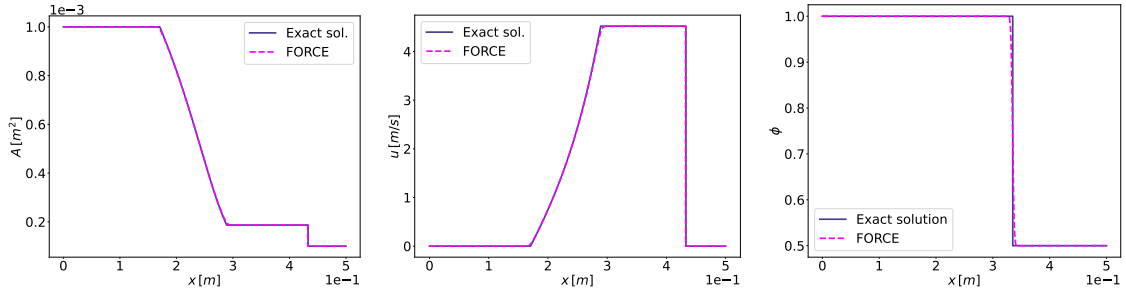

(d) $\alpha = 2$

Figure 2.4: Test 1. Artery. Left transonic rarefaction - contact discontinuity - right shock. Exact solution of the Riemann problem with $\alpha = 1$, $\alpha = 1.1$, $\alpha = 4/3$ and $\alpha = 2$ against FORCE numerical scheme. Initial data are in Tables 2.3, 2.4.

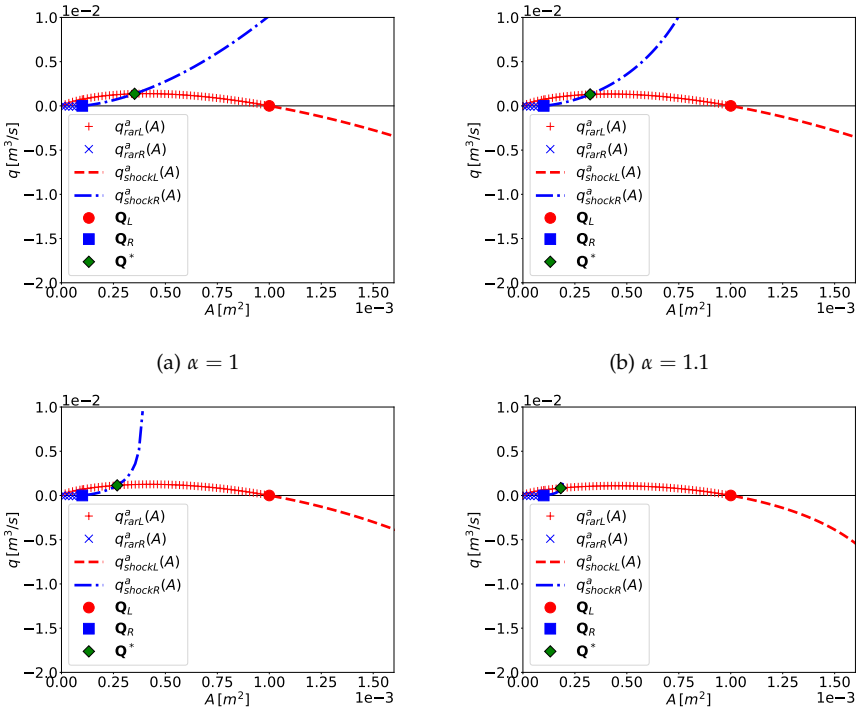

(a) $\alpha = 1$ (b) $\alpha = 1.1$

(c) $\alpha = 4/3$ (d) $\alpha = 2$

Figure 2.5: A detail of the graphic representations of the solutions in the (A, q) phase-plane for data of Test 1 in Tables 2.3, 2.4, for $\alpha = 1$, $\alpha = 1.1$, $\alpha = 4/3$ and $\alpha = 2$.

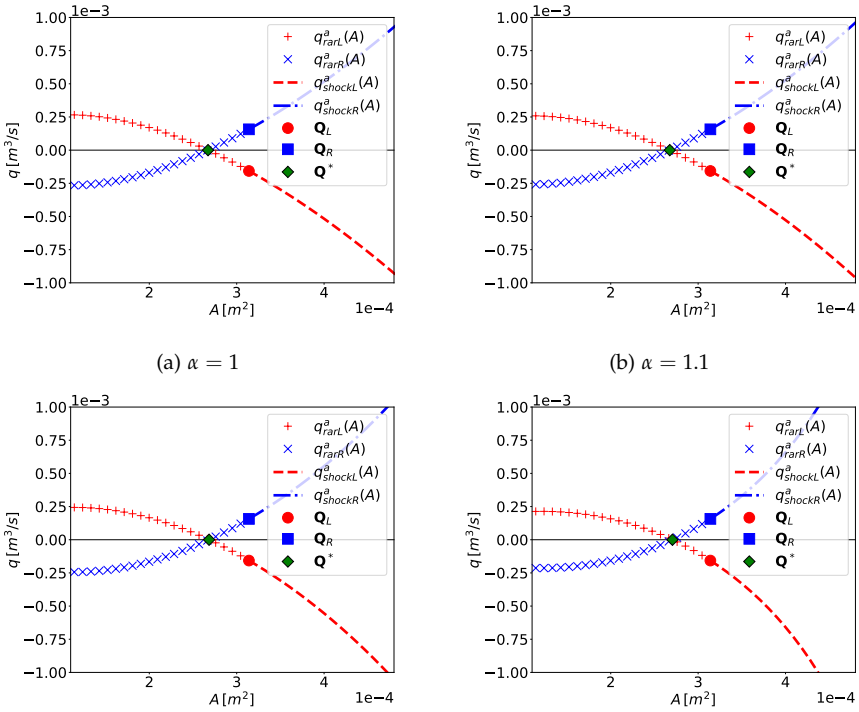

(a) $\alpha = 1$ (b) $\alpha = 1.1$

(c) $\alpha = 4/3$ (d) $\alpha = 2$

Figure 2.6: A detail of the graphic representations of the solutions in the (A, q) phase-plane for data of Test 2 in Tables 2.3, 2.4, for $\alpha = 1$, $\alpha = 1.1$, $\alpha = 4/3$ and $\alpha = 2$.

Test 2. Exact solution of the Riemann problem with $\alpha \in [1, 2]$

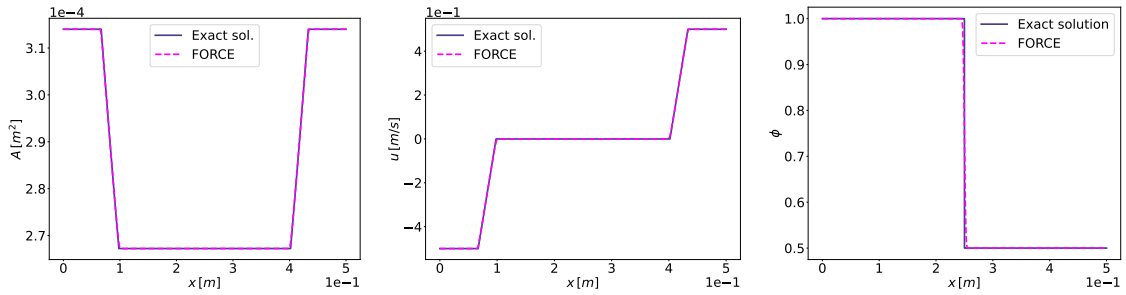

(a) $\alpha = 1$

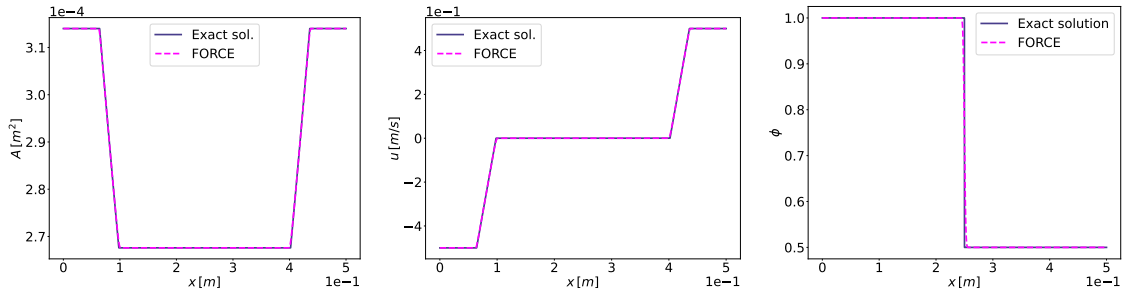

(b) $\alpha = 11/10$

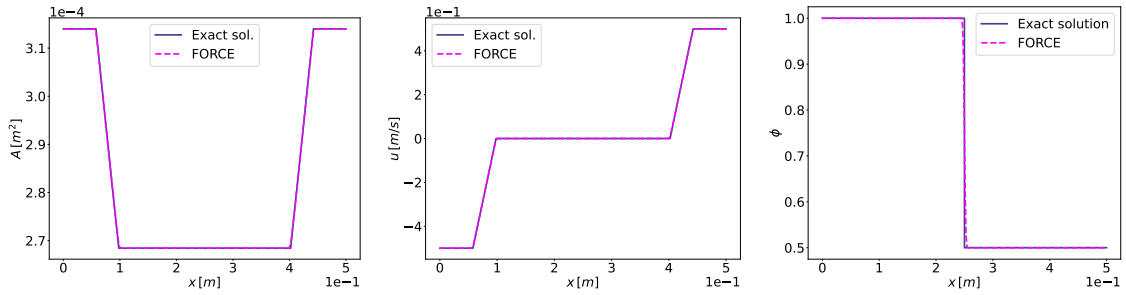

(c) $\alpha = 4/3$

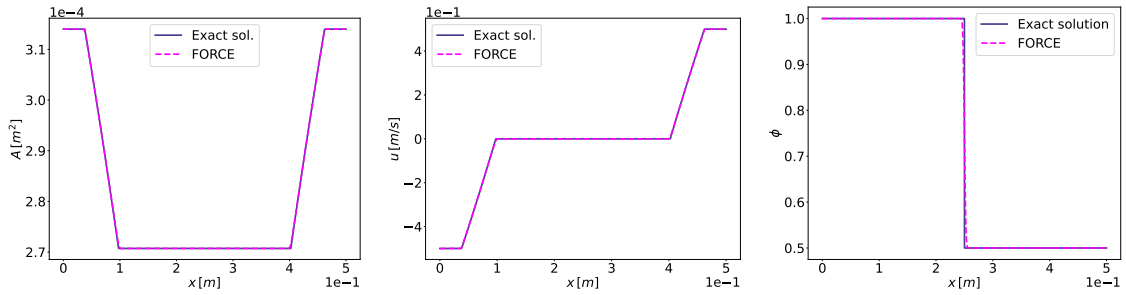

(d) $\alpha = 2$

Figure 2.7: Test 2. Artery. Left rarefaction - contact discontinuity - right rarefaction. Exact solution of the Riemann problem with $\alpha = 1$, $\alpha = 1.1$, $\alpha = 4/3$ and $\alpha = 2$ against FORCE numerical scheme. Initial data are in Tables 2.3, 2.4.

Test 3. Exact solution of the Riemann problem with $\alpha \in [1, 2]$

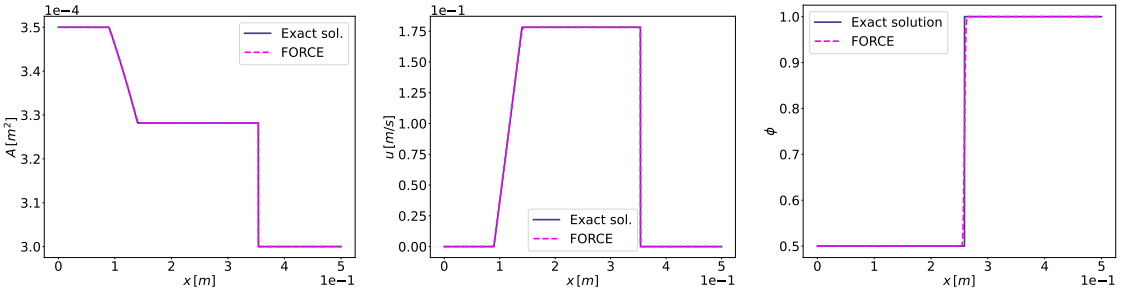

(a) $\alpha = 1$

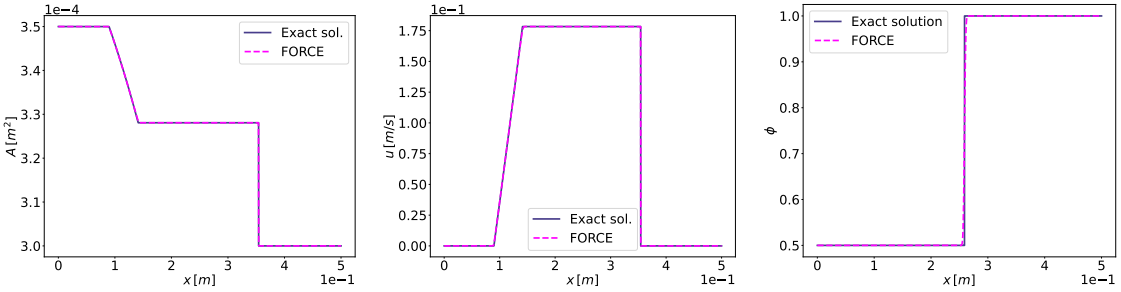

(b) $\alpha = 11/10$

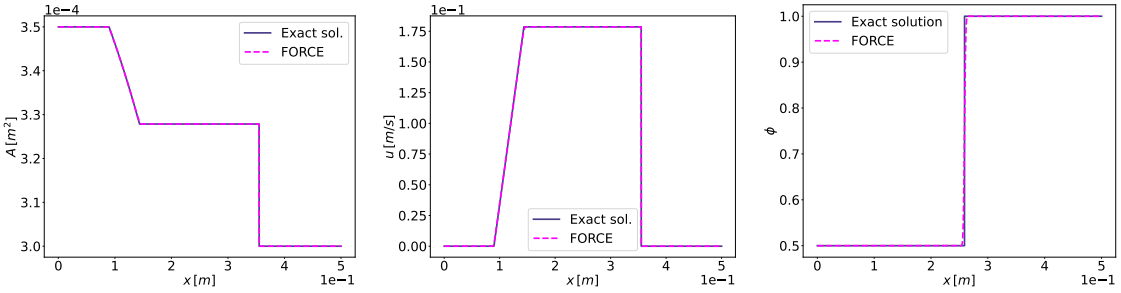

(c) $\alpha = 4/3$

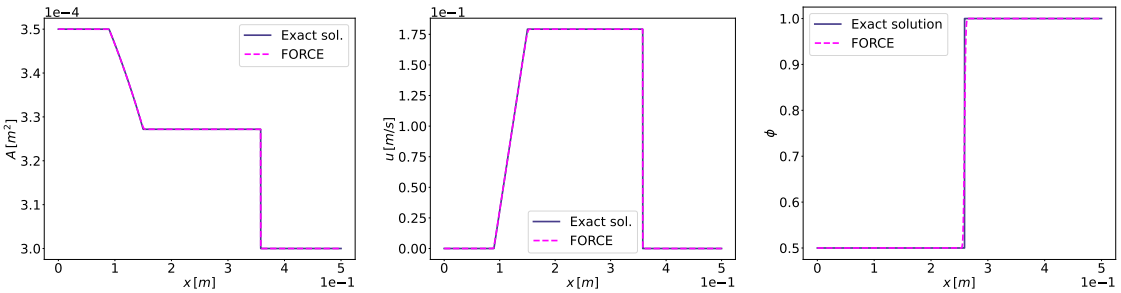

(d) $\alpha = 2$

Figure 2.8: Test 3. Vein. Left rarefaction - contact discontinuity - right shock. Exact solution of the Riemann problem with $\alpha = 1$, $\alpha = 1.1$, $\alpha = 4/3$ and $\alpha = 2$ against FORCE numerical scheme. Initial data are in Tables 2.3, 2.4.

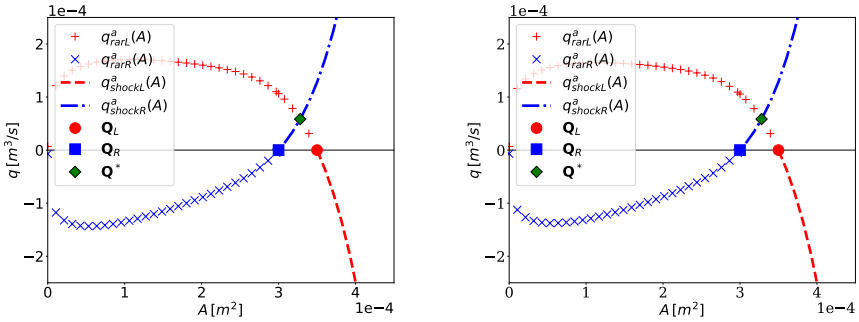

(a) $\alpha = 1$ (b) $\alpha = 1.1$

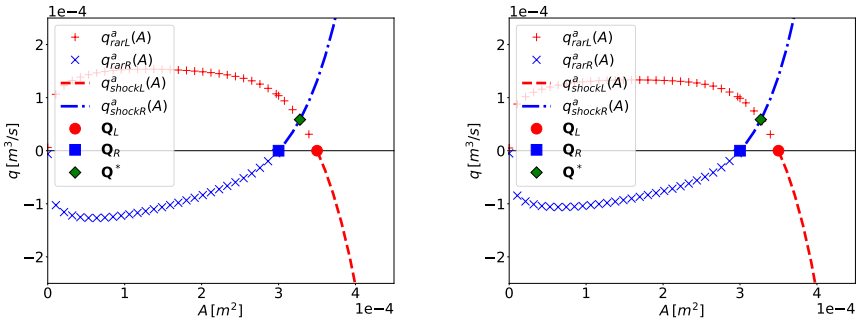

(c) $\alpha = 4/3$ (d) $\alpha = 2$

Figure 2.9: A detail of the graphic representations of the solutions in the (A, q) phase-plane for data of Test 3 in Tables 2.3, 2.4, for $\alpha = 1$, $\alpha = 1.1$, $\alpha = 4/3$ and $\alpha = 2$.

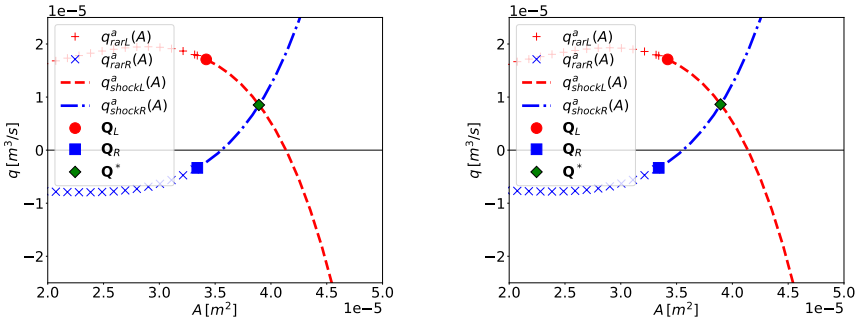

(a) $\alpha = 1$ (b) $\alpha = 1.1$

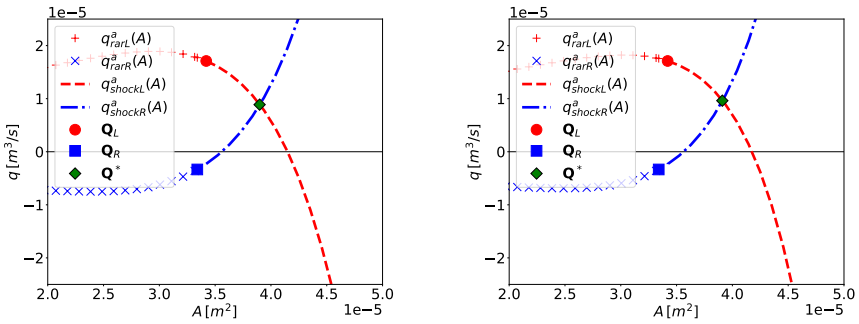

(c) $\alpha = 4/3$ (d) $\alpha = 2$

Figure 2.10: A detail of the graphic representations of the solutions in the (A, q) phase-plane for data of Test 4 in Tables 2.3, 2.4, for $\alpha = 1$, $\alpha = 1.1$, $\alpha = 4/3$ and $\alpha = 2$.

Test 4. Exact solution of the Riemann problem with $\alpha \in [1, 2]$

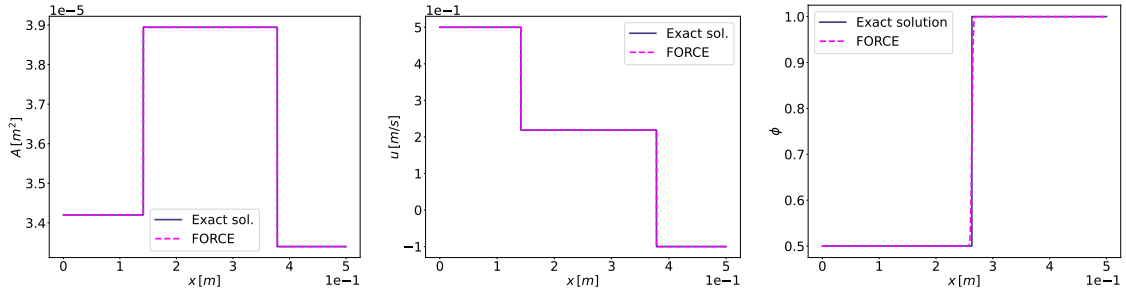

(a) $\alpha = 1$

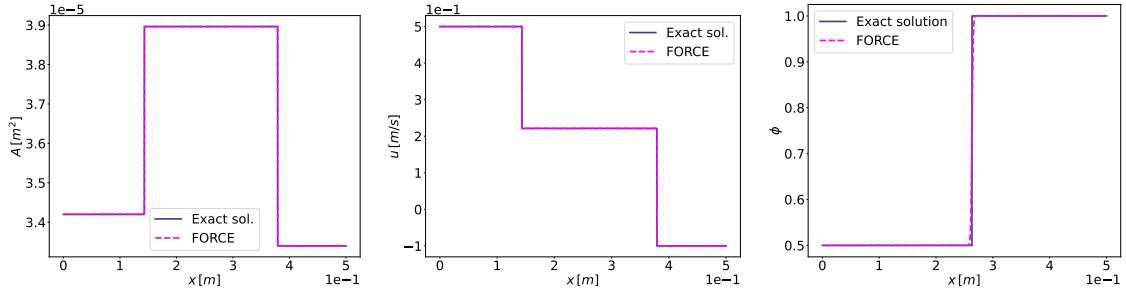

(b) $\alpha = 11/10$

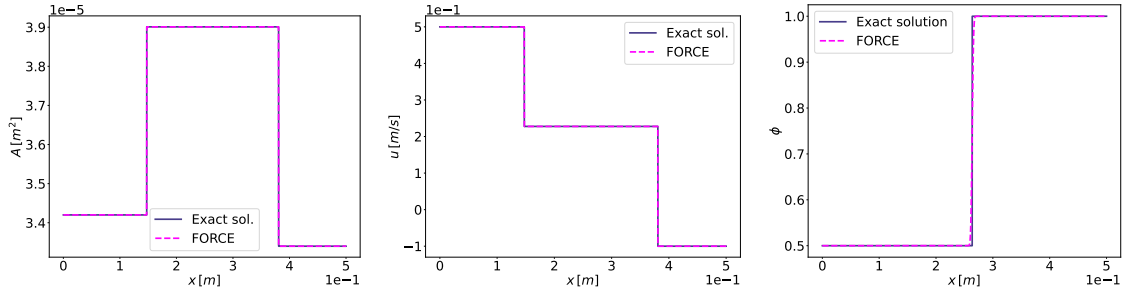

(c) $\alpha = 4/3$

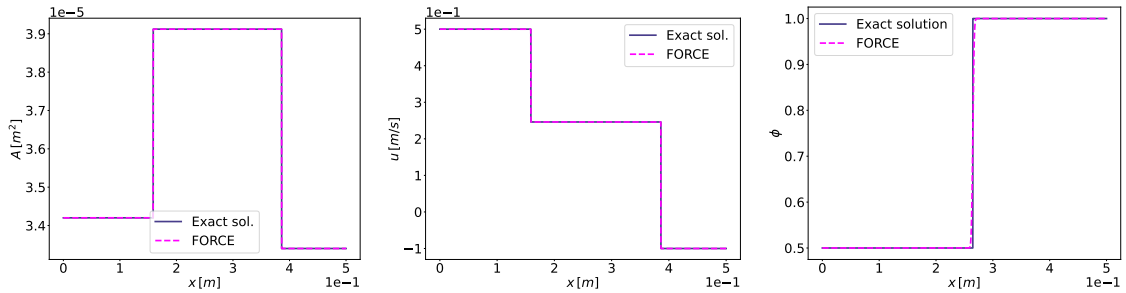

(d) $\alpha = 2$

Figure 2.11: Test 4. Vein. Left shock - contact discontinuity - right shock. Exact solution of the Riemann problem with $\alpha = 1$, $\alpha = 1.1$, $\alpha = 4/3$ and $\alpha = 2$ against FORCE numerical scheme. Initial data are in Tables 2.3, 2.4.

Test 5. Exact solution of the Riemann problem with $\alpha \in [1, 2]$

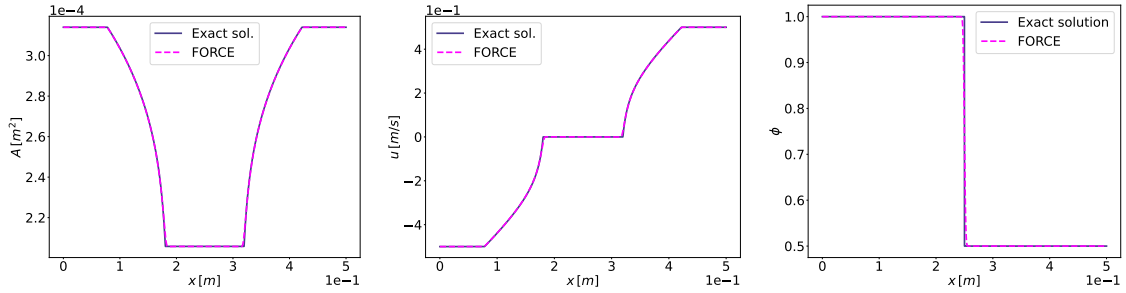

(a) $\alpha = 1$

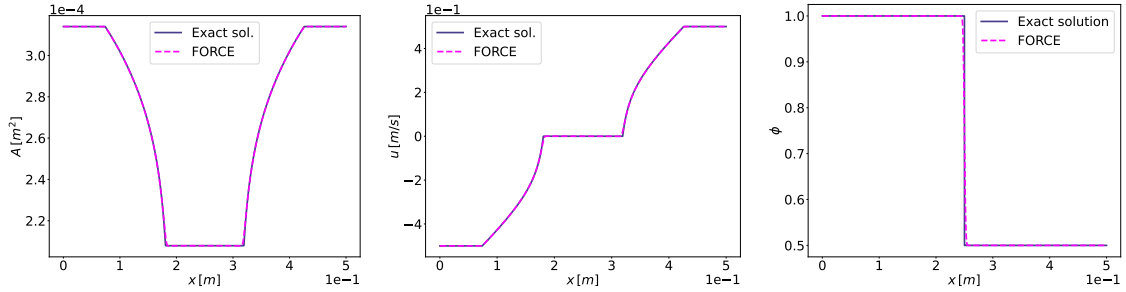

(b) $\alpha = 11/10$

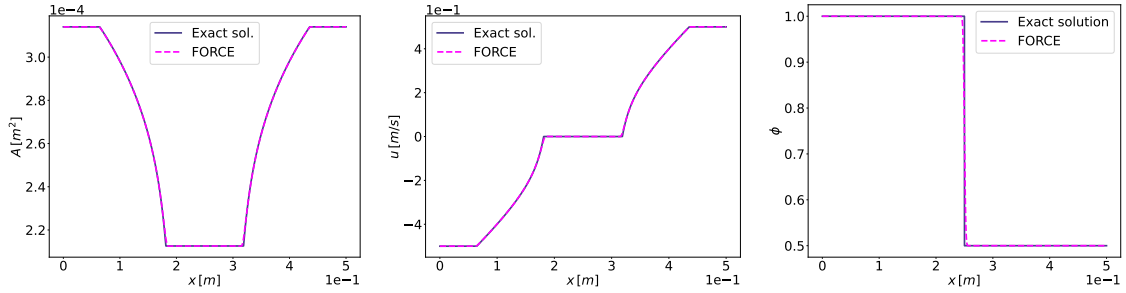

(c) $\alpha = 4/3$

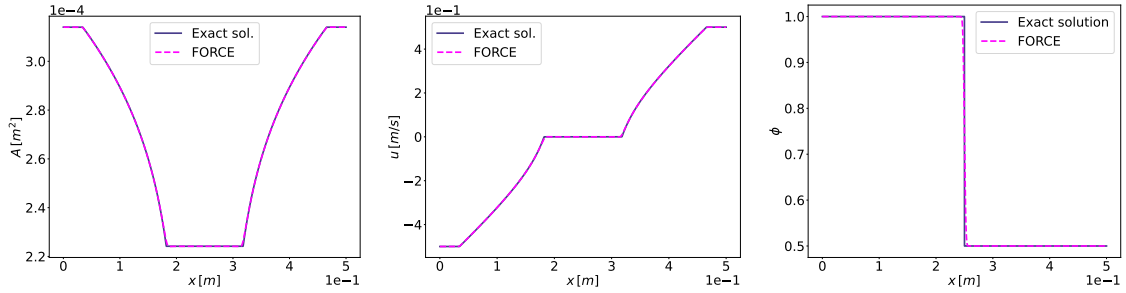

(d) $\alpha = 2$

Figure 2.12: Test 5. Vein. Left rarefaction - contact discontinuity - right rarefaction. Exact solution of the Riemann problem with $\alpha = 1$, $\alpha = 1.1$, $\alpha = 4/3$ and $\alpha = 2$ against FORCE numerical scheme. Initial data are in Tables 2.3, 2.4.

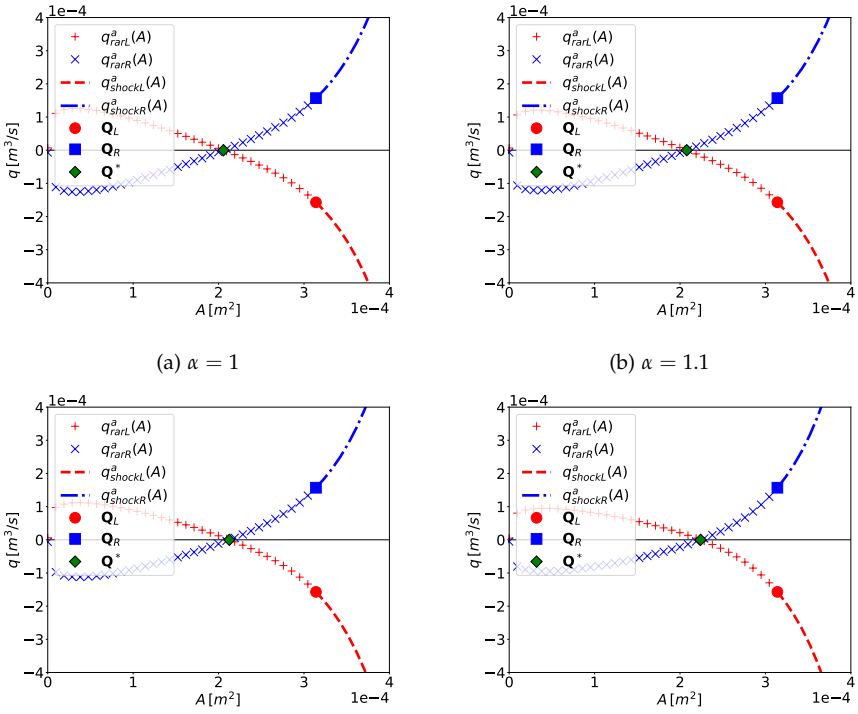

(a) $\alpha = 1$

(b) $\alpha = 1.1$

(c) $\alpha = 4/3$

(d) $\alpha = 2$

Figure 2.13: A detail of the graphic representations of the solutions in the (A, q) phase-plane for data of Test 5 in Tables 2.3, 2.4, for$\alpha = 1$, $\alpha = 1.1$, $\alpha = 4/3$ and $\alpha = 2$.

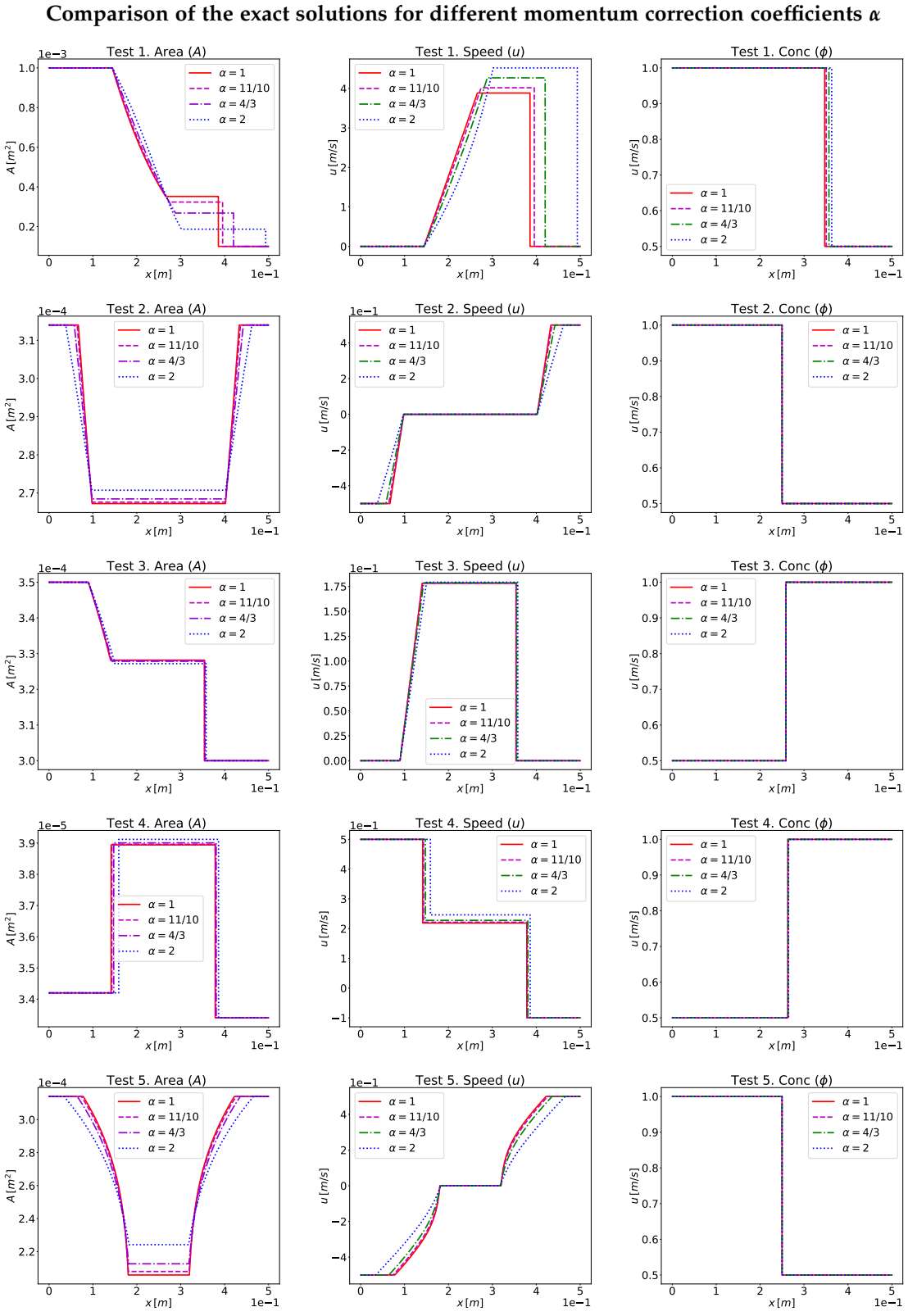

Figure 2.14: Comparison of the exact solutions of Tests in Table 2.3, 2.4 for different α.

2.2 The 1D blood flow model with discontinuous properties and transport

2.2.1 Governing equations

Assuming an axially symmetric vessel configuration in three space dimensions at time t, and assuming one-dimensional flow in the axial direction x, the 1D blood flow model with discontinuous properties reads

$$\begin{cases} \partial_t A + \partial_x(Au) = 0, \\ \partial_t(Au) + \partial_x(\alpha Au^2) + \dfrac{A}{\rho}\partial_x p = 0, \\ \partial_t(A\phi) + \partial_x(Au\phi) = 0, \end{cases} \tag{2.173}$$

where $A(x,t)$ is the cross-sectional area of the vessel or tube at position x and time t assumed $A \in \mathbb{R}^+$, $u(x,t) \in \mathbb{R}$ is the averaged velocity of blood at a cross section, $p(x,t) \in \mathbb{R}$ is the pressure, $\rho \in \mathbb{R}^+$ is the density of blood, assumed constant, $\phi(x,t) \in \mathbb{R}_0^+$ is the concentration of the passive scalar, $\alpha \in [1,2]$ is the momentum correction coefficient defined as in Section 2.1.1.
The first equation in (2.173) represents the mass conservation and the second implies the momentum conservation, the third is the advection equation for a passive scalar transport. To close the system, we adopt a tube law of the form

$$p = p_e + \psi(A, K, A_0), \tag{2.174}$$

where: $p_e(x)$ is the external pressure, $\psi(A,K,A_0)$ is the *transmural pressure*, assumed of the form

$$\psi(A,K,A_0) = K\left[\left(\frac{A}{A_0}\right)^m - \left(\frac{A}{A_0}\right)^n\right], \tag{2.175}$$

with

$$K(x) = \begin{cases} \dfrac{E(x)}{(1-\nu^2)}\left(\dfrac{h_0(x)}{R_0(x)}\right) & \text{for arteries,} \\ \dfrac{E(x)}{12(1-\nu^2)}\left(\dfrac{h_0(x)}{R_0(x)}\right)^3 & \text{for veins,} \end{cases} \tag{2.176}$$

$$m = \begin{cases} 1/2 & \text{for arteries,} \\ 10 & \text{for veins,} \end{cases} \qquad n = \begin{cases} 0 & \text{for arteries,} \\ -3/2 & \text{for veins.} \end{cases} \tag{2.177}$$

Here: $h_0(x)$ is the vessel wall thickness; $A_0(x)$ and $R_0(x)$ are the cross-sectional area of the vessel and the radius at equilibrium, i.e. $\psi(A,K,A_0) = 0$; $E(x)$ is the Young's modulus; ν is the Poisson ratio taken as $\nu = 0.5$, $m, n \in \mathbb{R}$ and in general are taken $m > 0$ and $-2 \le n \le 0$. $K \in \mathbb{R}^+$, $A_0 \in \mathbb{R}^+$, $p_e \in \mathbb{R}$, $R_0 \in \mathbb{R}^+$, $E \in \mathbb{R}^+$, $h_0 \in \mathbb{R}^+$.

Developing the partial derivative of the pressure, we have

$$\begin{cases} \partial_t A + \partial_x(Au) = 0, \\ \partial_t(Au) + \partial_x(\alpha Au^2) + \dfrac{A}{\rho}\psi_A\partial_x A = -\dfrac{A}{\rho}\psi_K\partial_x K - \dfrac{A}{\rho}\psi_{A_0}\partial_x A_0 - \dfrac{A}{\rho}\partial_x p_e, \\ \partial_t(A\phi) + \partial_x(Au\phi) = 0, \end{cases} \tag{2.178}$$

where

$$\begin{aligned}\psi_A &= \frac{\partial \psi}{\partial A} = \frac{K}{A}\left[m\left(\frac{A}{A_0}\right)^m - n\left(\frac{A}{A_0}\right)^n\right],\\ \psi_K &= \frac{\partial \psi}{\partial K} = \left[\left(\frac{A}{A_0}\right)^m - \left(\frac{A}{A_0}\right)^n\right],\\ \psi_{A_0} &= \frac{\partial \psi}{\partial A_0} = -\frac{K}{A_0}\left[m\left(\frac{A}{A_0}\right)^m - n\left(\frac{A}{A_0}\right)^n\right].\end{aligned} \tag{2.179}$$

We note that the right hand side of equation (2.178) has terms involving unknowns and spatial gradients of parameters. Such terms are normally called *geometric source terms*. Following [90] we consider the augmented system

$$\begin{cases}\partial_t A + \partial_x(Au) = 0,\\ \partial_t(Au) + \partial_x(\alpha A u^2) + \dfrac{A}{\rho}\psi_A \partial_x A + \dfrac{A}{\rho}\psi_K \partial_x K + \dfrac{A}{\rho}\psi_{A_0}\partial_x A_0 + \dfrac{A}{\rho}\partial_x p_e = 0,\\ \partial_t K = 0,\\ \partial_t A_0 = 0,\\ \partial_t p_e = 0,\\ \partial_t(A\phi) + \partial_x(Au\phi) = 0.\end{cases} \tag{2.180}$$

System (2.180) in quasi-linear form reads

$$\partial_t \mathbf{Q} + \mathbf{M}(\mathbf{Q})\partial_x \mathbf{Q} = \mathbf{0}, \tag{2.181}$$

where

$$\mathbf{Q} = \begin{bmatrix} A(x,t)\\ Au(x,t)\\ K(x)\\ A_0(x)\\ p_e(x)\\ A\phi(x,t)\end{bmatrix}, \quad \mathbf{M}(\mathbf{Q}) = \begin{bmatrix} 0 & 1 & 0 & 0 & 0 & 0\\ c^2 - \alpha u^2 & 2\alpha u & \dfrac{A}{\rho}\psi_K & \dfrac{A}{\rho}\psi_{A_0} & \dfrac{A}{\rho} & 0\\ 0 & 0 & 0 & 0 & 0 & 0\\ 0 & 0 & 0 & 0 & 0 & 0\\ 0 & 0 & 0 & 0 & 0 & 0\\ -u\phi & \phi & 0 & 0 & 0 & u\end{bmatrix}. \tag{2.182}$$

Here c is the *wave speed*

$$c(A,K,A_0) = \sqrt{\frac{A}{\rho}\frac{\partial p}{\partial A}} = \sqrt{\frac{A}{\rho}\psi_A} = \sqrt{\frac{K}{\rho}\left[m\left(\frac{A}{A_0}\right)^m - n\left(\frac{A}{A_0}\right)^n\right]}, \tag{2.183}$$

which is always real, being $\psi_A \in \mathbb{R}^+$ for the choices of m and n given in (2.177). The eigenvalues of $\mathbf{M}(\mathbf{Q})$ are given by

$$\lambda_1 = \alpha u - c_\alpha, \qquad \lambda_2 = \lambda_3 = \lambda_4 = 0, \qquad \lambda_5 = u, \qquad \lambda_6 = \alpha u + c_\alpha, \tag{2.184}$$

with

$$c_\alpha(\mathbf{Q}) = \sqrt{c^2 + \alpha(\alpha - 1)u^2}. \tag{2.185}$$

A possible choice of right eigenvectors of $\mathbf{M}(\mathbf{Q})$ corresponding to eigenvalues (2.184) is

$$\mathbf{R}_1 = \begin{bmatrix} 1 \\ \alpha u - c_\alpha \\ 0 \\ 0 \\ 0 \\ \phi \end{bmatrix}, \quad \mathbf{R}_2 = \begin{bmatrix} 0 \\ 0 \\ 1 \\ 0 \\ -\psi_K \\ 0 \end{bmatrix}, \quad \mathbf{R}_3 = \begin{bmatrix} 0 \\ 0 \\ 0 \\ 1 \\ -\psi_{A_0} \\ 0 \end{bmatrix},$$
$$\mathbf{R}_4 = \begin{bmatrix} 1 \\ 0 \\ 0 \\ 0 \\ \frac{\rho}{A}(\alpha u^2 - c^2) \\ \phi \end{bmatrix}, \quad \mathbf{R}_5 = \begin{bmatrix} 0 \\ 0 \\ 0 \\ 0 \\ 0 \\ 1 \end{bmatrix}, \quad \mathbf{R}_6 = \begin{bmatrix} 1 \\ \alpha u + c_\alpha \\ 0 \\ 0 \\ 0 \\ \phi \end{bmatrix}. \tag{2.186}$$

Remark 2.2.1. Please note that also in this Section we denote flow rate as Au or $q = Au$ interchangeably (and obviously $u = \frac{q}{A}$).

Being the considered domain $\Omega^d = [\mathbb{R}^+ \times \mathbb{R} \times \Omega_{\mathcal{P}} \times \mathbb{R}_0^+] \subset \mathbb{R}^6$, with $\Omega_{\mathcal{P}} \subseteq \mathbb{R}^+ \times \mathbb{R}^+ \times \mathbb{R}$, we will limit ourselves to consider subcritical states, i.e. situations in which $\alpha|u| < c_\alpha$, and we define the new domain

$$\overline{\Omega}^d = \left\{ \mathbf{Q} \in \Omega^d \quad | \quad \alpha|u| < c_\alpha \right\}. \tag{2.187}$$

Proposition 2.2.1 (Hyperbolicity)**.** *The system defined in* (2.181) *is hyperbolic under the following hypotheses:*

1. *the set of admissible solutions is restricted to* $\mathbf{Q} \in \overline{\Omega}^d$,
2. $\alpha \in [1, 2]$,
3. *the tube law is a monotonically increasing function of the cross-sectional area* A, *i.e.* $\dfrac{\partial p}{\partial A} > 0$.

Proof. Since $\alpha \in [1, 2]$ and for tube laws that satisfy the last hypothesis, it can be easily verified that $c_\alpha \in \mathbb{R}^+$ and thus eigenvalues (2.184) will always be real. Since we have 3 repeated eigenvalues $\lambda_k = 0$, with $k = 2, 3, 4$, strict hyperbolicity is lost $\forall \mathbf{Q} \in \overline{\Omega}^d$. □

Remark 2.2.2. It is worth noting that condition (1) of Proposition 2.2.1 is necessary for hyperbolicity only for $\alpha = 1$, for $\alpha > 1$, hyperbolicity is never lost.

Proposition 2.2.2 (Nature of the characteristic fields)**.** *Under the hypotheses of Proposition* 2.2.1, *the* λ_1*- and* λ_6*-characteristic fields for system* (2.181) *are genuinely non-linear for* $\mathbf{Q} \in \overline{\Omega}^d$. *Moreover the* λ_2*-,* λ_3*-,* λ_4*-,* λ_5*-characteristic fields, are linearly degenerate. In praticular provided* $m > 0$, $-2 \leq n \leq 0$, *we have*

$$\nabla \lambda_1(\mathbf{Q}) \cdot \mathbf{R}_1(\mathbf{Q}) < 0, \qquad \nabla \lambda_6(\mathbf{Q}) \cdot \mathbf{R}_6(\mathbf{Q}) > 0 \quad \forall \mathbf{Q} \in \overline{\Omega}^d. \tag{2.188}$$

Proof. Eigenvalues λ_1 and λ_6 are identical to the ones associated with genuinely non-linear fields of system (2.11). Comparing eigenvectors associated with corresponding eigenvalues in both systems, it is evident that the relations obtained by requiring that

$$\nabla \lambda_k(\mathbf{Q}) \cdot \mathbf{R}_k(\mathbf{Q}) \neq 0, \quad \forall \mathbf{Q} \in \overline{\Omega}^d, \tag{2.189}$$

and $k = 1, 6$, are identical to the ones obtained for the original 3×3 model with continuous tube law properties. Finally, it is easy to verify that the λ_k-characteristic fields $k = 2, 3, 4, 5$, are linearly degenerate by noting that

$$\nabla \lambda_k(\mathbf{Q}) \cdot \mathbf{R}_k(\mathbf{Q}) = 0, \quad k = 2, 3, 4, 5 \quad \forall \mathbf{Q} \in \overline{\Omega}^d. \tag{2.190}$$

□

2.2.2 Exact solution of the Riemann problem - Theoretical study

We now adapt the theory described in [90], [81], for a generic $\alpha \in [1, 2]$.

The Riemann problem for system (2.181) is the initial-value problem

$$\begin{cases} \partial_t \mathbf{Q} + \mathbf{M}(\mathbf{Q}) \partial_x \mathbf{Q} = \mathbf{0}, \quad x \in \mathbb{R}, \quad t > 0, \\ \mathbf{Q}(x, 0) = \begin{cases} \mathbf{Q}_L, & \text{if} \quad x < x_d \\ \mathbf{Q}_R, & \text{if} \quad x > x_d \end{cases} \quad \text{with } x_d \in \mathbb{R}, \end{cases} \tag{2.191}$$

being x_d the spatial coordinate of the discontinuity at $t = 0$. The initial conditions are given by the two constant states

$$\mathbf{Q}_L = \begin{bmatrix} A_L \\ A_L u_L \\ K_L \\ A_{0L} \\ p_{eL} \\ A_L \phi_L \end{bmatrix}, \qquad \mathbf{Q}_R = \begin{bmatrix} A_R \\ A_R u_R \\ K_R \\ A_{0R} \\ p_{eR} \\ A_R \phi_R \end{bmatrix}. \tag{2.192}$$

The unknowns are $\mathbf{Q}_L^*$ and $\mathbf{Q}_R^*$ defined

$$\mathbf{Q}_L^* = \begin{bmatrix} A_L^* \\ A_L^* u_L^* \\ K_L^* \\ A_{0L}^* \\ p_{eL}^* \\ A_L^* \phi_L^* \end{bmatrix}, \qquad \mathbf{Q}_R^* = \begin{bmatrix} A_R^* \\ A_R^* u_R^* \\ K_R^* \\ A_{0R}^* \\ p_{eR}^* \\ A_R^* \phi_R^* \end{bmatrix}. \tag{2.193}$$

Fig. 2.15 shows the structure of the exact solution of the Riemann problem (2.191) for the homogeneous blood flow equations (2.181). There are two wave families associated with the two real eigenvalues $\lambda_1 = \alpha u - c_\alpha$, $\lambda_6 = \alpha u + c_\alpha$. The two waves are associated with genuinely non-linear fields and can be either shocks (elastic jumps) or rarefactions [80]. The waves associated with the eigenvalues $\lambda_2 = \lambda_3 = \lambda_4 = 0$ and $\lambda_5 = u$ are related to linearly degenerate fields and are contact discontinuities.

As already stated in (2.187), in this work we stay always in *subsonic regime*.

Proposition 2.2.3 (Generalized Riemann invariants for the λ_1- and λ_6-characteristic fields)**.** *A not complete list of Riemann invariants is*

$$K = const, \quad A_0 = const, \quad p_e = const, \quad \phi = const, \tag{2.194}$$

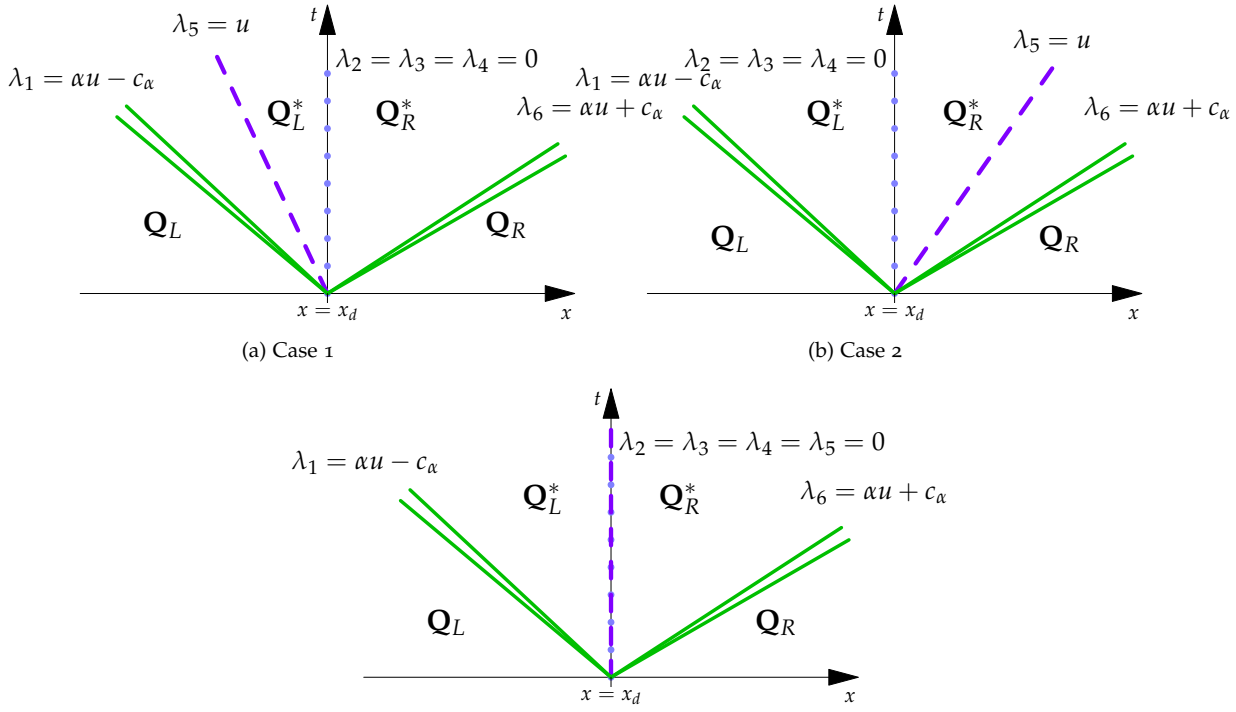

Figure 2.15: The three posssible configurations of the solution of Riemann problem for the complete system of 1D blood flow equations with discontinuous mechanical and geometrical parameters (2.191) within the subsonic regime. Green solid lines represent waves associated with genuinely non-linear fields that can be either shocks or rarefactions, while the dotted blue line and the dashed purple one depict contact discontinuities and are associated with linearly degenerate fields. In this Chapter the λ_1-wave will be sometimes called left wave, while the λ_6-one, right wave. It follows that the related wave patterns will be called left rarefaction/left shock or right rarefaction/right shock.

for the λ_1-characteristic field;

$$K = const, \quad A_0 = const, \quad p_e = const, \quad \phi = const, \tag{2.195}$$

for the λ_6-characteristic field. Regarding the relations between variables A and u no closed form is present for $\alpha > 1$.

Proof. The problem can be solved again applying the generalized Riemann invariants method (for example see [90]), i.e for a given hyperbolic system of n unknowns $[w_1, w_2, \dots, w_n]^T$, for any λ_k-characteristic field with right eigenvector $\mathbf{R}_k = [r_{1,k}, r_{2,k}, \dots, r_{n,k}]^T$ the generalized Riemann invariants are solutions of the following $n-1$ ordinary differential equations in phase-plane

$$\frac{dw_1}{r_{1,k}} = \frac{dw_2}{r_{2,k}} = \cdots = \frac{dw_n}{r_{n,k}}. \tag{2.196}$$

For the λ_1-characteristic field we have

$$\frac{dA}{1} = \frac{d(Au)}{\alpha u - c_\alpha} = \frac{dK}{0} = \frac{dA_0}{0} = \frac{dp_e}{0} = \frac{d(A\phi)}{\phi}. \tag{2.197}$$

From the first and the second term results

$$\frac{dq}{dA} = \alpha u - c_\alpha, \tag{2.198}$$

that is exactly the ODE in (2.51). From the third, fourth and fifth term

$$K = const, \quad A_0 = const, \quad p_e = const. \tag{2.199}$$

From the first and the last

$$\phi = const. \tag{2.200}$$

For the λ_6-characteristic field instead

$$\frac{dA}{1} = \frac{d(Au)}{\alpha u + c_\alpha} = \frac{dK}{0} = \frac{dA_0}{0} = \frac{dp_e}{0} = \frac{d(A\phi)}{\phi}. \tag{2.201}$$

From the first and the second term results

$$\frac{dq}{dA} = \alpha u + c_\alpha, \tag{2.202}$$

that is exactly the ODE in (2.52). From the third, fourth and fifth term

$$K = const, \quad A_0 = const, \quad p_e = const. \tag{2.203}$$

From the first and the last

$$\phi = const. \tag{2.204}$$

□

2.2.2.1 WAVE RELATIONS ACROSS THE CONTACT DISCONTINUITIES

Proposition 2.2.4 (Jump conditions across the stationary contact discontinuity associated with eigenvalues $\lambda_2 = \lambda_3 = \lambda_4 = 0$ (Case 1 and Case 2 of Fig. 2.15))**.** *Across the stationary contact discontinuity the following relations hold*

$$Au = const, \qquad \frac{1}{2}\alpha\rho u^2 + \psi + p_e = const, \quad \phi = const. \tag{2.205}$$

Proof. This problem can be solved by applying the generalized Riemann invariants method described in the proof of Proposition 2.2.3, following the approach presented in [81]. For an arbitrary right eigenvector $\mathbf{R} = [r_1, r_2, r_3, r_4, r_5, r_6]^T$ we clearly have

$$\mathbf{MR} = \lambda\mathbf{R}, \tag{2.206}$$

being $\mathbf{M}$ the system matrix defined in (2.182), which gives the algebraic system

$$\begin{cases} r_2 = \lambda r_1, \\ (c^2 - \alpha u^2) r_1 + 2\alpha u r_2 + \dfrac{A}{\rho}\psi_K r_3 + \dfrac{A}{\rho}\psi_{A_0} r_4 + \dfrac{A}{\rho} r_5 = \lambda r_2, \\ 0 = \lambda r_3, \\ 0 = \lambda r_4, \\ 0 = \lambda r_5, \\ -u\phi r_1 + \phi r_2 + u r_6 = \lambda r_6. \end{cases} \tag{2.207}$$

Substituting $\lambda = 0$ in (2.207), we first notice that $r_2 = 0$. Posing $r_1 = \beta$, $r_3 = \gamma$, $r_4 = \epsilon$, for β, γ, ϵ arbitrary constants, we obtain

$$\mathbf{R}_0 = \begin{bmatrix} \beta \\ 0 \\ \gamma \\ \epsilon \\ \left[(\alpha u^2 - c^2)\beta - \frac{A}{\rho}\psi_K\gamma - \frac{A}{\rho}\psi_{A_0}\epsilon\right]\frac{\rho}{A} \\ \phi\beta \end{bmatrix}. \tag{2.208}$$

This vector belongs to the subspace related to $\lambda = 0$, for every choice of β,γ and $\epsilon \in \mathbb{R}$, and every vector of that subspace has this form. At this point we can apply the generalized Riemann invariants method to vector (2.208), i.e.

$$\frac{dA}{\beta} = \frac{d(Au)}{0} = \frac{dK}{\gamma} = \frac{dA_0}{\epsilon} = \frac{dp_e}{\left[(\alpha u^2 - c^2)\beta - \frac{A}{\rho}\psi_K\gamma - \frac{A}{\rho}\psi_{A_0}\epsilon\right]\frac{\rho}{A}} = \frac{d(A\phi)}{\phi\beta}, \tag{2.209}$$

from the second of (2.209) we have

$$d(Au) = 0 \rightarrow Au = const, \tag{2.210}$$

from the first and the fifth of (2.209) we have

$$\frac{dA}{\beta} = \frac{dp_e}{\left[(\alpha u^2 - c^2)\beta - \frac{A}{\rho}\psi_K\gamma - \frac{A}{\rho}\psi_{A_0}\epsilon\right]\frac{\rho}{A}} \rightarrow (\alpha u^2 - c^2)\frac{\rho}{A}dA - \psi_K\frac{\gamma}{\beta}dA - \psi_{A_0}\frac{\epsilon}{\beta}dA = dp_e, \tag{2.211}$$

considering the first and the third of (2.209) coupled together and then the first and the fourth of (2.209), we have that

$$\gamma dA = \beta dK, \quad \epsilon dA = \beta dA_0. \tag{2.212}$$

Being c defined in (2.183) and $d(Au) = 0$, it follows that

$$(\alpha u^2 - c^2)\frac{\rho}{A}dA = -\alpha\rho u du - \psi_A dA, \tag{2.213}$$

so (2.211) becomes

$$-\alpha\rho u du - \psi_A dA - \psi_K dK - \psi_{A_0} dA_0 - dp_e = 0. \tag{2.214}$$

Considering that

$$d\psi = \psi_A dA + \psi_K dK + \psi_{A_0} dA_0, \tag{2.215}$$

(2.214) becomes

$$-\alpha\rho u du - d\psi - dp_e = 0, \tag{2.216}$$

from that, integrating, we obtain the second of (2.205). From the first and the last of (2.209) we have

$$\frac{dA}{\beta} = \frac{d(A\phi)}{\phi\beta} \rightarrow d\phi = 0 \rightarrow \phi = const. \tag{2.217}$$

□

Proposition 2.2.5 (Jump conditions across the contact discontinuity associated with eigenvalue $\lambda_5 = u \neq 0$ (Case 1 and Case 2 of Fig. 2.15)). *Across the contact discontinuity the following relations hold*

$$A = const, \qquad Au = const, \qquad K = const, \qquad A_0 = const, \qquad p_e = const. \tag{2.218}$$

Proof. Applying the generalized Riemann invariants method already described [90, 81], we obtain

$$\frac{dA}{0} = \frac{d(Au)}{0} = \frac{dK}{0} = \frac{dA_0}{0} = \frac{dp_e}{0} = \frac{d(A\phi)}{1}, \tag{2.219}$$

from which the statement is straightforward. □

Proposition 2.2.6 (Jump conditions across the stationary contact discontinuity associated with eigenvalues $\lambda_2 = \lambda_3 = \lambda_4 = \lambda_5 = 0$ (Case 3 of Fig. 2.15)). *Across the stationary contact discontinuity the following relations hold*

$$Au = 0, \qquad \psi + p_e = const. \tag{2.220}$$

Proof. This problem can again be solved by employing the generalized Riemann invariants method with the approach presented in [81], already described in the Proof of Proposition 2.2.4, now applied to matrix $\mathbf{M}$ in (2.182) but considering $u = 0$, i.e.

$$\widetilde{\mathbf{M}}(\mathbf{Q}) = \begin{bmatrix} 0 & 1 & 0 & 0 & 0 & 0 \\ c^2 & 0 & \frac{A}{\rho}\psi_K & \frac{A}{\rho}\psi_{A_0} & \frac{A}{\rho} & 0 \\ 0 & 0 & 0 & 0 & 0 & 0 \\ 0 & 0 & 0 & 0 & 0 & 0 \\ 0 & 0 & 0 & 0 & 0 & 0 \\ 0 & \phi & 0 & 0 & 0 & 0 \end{bmatrix}. \tag{2.221}$$

It follows that

$$\widetilde{\mathbf{M}}\mathbf{R} = \lambda\mathbf{R}, \tag{2.222}$$

which gives the algebraic system

$$\begin{cases} r_2 = \lambda r_1, \\ c^2 r_1 + \frac{A}{\rho}\psi_K r_3 + \frac{A}{\rho}\psi_{A_0} r_4 + \frac{A}{\rho} r_5 = \lambda r_2, \\ 0 = \lambda r_3, \\ 0 = \lambda r_4, \\ 0 = \lambda r_5, \\ \phi r_2 = \lambda r_6, \end{cases} \tag{2.223}$$

Substituting $\lambda = 0$ in (2.223), we first notice that $r_2 = 0$. Posing $r_1 = \beta$, $r_3 = \gamma$, $r_4 = \epsilon$, $r_6 = \delta$, for $\beta, \gamma, \epsilon, \delta \in \mathbb{R}$, arbitrary constants, we obtain

$$\mathbf{R}_0 = \begin{bmatrix} \beta \\ 0 \\ \gamma \\ \epsilon \\ \left[-c^2\beta - \frac{A}{\rho}\psi_K\gamma - \frac{A}{\rho}\psi_{A_0}\epsilon\right]\frac{\rho}{A} \\ \delta \end{bmatrix}. \tag{2.224}$$

This is a general form of a vector belonging to the subspace associated with $\lambda = 0$ for every choice of $\beta, \gamma, \epsilon, \delta, \in \mathbb{R}$. We then apply the generalized Riemann invariants method to this vector

$$\frac{dA}{\beta} = \frac{d(Au)}{0} = \frac{dK}{\gamma} = \frac{dA_0}{\epsilon} = \frac{dp_e}{\left[-c^2\beta - \frac{A}{\rho}\psi_K\gamma - \frac{A}{\rho}\psi_{A_0}\epsilon\right]\frac{\rho}{A}} = \frac{d(A\phi)}{\delta}. \tag{2.225}$$

From the second of (2.225) we have

$$Au = const, \tag{2.226}$$

that considering $u = 0$, becomes

$$Au = 0. \tag{2.227}$$

From the first and the fifth of (2.225) we have

$$\frac{dA}{\beta} = \frac{dp_e}{\left[-c^2\beta - \frac{A}{\rho}\psi_K\gamma - \frac{A}{\rho}\psi_{A_0}\epsilon\right]\frac{\rho}{A}} \rightarrow -c^2\frac{\rho}{A}dA - \psi_K\frac{\gamma}{\beta}dA - \psi_{A_0}\frac{\epsilon}{\beta}dA = dp_e, \tag{2.228}$$

considering the first and the third of (2.225) coupled together and then the first and the fourth of (2.225), we have that

$$\gamma dA = \beta dK, \quad \epsilon dA = \beta dA_0. \tag{2.229}$$

Being c as in (2.183), we have

$$-c^2\frac{\rho}{A}dA = -\psi_A dA, \tag{2.230}$$

so (2.228) becomes

$$-\psi_A dA - \psi_K dK - \psi_{A_0} dA_0 - dp_e = 0. \tag{2.231}$$

Considering that

$$d\psi = \psi_A dA + \psi_K dK + \psi_{A_0} dA_0, \tag{2.232}$$

we have that (2.231) becomes

$$-d\psi - dp_e = 0, \tag{2.233}$$

from that, integrating, we obtain the second of (2.220). From the first and the sixth of (2.225) we have

$$\frac{dA}{\beta} = \frac{d(A\phi)}{\delta}, \tag{2.234}$$

that leads to

$$\frac{dA}{A} = \left(\frac{\beta}{\delta - \beta\phi}\right)d\phi. \tag{2.235}$$

Unfortunately β and δ are arbitrary, so from (2.234) and (2.235) the only thing we can say is that

$$A\phi \neq const, \qquad \phi \neq const. \tag{2.236}$$

□

Remark 2.2.3. Propositions 2.2.3, 2.2.4, 2.2.5, 2.2.6, prove that the stationary contact discontinuities marked with $\lambda_2 = \lambda_3 = \lambda_4 = 0$ are the only discontinuities for the parameters K, A_0 and p_e,

while the λ_5-contact wave is the only discontinuity for the passive scalar. It follows that the unknowns (2.193) become

$$\mathbf{Q}_L^* = \begin{bmatrix} A_L^* \\ Au_L^* \\ K_L^* \\ A_{0L}^* \\ p_{eL}^* \\ A_L^*\phi_L^* \end{bmatrix} = \begin{bmatrix} A_L^* \\ Au_L^* \\ K_L \\ A_{0L} \\ p_{eL} \\ A_L^*\phi \end{bmatrix}, \qquad \mathbf{Q}_R^* = \begin{bmatrix} A_R^* \\ Au_R^* \\ K_R^* \\ A_{0R}^* \\ p_{eR}^* \\ A_R^*\phi_R^* \end{bmatrix} = \begin{bmatrix} A_R^* \\ Au_R^* \\ K_R \\ A_{0R} \\ p_{eR} \\ A_R^*\phi \end{bmatrix}, \tag{2.237}$$

where the concentration of the passive scalar ϕ does not follow the *left-right* classification and must be treated separately. However in this context, the use of the left parameters K_L, A_{0L}, p_{eL} for the construction of the left admissible rarefactions and shocks curves, and the use of the right parameters K_R, A_{0R}, p_{eR} for the construction of the right admissible rarefactions and shocks curves in Section 2.2.2.2, 2.2.2.3 are clear.

2.2.2.2 WAVE RELATIONS ACROSS RAREFACTIONS

As in the case of continuous properties, considering Propositions 2.2.3, 2.2.4, 2.2.5 and 2.2.6, across the waves associated with the genuinely non-linear fields the variable ϕ remain constant. The contact wave λ_5 is the only discontinuity for the passive scalar ϕ. Furthermore the third equation in (2.173) is not affecting the others, consequentially to study the relations across the waves associated with the genuinely non-linear fields we focus only on the first five variables, referring to the unknowns as

$$\mathbf{Q}_L^* = \begin{bmatrix} A_L^* \\ q_L^* \\ K_L \\ A_{0L} \\ p_{eL} \end{bmatrix}, \qquad \mathbf{Q}_R^* = \begin{bmatrix} A_R^* \\ q_R^* \\ K_R \\ A_{0R} \\ p_{eR} \end{bmatrix} \tag{2.238}$$

and addressing ϕ at a later point.

Clearly Proposition 2.1.7 now is stated in this form

Proposition 2.2.7 (Physically admissible rarefaction curves)**.**
If the λ_1-wave, associated with a genuinely non-linear field, is a physically admissible rarefaction, the related admissible rarefaction curve in the (A, q) phase-plane is

$$q_{rarL}^a(A) = \{[A, q_{rarL}(A)]^T, \text{ s.t. } A \in \mathbb{R}^+ \text{ and } A \leq A_L\}, \tag{2.239}$$

with $q_{rarL}(A)$ in (2.53). In particular $A_L^* \leq A_L$.

If the λ_6-wave, associated with a genuinely non-linear field, is a physically admissible rarefaction, the related admissible rarefaction curve in the (A, q) phase-plane is

$$q_{rarR}^a(A) = \{[A, q_{rarR}(A)]^T, \text{ s.t. } A \in \mathbb{R}^+ \text{ and } A \leq A_R\}, \tag{2.240}$$

with $q_{rarR}(A)$ in (2.53). In particular $A_R^* \leq A_R$.

Proof. The proof is the same considering for the left wave $\mathbf{Q}_L^*$ instead of $\mathbf{Q}^*$ and for the right wave $\mathbf{Q}_R^*$ instead of $\mathbf{Q}^*$, λ_6 and $\mathbf{R}_6$ instead of λ_3 and $\mathbf{R}_3$. The $q_{rarj}(A)$, $j = L, R$ curves are shown in Fig. 2.16c. □

2.2.2.3 Wave relations across shocks

As in the case of rarefactions, considering Propositions 2.2.3, 2.2.4, 2.2.5 and 2.2.6, the considered unknowns are (2.238).

Section 2.1.2.3 still holds because, as presented in [90] and in [81], in the subsonic regime the waves associated with genuinely non-linear fields remain "far from the discontinuity" of the parameters (blue dotted line in Fig. 2.15), thus we act as we were in the continuous parameter case. Being

$$\mathbf{Q} = \begin{bmatrix} A \\ Au \\ K \\ A_0 \\ p_e \end{bmatrix}, \qquad \mathbf{F}(\mathbf{Q}) = \begin{bmatrix} Au \\ \alpha Au^2 + \dfrac{KA}{\rho}\left(\dfrac{m}{m+1}\left(\dfrac{A}{A_0}\right)^m - \dfrac{n}{n+1}\left(\dfrac{A}{A_0}\right)^n\right) \\ 0 \\ 0 \\ 0 \end{bmatrix}, \tag{2.241}$$

we construct the wave relations across shocks using the Rankine-Hugoniot jump condition, i.e

$$\mathbf{F}(\mathbf{Q}_{\hat{R}}) - \mathbf{F}(\mathbf{Q}_{\hat{L}}) = S(\mathbf{Q}_{\hat{R}} - \mathbf{Q}_{\hat{L}}), \tag{2.242}$$

where $\mathbf{Q}_{\hat{R}}$ and $\mathbf{Q}_{\hat{L}}$ are the constant states to the right and to the left of the shock discontinuity and S is the shock speed. Substituting $\mathbf{Q}_{\hat{R}}$ with $\mathbf{Q}_j^* = [A_j^*, q_j^*]^T$, $\mathbf{Q}_{\hat{L}}$ with $\mathbf{Q}_j = [A_j, q_j]^T$, S with S_j and $q_j = A_j u_j$, with $j = L, R$; now we obtain two different systems

$$\begin{cases} q_j^* - q_j = S_j(A_j^* - A_j), \\ \alpha \dfrac{q_j^{*2}}{A_j^*} - \alpha \dfrac{q_j^2}{A_j} + B_j = S_j(q_j^* - q_j), \end{cases} \tag{2.243}$$

with

$$B_j(A_j^*) = \frac{K_j}{\rho}\left[\frac{m}{m+1}\frac{A_j^{*m+1} - A_j^{m+1}}{A_{0j}^m} - \frac{n}{n+1}\frac{A_j^{*n+1} - A_j^{n+1}}{A_{0j}^n}\right], \tag{2.244}$$

one for $j = L$ and one for $j = R$. We refer to Remark 2.2.3 as the reason for the use of parameters in formula (2.244).

Solving for q_j^* we obtain

$$q_j^* = \frac{A_j^* q_j}{A_j\alpha + A_j^* - \alpha A_j^*} \pm \sqrt{\frac{(A_j - A_j^*)A_j^*(-A_j(A_j\alpha + A_j^* - \alpha A_j^*)B_j + (-1+\alpha)\alpha(A_j - A_j^*)q_j^2)}{A_j(A_j\alpha + A_j^* - \alpha A_j^*)^2}}, \tag{2.245}$$

with $j = L, R$. In this way, we obtain two q_j^* values for each state $j = L, R$. Considering that there is one and only q_j^* for each state $j = L, R$ as the result of the Riemann problem (see for example [20]), we consider again Proposition 2.1.8 that holds also in the discontinuous case replacing λ_3 with λ_6, $\mathbf{R}_3$ with $\mathbf{R}_6$, considering B_j defined in (2.244) and replacing K with K_L and A_0 with A_{0L} for the left part and K with K_R and A_0 with A_{0R} for the right part (see Figs. 2.16a, 2.16b the example for a left shock - (stationary contact - contact discontinuity for the passive scalar) - right shock problem in an artery with $\alpha = 4/3$).

Proposition 2.1.9, is now stated in this form

Proposition 2.2.8 (Entropy-satisfying shock curves)**.**
If the λ_1-wave, associated with a genuinely non-linear field, is an admissible entropy-satisfying shock, the related admissible shock curve in the (A, q) phase-plane is

$$q^a_{shockL}(A) = \{[A, q_{shockL}(A)]^T \text{ s.t. } A > A_L\}, \tag{2.246}$$

with A sufficiently close to A_L and $q_{shockL}(A)$ in (2.82) with B_j defined in (2.244). In particular $A^*_L > A_L$.

If the λ_6-wave, associated with a genuinely non-linear field, is an admissible entropy-satisfying shock, the related admissible shock curve in the (A, q) phase-plane is

$$q^a_{shockR}(A) = \{[A, q_{shockR}(A)]^T \text{ s.t. } A > A_R\}, \tag{2.247}$$

with A sufficiently close to A_R and $q_{shockR}(A)$ in (2.83) with B_j defined in (2.244). In particular $A^*_R > A_R$.

Proof. The same as in Proposition 2.1.9 replacing $\mathbf{Q}^*$ with $\mathbf{Q}^*_L$, q^* with q^*_L and A^* with A^*_L for the left part and $\mathbf{Q}^*$ with $\mathbf{Q}^*_R$, q^* with q^*_R, A^* with A^*_R, λ_3 with λ_6 and $\mathbf{R}_3$ with $\mathbf{R}_6$ for the right part. □

2.2.2.4 Solution in the Star Region

Defining again the Star Region as the region in the half-plane (x, t) in Fig. 2.15 between the λ_1-wave and the λ_6-wave and considering that a wave associated with a genuinely non-linear field can be either a shock or a rarefaction (see for example [80]) Theorems 2.1.1 and 2.1.2 clearly are stated in this way

Theorem 2.2.1. *Given the Riemann problem (2.191), the λ_1-wave is a physically admissible (left) rarefaction if and only if*

$$A^*_L \leq A_L. \tag{2.248}$$

The λ_5-wave is a physically admissible right rarefaction if and only if

$$A^*_R \leq A_R. \tag{2.249}$$

Proof.
($\Longrightarrow$) Proposition 2.2.7.
($\Longleftarrow$) Proposition 2.2.8. □

Theorem 2.2.2. *Given the Riemann problem (2.191), the λ_1-wave is an entropy-satisfying (left) shock if and only if*

$$A^*_L > A_L. \tag{2.250}$$

The λ_5-wave is an entropy-satisfying right shock if and only if

$$A^*_R > A_R. \tag{2.251}$$

Proof.
($\Longrightarrow$) Proposition 2.2.8.
($\Longleftarrow$) Proposition 2.2.7. □

The final $q_{left}(A)$ and $q_{right}(A)$ curves in the phase-plane (A, q) are defined in (2.120), (2.121) (Fig. 2.16d), unfortunately Proposition 2.1.10 does not hold anymore, because now we are looking for two different states $\mathbf{Q}^*_L$ and $\mathbf{Q}^*_R$ so we can not consider any intersection of the obtained curves. In any case, we maintain this graphic representation of the curves for completeness, in which we

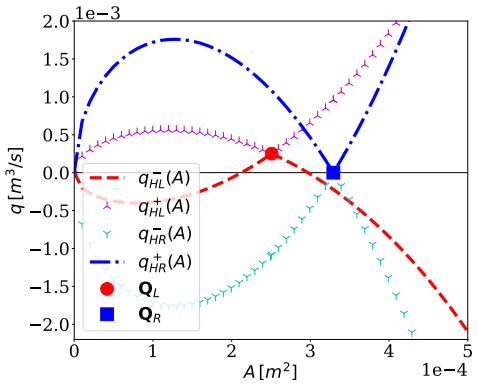

(a) The obtained shock curves for $\mathbf{Q}_L$ and $\mathbf{Q}_R$, for the Test 7 left shock - (stationary contact - contact discontinuity for the passive scalar) - right shock problem in an artery with discontinous properties, with α=4/3.

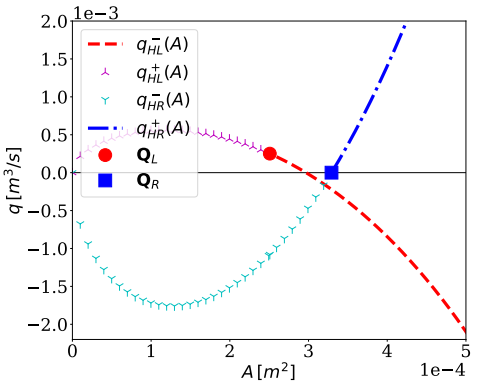

(b) The $q_{shockj}(A)$ $j = L, R$ curves for the Test 7 left shock - (stationary contact - contact discontinuity for the passive scalar) - right shock problem in an artery with discontinous properties, with α=4/3. $q_{shockj}(A)$ $j = L, R$ are defined in (2.82) and (2.83) but with B_j defined in (2.244).

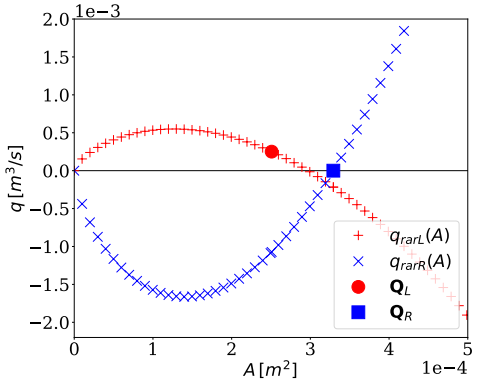

(c) The obtained $q_{rarj}(A)$ $j = L, R$ curves for the Test 7 left shock - (stationary contact - contact discontinuity for the passive scalar) - right shock problem in an artery with discontinous properties, with α=4/3.

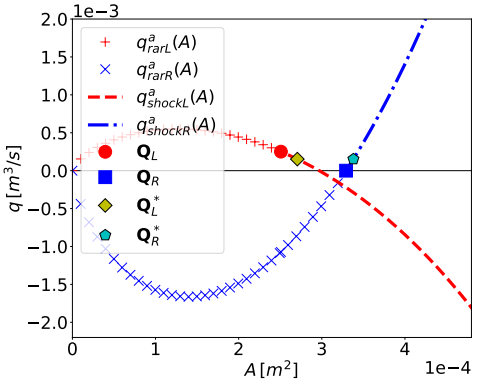

(d) The final $q_{left}(A)$ and $q_{right}(A)$ curves for the Test 7 left shock - (stationary contact - contact discontinuity for the passive scalar) - right shock problem in an artery with discontinous properties, with α=4/3, as defined in (2.120) and (2.121). The subscript a stands for *admissible*. It is clear that this Test is a left shock - right shock problem (plus the contact discontinuities here not depicted), due to the nature of the curves in the neighbourhood of $\mathbf{Q}^*_L$ and $\mathbf{Q}^*_R$.

Figure 2.16: Rarefaction and shock curves in the phase-plane (A, q) for data of Test 7 left shock - (stationary contact - contact discontinuity for the passive scalar) - right shock problem in an artery with discontinuous properties and $\alpha = 4/3$. Initial data are in Tables 2.7, 2.8.

add the actual exact solution of the Riemann problem in the Star Region as shown for example in Fig. 2.16d.

2.2.2.5 Solution inside the rarefactions

This is basically the same as in Section 2.1.2.5, considering A^*_j, $\mathbf{Q}^*_j$ with $j = L$ or $j = R$ for the corresponding waves, instead of A^*, $\mathbf{Q}^*$, and obviously λ_6 instead of λ_3.

2.2.2.6 The complete exact solution of the Riemann problem for the 1D blood flow equations with discontinuous parameters

The complete exact solution of the Riemann problem consists of the states $\mathbf{Q}_L$ and $\mathbf{Q}_R$ (initial data), $\mathbf{Q}_L^*$ and $\mathbf{Q}_R^*$ (the unknowns), $\mathbf{Q}_{irarL}$ and $\mathbf{Q}_{irarR}$ (solution inside the rarefactions when they exist). In Section 2.2.3 we will describe how we actually obtain these values.

2.2.3 Exact solution of the Riemann problem - Numerical resolution

Similarly to what presented in Section 2.1.3, we present a practical method to calculate the desired states.

Remark 2.2.4. Also in case of discontinuous parameters, to compute the exact solution in Section 2.2.2, we must actually approximate numerically the results just presented, as we will see in the next Sections. Nevertheless we always refer to the resulting solution as "exact".

We choose to follow the methodology presented in [87]. We recall that $u = \frac{q}{A}$.

2.2.3.1 Rarefaction and shock curves

We construct the two $u_{rarj}(A)$, $j = L, R$ functions solving (2.125) and (2.126) approximately, via *scipy.integrate.solve_ivp* Python function in the same way as described in Section 2.1.3.1, clearly now (2.126) regards the λ_6-wave and c_α in (2.125) is calculated with the left parameters in (2.272), instead in (2.126), c_α is calculated with the right parameters in (2.272). The two $u_{shockj}(A)$, $j = L, R$ functions are the same as in Section 2.1.3.2 but with B_j in (2.244).

2.2.3.2 Solution in the Star Region (without variable ϕ)

We proceed as presented, for the case of $\alpha = 1$, in [90, 81].

Proposition 2.2.9 (Solution in the Star Region)**.** *The exact solution of the Riemann problem for the 1D blood flow equations with discontinuous parameters in the Star Region is*

$$\mathbf{Q}_L^* = \begin{bmatrix} A_L^* \\ A_L^* u_L^* \\ K_L \\ A_{0L} \\ p_{eL} \end{bmatrix}, \qquad \mathbf{Q}_R^* = \begin{bmatrix} A_R^* \\ A_R^* u_R^* \\ K_R \\ A_{0R} \\ p_{eR} \end{bmatrix}, \tag{2.252}$$

and is found solving for the unknown

$$\mathbf{X} = \begin{bmatrix} x_1 \\ x_2 \\ x_3 \\ x_4 \end{bmatrix} = \begin{bmatrix} A_L^* \\ u_L^* \\ A_R^* \\ u_R^* \end{bmatrix}, \tag{2.253}$$

the system

$$\begin{cases} f_1(x_1,x_2) = x_2 - u_L + f_L(x_1) = 0, \\ f_2(x_3,x_4) = x_4 - u_R - f_R(x_3) = 0, \\ f_3(x_1,x_2,x_3,x_4) = x_1x_2 - x_3x_4 = 0, \\ f_4(x_1,x_2,x_3,x_4) = \frac{1}{2}\alpha\rho(x_2^2 - x_4^2) + K_L\left[\left(\frac{x_1}{A_{0L}}\right)^m - \left(\frac{x_1}{A_{0L}}\right)^n\right] - K_R\left[\left(\frac{x_3}{A_{0R}}\right)^m - \left(\frac{x_3}{A_{0R}}\right)^n\right] + \\ \qquad\qquad + (p_{eL} - p_{eR}) = 0, \end{cases} \tag{2.254}$$

where

$$f_L(x_1) = \begin{cases} u_L - u_{rarL}(x_1) & \text{if } x_1 \le A_L \text{ (left rarefaction)}, \\ u_L - u_{shockL}(x_1) & \text{if } x_1 > A_L \text{ (left shock)}, \end{cases} \tag{2.255}$$

$$f_R(x_3) = \begin{cases} -u_R + u_{rarR}(x_3) & \text{if } x_3 \le A_R \text{ (right rarefaction)}, \\ -u_R + u_{shockR}(x_3) & \text{if } x_3 > A_R \text{ (right shock)}. \end{cases} \tag{2.256}$$

Proof. The proof is similar to that of Proposition 2.1.12, but considering all the relations across the waves studied in Section 2.2.2 (for details see [90], [81]). □

Remark 2.2.5. (2.254) is solved with a globally convergent Newton-Raphson method with initial state $X_I = [A_L, 0, A_R, 0]^T$ (see Appendix B.1). $u_{rarL}(A)$, $u_{rarR}(A)$, $u_{shockL}(A)$ and $u_{shockR}(A)$ are constructed in Section 2.2.3.1. These initial guesses work fine in our case, but in case they fail it is possible to choose other possibilities, for example, in case of $\alpha \neq 1$, the exact solution of the considered Riemann problem for $\alpha = 1$ as presented in [81].

2.2.3.3 Solution inside the rarefactions (without variable ϕ)

Proposition 2.2.10 (Solution inside the left rarefaction)**.** *The exact solution of the Riemann problem inside the left rarefaction is*

$$\mathbf{Q}_{irarL} = \begin{bmatrix} A_{irarL} \\ A_{irarL}u_{irarL} \\ K_L \\ A_{0L} \\ p_{eL} \end{bmatrix}, \tag{2.257}$$

where A_{irarL} is obtained solving with respect to the unknown x the following

$$\frac{\mathcal{X}}{t} + c_\alpha(\mathbf{Q}_{rarL}(x)) - \alpha u_{rarL}(x) = 0, \tag{2.258}$$

with $\mathbf{Q}_{rarL}(x) = [x, x\,u_{rarL}(x), K_L, A_{0L}, p_{eL}]^T$, being $\mathcal{X} = x - x_d$ where x is the specific place of the domain (vessel) in which we are calculating the desired values, x_d is the vessel spatial coordinate of the initial discontinuity, t is the time, and $u_{rarL}(x)$ defined in Section 2.2.3.1, Afterwards the actual u_{irarL}, corresponding to the found A_{irarL}, is

$$u_{irarL} = u_{rarL}(A_{irarL}). \tag{2.259}$$

Proof. The proof is similar to that of Proposition 2.1.13. For the parameters K, A_0 and p_e we refer to Remark. 2.2.3. □

Proposition 2.2.11 (Solution inside the right rarefaction). *The exact solution of the Riemann problem inside the right rarefaction is*

$$\mathbf{Q}_{irarR} = \begin{bmatrix} A_{irarR} \\ A_{irarR} u_{irarR} \\ K_R \\ A_{0R} \\ p_{eR} \end{bmatrix}, \tag{2.260}$$

where A_{irarR} is obtained solving with respect the unknown χ the following

$$\frac{\mathcal{X}}{t} - c_\alpha(\mathbf{Q}_{rarR}(\chi)) - \alpha u_{rarR}(\chi) = 0, \tag{2.261}$$

with $\mathbf{Q}_{rarR}(\chi) = [\chi, \chi u_{rarR}(\chi), K_R, A_{0R}, p_{eR}]^T$, being $\mathcal{X} = x - x_d$ where x is the specific place of the domain (vessel) in which we are calculating the desired values, x_d is the vessel spatial coordinate of the initial discontinuity, t is the time and $u_{rarR}(\chi)$ defined in Section 2.2.3.1. Afterwards the actual u_{irarR}, corresponding to the found A_{irarR}, is

$$u_{irarR} = u_{rarR}(A_{irarR}). \tag{2.262}$$

Proof. Similar to that of Proposition 2.1.14. For the parameters K, A_0 and p_e we refer to Remark. 2.2.3. □

Again (2.258) and (2.261) are solved with a globally convergent Newton-Raphson method with initial points respectively A_L and A_R .

2.2.3.4 THE COMPLETE EXACT SOLUTION OF THE RIEMANN PROBLEM FOR THE 1D BLOOD FLOW EQUATIONS WITH DISCONTINUOUS PARAMETERS

In this Section we present the sampling of the complete exact solution of the Riemann problem for the 1D blood flow equations (2.191). Now we can add the last variable ϕ. Being as before $\mathcal{X} = x - x_d$, x is the specific place of the domain (vessel) in which we are calculating the desired values, x_d is the vessel spatial coordinate of the initial discontinuity, and t is the time, thanks to Theorems 2.2.1, 2.2.2, on the left side the complete solution is:

- if $A_L^* \leq A_L$ (left rarefaction):

$$\mathbf{Q}(x,t) = \begin{cases} \mathbf{Q}_L & \text{if} \quad \mathcal{X} < (\alpha u_L - c_\alpha(\mathbf{Q}_L))t, \\ \mathbf{Q}_{irarL} & \text{if} \quad (\alpha u_L - c_\alpha(\mathbf{Q}_L))t \leq \mathcal{X} \leq (\alpha u_L^* - c_\alpha(\mathbf{Q}_L^*))t, \\ \mathbf{Q}_L^* & \text{if} \quad (\alpha u_L^* - c_\alpha(\mathbf{Q}_L^*))t < \mathcal{X} \leq 0, \end{cases} \tag{2.263}$$

- if $A_L^* > A_L$ (left shock):

$$\mathbf{Q}(x,t) = \begin{cases} \mathbf{Q}_L & \text{if} \quad \mathcal{X} \leq S_L t, \\ \mathbf{Q}_L^* & \text{if} \quad S_L t < \mathcal{X} \leq 0. \end{cases} \tag{2.264}$$

Similarly on the right side the complete solution is

- if $A_R^* \leq A_R$ (right rarefaction):

$$\mathbf{Q}(x,t) = \begin{cases} \mathbf{Q}_R^* & \text{if} \quad 0 < \mathcal{X} < (\alpha u_R^* + c_\alpha(\mathbf{Q}_R^*))t, \\ \mathbf{Q}_{irarR} & \text{if} \quad (\alpha u_R^* + c_\alpha(\mathbf{Q}_R^*))t \leq \mathcal{X} \leq (\alpha u_R + c_\alpha(\mathbf{Q}_R))t, \\ \mathbf{Q}_R & \text{if} \quad \mathcal{X} > (\alpha u_R + c_\alpha(\mathbf{Q}_R))t, \end{cases} \tag{2.265}$$

- if $A_R^* > A_R$ (right shock):

$$\mathbf{Q}(x,t) = \begin{cases} \mathbf{Q}_R^* & \text{if} \quad 0 < \mathcal{X} \leq S_R t, \\ \mathbf{Q}_R & \text{if} \quad \mathcal{X} > S_R t. \end{cases} \tag{2.266}$$

Considering Proposition 2.1.15 and Remark 2.2.3, the considered quantities are $\mathbf{Q}_L$ and $\mathbf{Q}_R$ in (2.192),

$$\mathbf{Q}_{irarL} = \begin{bmatrix} A_{irarL} \\ A_{irarL} u_{irarL} \\ K_{irarL} \\ A_{0irarL} \\ p_{eirarL} \\ A_{irarL}\phi_L \end{bmatrix}, \qquad \mathbf{Q}_{irarR} = \begin{bmatrix} A_{irarR} \\ A_{irarR} u_{irarR} \\ K_{irarR} \\ A_{0irarR} \\ p_{eirarR} \\ A_{irarR}\phi_R \end{bmatrix}, \tag{2.267}$$

$$\mathbf{Q}_L^* = \begin{bmatrix} A_L^* \\ A_L^* u_L^* \\ K_L \\ A_{0L} \\ p_{eL} \\ A_L^*\phi \end{bmatrix}, \qquad \mathbf{Q}_R^* = \begin{bmatrix} A_R^* \\ A_R^* u_R \\ K_R^* \\ A_{0R} \\ p_{eR} \\ A_R^*\phi \end{bmatrix}, \tag{2.268}$$

All these unknowns have been already treated in the previous Sections, with the exception of ϕ in (2.268), that is defined

$$\phi(x,t) = \begin{cases} \phi_L & \text{if} \quad \mathcal{X} \leq u^* t, \\ \phi_R & \text{if} \quad \mathcal{X} > u^* t. \end{cases} \tag{2.269}$$

being

$$u^* = \begin{cases} u_L^* & \text{if} \quad u_L^* \leq 0, \\ u_R^* & \text{if} \quad u_R^* > 0. \end{cases} \tag{2.270}$$

This latter definition is straightforward remembering that $sgn(u_L^*) = sgn(u_R^*)$. c_α is defined in (2.185), S_L and S_R are the left and the right shock speeds and are defined according to the first of (2.243)

$$\begin{aligned} S_L &= \frac{q_L^* - q_L}{A_L^* - A_L} = \frac{A_L^* u_L^* - A_L u_L}{A_L^* - A_L}, \\ S_R &= \frac{q_R^* - q_R}{A_R^* - A_R} = \frac{A_L^* u_R^* - A_R u_R}{A_R^* - A_R}. \end{aligned} \tag{2.271}$$

Remark 2.2.6. Recalling Remark 2.2.3, and Fig. 2.15, the parameters are defined as follows

$$K(x) = \begin{cases} K_L & \text{if} \quad \mathcal{X} \leq 0, \\ K_R & \text{if} \quad \mathcal{X} > 0, \end{cases} \quad A_0(x) = \begin{cases} A_{0L} & \text{if} \quad \mathcal{X} \leq 0, \\ A_{0R} & \text{if} \quad \mathcal{X} > 0, \end{cases} \quad p_e(x) = \begin{cases} p_{eL} & \text{if} \quad \mathcal{X} \leq 0, \\ p_{eR} & \text{if} \quad \mathcal{X} > 0. \end{cases} \tag{2.272}$$

2.2.4 Numerical results

Having obtained the exact solution of the Riemann problem as presented in Section 2.2.3, we perform a mesh independence study to justify the choice of the mesh $E = 100$ to build the approximated integral curves in Section 2.2.3.1, also for the discontinuous case. After that, we evaluate the entire exact solution thus constructed on a suite of test problems involving arteries

and veins and different wave patterns, for different momentum correction coefficients α, against DOT Riemann solver [24] (see Appendix A.5).

2.2.4.1 MESH INDEPENDENCE STUDY

Table 2.6: Mesh independence study for vein, left rarefaction - contact discontinuity for the passive scalar- stationary contact - right rarefaction, Test 10 problem in Tables 2.7, 2.8.

α	Variable	Mesh	L^1-err	L^2-err	L^∞-err
1	A	50	-	-	-
		100	$4.8567e-15$	$2.5461e-14$	$1.6338e-13$
		200	$8.0954e-16$	$4.5177e-15$	$2.9203e-14$
	Au	50	-	-	-
		100	$1.7127e-14$	$3.5945e-14$	$8.7834e-14$
		200	$2.4470e-15$	$5.4011e-15$	$1.2445e-14$
11/10	A	50	-	-	-
		100	$5.8785e-15$	$3.0851e-14$	$1.9578e-13$
		200	$7.6170e-16$	$4.1755e-15$	$2.6616e-14$
	Au	50	-	-	-
		100	$1.4903e-14$	$3.1089e-14$	$9.2827e-14$
		200	$2.2018e-15$	$4.8336e-15$	$1.1104e-14$
4/3	A	50	-	-	-
		100	$5.5939e-15$	$2.8037e-14$	$1.7191e-13$
		200	$5.6236e-16$	$2.9147e-15$	$1.7943e-14$
	Au	50	-	-	-
		100	$1.1438e-14$	$2.4368e-14$	$1.1822e-13$
		200	$1.7497e-15$	$3.7779e-15$	$9.7998e-15$
2	A	50	-	-	-
		100	$2.0588e-15$	$8.4390e-15$	$8.8586e-14$
		200	$2.7271e-16$	$1.0108e-15$	$5.2546e-15$
	Au	50	-	-	-
		100	$9.0131e-15$	$3.1157e-14$	$2.6412e-13$
		200	$1.0944e-15$	$2.4385e-15$	$1.5819e-14$

To verify that our exact solution constructed in Section 2.2.3 is mesh independent with respect to the one used to approximate the integral curves (see Section 2.2.3.1), we perform a study with meshes $E_n \in E = [50, 100, 200]$ computational cells choosing tests in which only rarefactions waves are involved. We construct the $u_{rarj}(A)$ curves as presented in Section 2.2.3.1 with each of the prescribed E_n meshes, and then we build the complete solution of the Riemann problem as presented in Section 2.2.3.4 with a mesh of $I = 3000$ computational cells. Then we calculate L^1_{err}, L^2_{err} and L^∞_{err} as defined in (2.170). The results are shown in Table 2.6, the test data are those of Test 10 (left rarefaction - contact discontinuity for the passive scalar- stationary contact - right rarefaction in a vein) in Tables 2.7, 2.8. As result of this procedure, we choose the mesh $E = 100$ computational cells also for the discontinuous parameters part.

2.2.4.2 RESULTS

We plot the exact solution of the Riemann problem for the 1D blood flow equations with discontinuous parameters presented so far, for test problems that involve both arteries and veins, whose initial data are in Tables 2.7, 2.8, against DOT solver (Appendix A.5), with a Courant–Friedrichs–Lewy number $C_{cfl} = 0.9$ defined in Def. 2.1.1, both in a $I = 3000$ computational cells mesh, for different momentum correction coefficents $\alpha = [1, 1.1, 4/3, 2]$. The numerical results are described in Figs. 2.17, 2.18, 2.19, 2.20, 2.21, 2.22, 2.23, 2.24, 2.25, 2.26. In Fig. 2.27 is shown a comparison of the different exact solutions of some tests for the considered α. In Table 2.9 is reported the exact solution in the Star Region for each test and for the considered α.

Table 2.7: Parameters used for Tests 6 to 10: blood density ρ; reference vessel wall stiffness K_{ref}; reference cross-sectional area $A_{0,ref}$; domain length ℓ; location of the initial discontinuity x_d and output time t_{End}. Regarding the resulting wave pattern, *R=rarefaction*, *S=shock*, C_u=*contact discontinuity associated with* $\lambda = u$, C_0=*contact discontinuity associated with* $\lambda = 0$.

Test	Vessel	Wave pattern	$\rho[kg/m^3]$	$K_{ref}[Pa]$	$A_{0,ref}[m^2]$	$\ell[m]$	$x_d[m]$	$t_{End}[s]$
6	Artery	Stationary	1050	58725.0	$3.1353 \cdot 10^{-4}$	0.2	0.5ℓ	0.007
7	Artery	SC_0C_uS	1050	58725.0	$3.1353 \cdot 10^{-4}$	0.2	0.3ℓ	0.007
8	Vein	SC_uC_0R	1050	33.3333	$2.8274 \cdot 10^{-5}$	0.5	0.3ℓ	0.025
9	Vein	SC_0C_uS	1050	33.3333	$2.8274 \cdot 10^{-5}$	0.5	0.5ℓ	0.05
10	Vein	RC_uC_0R	1050	33.3333	$2.8274 \cdot 10^{-5}$	0.5	0.3ℓ	0.05

Table 2.8: Left and right initial conditions for Tests from 6 to 10. The units of measures used for this Thesis are: m, s, kg, Pa.

	Test	$A_L[m^2]$	$u_L[m/s]$	$K_L[Pa]$	$A_{0L}[m^2]$	$p_{eL}[Pa]$	ϕ_L
Left data	6	$1.0228A_{0L}$	0.0	K_{ref}	$2.0A_{0,ref}$	9999.15	1.0
	7	$1.6A_{0L}$	1.0	K_{ref}	$0.5A_{0,ref}$	3999.66	1.0
	8	$2.9 \cdot 10^{-5}$	0.2	K_{ref}	$A_{0,ref}$	66.661	1.0
	9	$3.42 \cdot 10^{-5}$	0.5	K_{ref}	$A_{0,ref}$	66.661	0.5
	10	$3.1 \cdot 10^{-5}$	-0.2	K_{ref}	$A_{0,ref}$	66.661	0.5
	Test	$A_R[m^2]$	$u_R[m/s]$	$K_R[Pa]$	$A_{0R}[m^2]$	$p_{eR}[Pa]$	ϕ_R
Right data	6	$0.9977A_{0R}$	0.0	$10K_{ref}$	$A_{0,ref}$	11340.56820743433	0.5
	7	$1.05A_{0R}$	0.0	$10K_{ref}$	$A_{0,ref}$	0.0	0.5
	8	$3.2 \cdot 10^{-5}$	0.1	$100K_{ref}$	$1.05A_{0,ref}$	66.661	0.5
	9	$3.34 \cdot 10^{-5}$	-0.1	$40K_{ref}$	$1.15A_{0,ref}$	66.661	1.0
	10	$3.1 \cdot 10^{-5}$	0.1	$30K_{ref}$	$1.05A_{0,ref}$	66.661	1.0

Table 2.9: Exact solution in the Star Region of Tests from 6 to 10.

Test	α	$A_L^*[m^2]$	$u_L^*[m/s]$	$A_R^*[m^2]$	$u_R^*[m/s]$
6	1	$6.4136 \cdot 10^{-4}$	0.0	$3.1281 \cdot 10^{-4}$	0.0
	11/10	$6.4136 \cdot 10^{-4}$	0.0	$3.1281 \cdot 10^{-4}$	0.0
	4/3	$6.4136 \cdot 10^{-4}$	0.0	$3.1281 \cdot 10^{-4}$	0.0
	2	$6.4136 \cdot 10^{-4}$	0.0	$3.1281 \cdot 10^{-4}$	0.0
7	1	$2.7010 \cdot 10^{-4}$	0.5553	$3.3792 \cdot 10^{-4}$	0.4439
	11/10	$2.7024 \cdot 10^{-4}$	0.5576	$3.3795 \cdot 10^{-4}$	0.4459
	4/3	$2.7056 \cdot 10^{-4}$	0.5631	$3.3802 \cdot 10^{-4}$	0.4507
	2	$2.7145 \cdot 10^{-4}$	0.5791	$3.3821 \cdot 10^{-4}$	0.4648
8	1	$3.8612 \cdot 10^{-5}$	-0.2578	$3.0202 \cdot 10^{-5}$	-0.3296
	11/10	$3.8597 \cdot 10^{-5}$	-0.2579	$3.0198 \cdot 10^{-5}$	-0.3296
	4/3	$3.8563 \cdot 10^{-5}$	-0.2581	$3.0190 \cdot 10^{-5}$	-0.3297
	2	$3.8465 \cdot 10^{-5}$	-0.2586	$3.0167 \cdot 10^{-5}$	-0.3297
9	1	$4.0863 \cdot 10^{-5}$	0.0607	$3.4649 \cdot 10^{-5}$	0.0716
	11/10	$4.0894 \cdot 10^{-5}$	0.0623	$3.4661 \cdot 10^{-5}$	0.0735
	4/3	$4.0967 \cdot 10^{-5}$	0.0659	$3.4692 \cdot 10^{-5}$	0.0779
	2	$4.1171 \cdot 10^{-5}$	0.0765	$3.4778 \cdot 10^{-5}$	0.0906
10	1	$2.5291 \cdot 10^{-5}$	-0.0767	$2.9616 \cdot 10^{-5}$	-0.0655
	11/10	$2.5429 \cdot 10^{-5}$	-0.0760	$2.9618 \cdot 10^{-5}$	-0.0653
	4/3	$2.5728 \cdot 10^{-5}$	-0.0746	$2.9624 \cdot 10^{-5}$	-0.0648
	2	$2.6430 \cdot 10^{-5}$	-0.0714	$2.9639 \cdot 10^{-5}$	-0.0636

Test 6 The solution of Test 6 consists of a stationary solution in an artery, i.e. a solution in which $u(x,t) = 0\ \forall x \in \mathbb{R}$ and $\forall t \in \mathbb{R}^+$. The variation of α does not change the stationary nature of the solution, however we can appreciate an accentuation of the curvatures of the $q_{left}(A)$ and $q_{right}(A)$ curves (Figs. 2.17, 2.18).

Test 7 The solution of Test 7 describes a left shock, a stationary contact, a contact discontinuity for the passive scalar and a right shock in an artery (SC_0C_uS). In this case we face a variation of both A_j^* and u_j^*, $j = L, R$, with both of them growing when α increases (Fig. 2.27), again (A, q) plots describe a small accentuation of the curvature of the $q_{left}(A)$ and $q_{right}(A)$ curves with the rise of α (Fig. 2.20, 2.19).

Test 8 The solution of Test 8 consists of a left shock, a contact discontinuity for the passive scalar, a stationary contact and a right rarefaction in a vein (SC_uC_0R). Also in this case we face a variation of both A_j^* and u_j^*, with both of them decreasing when α increases (Fig. 2.27). The accentuation of the curvatures of the left and right curves is present but minimal (Fig. 2.21, 2.22).

Test 9 Test 9 presents a left shock, a stationary contact, a contact discontinuity for the passive scalar, and a right shock in a vein (SC_0C_uS). In this test both A_j^* and u_j^* increase with α (Fig. 2.27). The same discussion as before for the $q_{left}(A)$ and $q_{right}(A)$ curves (Fig. 2.24, 2.23).

Test 10 In Test 10 a left rarefaction, a contact discontinuity for the passive scalar, a stationary contact and a right rarefaction in a vein (RC_uC_0R) are depicted with both A_j^* and u_j^* increasing with α (Fig. 2.27). Also a small variation in the inclination of the rarefaction is observed. For the curvature of the left and right curve the discussion is the same as before (Fig. 2.25, 2.26).

Figs. 2.17, 2.20, 2.21, 2.24, 2.25 show a very good matching between the exact solutions and the DOT solver. Regarding the passive scalar ϕ, Fig. 2.27 does not show remarkable differences in depicting the related discontinuities for the different values of α.

Test 6. Exact solution of the Riemann problem with $\alpha \in [1, 2]$

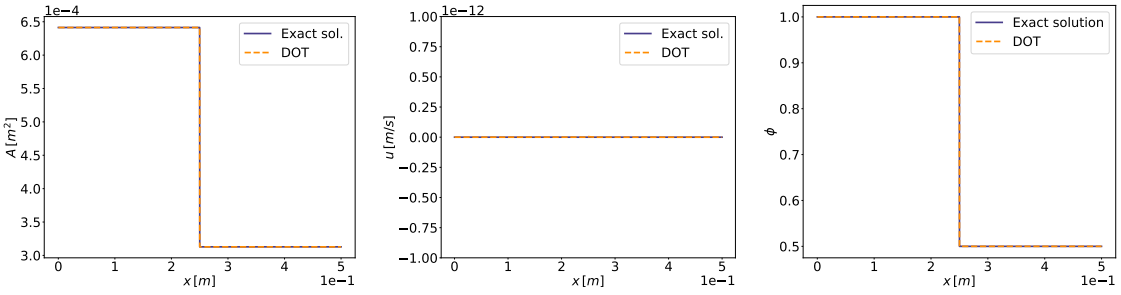

(a) $\alpha = 1$

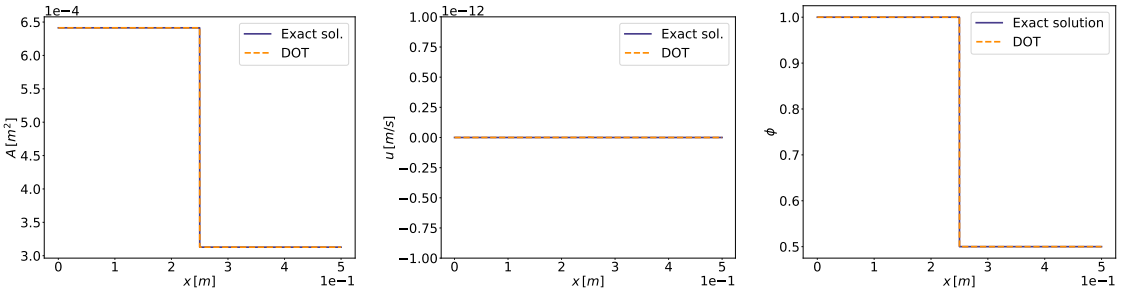

(b) $\alpha = 11/10$

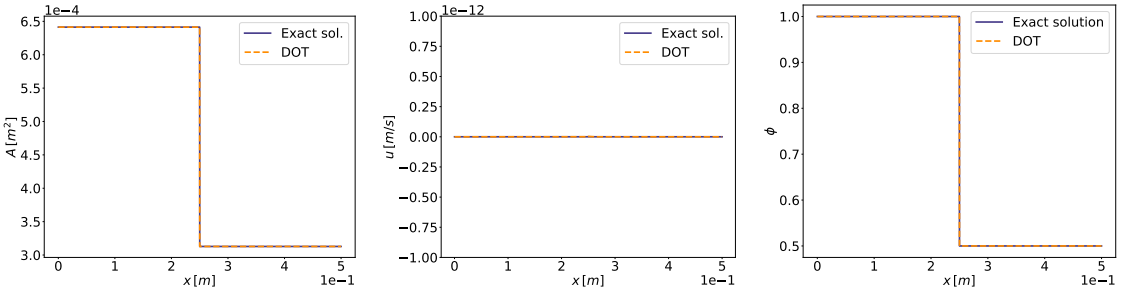

(c) $\alpha = 4/3$

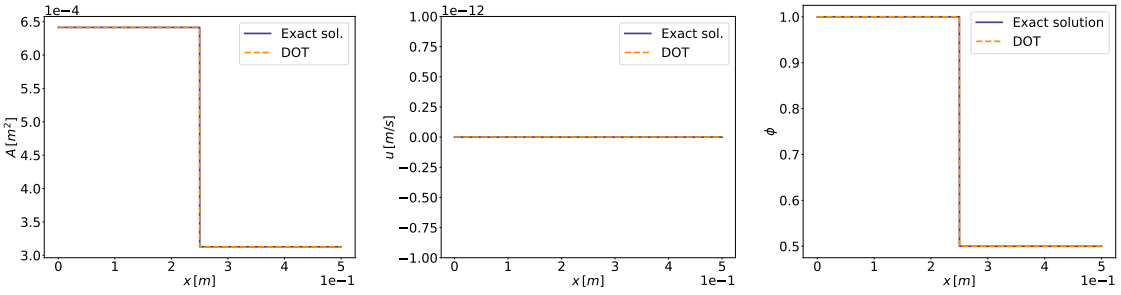

(d) $\alpha = 2$

Figure 2.17: Test 6. Artery. Stationary. Exact solution of the Riemann problem with $\alpha = 1$, $\alpha = 1.1$, $\alpha = 4/3$, $\alpha = 2$ against DOT Riemann solver. Initial data are in Tables 2.7, 2.8.

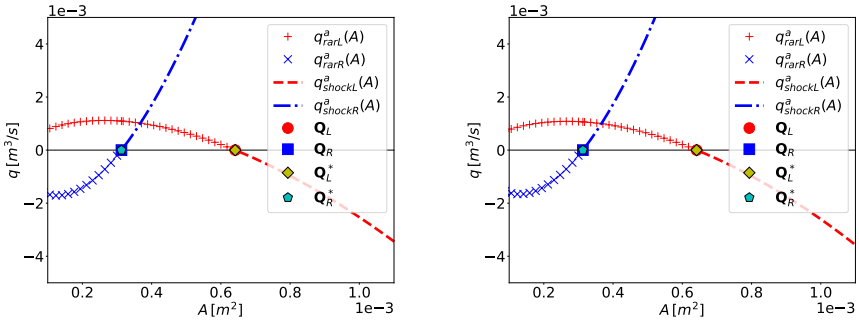

(a) $\alpha = 1$ (b) $\alpha = 1.1$

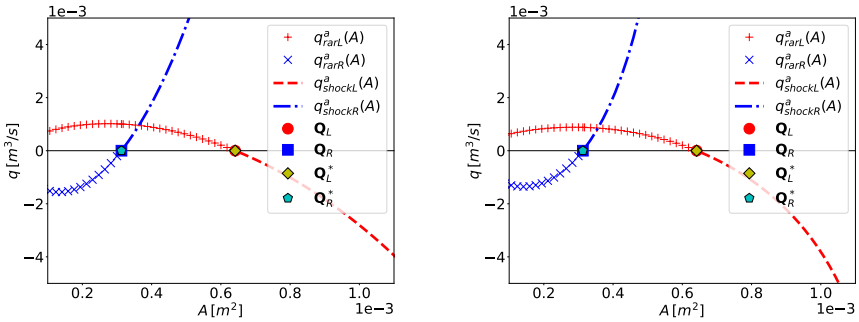

(c) $\alpha = 4/3$ (d) $\alpha = 2$

Figure 2.18: A detail of the graphic representations of the solutions in the (A, q) phase-plane for data of Test 6 in Tables 2.7, 2.8, for $\alpha = 1$, $\alpha = 1.1$, $\alpha = 4/3$ and $\alpha = 2$.

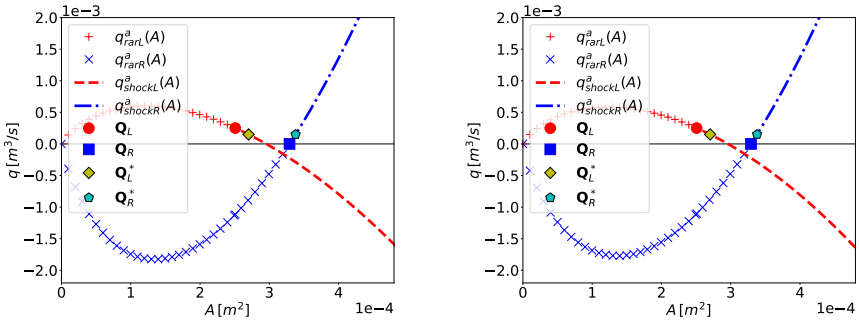

(a) $\alpha = 1$ (b) $\alpha = 1.1$

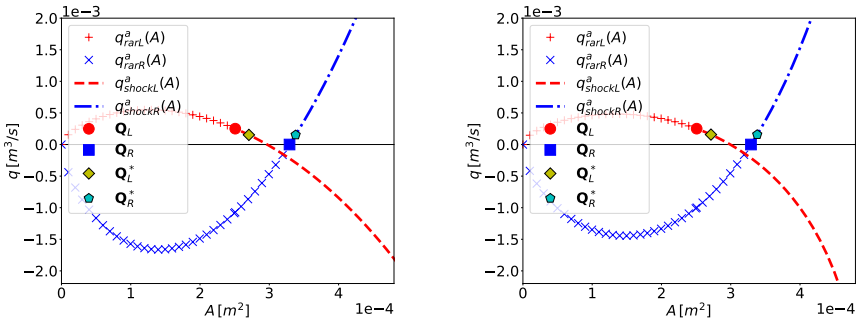

(c) $\alpha = 4/3$ (d) $\alpha = 2$

Figure 2.19: A detail of the graphic representations of the solutions in the (A, q) phase-plane for data of Test 7 in Tables 2.7, 2.8, for $\alpha = 1$, $\alpha = 1.1$, $\alpha = 4/3$ and $\alpha = 2$.

Test 7. Exact solution of the Riemann problem with $\alpha \in [1, 2]$

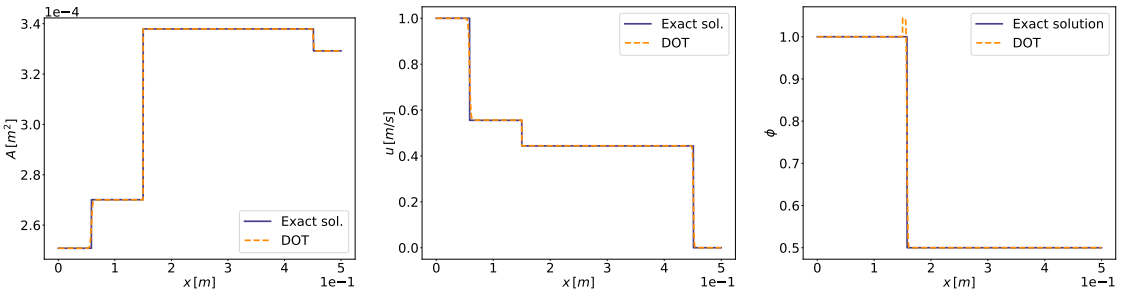

(a) $\alpha = 1$

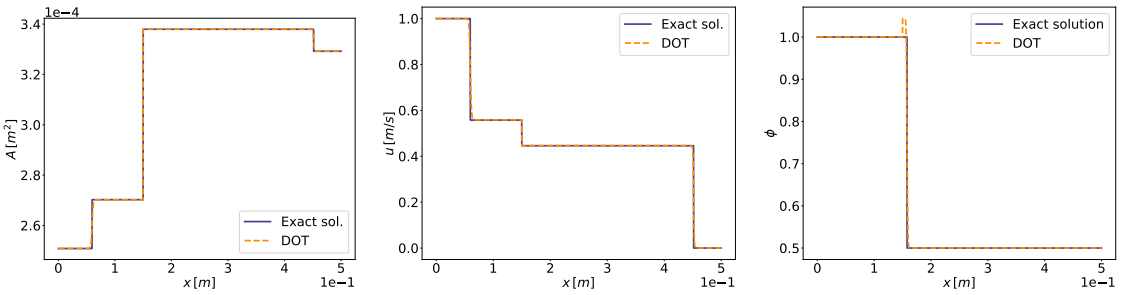

(b) $\alpha = 11/10$

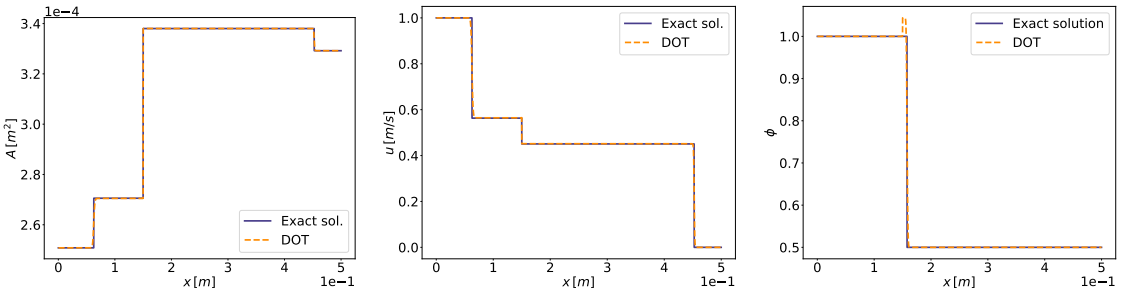

(c) $\alpha = 4/3$

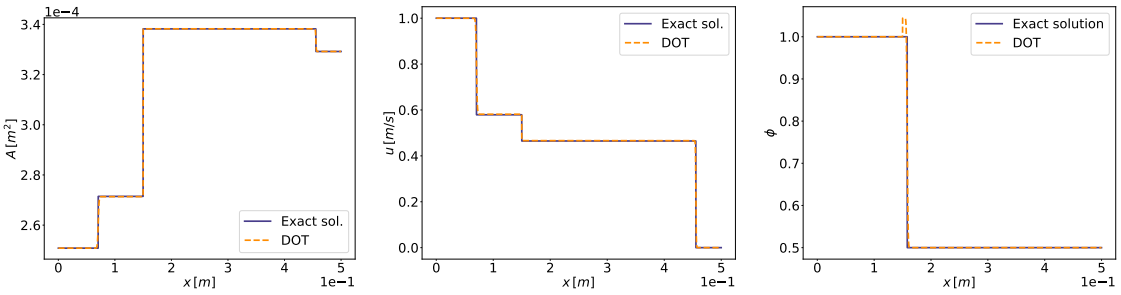

(d) $\alpha = 2$

Figure 2.20: Test 7. Artery. Left shock - stationary contact - contact discontinuity for the passive scalar - right shock. Exact solution of the Riemann problem with $\alpha = 1$, $\alpha = 11/10$, $\alpha = 4/3$, $\alpha = 2$ against DOT Riemann solver. Initial data are in Tables 2.7, 2.8.

Test 8. Exact solution of the Riemann problem with $\alpha \in [1, 2]$

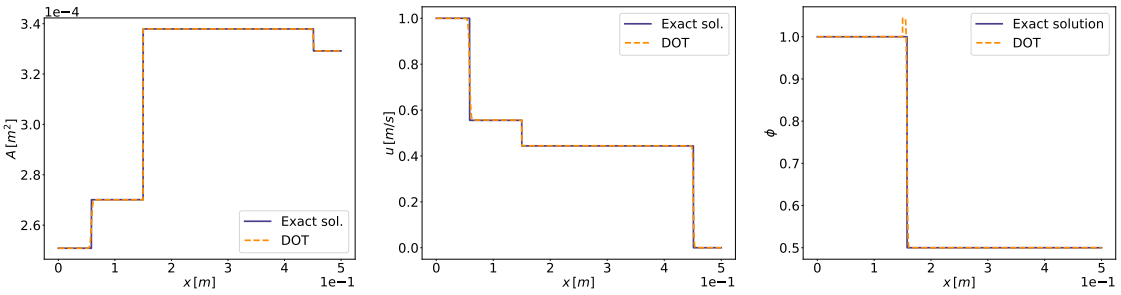

(a) $\alpha = 1$

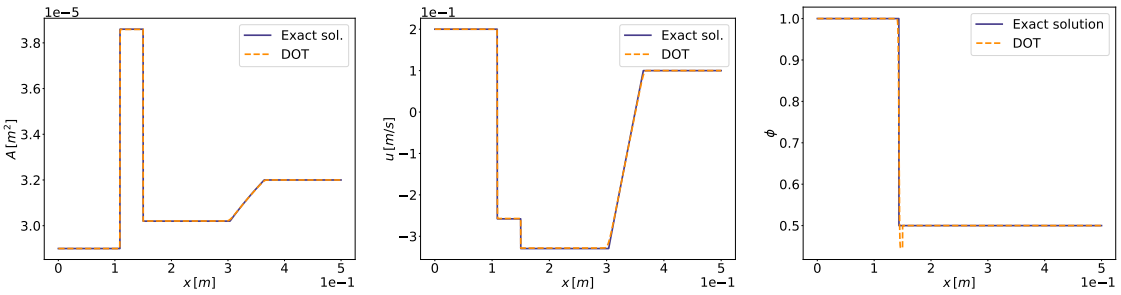

(b) $\alpha = 11/10$

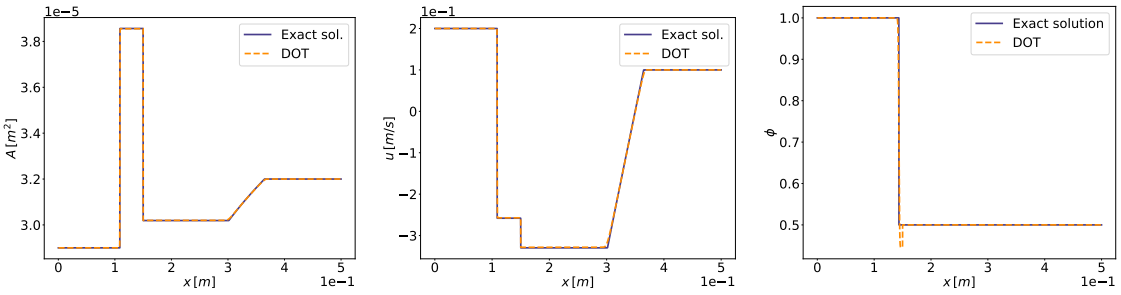

(c) $\alpha = 4/3$

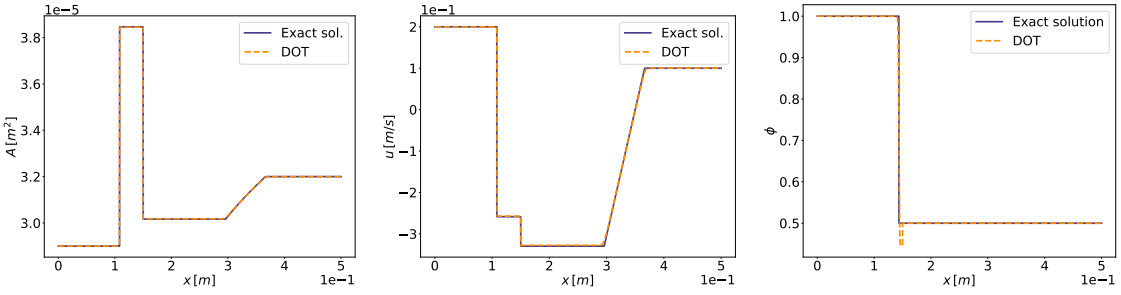

(d) $\alpha = 2$

Figure 2.21: Test 8. Vein. Left shock - contact discontinuity for the passive scalar - stationary contact - right rarefaction. Exact solution of the Riemann problem with $\alpha = 1$, $\alpha = 1.1$, $\alpha = 4/3$, $\alpha = 2$ against DOT Riemann solver. Initial data are in Tables 2.7, 2.8.

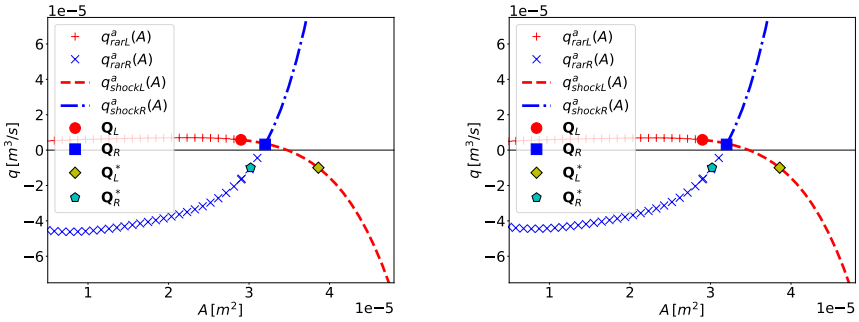

(a) $\alpha = 1$ (b) $\alpha = 1.1$

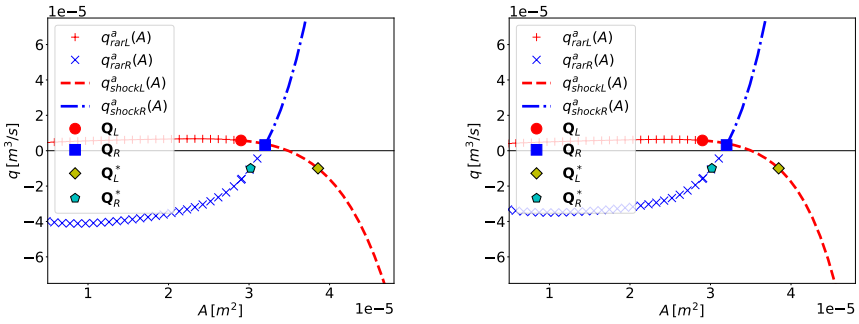

(c) $\alpha = 4/3$ (d) $\alpha = 2$

Figure 2.22: A detail of the graphic representations of the solutions in the (A, q) phase-plane for data of Test 8 in Tables 2.7, 2.8, for $\alpha = 1$, $\alpha = 1.1$, $\alpha = 4/3$ and $\alpha = 2$.

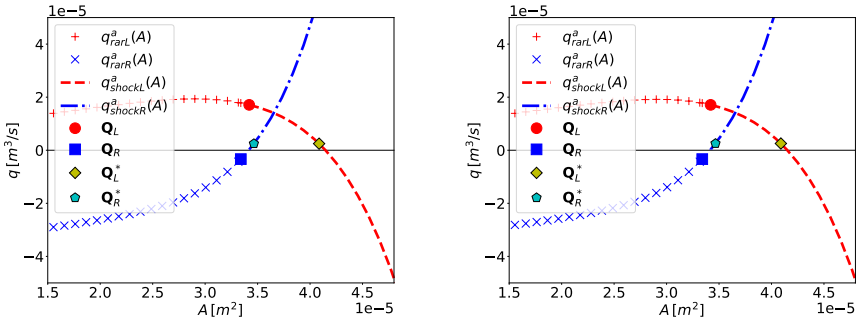

(a) $\alpha = 1$ (b) $\alpha = 1.1$

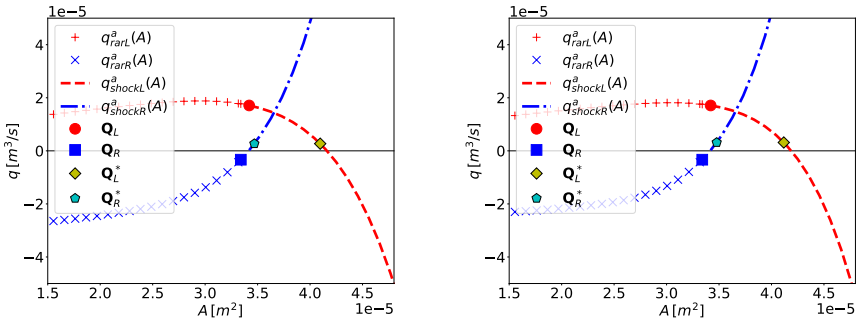

(c) $\alpha = 4/3$ (d) $\alpha = 2$

Figure 2.23: A detail of the graphic representations of the solutions in the (A, q) phase-plane for data of Test 9 in Tables 2.7, 2.8, for $\alpha = 1$, $\alpha = 1.1$, $\alpha = 4/3$ and $\alpha = 2$.

Test 9. Exact solution of the Riemann problem with $\alpha \in [1, 2]$

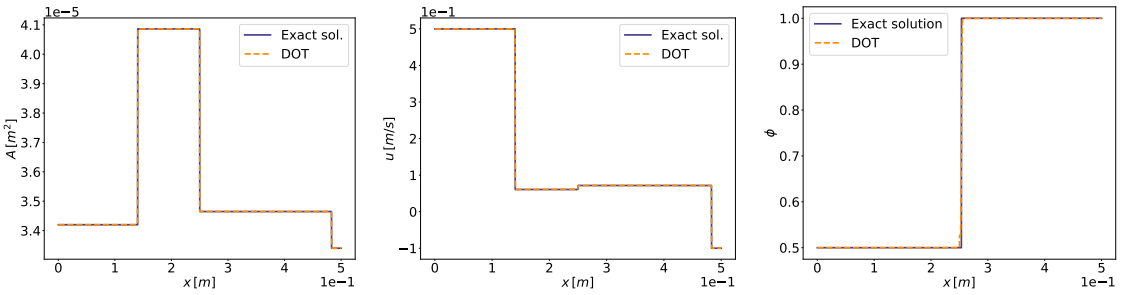

(a) $\alpha = 1$

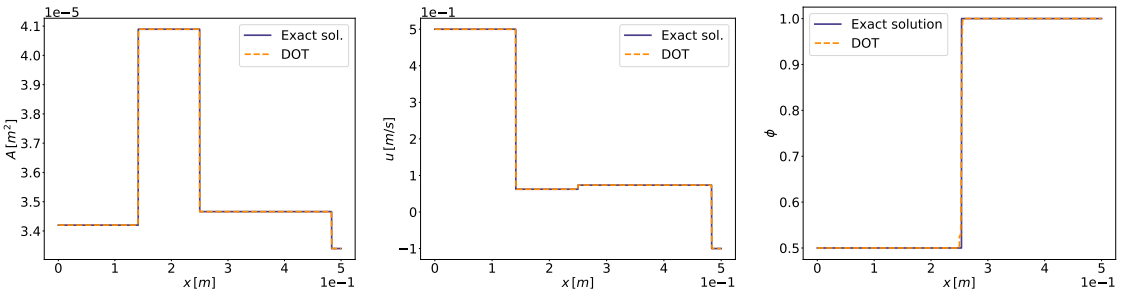

(b) $\alpha = 11/10$

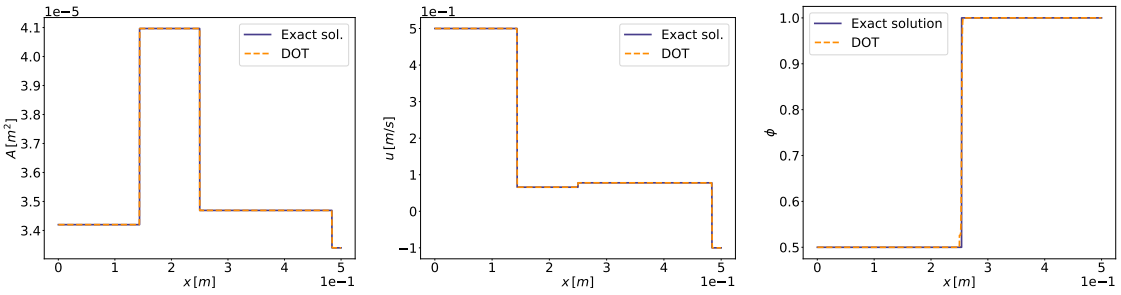

(c) $\alpha = 4/3$

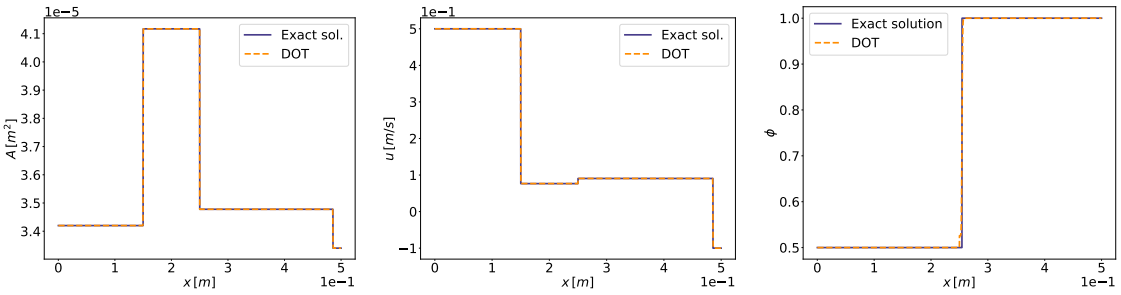

(d) $\alpha = 2$

Figure 2.24: Test 9. Vein. Left shock - stationary contact - contact discontinuity for the passive scalar -right shock. Exact solution of the Riemann problem with $\alpha = 1$, $\alpha = 1.1$, $\alpha = 4/3$, $\alpha = 2$ against DOT Riemann solver. Initial data are in Tables 2.7, 2.8.

Test 10. Exact solution of the Riemann problem with $\alpha \in [1, 2]$

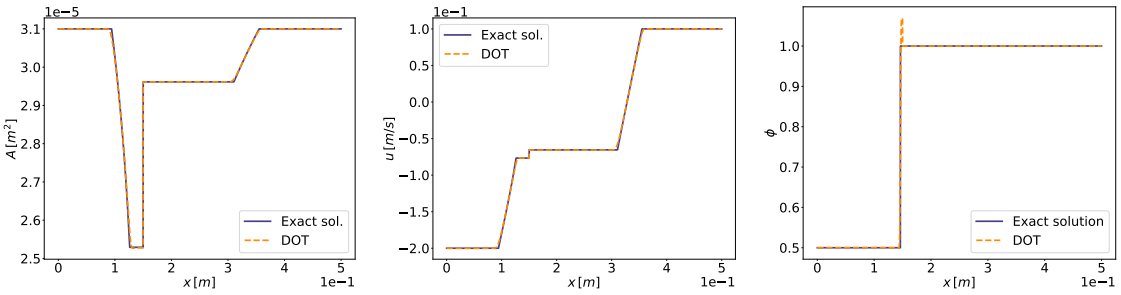

(a) $\alpha = 1$

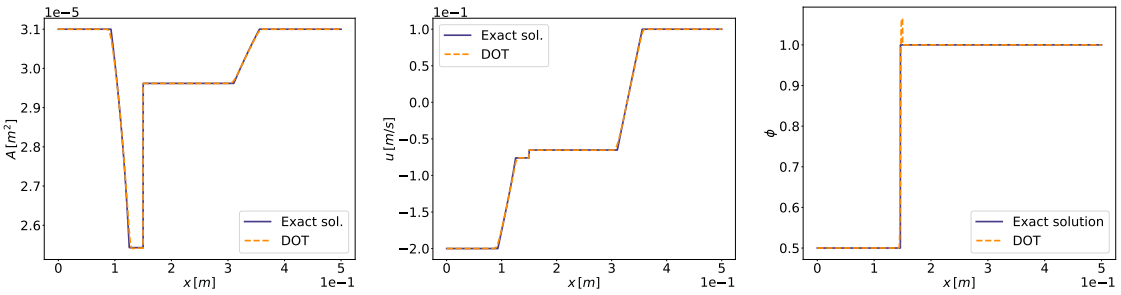

(b) $\alpha = 11/10$

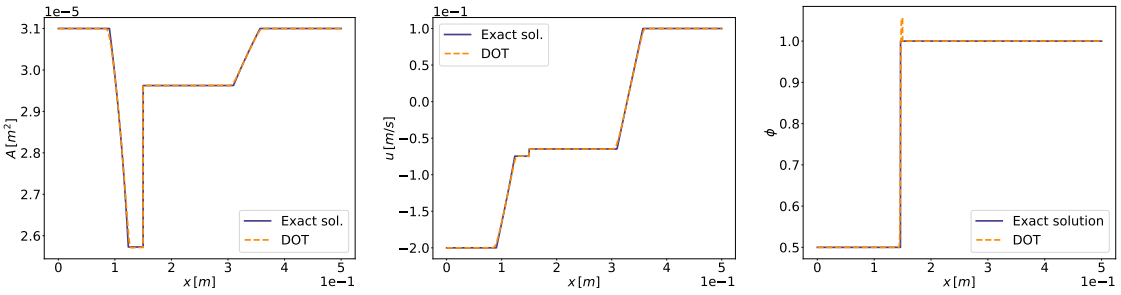

(c) $\alpha = 4/3$

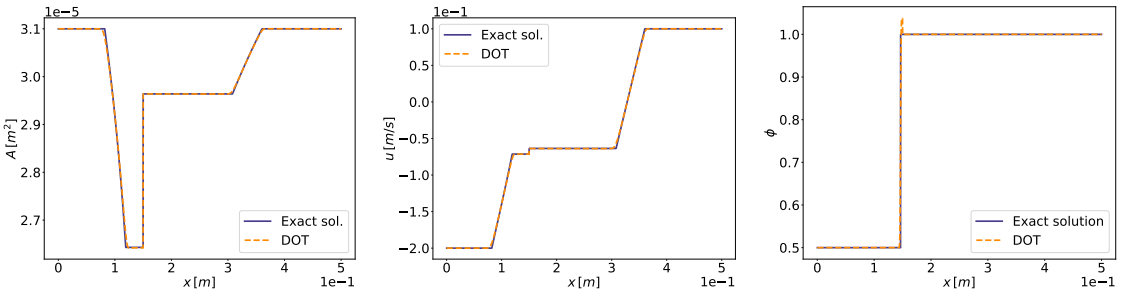

(d) $\alpha = 2$

Figure 2.25: Test 10. Vein. Left rarefaction - contact discontinuity for the passive scalar - stationary contact - right rarefaction. Exact solution of the Riemann problem with $\alpha = 1$, $\alpha = 1.1$, $\alpha = 4/3$, $\alpha = 2$ against DOT Riemann solver.Initial data are in Tables 2.7, 2.8.

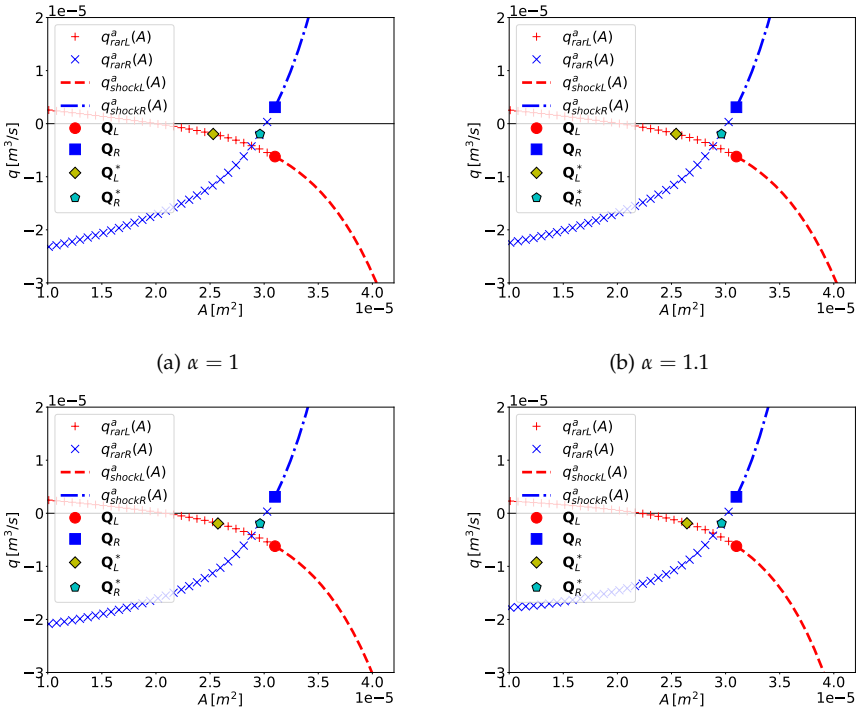

(a) $\alpha = 1$

(b) $\alpha = 1.1$

(c) $\alpha = 4/3$

(d) $\alpha = 2$

Figure 2.26: A detail of the graphic representations of the solutions in the (A, q) phase-plane for data of Test 10 in Tables 2.7, 2.8, for $\alpha = 1$, $\alpha = 1.1$, $\alpha = 4/3$ and $\alpha = 2$.

Comparison of the exact solutions for different momentum correction coefficients α

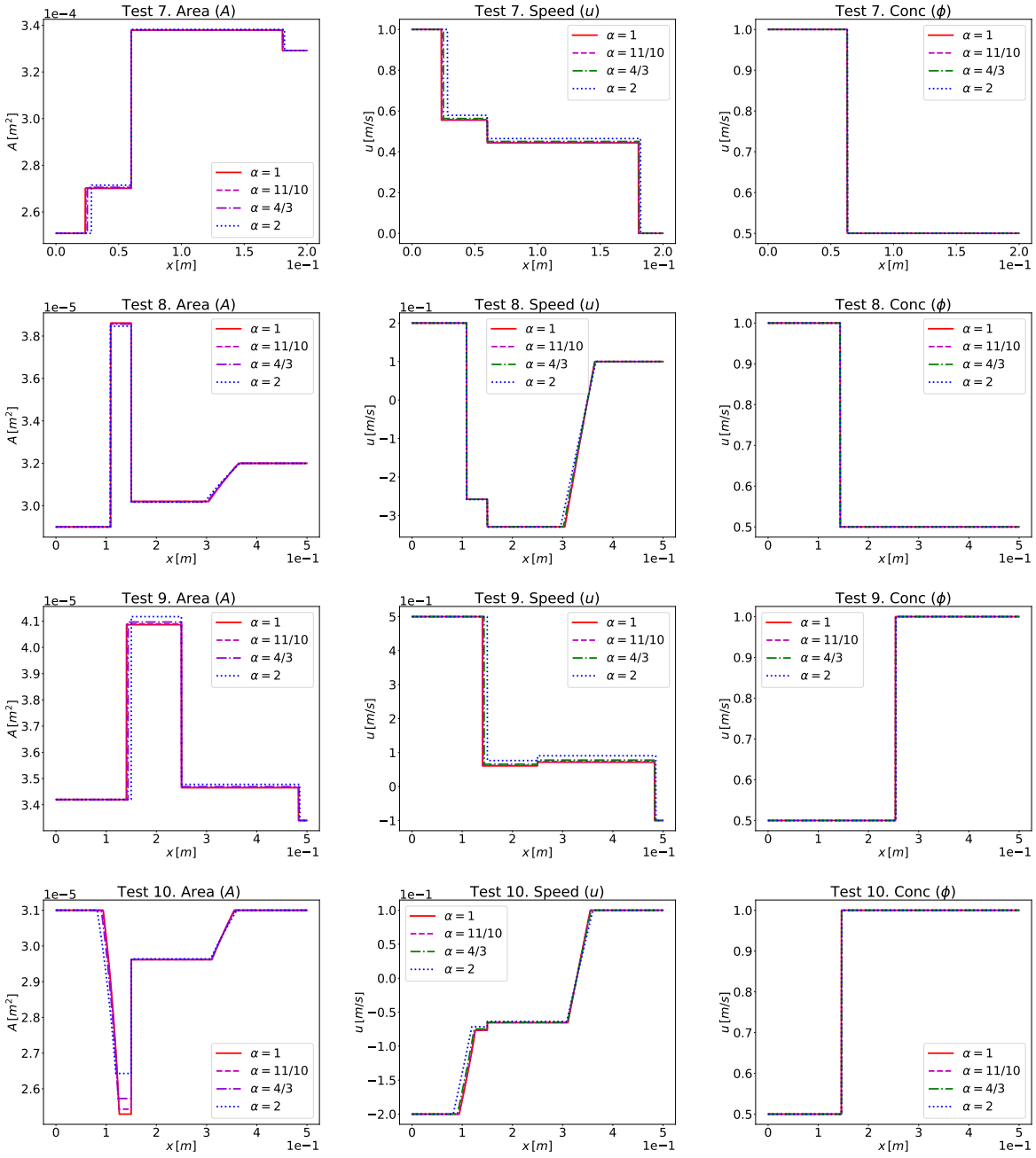

Figure 2.27: Comparison of the exact solutions for different α of some of the Tests considered in Tables 2.7, 2.8.

2.3 Conclusions

In this Chapter we have presented the exact solution of the Riemann problem for the 1D blood flow equations with continuous and discontinuous parameters with a constant momentum correction coefficient $\alpha \in [1,2]$ in the case of arteries and veins. The momentum correction coefficient in the 1D blood flow models is related to the velocity profile: for example $\alpha = 1$ corresponds to a flat velocity profile, i.e. to an inviscid fluid, $\alpha = 4/3$ is related to a parabolic velocity profile. This exact solution already exists in literature but only for a momentum correction coefficient $\alpha = 1$. We have given a detailed mathematical analysis for the case of $\alpha \in [1,2]$, although limiting our discussion to the subsonic regime in case of discontinuous parameters, describing the relations across each wave pattern, i.e.: rarefactions, elastic jumps (shocks), and contact discontinuities, and we have given a condition of physical admissibility of shocks and rarefactions in waves associated with genuinely non-linear fields. Finally we have added a graphic interpretation of the results. After, we have presented a simple and efficient numerical procedure to compute the constructed exact solution, following the methodology of [87], [90], [81]; adapting it for $\alpha \in [1,2]$. The obtained exact solution has then been verified against FORCE [88], first order, conservative, centred numerical scheme, for the case of continuous parameters (conservative hyperbolic system of PDEs) and DOT Riemann solver [23], first order, path-conservative numerical scheme, for the case of discontinuous parameters (non-conservative hyperbolic system of PDEs). The DOT solver has been adapted for the case of a momentum correction coefficient $\alpha \in [1,2]$ and the well-balanced properties have been proved analitically also in this case.

It is worth noticing that the goal of our work was to describe the exact solution of a Riemann problem, and to then validate the numerical solution strategy by comparing the exact solution to numerical solutions obtained using centered numerical schemes. Therefore, the relevance of our work lies in providing reference solutions for the construction of numerical solvers, as well as in laying the ground for the determination of boundary and coupling conditions for blood flow in networks of one-dimensional domains. Importantly, we have not assessed the efficiency of the proposed solver in the context of Godunov-type schemes. While this will be the subject of future work, we can anticipate that it is highly unlikely that the exact solver will turn out to be an efficient alternative, especially because of the lack of an explicit formulation of generalized Riemann invariants.

Chapter 3

Advection-Pressure splitting at the level of PDEs

In this Chapter we present the actual advection-pressure splitting we propose for the complete system of hyperbolic 1D blood flow equations described in Chapter 2, both for the case of continuous parameters (Section 2.1) and for the case of discontinuous parameters (Section 2.2). This is a modification of the flux splitting approach introduced in Toro and Vázquez [92] for the Euler equations. Following this method the original complete system of 1D blood flow equations is split into two hyperbolic subsystems of PDEs: the advection system and the pressure one, both showing a simpler eigenstructure with respect to the complete system. As described in the Introduction to this Thesis, this turns out to be advantageous when dealing with coupling conditions in large networks of vessels.

In both conservative and non-conservative cases the flux of the continuity equation is assigned to the pressure system, differently from the TV approach. The decision is influenced by the alignment with zero-dimensional models and the absence of hyperbolicity in the subsystems of PDEs that arises conversely.

It is worth noting that the expression *advection-pressure* is a more general way to refer to flux vector splitting methods, this latter name suitable only for conservative 1D blood flow models (i.e. the particular models with continuous mechanical and geometrical properties).

In Section 3.1 we present the flux splitting at the level of PDEs for the conservative 1D blood flow model with transport described in Section 2.1, while in Section 3.2 we present the advection-pressure splitting for the non-conservative 1D blood flow model with transport depicted in Section 2.2.

This Chapter is partially presented in Toro et al. [91] and in Spilimbergo et al. [83].

3.1 Splitting for the conservative 1D blood flow model with transport

Given the conservative hyperbolic system of PDEs

$$\partial_t \mathbf{Q} + \partial_x \mathbf{F}(\mathbf{Q}) = \mathbf{0}, \tag{3.1}$$

defined in (2.12), we split $\mathbf{F}(\mathbf{Q})$ in (2.13) into the sum of advection and pressure fluxes as follows

$$\mathbf{F}(\mathbf{Q}) = \mathcal{A}(\mathbf{Q}) + \mathcal{P}(\mathbf{Q}), \tag{3.2}$$

and we propose to split system (2.12) via (3.2) into the two subsystems

$$\begin{cases} \partial_t \mathbf{Q} + \partial_x \boldsymbol{\mathcal{A}}(\mathbf{Q}) = \mathbf{0}, & (3.3) \\ \partial_t \mathbf{Q} + \partial_x \boldsymbol{\mathcal{P}}(\mathbf{Q}) = \mathbf{0}, & (3.4) \end{cases}$$

where

$$\begin{aligned} \mathbf{Q} = \begin{bmatrix} A \\ Au \\ A\phi \end{bmatrix}, \qquad \boldsymbol{\mathcal{A}}(\mathbf{Q}) = \begin{bmatrix} 0 \\ \alpha A u^2 \\ Au\phi \end{bmatrix}, \\ \boldsymbol{\mathcal{P}}(\mathbf{Q}) = \begin{bmatrix} Au \\ \int c(A)^2 \, dA \\ 0 \end{bmatrix} = \begin{bmatrix} Au \\ \frac{KA}{\rho} \left(\frac{m}{m+1} \left(\frac{A}{A_0} \right)^m - \frac{n}{n+1} \left(\frac{A}{A_0} \right)^n \right) \\ 0 \end{bmatrix}. \end{aligned} \tag{3.5}$$

System (3.3) is called "advection system", system (3.4) is called "pressure system". As it will be presented in Chapter 6, the aim is to compute a numerical flux

$$\mathbf{F}_{i+\frac{1}{2}} = \boldsymbol{\mathcal{A}}_{i+\frac{1}{2}} + \boldsymbol{\mathcal{P}}_{i+\frac{1}{2}}, \tag{3.6}$$

The numerical strategy to determine the advection and pressure numerical fluxes $\boldsymbol{\mathcal{A}}_{i+\frac{1}{2}}$ and $\boldsymbol{\mathcal{P}}_{i+\frac{1}{2}}$ in (3.6) relies on first solving the Riemann problem for the pressure system in (3.4). The solution of this system will fully determine the pressure numerical flux $\boldsymbol{\mathcal{P}}_{i+\frac{1}{2}}$ and will also provide the information for determining the advection numerical flux $\boldsymbol{\mathcal{A}}_{i+\frac{1}{2}}$ (Chapters 6, 7).

3.2 SPLITTING FOR THE NON-CONSERVATIVE 1D BLOOD FLOW MODEL WITH TRANSPORT

Given the non-conservative hyperbolic system of PDEs

$$\partial_t \mathbf{Q} + \mathbf{M}(\mathbf{Q}) \partial_x \mathbf{Q} = \mathbf{0} \tag{3.7}$$

defined in (2.181), we split $\mathbf{M}(\mathbf{Q})$ in (2.182) into the sum of an advection and a pressure matrix as follows

$$\mathbf{M}(\mathbf{Q}) = \boldsymbol{\mathcal{A}}(\mathbf{Q}) + \boldsymbol{\mathcal{P}}(\mathbf{Q}), \tag{3.8}$$

and we propose to split system (2.181) via (3.8) into the two subsystems

$$\begin{cases} \partial_t \mathbf{Q} + \boldsymbol{\mathcal{A}}(\mathbf{Q}) \partial_x \mathbf{Q} = \mathbf{0}, & (3.9) \\ \partial_t \mathbf{Q} + \boldsymbol{\mathcal{P}}(\mathbf{Q}) \partial_x \mathbf{Q} = \mathbf{0}, & (3.10) \end{cases}$$

where

$$\mathbf{Q} = \begin{bmatrix} A \\ Au \\ K \\ A_0 \\ p_e \\ A\phi \end{bmatrix}, \quad \mathcal{A}(\mathbf{Q}) = \begin{bmatrix} 0 & 0 & 0 & 0 & 0 & 0 \\ -\alpha u^2 & 2\alpha u & 0 & 0 & 0 & 0 \\ 0 & 0 & 0 & 0 & 0 & 0 \\ 0 & 0 & 0 & 0 & 0 & 0 \\ 0 & 0 & 0 & 0 & 0 & 0 \\ -u\phi & \phi & 0 & 0 & 0 & u \end{bmatrix},$$
$$\boldsymbol{\mathcal{P}}(\mathbf{Q}) = \begin{bmatrix} 0 & 1 & 0 & 0 & 0 & 0 \\ c^2 & 0 & \frac{A}{\rho}\psi_K & \frac{A}{\rho}\psi_{A_0} & \frac{A}{\rho} & 0 \\ 0 & 0 & 0 & 0 & 0 & 0 \\ 0 & 0 & 0 & 0 & 0 & 0 \\ 0 & 0 & 0 & 0 & 0 & 0 \\ 0 & 0 & 0 & 0 & 0 & 0 \end{bmatrix}. \tag{3.11}$$

where c is the *wave speed* (2.183). System (3.9) is called *advection system*, system (3.10) is called *pressure system*. The aim is to build a numerical scheme from the solution of the Riemann problem for the pressure systems (3.10). This solution will fully determine the different part of the final numerical scheme.

Chapter 4

Exact solution of the Riemann problem for the 1D advection system with general constant momentum correction coefficient without transport

In this Chapter we solve exactly the Riemann problem for the advection system arising in the advection-pressure splitting for conservative 1D blood flow models presented in Chapter 3.1, and for non-conservative 1D blood flow models described in Chapter 3.2, for tube laws describing arteries and veins with a constant momentum correction coefficient different from one without considering the passive scalar transport equation. The resulting system is a hyperbolic system of conservation laws both in case of continuous or discontinuous parameters. We give a detailed mathematical analysis and a numerical procedure to compute the resulting solution. Finally we further verify the obtained mathematical results against a second order extension of FORCE numerical scheme.

In detail: in Section 4.1, we present exact solution of the Riemann problem for the advection system generated from the splitting of the conservative 1D blood flow equations, in Section 4.2 the one arising from the splitting of the non-conservative one. In Section 4.3 the conclusions are drawn.

The research article regarding this topic is in preparation.

4.1 Exact solution of the Riemann problem for the advection system

The advection system is

$$\begin{cases} \partial_t A = 0, \\ \partial_t (Au) + \alpha \partial_x (Au^2) = 0, \end{cases} \tag{4.1}$$

i.e

$$\partial_t \mathbf{Q} + \partial_x \mathcal{A}(\mathbf{Q}) = \mathbf{0}, \tag{4.2}$$

with

$$\mathbf{Q} = \begin{bmatrix} A(x,t) \\ Au(x,t) \end{bmatrix}, \quad \mathcal{A}(\mathbf{Q}) = \begin{bmatrix} 0 \\ \alpha Au^2 \end{bmatrix}, \tag{4.3}$$

where $A(x,t)$ is the cross-sectional area of the vessel, $u(x,t)$ is the blood speed, α is the momentum correction coefficient, constant, considered $\alpha \in [1,2]$.

The Jacobian of (4.2) is

$$\widehat{\mathcal{A}}(\mathbf{Q}) = \begin{bmatrix} 0 & 0 \\ -\alpha u^2 & 2\alpha u \end{bmatrix}, \tag{4.4}$$

The eigenvalues of $\widehat{\mathcal{A}}$ are all real and given by

$$\lambda_{\mathcal{A}1} = 2\alpha u \qquad \lambda_{\mathcal{A}2} = 0. \tag{4.5}$$

A possible choice of right eigenvectors corresponding to eigenvalues (4.5) is

$$\mathbf{R}_{\mathcal{A}1} = \begin{bmatrix} 0 \\ 1 \end{bmatrix}, \qquad \mathbf{R}_{\mathcal{A}2} = \begin{bmatrix} 1 \\ \frac{u}{2} \end{bmatrix}. \tag{4.6}$$

Proposition 4.1.1 (Hyperbolicity). *System (4.1) is hyperbolic* $\forall \mathbf{Q} \in \Omega = [\mathbb{R}^+ \times \mathbb{R}]$.

Proof. It is straightforward to see that eigenvalues (4.5) are always real and eigenvectors (4.6) are linearly independent in the entire domain Ω. System (4.1) however, is not strictly hyperbolic since for $u = 0$ the two eigenvalues (4.5) are the same. □

Proposition 4.1.2 (Nature of $\lambda_{\mathcal{A}1}$-characteristic field). *The $\lambda_{\mathcal{A}1}$-characteristic field is genuinely non-linear* $\forall \mathbf{Q} \in \Omega$.

Proof. It can be easily verified that

$$\nabla \lambda_{\mathcal{A}1}(\mathbf{Q}) \cdot \mathbf{R}_{\mathcal{A}1}(\mathbf{Q}) = \frac{2\alpha}{A} > 0 \quad \forall \mathbf{Q} \in \Omega. \tag{4.7}$$

□

Proposition 4.1.3 (Nature of $\lambda_{\mathcal{A}2}$-characteristic field). *The $\lambda_{\mathcal{A}2}$-characteristic field is linearly degenerate* $\forall \mathbf{Q} \in \Omega$.

Proof. It can be easily verified that

$$\nabla \lambda_{\mathcal{A}2}(\mathbf{Q}) \cdot \mathbf{R}_{\mathcal{A}2}(\mathbf{Q}) = 0 \quad \forall \mathbf{Q} \in \Omega. \tag{4.8}$$

□

The Riemann problem for system (4.2) is

$$\begin{cases} \partial_t \mathbf{Q} + \partial_x \mathcal{A}(\mathbf{Q}) = \mathbf{0}, \quad x \in \mathbb{R}, \quad t > 0, \\ \mathbf{Q}(x,0) = \begin{cases} \mathbf{Q}_L & \text{if} \quad x < x_d, \\ \mathbf{Q}_R & \text{if} \quad x > x_d, \end{cases} \end{cases} \tag{4.9}$$

where $x_d \in \mathbb{R}$ is the initial discontinuity of the data

$$\mathbf{Q}_L = \begin{bmatrix} A_L \\ Au_L \end{bmatrix}, \qquad \mathbf{Q}_R = \begin{bmatrix} A_R \\ Au_R \end{bmatrix}. \tag{4.10}$$

There are three possible configuration of the solution in the (x,t) half-plane, as shown in Fig. 4.1. As will be proved in this Chapter, the actual formula for $\mathbf{Q}^*_{\mathcal{A}}$ varies according to the "position" to the left or to the right of the $\lambda_{\mathcal{A}2}$ discontinuity in Fig. 4.1, or in case the two waves are superimposed (Case 3 of Fig. 4.1). To build the final exact solution we adopt the scheme in Fig. 4.2, i.e. we pretend to have two fake unknowns

$$\mathbf{Q}^*_{\mathcal{A}L} = \begin{bmatrix} A^*_L \\ Au^*_L \end{bmatrix}, \qquad \mathbf{Q}^*_{\mathcal{A}R} = \begin{bmatrix} A^*_R \\ Au^*_R \end{bmatrix}, \tag{4.11}$$

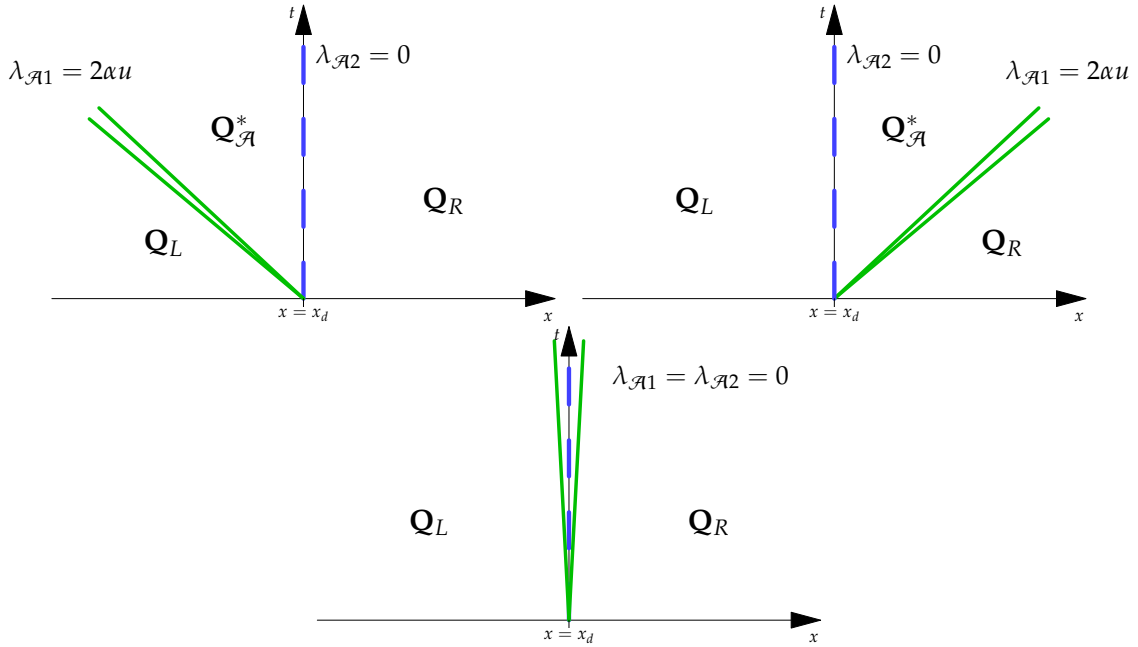

Figure 4.1: The three possible configurations of the solution of Riemann problem (4.9). The green solid lines represent the wave associated with the genuinely non-linear field, that can be either a shock or a rarefaction, the blue dashed line is the contact discontinuity associated with the linearly degenerate field. The top-left picture depicts the case of $\lambda_{\mathcal{A}1} < 0$, the top-right one the case $\lambda_{\mathcal{A}1} > 0$ and the bottom picture the case $\lambda_{\mathcal{A}1} = \lambda_{\mathcal{A}2} = 0$. The last case presents a not trivial configuration of the solution and will be treated in Section 4.1.4.

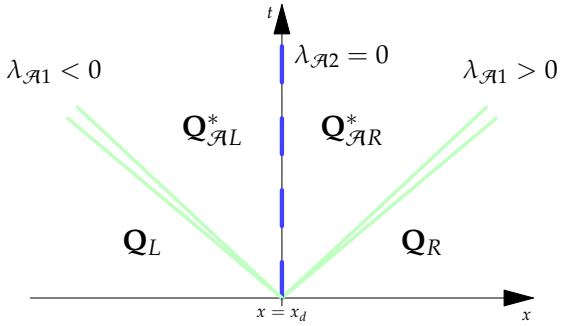

Figure 4.2: The theoretical approach we use in this Chapter to calculate the unknown $\mathbf{Q}^*_{\mathcal{A}}$. We suppose to have two "virtual" unknowns $\mathbf{Q}^*_{\mathcal{A}L}$ and $\mathbf{Q}^*_{\mathcal{A}R}$ that are supposed to exist in any case of Fig. 4.1, clearly with different values. The green solid lines are now lighter than in Fig. 4.1 because we don't know a priori in which position the *one and only* $\lambda_{\mathcal{A}1}$ wave actually is. In this Chapter we name *left part* the part of the (x,t) plane that is *to the left* of the $\lambda_{\mathcal{A}2}$ discontinuity, *right part* the part of the (x,t) plane that is *to the right* of the $\lambda_{\mathcal{A}2}$ discontinuity.

to which finally we will assign the proper value according to the position of the $\lambda_{\mathcal{A}1}$ wave, as explained in Section 4.1.5.

Before describing the relations across each wave, necessary for the exact solution of the Riemann problem, we present this result

Proposition 4.1.4. *For the Riemann problem* (4.9)

$$A^*_L = A_L, \quad A^*_R = A_R, \tag{4.12}$$

regardless of the type of wave.

Proof. Considering that, for the first of (4.1)

$$\partial_t A = 0, \tag{4.13}$$

i.e

$$A = const, \quad \forall t \in \mathbb{R}_0^+, \tag{4.14}$$

it is clear that given a discontinuous initial condition for A

$$A(x,0) = \begin{cases} A_L & \text{for} \quad x < x_d, \\ A_R & \text{for} \quad x > x_d, \end{cases} \tag{4.15}$$

results

$$A(x,t) = A(x,0), \quad \forall x \in \mathbb{R}, \quad \forall t \in \mathbb{R}_0^+, \tag{4.16}$$

in other words

$$A_L^* = A_L, \qquad A_R^* = A_R. \tag{4.17}$$

□

4.1.1 Wave relations for the case $\lambda_{\mathcal{A}1} \neq 0$

In this Section we propose the relations across the waves presented before in case the genuinely non-linear one and the contact discontinuity are not superimposed (Cases 1 and 2 of Fig. 4.1).

Proposition 4.1.5 (Generalized Riemann invariants for the $\lambda_{\mathcal{A}1}$ - characteristic field)**.** *The Riemann invariants for the $\lambda_{\mathcal{A}1} = 2\alpha u \neq 0$ characteristic field, are given by*

$$A = const, \qquad q \neq const \tag{4.18}$$

i.e.

$$A = const, \qquad u \neq const \tag{4.19}$$

for the $\lambda_{\mathcal{A}1}$ -characteristic field.

Proof. The Riemann invariants are the solution of the following ODE [90]

$$\frac{dA}{0} = \frac{dq}{1}. \tag{4.20}$$

From $dA = 0$ we have $A = const$ and being $dq \neq const$ we have $u \neq const$. □

Proposition 4.1.6 (Shock speed)**.** *The shock speed is*

$$S_j = \frac{\alpha}{A_j}(q_j^* + q_j) = \alpha(u_j^* + u_j), \quad j = L, R. \tag{4.21}$$

Proof. Being the actual system (4.1), we recall that if a discontinuity propagating with speed S has constant values $\widehat{\mathbf{Q}}$, $\widetilde{\mathbf{Q}}$ on either side of the discontinuity, then the Rankine-Hugoniot jump condition

$$\mathcal{A}(\widehat{\mathbf{Q}}) - \mathcal{A}(\widetilde{\mathbf{Q}}) = S_j(\widehat{\mathbf{Q}} - \widetilde{\mathbf{Q}}), \tag{4.22}$$

must hold, with $\mathcal{A}$ in (4.3) (see for example [44]). So, considering Fig. 4.2, (4.22) becomes

$$\mathcal{A}(\mathbf{Q}_{\mathcal{A}j}^*) - \mathcal{A}(\mathbf{Q}_j) = S_j(\mathbf{Q}_{\mathcal{A}j}^* - \mathbf{Q}_j), \quad j = L, R. \tag{4.23}$$

(4.23) becomes

$$\begin{cases} 0 = S_j(A_j^* - A_j), \\ \alpha \dfrac{q_j^{2*}}{A_j^*} - \alpha \dfrac{q_j^2}{A_j} = S_j(q_j^* - q_j). \end{cases} \tag{4.24}$$

For Proposition 4.1.4 system (4.24) becomes

$$\begin{cases} 0 = 0, \\ \alpha \dfrac{q_j^{2*}}{A_j} - \alpha \dfrac{q_j^2}{A_j} = S_j(q_j^* - q_j), \end{cases} \tag{4.25}$$

from which we obtain the results for the shock speed

$$S_j = \frac{\alpha}{A_j}(q_j^* + q_j) = \alpha(u_j^* + u_j), \quad j = L, R. \tag{4.26}$$

Clearly, having one and only shock wave, formula (4.26) becomes

$$S = \alpha(u^* + u_j), \tag{4.27}$$

where u_j is initial value of u to the side of the actual shock, side that is still unknown. The same for the actual side of u^* and its value. An explicit formula for u^* will be given later. □

Proposition 4.1.7 (Generalized Riemann invariants for the $\lambda_{\mathcal{A}2}$ - characteristic field. Case $\lambda_{\mathcal{A}1} \neq 0$)**.** *The generalized Riemann invariants for the $\lambda_{\mathcal{A}2}$- contact discontinuity, with $\lambda_{\mathcal{A}1} \neq 0$, are given by*

$$A \neq const, \qquad ln(|u|) + \frac{1}{2} ln(A) = const. \tag{4.28}$$

Proof. Applying the generalized Riemann invariants method [90] to the $\lambda_{\mathcal{A}2}$-wave and to the related right eigenvector we obtain

$$\frac{dA}{1} = \frac{d(Au)}{\frac{u}{2}}, \tag{4.29}$$

i.e.

$$\frac{u}{2} dA = d(Au) \rightarrow A du + \frac{u}{2} dA = 0, \tag{4.30}$$

via separation of variables,

$$\frac{1}{u} du = -\frac{1}{2A} dA, \tag{4.31}$$

integrating,

$$\int \frac{1}{u} du = -\frac{1}{2} \int \frac{1}{A} dA, \tag{4.32}$$

and consequently we obtain the second of (4.28), being $A > 0$ by hypothesis. □

4.1.2 Solution in the Star Region in case of $\lambda_{\mathcal{A}1} \neq 0$

Being the Star Region, as usual, the region in the (x, t) plane included between the $\lambda_{\mathcal{A}1}$ and the $\lambda_{\mathcal{A}2}$ wave, we obtain the following results.

Proposition 4.1.8 (Definition of u^* under certain conditions). *In case of $\lambda_{\mathcal{A}1} \neq 0$, i.e. $u^* \neq 0$, u^* is defined as*

$$u^* = \begin{cases} u_R^* = \sqrt{\dfrac{A_L}{A_R}}|u_L| \quad \text{with } u_L > 0 \qquad \text{if} \quad \lambda_{\mathcal{A}1} > 0, \\ u_L^* = -\sqrt{\dfrac{A_R}{A_L}}|u_R| \quad \text{with } u_R < 0 \quad \text{if} \quad \lambda_{\mathcal{A}1} < 0, \end{cases} \tag{4.33}$$

either in case of rarefaction or shock in the $\lambda_{\mathcal{A}1}$-wave.

Proof. Using what stated in Proposition 4.1.7, across $\lambda_{\mathcal{A}2} = 0$ discontinuity we have

$$\int \frac{1}{u} du = -\frac{1}{2} \int \frac{1}{A} dA. \tag{4.34}$$

Considering Fig. 4.2 and carrying out the calculations, (4.34) becomes

$$\int_{u_L^*}^{u_R^*} \frac{1}{u} du = -\frac{1}{2} \int_{A_L^*}^{A_R^*} \frac{1}{A} dA. \tag{4.35}$$

For Proposition 4.1.4, (4.35) becomes

$$\int_{u_L^*}^{u_R^*} \frac{1}{u} du = -\frac{1}{2} \int_{A_L}^{A_R} \frac{1}{A} dA. \tag{4.36}$$

Now we consider some cases

1. $\lambda_{\mathcal{A}1} > 0$
   In this case as shown in Fig. (4.2), the $\lambda_{\mathcal{A}1}$- wave lays to the right of the discontinuity. It follows that $\mathbf{Q}_{\mathcal{A}R}^* = \mathbf{Q}_{\mathcal{A}}^*$, i.e. is the real $\mathbf{Q}_{\mathcal{A}}^*$, instead $\mathbf{Q}_{\mathcal{A}L}^*$ does not actually exist. It is straightforward to put $\mathbf{Q}_{\mathcal{A}L}^* = \mathbf{Q}_L$ for computational simplicity. It follows that $u_R^* = u^*$, while $u_L^* = u_L$:

   $$\int_{u_L}^{u_R^* = u^*} \frac{1}{u} du = -\frac{1}{2} \int_{A_L}^{A_R} \frac{1}{A} dA. \tag{4.37}$$

   Now considering that

   $$\lambda_{\mathcal{A}1} = 2\alpha u^* > 0 \Rightarrow u^* = u_R^* > 0, \tag{4.38}$$

   and considering that function $\dfrac{1}{u}$ presents a vertical asymptote for $u = 0$, it is clear that in this case we can only consider $u_R^* > 0$ and $u_L > 0$.
   So (4.37) becomes

   $$ln(u_R^*) - ln(u_L) = -\frac{1}{2}(ln(A_R) - ln(A_L)) \longrightarrow \frac{u_R^*}{u_L} = \sqrt{\frac{A_L}{A_R}}. \tag{4.39}$$

   So in conclusion, if $\lambda_{\mathcal{A}1} > 0$

   $$u_L^* = u_L > 0, \qquad u_R^* = u^* = \sqrt{\frac{A_L}{A_R}} u_L = \sqrt{\frac{A_L}{A_R}} |u_L|, \tag{4.40}$$

   either if $u_R^* > u_L$ or $u_R^* < u_L$.

2. $\lambda_{\mathcal{A}1} < 0$
   In this case according to Fig. (4.2), the $\lambda_{\mathcal{A}1}$- wave lays to the left of the discontinuity. It

follows that $\mathbf{Q}^*_{\mathcal{A}L} = \mathbf{Q}^*_{\mathcal{A}}$, i.e. is the real $\mathbf{Q}^*_{\mathcal{A}}$, instead $\mathbf{Q}^*_{\mathcal{A}R}$ does not actually exist. It is straightforward to put $\mathbf{Q}^*_{\mathcal{A}R} = \mathbf{Q}_R$ for computational simplicity. It follows that $u^*_L = u^*$, while $u^*_R = u_R$:

$$\int_{u^*_L = u^*}^{u_R} \frac{1}{u} du = -\frac{1}{2} \int_{A_L}^{A_R} \frac{1}{A} dA. \tag{4.41}$$

Now considering that

$$\lambda_{\mathcal{A}1} = 2\alpha u^* < 0 \Rightarrow u^* = u^*_L < 0, \tag{4.42}$$

and considering that function $\frac{1}{u}$ presents a vertical asymptote for $u = 0$, it is clear that in this case we can only consider $u^*_L < 0$ and $u_R < 0$.

So (4.41) becomes

$$ln(|u_R|) - ln(|u^*_L|) = -\frac{1}{2}(ln(A_R) - ln(A_L)) \longrightarrow \left|\frac{u_R}{u^*_L}\right| = \sqrt{\frac{A_L}{A_R}}. \tag{4.43}$$

In conclusion, for $\lambda_{\mathcal{A}1} < 0$

$$u^*_L = u^* = \sqrt{\frac{A_R}{A_L}} u_R = -\sqrt{\frac{A_R}{A_L}} |u_R|, \qquad u^*_R = u_R < 0, \tag{4.44}$$

both for $|u^*_L| < |u_R|$ and $|u^*_L| > |u_R|$.

So we have the results. □

Remark 4.1.1. The definition of u^* given in (4.33), as emphasized, is, by construction, admissible only under specific conditions

- $u^*_R > 0$ is defined only for $u_L > 0$,
- $u^*_L < 0$ is defined only for $u_R < 0$.

The cases including $u_L \leq 0$ and $u_R \geq 0$ are treated in Section 4.1.4.

Remark 4.1.2. The formulas treated in Proposition 4.1.8 are given without specifying in which actual side the real $\mathbf{Q}^*_{\mathcal{A}}$ is. This issue will be treated in Section 4.1.4.

4.1.3 Wave relations for the case $\lambda_{\mathcal{A}1} = \lambda_{\mathcal{A}2} = 0 \quad (u^* = 0)$

This case (n° 3 of Fig. 4.1), is not trivial and includes different possibilities and will be treated in Section 4.1.4. However it is possible to notice that being

$$\mathbf{Q}^* = \begin{bmatrix} A^* \\ Au^* \end{bmatrix}, \tag{4.45}$$

clearly we expect that in this case

$$\mathbf{Q}^* = \begin{bmatrix} A^* \\ 0 \end{bmatrix}. \tag{4.46}$$

At this point we should determine which of the two A^*_j, $j = L, R$, is appropriate in this case. This issue is treated in Section 4.1.4, where we want to determine the actual side of the $\lambda_{\mathcal{A}1}$-wave and the presence of shocks or rarefactions only from the initial data.

Remark 4.1.3. As it will be proved in Corollary. 4.1.16.1 the case $\lambda_{\mathcal{A}1} = 0$ does not correspond necessarily to a stationary solution. Actually it corresponds to a stationary solution $\iff$ ($u_L = 0$ and $u_R = 0$).

4.1.4 SIDES AND CONDITIONS FOR THE DIFFERENT TYPES OF WAVES

Developing the calculations for system (4.1) we obtain

$$\begin{cases} \partial_t A = 0, \\ A\partial_t u + u\partial_t A + \alpha A \partial_x (u^2) + \alpha u^2 \partial_x A = 0, \end{cases} \tag{4.47}$$

that becomes

$$\begin{cases} \partial_t A = 0, \\ \partial_t u + \alpha \partial_x (u^2) + \alpha \dfrac{u^2}{A} \partial_x A = 0. \end{cases} \tag{4.48}$$

For Proposition 4.1.4, $A(x,t)$ is a piecewise constant function, for every $t \in \mathbb{R}_0^+$. So $\partial_x A = 0$ in each point where this spatial derivative exists: i.e. everywhere with the exception of the discontinuity $x = x_d$. So, for $x < x_d$ and $x > x_d$, system (4.48) reduces to the conservative, unidimensional equation

$$\partial_t u + \alpha \partial_x (u^2) = 0, \tag{4.49}$$

that holds *separately* in each of the two sides (sides L and R of Fig. 4.2).

Analysing this equation we obtain

$$\lambda(u) = 2\alpha u, \tag{4.50}$$

that is the eigenvalue $\lambda_{\mathcal{A}1}$ of (4.5).

Remark 4.1.4. As remarked in caption of Fig. 4.2, in this Chapter we name *left part* the part of the (x,t) plane in Fig. 4.2 that is *to the left* of the $\lambda_{\mathcal{A}2}$ discontinuity, on the contrary we name *right part* the part of the (x,t) plane in Fig. 4.2 that is *to the right* of the $\lambda_{\mathcal{A}2}$ discontinuity.

Proposition 4.1.9. *Given* (4.49) *that holds in each left and right part, and considering Fig.* 4.2*, we have*

- *in the left part*

$$\text{left rarefaction} \iff u_L \leq u_L^*, \tag{4.51}$$

$$\text{entropy-satisfying left shock} \iff u_L > u_L^*, \tag{4.52}$$

- *in the right part*

$$\text{right rarefaction} \iff u_R^* \leq u_R, \tag{4.53}$$

$$\text{entropy-satisfying right shock} \iff u_R^* > u_R. \tag{4.54}$$

Proof. A discontinuity of a weak solution of the conservation law (4.49) satisfies the Rankine-Hugoniot jump condition across it, named

$$f(u_{\widehat{R}}) - f(u_{\widehat{L}}) = S(u_{\widehat{R}} - u_{\widehat{L}}) \Rightarrow \alpha u_{\widehat{R}}^2 - \alpha u_{\widehat{L}}^2 = S(u_{\widehat{R}} - u_{\widehat{L}}), \tag{4.55}$$

where $u_{\widehat{L}}$ and $u_{\widehat{R}}$, are the constant values of u to the left and to the right of the jump. From (4.55) we obtain the shock speed S

$$S = \alpha(u_{\widehat{R}} + u_{\widehat{L}}). \tag{4.56}$$

According to the Lax-Entropy condition [42], an entropy-satisfying shock in a wave associated with a genuinely non-linear field satisfies

$$\lambda(u_{\widehat{L}}) > S > \lambda(u_{\widehat{R}}), \tag{4.57}$$

in other words

$$2\alpha u_{\widehat{L}} > S > 2\alpha u_{\widehat{R}} \implies u_{\widehat{L}} > u_{\widehat{R}}. \tag{4.58}$$

This means that, according to Fig. 4.2,

$$\begin{aligned} &\text{Entropy-satisfying left shock} \implies u_L > u_L^*, \\ &\text{Entropy-satisfying right shock} \implies u_R^* > u_R, \end{aligned} \tag{4.59}$$

while (4.56) is (4.21).

On the contrary, having an admissible rarefaction in a wave associated with a genuinely non-linear field, being that a smooth wave, leads the opposite of (4.57) to hold, i.e.

$$\lambda(u_{\widehat{L}}) \leq \lambda(u_{\widehat{rar}}) \leq \lambda(u_{\widehat{R}}), \tag{4.60}$$

where $u_{\widehat{rar}}$ are the states *inside* the rarefaction, and $u_{\widehat{L}}$ and $u_{\widehat{R}}$ are the states that define its border. In other words

$$2\alpha u_{\widehat{L}} \leq 2\alpha u_{\widehat{rar}} \leq 2\alpha u_{\widehat{R}} \implies u_{\widehat{L}} \leq u_{\widehat{R}}. \tag{4.61}$$

According to Fig. 4.2

$$\begin{aligned} &\text{Left rarefaction} \implies u_L \leq u_L^*, \\ &\text{Right rarefaction} \implies u_R^* \leq u_R. \end{aligned} \tag{4.62}$$

Considering that a wave associated with a genuinely non-linear field can be either a rarefaction or a shock [80], and putting together (4.59) and (4.62), we obtain the if and only if statement. □

We can extend the definition of u^* in Proposition 4.1.8 to 0 only in particular cases, as explained in the following Proposition.

Proposition 4.1.10 (Extension of the definition of u^* in Proposition 4.1.8)**.**
In case of $u_R = 0$

$$u_L^* = u^* = 0 \iff \text{there is a left rarefaction.} \tag{4.63}$$

In case of $u_L = 0$

$$u_R^* = u^* = 0 \iff \text{there is a right rarefaction.} \tag{4.64}$$

Proof. Even if (4.33) are not given for $u_L = 0$ and $u_R = 0$ we can notice that

$$\begin{aligned} \lim_{u_L \to 0} u_R^* &= \lim_{u_L \to 0} \sqrt{\frac{A_L}{A_R}} |u_L| = 0, \\ \lim_{u_R \to 0} u_L^* &= \lim_{u_R \to 0} -\sqrt{\frac{A_R}{A_L}} |u_R| = 0, \end{aligned} \tag{4.65}$$

so it is possible to extend (4.33) by continuity to 0 and now we will prove in which particular cases.

($\Longleftarrow$)Now we will prove that

$$(\text{an admissible left rarefaction with} \quad u_R = 0) \implies u^* = 0. \tag{4.66}$$

In case of admissible rarefactions, by definition these latter are smooth waves characterized by the property

$$\begin{aligned} &\lambda_{\mathcal{A}1}(u_L) \leq \lambda_{\mathcal{A}1}(u_{rarL}) \leq \lambda_{\mathcal{A}1}(u_L^* = u^*) \quad \text{for an admissible left rarefaction,} \\ &\lambda_{\mathcal{A}1}(u_R^* = u^*) \leq \lambda_{\mathcal{A}1}(u_{rarR}) \leq \lambda_{\mathcal{A}1}(u_R) \quad \text{for an admissible right rarefaction,} \end{aligned} \tag{4.67}$$

where u_{rarL} and u_{rarR} are the states *inside* the left and the right rarefactions. In case of left rarefaction, for example, $u_R = 0$ leads to $u_L^* = 0$ for (4.65) and this implies that

$$\lambda_{\mathcal{A}1}(u_L) \leq \lambda_{\mathcal{A}1}(u_{rarL}) \leq 0 \Longrightarrow 2\alpha u_L \leq 2\alpha u_{rarL} \leq 0, \tag{4.68}$$

in (4.67), that is consistent with the hypothesis of a left rarefaction.

A similar proof for the right rarefaction.

($\Longrightarrow$)To prove the opposite implication, considering that a genuinely non-linear field can present only either a shock or a rarefaction [80], we prove that

$$(\text{an entropy-satisfying left shock with} \quad u_L = 0) \Longrightarrow u^* \neq 0. \tag{4.69}$$

The Lax-Entropy condition (4.57) becomes

$$\lambda_{\mathcal{A}1}(u_L) > S_L > \lambda_{\mathcal{A}1}(u_L^* = u^*) \Longrightarrow 2\alpha u_L > S_L > 2\alpha u_L^*, \tag{4.70}$$

so $u_R = 0$ leads to $u_L^* = 0$ by (4.65) but this implies that

$$2\alpha u_L > S_L > 0, \tag{4.71}$$

that leads to a contradiction, because by construction for a left shock $S_L \leq 0$ (see Remark 4.1.5).

An analogue proof for a right shock that must have $S_R \geq 0$, with the related Lax-Entropy condition

$$\lambda_{\mathcal{A}1}(u_R^* = u^*) > S_R > \lambda_{\mathcal{A}1}(u_R). \tag{4.72}$$

Putting together (4.66) and (4.69) we obtain the statement. □

Remark 4.1.5. In case of shock, the shock discontinuity with speed S is a characteristic in the (x,t) plane having angular coefficient $m_S = \dfrac{1}{S}$ that is thus of the same sign as the shock speed. By construction (Remark 4.1.4), we named *left shock* the ones whose shock discontinuity is *to the left* of the $\lambda_{\mathcal{A}2}$ discontinuity on the (x,t) plane. On the contrary we named *right shock* the ones whose shock discontinuity is *to the right* of the $\lambda_{\mathcal{A}2}$ discontinuity on the (x,t) plane. It follows that a left shock must have $S_L \leq 0$ and a right shock $S_R \geq 0$.

Proposition 4.1.9 and Proposition 4.1.10 lead to

Proposition 4.1.11 (Final conditions for rarefactions)**.** *We have a*

- *left rarefaction* $\Longleftrightarrow$

$$u_L \leq -\sqrt{\frac{A_R}{A_L}}|u_R| \quad \text{with} \quad u_L \leq 0 \quad \text{and} \quad u_R \leq 0, \tag{4.73}$$

- *right rarefaction* $\Longleftrightarrow$

$$u_R \geq \sqrt{\frac{A_L}{A_R}}|u_L| \quad \text{with} \quad u_L \geq 0 \quad \text{and} \quad u_R \geq 0. \tag{4.74}$$

Proof. According to Proposition 4.1.9 and Proposition 4.1.10 there is a left rarefaction $\iff u_L \leq u_L^* \leq 0$ with $u_R \leq 0$, i.e $\iff$

$$u_L \leq -\sqrt{\frac{A_R}{A_L}}|u_R| \leq 0 \quad \text{with} \quad u_R \leq 0, \tag{4.75}$$

that necessarily implies $u_L \leq 0$.

According to Proposition 4.1.9 and Proposition 4.1.10 there is a right rarefaction $\iff 0 \leq u_R^* \leq u_R$ with $u_L \geq 0$, i.e $\iff$

$$0 \leq \sqrt{\frac{A_L}{A_R}}|u_L| \leq u_R \quad \text{with} \quad u_L \geq 0, \tag{4.76}$$

that necessarily implies $u_R \geq 0$. □

Proposition 4.1.12 (Shocks-part1)**.** *We have a*

- *left shock* if

$$u_L > -\sqrt{\frac{A_R}{A_L}}|u_R| \quad \text{with} \quad u_L \leq 0 \quad \text{and} \quad u_R < 0, \tag{4.77}$$

- *right shock* if

$$u_R < \sqrt{\frac{A_L}{A_R}}|u_L| \quad \text{with} \quad u_L > 0 \quad \text{and} \quad u_R \geq 0. \tag{4.78}$$

Proof. According to Proposition 4.1.9 and Proposition 4.1.10, we have a shock on the left side $\iff u_L > u_L^*$ with $u_L^* < 0$, i.e. $\iff$

$$u_L > -\sqrt{\frac{A_R}{A_L}}|u_R| \quad \text{with} \quad u_R < 0. \tag{4.79}$$

According to Proposition 4.1.9 and Proposition 4.1.10, we have a shock on the right side $\iff u_R^* > u_R$ with $u_R^* > 0$, i.e. $\iff$

$$u_R < \sqrt{\frac{A_L}{A_R}}|u_L| \quad \text{with} \quad u_L > 0. \tag{4.80}$$

Unfortunately given the definition (4.33) the two conditions are partially superimposed, in details

$$\begin{cases} u_L > -\sqrt{\frac{A_R}{A_L}}|u_R| \quad \text{with} \quad u_R < 0, \\ u_R < \sqrt{\frac{A_L}{A_R}}|u_L| \quad \text{with} \quad u_L > 0, \end{cases} = u_L > -\sqrt{\frac{A_R}{A_L}}|u_R| \quad \text{with} \quad u_R < 0 \quad \text{and} \quad u_L > 0. \tag{4.81}$$

While under condition (4.81) we actually know that there is a shock but we still do not know on which side, we are sure that under the complementary conditions

$$u_L > -\sqrt{\frac{A_R}{A_L}}|u_R| \quad \text{with} \quad u_L \leq 0 \quad \text{and} \quad u_R < 0, \tag{4.82}$$

for the left shock, and

$$u_R < \sqrt{\frac{A_L}{A_R}}|u_L| \quad \text{with} \quad u_L > 0 \quad \text{and} \quad u_R \geq 0, \tag{4.83}$$

for the right shock, we have the desired results. □

Proposition 4.1.13. *Under conditions $u_L > 0$ and $u_R < 0$, we have an admissible j-shock (j=L,R)* $\iff$

$$\begin{aligned} &S_L < 0 \quad \text{for left shocks,} \\ &S_R > 0 \quad \text{for right shocks.} \end{aligned} \tag{4.84}$$

Proof. we must prove that we can not have both $S_L < 0$ and $S_R > 0$. Shock speeds are defined in (4.21).

$$\begin{cases} S_L = a(u_L - \sqrt{\frac{A_R}{A_L}}|u_R|) < 0 \iff u_L < -\sqrt{\frac{A_R}{A_L}}u_R, \\ S_R = a(u_R + \sqrt{\frac{A_L}{A_R}}|u_L|) > 0 \iff u_R > -\sqrt{\frac{A_L}{A_R}}u_L \iff u_L > -\sqrt{\frac{A_R}{A_L}}u_R. \end{cases} \tag{4.85}$$

So S_L and S_R are either both positive or negative considering conditions $u_L > 0$ and $u_R < 0$. □

Proposition 4.1.14 (Shocks-part2)**.** *We have a*

- *left shock* if
$$u_L > 0 \quad \text{and} \quad u_R < 0 \quad \text{and} \quad S_L < 0, \tag{4.86}$$
- *right shock* if
$$u_L > 0 \quad \text{and} \quad u_R < 0 \quad \text{and} \quad S_R > 0. \tag{4.87}$$

Proof. Follows directly from (4.81) and Proposition 4.1.13. Please note that conditions

$$u_L > -\sqrt{\frac{A_R}{A_L}}|u_R|, \qquad u_R < \sqrt{\frac{A_L}{A_R}}|u_L|, \tag{4.88}$$

in (4.81), are redundant for $u_L > 0$ and $u_R < 0$. □

Proposition 4.1.15 (Final conditions for shocks)**.** *We have a*

- *left shock* $\iff$
$$u_L > -\sqrt{\frac{A_R}{A_L}}|u_R| \quad \text{with} \quad u_L \leq 0 \quad \text{and} \quad u_R < 0, \tag{4.89}$$
or
$$u_L < \sqrt{\frac{A_R}{A_L}}|u_R| \quad \text{with} \quad u_L > 0 \quad \text{and} \quad u_R < 0, \tag{4.90}$$
- *right shock* $\iff$
$$u_R < \sqrt{\frac{A_L}{A_R}}|u_L| \quad \text{with} \quad u_L > 0 \quad \text{and} \quad u_R \geq 0, \tag{4.91}$$
or
$$u_R > -\sqrt{\frac{A_L}{A_R}}|u_L| \quad \text{with} \quad u_L > 0 \quad \text{and} \quad u_R < 0. \tag{4.92}$$

Proof. Given in Proposition 4.1.12 and 4.1.14. □

Now we consider what happens under initial conditions not given in Proposition 4.1.8, i.e. $u_L \leq 0$ and $u_R \geq 0$. As marked in Remark 4.1.1, u_L^* and u_R^* in this case are not defined as in Proposition 4.1.8.

Proposition 4.1.16 (Conditions for a transonic rarefaction)**.** *We have a single rarefaction that overtakes the $\lambda_{\mathcal{A}2}$ discontinuity $\iff$ $u_L \leq 0$ and $u_R \geq 0$.*

Proof. Let us analyse the characteristics of the leading equation (4.49).

We briefly recall that for a general Cauchy problem

$$\begin{cases} \partial_t u + \partial_x f(u) = 0, \\ u(x,0) = h(x), \end{cases} \tag{4.93}$$

the characteristic curves $x = x(t)$ are defined

$$\begin{cases} \dfrac{dx}{dt} = \lambda(u(x,t)), \\ x(0) = x_0. \end{cases} \tag{4.94}$$

and the total derivative of u along one of these curves is

$$\frac{du}{dt} = \frac{\partial u}{\partial t}\frac{dt}{dt} + \frac{\partial u}{\partial x}\frac{dx}{dt} = \partial_t u + \lambda(u)\partial_x u. \tag{4.95}$$

Considering our Riemann problem

$$\begin{cases} \partial_t u + \alpha \partial_x (u^2) = 0 \\ u(x,0) = \begin{cases} u_L & \text{if} \quad x < x_d, \\ u_R & \text{if} \quad x > x_d, \end{cases} \end{cases} \tag{4.96}$$

it follows that

$$\frac{du}{dt} = 0, \tag{4.97}$$

so $u(x,t)$ is constant along the characteristics satisfying (4.94), and this implies that $\lambda(u) = 2\alpha u$ is also constant along the characteristics.

From (4.94) it follows that the equation of the characteristics is

$$x = x_0 + \lambda(u(x,t))t, \tag{4.98}$$

from which it is clear that the characteristics are straight lines in the (x,t) plane and $\lambda(u) = 2\alpha u$ is the inverse of the angular coefficient of the straight lines.

Being u constant along the characteristics, it is clear that

$$u(x,t) = h(x_0), \tag{4.99}$$

where $x_0 = x(0)$ is the foot of the characteristic of the considered $u(x,t)$, and

$$h(x_0) = \begin{cases} u_L & \text{if} \quad x_0 < x_d, \\ u_R & \text{if} \quad x_0 > x_d, \end{cases} \tag{4.100}$$

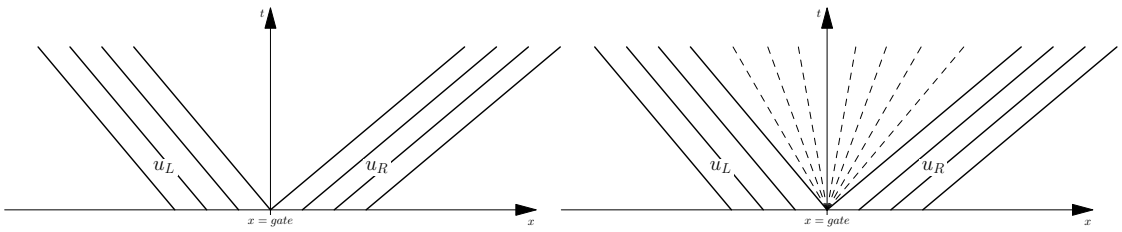

Figure 4.3: In the left picture the characteristics for generic initial data $u_L < 0$ and $u_R > 0$. In the right picture the complete solution with characteristics *inside* the rarefaction. We remind that the angular coefficent of the characteristics is $m = \dfrac{1}{2\alpha u}$, from which the graphs are straightforward.

so $u(x,t)$ in (4.99) is s.t.

$$u(x,t) = h(x_0) = \begin{cases} u_L & \text{if} \quad x - \lambda(u_L)t < x_d, \\ u_R & \text{if} \quad x - \lambda(u_R)t > x_d, \end{cases} = \begin{cases} u_L & \text{if} \quad x - 2\alpha u_L t < x_d, \\ u_R & \text{if} \quad x - 2\alpha u_R t > x_d, \end{cases} \tag{4.101}$$

in other words

$$u(x,t) = \begin{cases} u_L & \text{if} \quad \dfrac{x - x_d}{t} < 2\alpha u_L, \\ u_R & \text{if} \quad \dfrac{x - x_d}{t} > 2\alpha u_R, \end{cases} \tag{4.102}$$

and for $u_L < 0$, $u_R > 0$, we obtain Fig. 4.3-left.

It is quite clear that we are in presence of a single rarefaction that overtakes the discontinuity marked with $\lambda_{\mathcal{A}2}$ (the latter superimposed on the t-axis), Fig. 4.3-right.

In particular the case $u_L = 0$ and $u_R = 0$ leads to a single rarefaction with both borders superimposed on the $\lambda_{\mathcal{A}2}$ discontinuity, i.e. a stationary solution (please see Corollary 4.1.16.1).

Please note that under the considered conditions u^* is not defined in Proposition 4.1.8 anymore, it is only defined for $u_L = 0$ and $u_R = 0$ (case stationary solution seen as a particular case of a left and a right null rarefaction) thanks to Proposition 4.1.10. Actually the Star Region (defined as the region in the (x,t) plane between the $\lambda_{\mathcal{A}1}$ and $\lambda_{\mathcal{A}2}$-wave) does not exist in any of the cases treated in this Proposition. We choose to put $u^* = u_L^* = u_R^* = 0$ for computational simplicity due to the fact that $\lambda_{\mathcal{A}1} = 2\alpha u = 0$.

In case $u_L = 0$ *or* $u_R = 0$, according to (4.102) we obtain again a single rarefaction with one or two boundaries superimposed on the $\lambda_{\mathcal{A}2}$-discontinuity, cases already seen in Proposition 4.1.11. This is not a contradiction in fact actually the result is a single right or left rarefaction (for description of boundaries of a rarefaction please see Section 4.1.6).

□

Remark 4.1.6. It is clear that Riemann problem (4.96) is not really accurate since the equation proposed is valid for $x < x_d$ and $x > x_d$ but not in $x = x_d$. However we chose to ignore the discontinuity to draw the characteristics for the intitial data u_L and u_R that do not cross the $\lambda_{\mathcal{A}2}$-discontinuity and study the solution through them. Given the characteristics in Fig. 4.3 in fact only a rarefaction is admissible.

Corollary 4.1.16.1 (Stationary solutions)**.** *We have stationary solutions* $(u(x,t) = 0,\ \forall x,t) \iff (u_L = 0$ *and* $u_R = 0)$. *This implies* $u^* = u_L^* = u_R^* = 0$.

Proof. The only possibilities so far that allow these initial data are in Proposition 4.1.11 and Proposition 4.1.16. According to the cited Propositions, this is a particular case of a left, a right, or a transonic rarefaction. In particular according to Proposition 4.1.11 we should have both a left and a right rarefaction at the same time. So considering Proposition 4.1.10 we obtain

$u^* = u_L^* = u_R^* = 0$. Clearly $\lambda_{\mathcal{A}1} = 0$. On the other hand considering Proposition 4.1.16, according to (4.102) we have

$$u(x,t) = \begin{cases} 0 & \text{if} \quad \dfrac{x - x_d}{t} < 0, \\ 0 & \text{if} \quad \dfrac{x - x_d}{t} > 0, \end{cases} \tag{4.103}$$

i.e a stationary solution. □

Proposition 4.1.16 and Corollary 4.1.16.1 are the two possibilites of case 3 in Fig. 4.1.

Proposition 4.1.17 (Steady-state solutions not stationary). *We have steady-state solutions that are not stationary (i.e. solutions for which $\partial_t u = 0$ but $u(x,t) \neq 0$) $\iff$*

$$u_L = \sqrt{\frac{A_R}{A_L}} u_R, \quad \text{with} \quad u_L < 0, \quad \text{and} \quad u_R < 0, \tag{4.104}$$

or

$$u_L = \sqrt{\frac{A_R}{A_L}} u_R, \quad \text{with} \quad u_L > 0, \quad \text{and} \quad u_R > 0, \tag{4.105}$$

or

$$u_L = \sqrt{\frac{A_R}{A_L}} |u_R|, \quad \text{with} \quad u_L > 0, \quad \text{and} \quad u_R < 0. \tag{4.106}$$

Proof. Steady-state solutions are clearly obtained when

$$\begin{cases} u_L = u_L^*, \\ u_R = u_R^*. \end{cases} \tag{4.107}$$

There are some possibilities. First we must notice that by our construction, only one between u_L^* and u_R^* could be the real u^* (see Fig. 4.1 top-left and top-right) with the exception of the case of transonic rarefactions in Proposition 4.1.16, and stationary solutions in Corollary 4.1.16.1. These are the only cases in which we could have $u_L = u_R = u_L^* = u_R^* = 0$, i.e. when there is a stationary solution, that is actually steady, and has been already treated in Corollary 4.1.16.1.

Considering the case in which

$$u^* = u_L^*, \tag{4.108}$$

for computational simplicity we pose $u_R^* = u_R$ (as explained in the proof of Proposition 4.1.8). (4.108) and (4.107) lead us to $u^* = u_L^* = u_L$, i.e. by (4.42)

$$u_L < 0. \tag{4.109}$$

With the exception of the cases of transonic rarefactions and stationary solutions, u_L^* is defined in Proposition 4.1.8 and as reminded in Remark 4.1.1, only for $u_R < 0$, so

$$u_L = u_L^* \Longrightarrow u_L = \sqrt{\frac{A_R}{A_L}} u_R. \tag{4.110}$$

This is a limiting case of a left rarefaction (Proposition 4.1.11) in which the two borders of the rarefaction are superimposed on each other but not on the $\lambda_{\mathcal{A}2}$-wave.

Considering now the case in which

$$u^* = u_R^*, \tag{4.111}$$

for computational simplicity we pose $u_L^* = u_L$ (as explained in the proof of Proposition 4.1.8). (4.111) and (4.107) lead us to $u^* = u_R^* = u_R$, i.e. by (4.38)

$$u_R > 0. \tag{4.112}$$

With the exception of the cases of transonic rarefaction and stationary solutions, u_R^* is defined in Proposition 4.1.8 and as reminded in Remark 4.1.1, only for $u_L > 0$, so

$$u_R = u_R^* \Longrightarrow u_R = \sqrt{\frac{A_L}{A_R}} u_L. \tag{4.113}$$

This is a limiting case of a right rarefaction (Proposition 4.1.11) in which the two borders of the rarefaction are superimposed on each other but not on the $\lambda_{\mathcal{A}2}$-wave.

There is however, another possibility. Having $u_L > 0$, $u_R < 0$ and $u_L = \sqrt{\frac{A_R}{A_L}}|u_R|$, with some calculations we obtain

$$\begin{aligned} &u_L = -u_L^*, \\ &\textit{or} \\ &u_R = -u_R^*. \end{aligned} \tag{4.114}$$

The only possibility for $u_L > 0$, $u_R < 0$ is to have a shock somewhere (4.81), however due to (4.21), $S_L = \alpha(u_L + u_L^*)$ and $S_R = \alpha(u_R + u_R^*)$, so (4.114) leads to $S_L = 0$ or $S_R = 0$. In Proposition 4.1.13 we treated the case $u_L > 0$, $u_R < 0$ and $S_j \neq 0$, but we did not mention what happens when $S_L = 0$ or $S_R = 0$. Clearly in this case we have a shock somewhere with speed 0, i.e. a steady-state solution. □

All we have seen lead us to the final

Theorem 4.1.1 (Sides and conditions for the waves)**.** *In the advection system described in* (4.1) *we have*

- *a left rarefaction* $\Longleftrightarrow$

$$\begin{cases} u_L \leq 0, \\ u_R \leq 0, \\ u_L \leq -\sqrt{\frac{A_R}{A_L}}|u_R|, \end{cases} \tag{4.115}$$

- *a left shock* $\Longleftrightarrow$

$$\begin{cases} u_L \leq 0, \\ u_R < 0, \\ u_L > -\sqrt{\frac{A_R}{A_L}}|u_R|, \end{cases} \quad \text{or} \quad \begin{cases} u_L > 0, \\ u_R < 0, \\ u_L < \sqrt{\frac{A_R}{A_L}}|u_R|, \end{cases} \tag{4.116}$$

- *a right rarefaction* $\Longleftrightarrow$

$$\begin{cases} u_L \geq 0, \\ u_R \geq 0, \\ u_R \geq \sqrt{\frac{A_L}{A_R}}|u_L|, \end{cases} \tag{4.117}$$

- *a right shock* $\Longleftrightarrow$

$$\begin{cases} u_L > 0, \\ u_R \geq 0, \\ u_R < \sqrt{\dfrac{A_L}{A_R}}|u_L|, \end{cases} \quad \text{or} \quad \begin{cases} u_L > 0, \\ u_R < 0, \\ u_R > -\sqrt{\dfrac{A_L}{A_R}}|u_L|, \end{cases} \tag{4.118}$$

- *a transonic rarefaction* $\Longleftrightarrow$

$$\begin{cases} u_L \leq 0, \\ u_R \geq 0, \end{cases} \tag{4.119}$$

- *a stationary solution* $\Longleftrightarrow$

$$\begin{cases} u_L = 0, \\ u_R = 0, \end{cases} \tag{4.120}$$

- *a steady-state solution not stationary* $\Longleftrightarrow$

$$\begin{cases} u_L < 0, \\ u_R < 0, \\ u_L = -\sqrt{\dfrac{A_R}{A_L}}|u_R|, \end{cases} \text{or} \quad \begin{cases} u_L > 0, \\ u_R > 0, \\ u_L = \sqrt{\dfrac{A_R}{A_L}}u_R, \end{cases} \text{or} \quad \begin{cases} u_L > 0, \\ u_R < 0, \\ u_L = \sqrt{\dfrac{A_R}{A_L}}|u_R|. \end{cases} \tag{4.121}$$

Proof. The entire Section 4.1.4. □

Remark 4.1.7. Please note that some items in Theorem 4.1.1 are superimposed. However this is not a mistake. For example as described in the proof of Corollary. 4.1.16.1, stationary solutions are limiting cases of left rarefactions, right rarefactions, and transonic ones. A same description for rarefactions that have an initial condition equal to $u_j = 0$, that can be seen as limiting cases of j-rarefactions or transonic ones, indeed the third condition for steady state solution is a particular case of a shock with speed $S = 0$ etc....

4.1.5 Solution in the Star Region

The Star Region is the region in the (x, t) plane between the $\lambda_{\mathcal{A}1}$ and the $\lambda_{\mathcal{A}2}$-waves. Putting together what stated in Section 4.1.4, we obtain:

- initial data

$$\mathbf{Q}_L = \begin{bmatrix} A_L \\ A_L u_L \end{bmatrix}, \qquad \mathbf{Q}_R = \begin{bmatrix} A_R \\ A_R u_R \end{bmatrix}, \tag{4.122}$$

- case *left rarefaction* or *left shock*:

$$\mathbf{Q}^* = \mathbf{Q}^*_{\mathcal{A}L} = \begin{bmatrix} A_L \\ A_L u^*_L \end{bmatrix}, \qquad \mathbf{Q}^*_{\mathcal{A}R} = \mathbf{Q}_R, \tag{4.123}$$

- case *right rarefaction* or *right shock*:

$$\mathbf{Q}^*_{\mathcal{A}L} = \mathbf{Q}_L \qquad \mathbf{Q}^* = \mathbf{Q}^*_{\mathcal{A}R} = \begin{bmatrix} A_R \\ A_R u^*_R \end{bmatrix}, \tag{4.124}$$

- case *transonic rarefaction* or *stationary solution*:

$$\mathbf{Q}^* = \mathbf{Q}^*_{\mathcal{A}L} = \begin{bmatrix} A_L \\ 0 \end{bmatrix}, \qquad \mathbf{Q}^* = \mathbf{Q}^*_{\mathcal{A}R} = \begin{bmatrix} A_R \\ 0 \end{bmatrix}, \tag{4.125}$$

- case *steady-state solution not stationary*:

$$\text{(cases 1 and 2 of (4.121))} \quad \mathbf{Q}^*_{\mathcal{A}L} = \mathbf{Q}_L \qquad \mathbf{Q}^*_{\mathcal{A}R} = \mathbf{Q}_R, \tag{4.126}$$

$$\text{(case 3 of (4.121))} \quad \mathbf{Q}^*_{\mathcal{A}L} = \begin{bmatrix} A_L \\ -A_L u_L \end{bmatrix}, \qquad \mathbf{Q}^*_{\mathcal{A}R} = \begin{bmatrix} A_R \\ -A_R u_R \end{bmatrix}, \tag{4.127}$$

where u^*_L and u^*_R are as in (4.33).

Remark 4.1.8. Please note that (4.127) are the actual values of $\mathbf{Q}^*_{\mathcal{A}j}$ for the considered case, but they do not compare in the actual final solution, due to the fact that the final solution is steady-state, i.e. remains equal to the initial conditions.

4.1.6 SOLUTION INSIDE THE RAREFACTIONS

To calculate the solution inside a rarefaction, being $\mathcal{X} = x - x_d$, x being the spatial coordinate of the vessel domain and x_d the spatial coordinate of the $\lambda_{\mathcal{A}2}$ discontinuity, we look for a similarity solution of equation (4.49)

$$u(x,t) = g\left(\frac{\mathcal{X}}{t}\right), \tag{4.128}$$

with $g\left(\frac{\mathcal{X}}{t}\right)$ smooth, then

$$\partial_t u = -\frac{\mathcal{X}}{t^2} g'\left(\frac{\mathcal{X}}{t}\right), \tag{4.129}$$

$$\partial_x u = \frac{1}{t} g'\left(\frac{\mathcal{X}}{t}\right), \tag{4.130}$$

so (4.49) becomes

$$g'\left(\frac{\mathcal{X}}{t}\right)\left[-\frac{\mathcal{X}}{t^2} + \frac{1}{t}\lambda\left(g\left(\frac{\mathcal{X}}{t}\right)\right)\right] = 0, \tag{4.131}$$

that holds $\iff$

$$g'\left(\frac{\mathcal{X}}{t}\right) = 0, \tag{4.132}$$

trivial solution, or

$$\lambda\left(g\left(\frac{\mathcal{X}}{t}\right)\right) = \frac{\mathcal{X}}{t}. \tag{4.133}$$

It follows that

$$\lambda_{\mathcal{A}1}(u_{rar}(x,t)) = 2\alpha u_{rar}(x,t) = \frac{\mathcal{X}}{t}, \tag{4.134}$$

so

$$u_{rar} = \frac{\mathcal{X}}{2\alpha t}, \tag{4.135}$$

where u_{rar} is the value of u inside the rarefaction. Clearly inside a rarefaction will hold

$$\mathbf{Q}_{rarL} = \begin{bmatrix} A_L \\ A_L u_{rar} \end{bmatrix}, \qquad \text{or} \qquad \mathbf{Q}_{rarR} = \begin{bmatrix} A_R \\ A_R u_{rar} \end{bmatrix}, \tag{4.136}$$

according to the actual side of the rarefaction.

Please note that for (4.61), (4.102) and (4.134), the actual borders of a rarefaction in the (x,t) plane are

$$\text{for a left rarefaction} \quad \begin{aligned} &\text{left border} \quad \frac{\mathcal{X}}{t} = \lambda_{\mathcal{A}1}(u_L) = 2\alpha u_L, \\ &\text{right border} \quad \frac{\mathcal{X}}{t} = \lambda_{\mathcal{A}1}(u_L^*) = 2\alpha u_L^*, \end{aligned} \tag{4.137}$$

$$\text{for a right rarefaction} \quad \begin{aligned} &\text{left border} \quad \frac{\mathcal{X}}{t} = \lambda_{\mathcal{A}1}(u_R^*) = 2\alpha u_R^*, \\ &\text{right border} \quad \frac{\mathcal{X}}{t} = \lambda_{\mathcal{A}1}(u_R) = 2\alpha u_R, \end{aligned} \tag{4.138}$$

$$\text{for a transonic rarefaction} \quad \begin{aligned} &\text{left border} \quad \frac{\mathcal{X}}{t} = \lambda_{\mathcal{A}1}(u_L) = 2\alpha u_L, \\ &\text{right border} \quad \frac{\mathcal{X}}{t} = \lambda_{\mathcal{A}1}(u_R) = 2\alpha u_R. \end{aligned} \tag{4.139}$$

4.1.7 Complete exact solution of the Riemann problem for the advection system

Here we present the complete exact solution in the entire vessel domain according to the wave pattern of the $\lambda_{\mathcal{A}1}$ wave. Being again $\mathcal{X} = x - x_d$, x being the spatial coordinate of the vessel domain and x_d the spatial coordinate of the $\lambda_{\mathcal{A}2}$ discontinuity and t the time, we obtain the complete solution according to the cases of Theorem 4.1.1.

- Case of left rarefaction:

$$\mathbf{Q}(x,t) = \begin{cases} \mathbf{Q}_L & \text{if} \quad \mathcal{X} < (2\alpha u_L)t, \\ \mathbf{Q}_{rarL} & \text{if} \quad (2\alpha u_L)t \le \mathcal{X} \le (2\alpha u_L^*)t, \\ \mathbf{Q}^*_{\mathcal{A}L} & \text{if} \quad (2\alpha u_L^*)t < \mathcal{X} \le 0 \\ \mathbf{Q}_R & \text{if} \quad \mathcal{X} > 0. \end{cases} \tag{4.140}$$

- Case of left shock:

$$\mathbf{Q}(x,t) = \begin{cases} \mathbf{Q}_L & \text{if} \quad \mathcal{X} \le S_L t, \\ \mathbf{Q}^*_{\mathcal{A}L} & \text{if} \quad S_L t < \mathcal{X} \le 0, \\ \mathbf{Q}_R & \text{if} \quad \mathcal{X} > 0. \end{cases} \tag{4.141}$$

- Case of right rarefaction:

$$\mathbf{Q}(x,t) = \begin{cases} \mathbf{Q}_L & \text{if} \quad \mathcal{X} \le 0, \\ \mathbf{Q}^*_{\mathcal{A}R} & \text{if} \quad 0 < \mathcal{X} \le (2\alpha u_R^*)t, \\ \mathbf{Q}_{rarR} & \text{if} \quad (2\alpha u_R^*)t \le \mathcal{X} \le (2\alpha u_R)t, \\ \mathbf{Q}_R & \text{if} \quad \mathcal{X} > 2\alpha u_R t. \end{cases} \tag{4.142}$$

- Case of right shock:

$$\mathbf{Q}(x,t) = \begin{cases} \mathbf{Q}_L & \text{if} \quad \mathcal{X} \le 0, \\ \mathbf{Q}^*_{\mathcal{A}R} & \text{if} \quad 0 < \mathcal{X} \le S_R t, \\ \mathbf{Q}_R & \text{if} \quad \mathcal{X} > S_R t. \end{cases} \tag{4.143}$$

- Case of transonic rarefaction:

$$\mathbf{Q}(x,t) = \begin{cases} \mathbf{Q}_L & \text{if} \quad \mathcal{X} < (2\alpha u_L)t, \\ \mathbf{Q}_{rarL} & \text{if} \quad (2\alpha u_L)t \leq \mathcal{X} \leq 0, \\ \mathbf{Q}_{rarR} & \text{if} \quad 0 < \mathcal{X} \leq (2\alpha u_R)t, \\ \mathbf{Q}_R & \text{if} \quad \mathcal{X} > (2\alpha u_R)t. \end{cases} \tag{4.144}$$

- Case of steady-state solution or stationary solution:

$$\mathbf{Q}(x,t) = \begin{cases} \mathbf{Q}_L & \text{if} \quad \mathcal{X} \leq 0, \\ \mathbf{Q}_R & \text{if} \quad \mathcal{X} > 0. \end{cases} \tag{4.145}$$

$\mathbf{Q}_L$, $\mathbf{Q}_R$ are defined in (4.122), $\mathbf{Q}_{rarL}$ and $\mathbf{Q}_{rarR}$ are defined in (4.136) and (4.135), while $\mathbf{Q}^*_{\mathcal{A}L}$, $\mathbf{Q}^*_{\mathcal{A}R}$ as described in Section 4.1.5, are defined as

$$\mathbf{Q}^*_{\mathcal{A}L} = \begin{bmatrix} A_L \\ A_L u^*_L \end{bmatrix}, \quad \mathbf{Q}^*_{\mathcal{A}R} = \begin{bmatrix} A_R \\ A_R u^*_R \end{bmatrix}, \tag{4.146}$$

with u^*_L and u^*_R in Proposition 4.1.8. S_L and S_R are defined in (4.21).

4.1.8 Results

We propose 7 test problems including arteries and veins. However the parameters that distinguish arteries and veins are not involved in the advection system, so the type of vessel is not specified. The solution of Test 1 describes a right rarefaction. In Test 2 is proposed a left shock, in Test 3 a left rarefaction,that can be also classified as a transonic one, Test 4 produces a steady state solution not stationary. In Test 5 the solution is stationary, in Test 6 a right rarefaction is produced, and finally in Test 7 a transonic rarefaction is given. These exact solutions are further validated by the comparison with a numerical, mesh-independent solution obtained with a second order, centred, extension of FORCE scheme, FORCEII (Appendix A.2) for different values of $\alpha \in [1,2]$ with a mesh of $I = 3000$ computational cells and a Courant-Friederich-Lewy coefficient $C_{Cfl} = 0.9$.

Initial data are in Tables 4.1, 4.2, while in Table 4.3 the exact solution of the Riemann problem in the Star Region is depicted. Results are in Figs. 4.4, 4.5, 4.6, 4.7, 4.8, 4.9, 4.10.

4.2 Exact solution of the Riemann problem for the advection system derived from the 1D blood flow equations with discontinuous parameters

The splitting is treated in Section 3.2. The resulting advection system is now

$$\begin{cases} \partial_t A = 0, \\ \partial_t (Au) + \alpha \partial_x (Au^2) = 0, \\ \partial_t K = 0, \\ \partial_t A_0 = 0, \\ \partial_t p_e = 0. \end{cases} \tag{4.147}$$

Table 4.1: Parameters used for Tests 1 to 7: momentum correction coefficient α, domain length ℓ; location of the initial discontinuity x_d and output time t_{End}. The units of measures used for this Thesis are: m, s, kg, Pa.

Test	α	$\ell[m]$	$x_d[m]$	$t_{End}[s]$
1	1.0	0.5	0.5ℓ	0.3
2	1.1	0.5	0.5ℓ	0.15
3	1.0	0.5	0.5ℓ	0.2
4	1.0	0.5	0.5ℓ	0.1
5	2.0	0.5	0.5ℓ	0.05
6	4/3	0.5	0.5ℓ	0.05
7	1.0	0.5	0.5ℓ	0.1

Table 4.2: Initial conditions and wave patterns for Tests from 1 to 7.

Test	$A_L[m^2]$	$u_L[m/s]$	$A_R[m^2]$	$u_R[m/s]$	Wave pattern
1	$3.5 \cdot 10^{-4}$	0.1	$3.0 \cdot 10^{-4}$	0.3	right rarefaction
2	$2.9 \cdot 10^{-4}$	-0.5	$3.5 \cdot 10^{-4}$	-0.5	left shock
3	$3.5 \cdot 10^{-4}$	0.5	$3.05 \cdot 10^{-4}$	0.1	right shock
4	$3.14 \cdot 10^{-4}$	0.5	$3.14 \cdot 10^{-4}$	-0.5	steady-state solution not stationary
5	$3.5 \cdot 10^{-4}$	0.0	$3.0 \cdot 10^{-4}$	0.0	stationary solution
6	$3.1 \cdot 10^{-4}$	-0.5	$3.0 \cdot 10^{-4}$	0.0	left rarefaction/transonic rarefaction
7	$2.0 \cdot 10^{-5}$	-0.2	$1.9 \cdot 10^{-5}$	0.7	transonic rarefaction

Table 4.3: Exact solution in the Star Region of the Riemann problem for the advection system.

Test	$A_L^*[m^2]$	$u_L^*[m/s]$	$A_R^*[m^2]$	$u_R^*[m/s]$	Note
1	$3.5 \cdot 10^{-4}$	0.1	$3.0 \cdot 10^{-4}$	0.1080	$\mathbf{Q}^*_{\mathcal{A}} = \mathbf{Q}^*_{\mathcal{A}R}$
2	$2.9 \cdot 10^{-4}$	-0.5493	$3.5 \cdot 10^{-4}$	-0.5	$\mathbf{Q}^* = \mathbf{Q}^*_{\mathcal{A}L}$
3	$3.5 \cdot 10^{-4}$	0.5	$3.05 \cdot 10^{-4}$	0.5356	$\mathbf{Q}^* = \mathbf{Q}^*_{\mathcal{A}R}$ Otherwise both are considered.
4	$3.14 \cdot 10^{-4}$	-0.5	$3.14 \cdot 10^{-4}$	0.5	$\mathbf{Q}^*_{\mathcal{A}L}$ and $\mathbf{Q}^*_{\mathcal{A}R}$
5	$3.5 \cdot 10^{-4}$	0.0	$3.0 \cdot 10^{-4}$	0.0	$\mathbf{Q}^*_{\mathcal{A}L}$ and $\mathbf{Q}^*_{\mathcal{A}R}$
6	$3.1 \cdot 10^{-5}$	0.0	$3.0 \cdot 10^{-5}$	0.0	$\mathbf{Q}^*_{\mathcal{A}} = \mathbf{Q}^*_{\mathcal{A}L}$ as a left rarefaction.
7	$2.0 \cdot 10^{-5}$	0.0	$1.9 \cdot 10^{-5}$	0.0	$\mathbf{Q}^*_{\mathcal{A}L}$ and $\mathbf{Q}^*_{\mathcal{A}R}$

The resulting system is still conservative, i.e.

$$\partial_t \mathbf{Q} + \partial_x \boldsymbol{\mathcal{A}}(\mathbf{Q}) = \mathbf{0}, \tag{4.148}$$

where

$$\mathbf{Q} = \begin{bmatrix} A(x,t) \\ Au(x,t) \\ K(x) \\ A_0(x) \\ p_e(x) \end{bmatrix}, \quad \boldsymbol{\mathcal{A}}(\mathbf{Q}) = \begin{bmatrix} Au \\ \alpha Au^2 \\ 0 \\ 0 \\ 0 \end{bmatrix}. \tag{4.149}$$

The jacobian of (4.149) is

$$\widehat{\boldsymbol{\mathcal{A}}}(\mathbf{Q}) = \begin{bmatrix} 0 & 0 & 0 & 0 & 0 \\ -\alpha u^2 & 2\alpha u & 0 & 0 & 0 \\ 0 & 0 & 0 & 0 & 0 \\ 0 & 0 & 0 & 0 & 0 \\ 0 & 0 & 0 & 0 & 0 \end{bmatrix}. \tag{4.150}$$

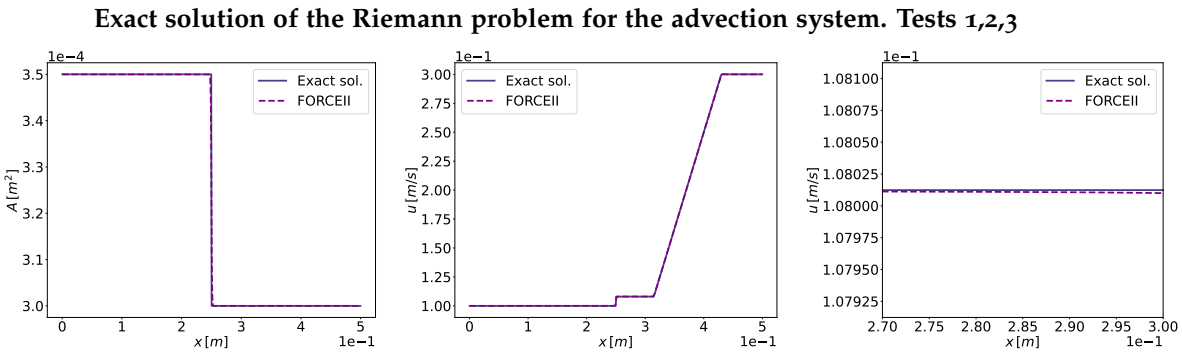

Figure 4.4: Test 1. Right rarefaction. Momentum correction coefficient $\alpha = 1$. Exact solution vs. FORCEII numerical scheme. The plot to the right shows a detail of the solution in the *Star Region* for velocity u. Initial data in Tables 4.1, 4.2.

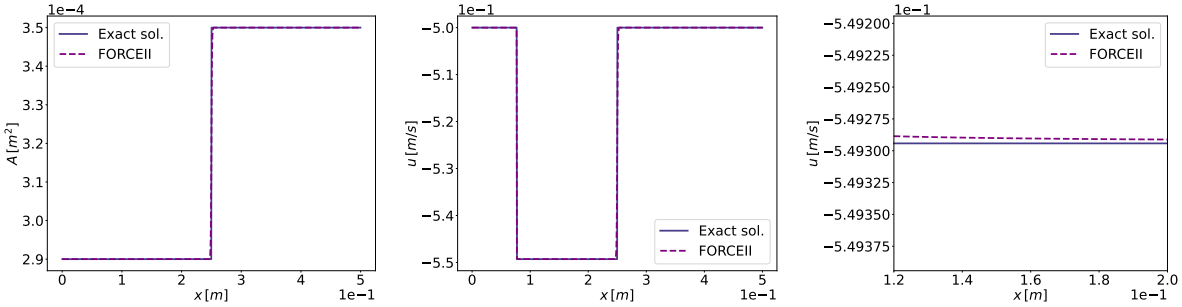

Figure 4.5: Test 2. Left shock. Momentum correction coefficient $\alpha = 1.1$. Exact solution vs. FORCEII numerical scheme. The plot to the right shows a detail of the solution in the *Star Region* for velocity u. Initial data in Tables 4.1, 4.2.

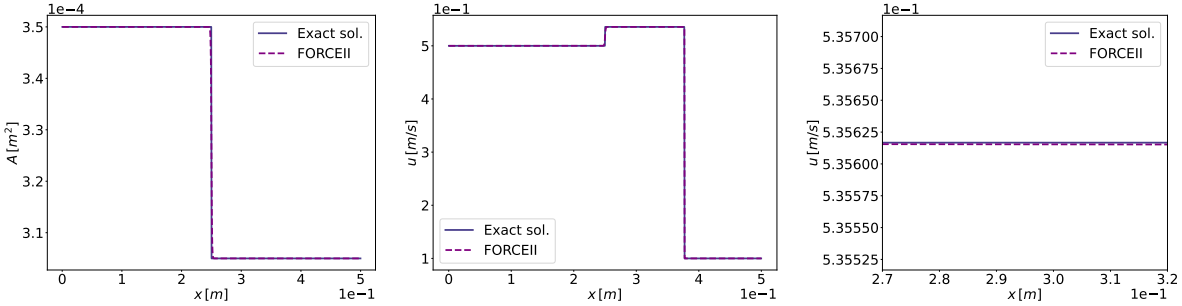

Figure 4.6: Test 3. Right shock. Momentum correction coefficient $\alpha = 1$. Exact solution vs. FORCEII numerical scheme. The plot to the right shows a detail of the solution in the *Star Region* for velocity u. Initial data in Tables 4.1, 4.2.

The eigenvalues of (4.150) are all real and given by

$$\lambda_{\mathcal{A}1} = 2\alpha u \qquad \lambda_{\mathcal{A}2} = \lambda_{\mathcal{A}3} = \lambda_{\mathcal{A}4} = \lambda_{\mathcal{A}5} = 0. \tag{4.151}$$

A possible choice of right eigenvectors corresponding to eigenvalues (4.151) is

$$\mathbf{R}_1 = \begin{bmatrix} 0 \\ 1 \\ 0 \\ 0 \\ 0 \end{bmatrix}, \quad \mathbf{R}_2 = \begin{bmatrix} 0 \\ 0 \\ 0 \\ 0 \\ 1 \end{bmatrix}, \quad \mathbf{R}_3 = \begin{bmatrix} 0 \\ 0 \\ 0 \\ 1 \\ 0 \end{bmatrix}, \quad \mathbf{R}_4 = \begin{bmatrix} 0 \\ 0 \\ 1 \\ 0 \\ 0 \end{bmatrix}, \quad \mathbf{R}_5 = \begin{bmatrix} 1 \\ \frac{u}{2} \\ 0 \\ 0 \\ 0 \end{bmatrix}. \tag{4.152}$$

Proposition 4.2.1 (Hyperbolicity). *System* (4.147) *is hyperbolic* $\forall \mathbf{Q} \in \Omega = [\mathbb{R}^+ \times \mathbb{R} \times \mathbb{R}^+ \times \mathbb{R}^+ \times \mathbb{R}]$.

Proof. It is straightforward to see that eigenvalues (4.151) are always real and eigenvectors (4.152) are linearly independent in the entire domain Ω. System (4.147) however, is not strictly hyperbolic since there are four identical eigenvalues. □

Proposition 4.2.2 (Nature of the $\lambda_{\mathcal{A}1}$-characteristic field). *The $\lambda_{\mathcal{A}1}$-characteristic field is genuinely non-linear* $\forall \mathbf{Q} \in \Omega$.

Proof. It can be easily verified that

$$\nabla \lambda_{\mathcal{A}1}(\mathbf{Q}) \cdot \mathbf{R}_{\mathcal{A}1}(\mathbf{Q}) = \frac{2\alpha}{A} > 0 \quad \forall \mathbf{Q} \in \Omega. \tag{4.153}$$

□

Proposition 4.2.3 (Nature of $\lambda_{\mathcal{A}k}$-characteristic field, $k = 2,3,4,5$). *The $\lambda_{\mathcal{A}k}$-characteristic field $k = 2,3,4,5$ is linearly degenerate* $\forall \mathbf{Q} \in \Omega$.

Proof. It can be easily verified that

$$\nabla \lambda_{\mathcal{A}k}(\mathbf{Q}) \cdot \mathbf{R}_{\mathcal{A}k}(\mathbf{Q}) = 0 \quad k = 2,3,4,5 \quad \forall \mathbf{Q} \in \Omega. \tag{4.154}$$

□

The Riemann problem for system (4.148) is

$$\begin{cases} \partial_t \mathbf{Q} + \partial_x \mathcal{A}(\mathbf{Q}) = \mathbf{0}, \quad x \in \mathbb{R}, \quad t > 0, \\ \mathbf{Q}(x,0) = \begin{cases} \mathbf{Q}_L & \text{if} \quad x < x_d, \\ \mathbf{Q}_R & \text{if} \quad x > x_d, \end{cases} \end{cases} \tag{4.155}$$

with

$$\mathbf{Q}_L = \begin{bmatrix} A_L \\ Au_L \\ K_L \\ A_{0L} \\ p_{eL} \end{bmatrix}, \quad \mathbf{Q}_R = \begin{bmatrix} A_R \\ Au_R \\ K_R \\ A_{0R} \\ p_{eR} \end{bmatrix}. \tag{4.156}$$

Regarding the parameters from (4.147) we have

$$\partial_t K = 0 \quad \partial_t A_0 = 0, \quad \partial_t p_e = 0, \tag{4.157}$$

in other words the parameters do not change with time, i.e. remain equal to the initial conditions

$$\begin{aligned} K(x) &= \begin{cases} K_L & \text{for the left part,} \\ K_R & \text{for the right part,} \end{cases} \\ A_0(x) &= \begin{cases} A_{0L} & \text{for the left part,} \\ A_{0R} & \text{for the right part,} \end{cases} \\ p_e(x) &= \begin{cases} p_{eL} & \text{for the left part,} \\ p_{eR} & \text{for the right part,} \end{cases} \end{aligned} \tag{4.158}$$

where the *left part* is s.t $\mathcal{X} < 0$ and the *right part* is s.t. $\mathcal{X} > 0$ with $\mathcal{X} = x - x_d$ and x_d is the initial discontinuity of the parameters, as defined in Section 4.1.7, and proved in the following

Proposition 4.2.4 (Wave relations across the $\lambda_{\mathcal{A}2} = \lambda_{\mathcal{A}3} = \lambda_{\mathcal{A}4} = \lambda_{\mathcal{A}5}$-wave for the case $\lambda_{\mathcal{A}1} \neq 0$)**.** *The relations across the contact discontinuity marked with $\lambda_{\mathcal{A}2} = \lambda_{\mathcal{A}3} = \lambda_{\mathcal{A}4} = \lambda_{\mathcal{A}5}$, with $\lambda_{\mathcal{A}1} \neq 0$, are given by*

$$A \neq const, \qquad ln(|u|) + \frac{1}{2} ln(A) = const, \qquad K \neq const, \qquad A_0 \neq const, \qquad p_e \neq const. \tag{4.159}$$

Proof. Following the method presented in [81], we consider matrix $\mathcal{A}(\mathbf{Q})$ in (4.150). For an arbitrary right eigenvector $\mathbf{R} = [r_1, r_2, r_3, r_4, r_5, r_6]^T$ we have

$$\mathcal{A}\mathbf{R} = \lambda \mathbf{R}, \tag{4.160}$$

which gives the algebraic system

$$\begin{cases} 0 = \lambda r_1, \\ -\alpha u^2 r_1 + 2\alpha u r_2 = \lambda r_2, \\ 0 = \lambda r_3, \\ 0 = \lambda r_4, \\ 0 = \lambda r_5. \end{cases} \tag{4.161}$$

Putting $\lambda = 0$ in (4.161), $r_1 = \beta$, $r_3 = \gamma$, $r_4 = \epsilon$, $r_5 = \delta$, for $\beta, \gamma, \epsilon, \delta \in \mathbb{R}$, arbitrary constants, we obtain

$$\mathbf{R}_0 = \begin{bmatrix} \beta \\ \frac{u\beta}{2} \\ \gamma \\ \epsilon \\ \delta \end{bmatrix}. \tag{4.162}$$

This is a general form of a vector belonging to the subspace associated with $\lambda = 0$ for every choice of β, γ, ϵ, δ, $\in \mathbb{R}$. We then apply the generalized Riemann invariants method to this vector

$$\frac{dA}{\beta} = \frac{dq}{\frac{u\beta}{2}} = \frac{dK}{\gamma} = \frac{dA_0}{\epsilon} = \frac{dp_e}{\delta}. \tag{4.163}$$

From the first and the second of (4.163) we have

$$\frac{u}{2} dA = d(Au) \tag{4.164}$$

that has been already treated in Proposition 4.1.7. From the third, the fourth and the fifth the only thing we can say is that

$$K \neq const, \qquad A_0 \neq const, \qquad p_e \neq const. \tag{4.165}$$

□

Proposition 4.2.5 (Wave relations across rarefactions for the case $\lambda_{\mathcal{A}1} \neq 0$)**.** *The generalized Riemann invariants for the case $\lambda_{\mathcal{A}1} = 2\alpha u \neq 0$, are given by*

$$A = const, \qquad q \neq const, \qquad K = const, \quad A_0 = const, \quad p_e = const, \tag{4.166}$$

for the $\lambda_{\mathcal{A}1}$ -characteristic field.

Proof. It is straightforward (please see [90]) to show that Riemann invariants can be obtained from

$$\frac{dA}{0} = \frac{dq}{1} = \frac{dK}{0} = \frac{dA_0}{0} = \frac{dp_e}{0}. \tag{4.167}$$

So, from the first we have $A = const$, from the third we have $K = const$, from the fourth we have $A_0 = const$ from the fifth we have $p_e = const$, and being $dq \neq const$ we have $u \neq const$. □

In conclusion it is straightforward to note that parameters K, A_0 and p_e are not involved in the computation of variable A and u so their presence and values does not change the final results that are exactly those presented in Section 4.1.8.

4.3 Conclusions

In this Chapter we have built the exact solution of the Riemann problem for the advection system (4.1) arising from the flux splitting of the complete conservative 1D blood flow equations for arteries and veins, with general constant momentum correction coefficient, presented in Chapter 3.1, and the advection-pressure splitting of the complete non-conservative 1D blood flow equations for arteries and veins, with general constant momentum correction coefficient, described in Chapter 3.2 We have given a complete mathematical analysis of the wave relations and have presented the conditions to obtain each type of wave. Through a comparison with the solutions obtained with the centred, second order numerical scheme FORCEII (Appendix A.2) we have further proved its correctness.

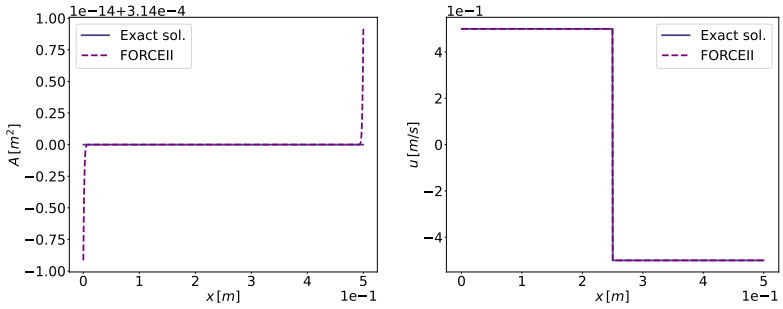

Figure 4.7: Test 4. Steady-state solution not stationary. Momentum correction coefficient $\alpha = 1$. Exact solution vs. FORCEII numerical scheme. Initial data in Tables 4.1, 4.2.

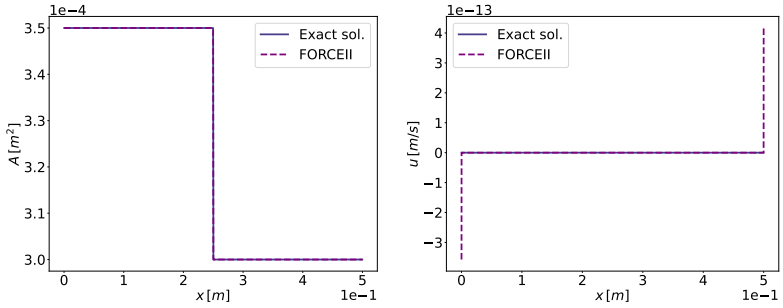

Figure 4.8: Test 5. Stationary solution. Momentum correction coefficient $\alpha = 2$. Exact solution vs. FORCEII numerical scheme. Initial data in Tables 4.1, 4.2.

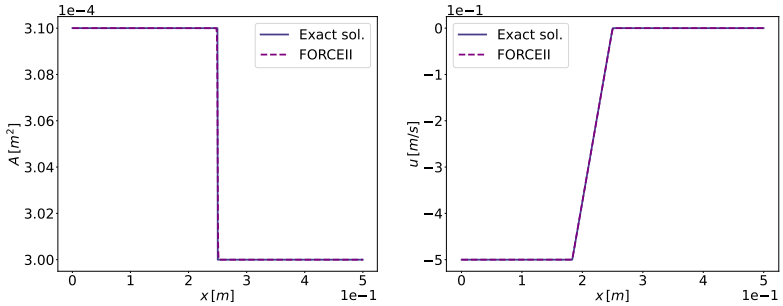

Figure 4.9: Test 6. Left rarefaction. Momentum correction coefficient $\alpha = 4/3$. Exact solution vs. FORCEII numerical scheme. Initial data in Tables 4.1, 4.2.

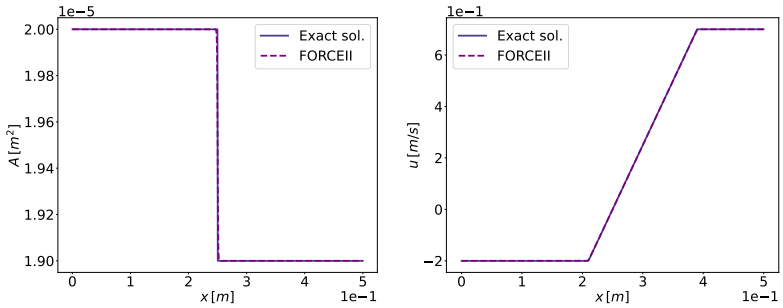

Figure 4.10: Test 7. Transonic rarefaction. Momentum correction coefficient $\alpha = 1$. Exact solution vs. FORCEII numerical scheme. Initial data in Tables 4.1, 4.2.

Chapter 5

Exact solution of the Riemann problem for the conservative 1D pressure system with transport

In this Chapter we solve exactly the Riemann problem for the pressure system arising in the advection-pressure splitting for conservative 1D blood flow models presented in Chapter 3.1, for tube laws describing arteries and veins with a constant momentum correction coefficient different from one and a passive scalar transport equation added.

In case of arteries the genuine non-linearity of the characteristic fields originates rarefactions and shocks, in addition to contact waves corresponding to the linearly degenerate fields. On the contrary in case of veins, the loss of genuine non-linearity leads to the presence of compound waves, i.e. mixed waves, composed by rarefactions and shocks. We give a detailed mathematical analysis and a numerical procedure to compute the resulting solution. Finally we further verify the obtained mathematical results against a second order extension of FORCE numerical scheme.

In detail: in Section 5.1, we present the (conservative) pressure system, in Section 5.2, we present the Riemann problem for the pressure system, in cases of both arteries and veins. In Section 5.3 we describe in detail the relations across each wave and the construction of the final complete exact solution of the Riemann problem for the pressure system in case of arteries, with the numerical procedure we use to compute it. In Section 5.4 we present the theoretical analysis of the mathematical relations across the waves in case of veins, and the numerical procedure we use to construct the exact solution also in this case, facing the loss of genuine non-linearity and the formation of compound waves. in Section 5.5 the conclusions are drawn.

The research article regarding this topic is in preparation.

5.1 The conservative pressure system with transport

The pressure system arising after the splitting for the conservative 1D blood flow equations has been introduced in Chapter 3.1 and is here recalled for convenience. The system is

$$\begin{cases} \partial_t A + \partial_x (Au) = 0, \\ \partial_t (Au) + \partial_x \left(\int c^2(A) dA \right) = 0, \\ \partial_t (A\phi) = 0, \end{cases} \tag{5.1}$$

where as usual $A(x,t)$ is the cross-sectional area of the vessel at position x and time t, assumed to be $A \in \mathbb{R}^+$, $u(x,t)$ is the averaged velocity of blood at a cross section, $\phi(x,t) \in \mathbb{R}_0^+$ is the concentration of the passive scalar. c is the *wave speed* already defined in (2.14)

$$c(A) = \sqrt{\frac{K}{\rho}\left[m\left(\frac{A}{A_0}\right)^m - n\left(\frac{A}{A_0}\right)^n\right]}, \tag{5.2}$$

with

$$K = \begin{cases} \dfrac{E}{(1-\nu^2)}\left(\dfrac{h_0}{R_0}\right) & \text{for arteries,} \\ \dfrac{E}{12(1-\nu^2)}\left(\dfrac{h_0}{R_0}\right)^3 & \text{for veins,} \end{cases} \tag{5.3}$$

$$m = \begin{cases} 1/2 & \text{for arteries,} \\ 10 & \text{for veins,} \end{cases} \qquad n = \begin{cases} 0 & \text{for arteries,} \\ -3/2 & \text{for veins.} \end{cases} \tag{5.4}$$

h_0 is the vessel wall thickness, A_0 and R_0 are the cross-sectional area of the vessel and the radius at equilibrium, E is the Young's modulus, ν is the Poisson ratio taken as $\nu = 0.5$, $m, n \in \mathbb{R}$ and in general are taken $m > 0$ and $-2 \leq n \leq 0$. $K \in \mathbb{R}^+$, $A_0 \in \mathbb{R}^+$, $R_0 \in \mathbb{R}^+$, $E \in \mathbb{R}^+$, $h_0 \in \mathbb{R}^+$ are constants. ρ is the density of blood, assumed constant. c is always real, for the choices of m and n given in (5.4).

(5.1) can be written as

$$\partial_t \mathbf{Q} + \partial_x \boldsymbol{\mathcal{P}}(\mathbf{Q}) = \mathbf{0}, \tag{5.5}$$

where

$$\begin{aligned} \mathbf{Q} &= \begin{bmatrix} A \\ Au \\ A\phi \end{bmatrix}, \\ \boldsymbol{\mathcal{P}}(\mathbf{Q}) &= \begin{bmatrix} Au \\ \displaystyle\int c^2(A)\, dA \\ 0 \end{bmatrix} = \begin{bmatrix} Au \\ \dfrac{KA}{\rho}\left(\dfrac{m}{m+1}\left(\dfrac{A}{A_0}\right)^m - \dfrac{n}{n+1}\left(\dfrac{A}{A_0}\right)^n\right) \\ 0 \end{bmatrix} \end{aligned} \tag{5.6}$$

The Jacobian of system (5.1) is

$$\mathcal{J}_{\boldsymbol{\mathcal{P}}}(\mathbf{Q}) = \begin{bmatrix} 0 & 1 & 0 \\ c^2 & 0 & 0 \\ 0 & 0 & 0 \end{bmatrix}. \tag{5.7}$$

The eigenvalues of $\mathcal{J}_{\boldsymbol{\mathcal{P}}}(\mathbf{Q})$ are

$$\lambda_{\mathcal{P}1} = -c, \qquad \lambda_{\mathcal{P}2} = 0, \qquad \lambda_{\mathcal{P}3} = +c, \tag{5.8}$$

moreover a possible choice of right eigenvectors corresponding to eigenvalues (5.8) is

$$\mathbf{R}_{\mathcal{P}1} = \begin{bmatrix} 1 \\ -c \\ 0 \end{bmatrix}, \qquad \mathbf{R}_{\mathcal{P}2} = \begin{bmatrix} 0 \\ 0 \\ 1 \end{bmatrix}, \qquad \mathbf{R}_{\mathcal{P}3} = \begin{bmatrix} 1 \\ c \\ 0 \end{bmatrix}, \tag{5.9}$$

where and c is the wave speed (5.2).

Proposition 5.1.1 (Hyperbolicity). *System (5.1) is strictly hyperbolic under the following hypotheses:*

1. *the set of admissible solutions is restricted to* $\mathbf{Q} \in \Omega = [\mathbb{R}^+ \times \mathbb{R} \times \mathbb{R}_0^+] \subset \mathbb{R}^3$;

2. *the tube law is a monotonically increasing function of the cross-sectional area A, i.e.* $\dfrac{\partial p}{\partial A} > 0$.

Proof. This can be clearly seen from the definition of wave speed given in (5.2). Under the conditions considered in this proposition $c \in \mathbb{R}^+ \ \forall \mathbf{Q} \in \Omega$, which results in $\lambda_{\mathcal{P}1} \in \mathbb{R}^-$, $\lambda_{\mathcal{P}3} \in \mathbb{R}^+$, $\forall \mathbf{Q} \in \Omega$. In particular this is true for the parameters given in (5.3), (5.4). □

Proposition 5.1.2 (Nature of the $\lambda_{\mathcal{P}1}$ and $\lambda_{\mathcal{P}3}$ - characteristic fields)**.** *Under the hypotheses of Proposition 5.1.1, in case of arteries (parameters are given in (5.4)) the $\lambda_{\mathcal{P}1}$ and $\lambda_{\mathcal{P}3}$ - characteristic fields are genuinely non-linear with*

$$\begin{aligned} \nabla\lambda_{\mathcal{P}1}(\mathbf{Q}) \cdot \mathbf{R}_{\mathcal{P}1}(\mathbf{Q}) < 0, \quad \forall \mathbf{Q} \in \Omega, \\ \nabla\lambda_{\mathcal{P}3}(\mathbf{Q}) \cdot \mathbf{R}_{\mathcal{P}3}(\mathbf{Q}) > 0, \quad \forall \mathbf{Q} \in \Omega, \end{aligned} \tag{5.10}$$

instead in case of veins, they are not. In fact

$$\begin{aligned} \nabla\lambda_{\mathcal{P}1}(\mathbf{Q}) \cdot \mathbf{R}_{\mathcal{P}1}(\mathbf{Q}) \quad & \begin{cases} > 0 & \text{for} \quad A < A_c, \\ = 0 & \text{for} \quad A = A_c, \\ < 0 & \text{for} \quad A > A_c; \end{cases} \\ \nabla\lambda_{\mathcal{P}3}(\mathbf{Q}) \cdot \mathbf{R}_{\mathcal{P}3}(\mathbf{Q}) \quad & \begin{cases} < 0 & \text{for} \quad A < A_c, \\ = 0 & \text{for} \quad A = A_c, \\ > 0 & \text{for} \quad A > A_c, \end{cases} \end{aligned} \tag{5.11}$$

where A_c, for parameters in (5.4), is

$$A_c \approx 0.7190\, A_0. \tag{5.12}$$

A characteristic field in which (5.11) occurs is called nongenuinely non-linear [17].

Proof. It can be easily verified that

$$\nabla\lambda_{\mathcal{P}1}(\mathbf{Q}) \cdot \mathbf{R}_{\mathcal{P}1}(\mathbf{Q}) = -\frac{\partial c}{\partial A}, \tag{5.13}$$

and

$$\nabla\lambda_{\mathcal{P}3}(\mathbf{Q}) \cdot \mathbf{R}_{\mathcal{P}3}(\mathbf{Q}) = \frac{\partial c}{\partial A}, \tag{5.14}$$

where $\mathbf{R}_{\mathcal{P}1}$ and $\mathbf{R}_{\mathcal{P}3}$ are the right eigenvectors (5.9).
For genuine non-linearity we must prove that $\dfrac{\partial c}{\partial A} \neq 0$. Having

$$\frac{\partial c}{\partial A} = \frac{\dfrac{K}{\rho}\left(\left(\dfrac{A}{A_0}\right)^m m^2 - \left(\dfrac{A}{A_0}\right)^n n^2\right)}{2A\sqrt{\dfrac{K}{\rho}\left(\left(\dfrac{A}{A_0}\right)^m m - \left(\dfrac{A}{A_0}\right)^n n\right)}}, \tag{5.15}$$

being

$$\sqrt{\frac{K}{\rho}\left(\left(\frac{A}{A_0}\right)^m m - \left(\frac{A}{A_0}\right)^n n\right)} = c > 0, \tag{5.16}$$

by hypothesis, with c as in (5.2) and being by hypothesis $K > 0$, $\rho > 0$, $A_0 > 0$ and $A > 0$, we must prove that

$$\left(\left(\frac{A}{A_0}\right)^m m^2 - \left(\frac{A}{A_0}\right)^n n^2\right) \neq 0, \tag{5.17}$$

for our considered values of variables and parameters.
It is easy to verify that for the case of arteries, i.e $m = 0.5$ and $n = 0$, (5.17) always holds, and in particular

$$\frac{\partial c}{\partial A} > 0, \quad \forall A \in \mathbb{R}^+, \tag{5.18}$$

that gives the result. On the contrary, for the case of veins i.e $m = 10$ and $n = -1.5$

$$y(\zeta) = \zeta^{10} 10^2 - \zeta^{-1.5} 1.5^2, \tag{5.19}$$

with $\zeta = \dfrac{A}{A_0}$, changes its sign from negative to positive and exists one and only ζ_z in the interval $\mathcal{I} =]0, \infty[$ s.t. $y(\zeta_z) = 0$, that is approximately

$$\zeta_z = \frac{A_c}{A_0} \approx 0.7190, \tag{5.20}$$

this means that in case of veins

$$\frac{\partial c}{\partial A} \quad \begin{cases} < 0 & \text{for} \quad A < A_c, \\ = 0 & \text{for} \quad A = A_c, \\ > 0 & \text{for} \quad A > A_c, \end{cases} \tag{5.21}$$

the statement briefly follows. □

Proposition 5.1.3 (Generalization of Proposition 5.1.2)**.** *In case of arteries* ($m > 0$, $n = 0$) *the* $\lambda_{\mathcal{P}1}$ *and* $\lambda_{\mathcal{P}3}$ *- characteristic fields are genuinely non-linear, instead in case of veins* ($m > 0$, $-2 \leq n < 0$), *they are not.*

Proof. Condition (5.17) holds for any $m > 0$, $n = 0$, while it is always false for any $m > 0$, $-2 \leq n < 0$. The proof is straightforward, having

$$\zeta^m m^2 - \zeta^n n^2 = 0, \tag{5.22}$$

that, considering generic $m > 0$ and $-2 \leq n \leq 0$, can be written as

$$\frac{\zeta^{m+|n|} m^2 - n^2}{\zeta^{|n|}} = 0, \tag{5.23}$$

by hypothesis

$$\zeta \in \mathbb{R}^+, \tag{5.24}$$

so we must check

$$g(\zeta) = \zeta^{m+|n|} m^2 - n^2. \tag{5.25}$$

g in (5.25) is s.t. $g(0) = -n^2$ and is continuous in $\mathbb{R}^+$ for any $m + |n| > 0$, the derivative

$$g'(\zeta) = m^2 (m + |n|) \zeta^{m+|n|-1} > 0 \qquad \forall \zeta \in \mathbb{R}^+, \tag{5.26}$$

(5.25) is increasing in $\mathbb{R}^+$ and

$$\lim_{\zeta \to +\infty} g(\zeta) = +\infty. \tag{5.27}$$

Consequently if $n \neq 0$, $g(0) < 0$ and $g(\zeta) > 0$ for large enough ζ, so, for the Intermediate Value Theorem, there exists at least one zero for (5.25). Furthermore, as $g(\zeta)$ is a strictly increasing function, the root is unique. In other words, if $n \neq 0$ there is always a unique state $\zeta_z \in \mathbb{R}^+$ s.t.

$$g(\zeta_z) = \zeta_z^{m+|n|} m^2 - n^2 = 0, \tag{5.28}$$

othewise for $n = 0$ (5.25) is always positive. □

Proposition 5.1.4 (Nature of the $\lambda_{\mathcal{P}2}$ - characteristic field)**.** *Under the hypotheses of Proposition 5.1.1, the $\lambda_{\mathcal{P}2}$ - characteristic field is linearly degenerate.*

Proof. It is straightforward to show that

$$\nabla \lambda_{\mathcal{P}2}(\mathbf{Q}) \cdot \mathbf{R}_{\mathcal{P}2}(\mathbf{Q}) = 0, \quad \forall \mathbf{Q} \in \Omega. \tag{5.29}$$

□

5.2 The Riemann problem for the pressure system

The Riemann problem (later also named RP) for system (5.1) is

$$\begin{cases} \partial_t \mathbf{Q} + \partial_x \boldsymbol{\mathcal{P}}(\mathbf{Q}) = \mathbf{0}, & x \in \mathbb{R}, \quad t > 0, \\ \mathbf{Q}(x,0) = \begin{cases} \mathbf{Q}_L & \text{if} \quad x < x_d, \\ \mathbf{Q}_R, & \text{if} \quad x > x_d, \end{cases} \end{cases} \tag{5.30}$$

where $x_d \in \mathbb{R}$ is the spatial location of the initial discontinuity. The initial conditions are given by the two constant states

$$\mathbf{Q}_L = \begin{bmatrix} A_L \\ A_L u_L \\ A_L \phi_L \end{bmatrix}, \quad \mathbf{Q}_R = \begin{bmatrix} A_R \\ A_R u_R \\ A_R \phi_R \end{bmatrix}. \tag{5.31}$$

The unknowns are $\mathbf{Q}^*_{\mathcal{P}L}$ and $\mathbf{Q}^*_{\mathcal{P}R}$ defined

$$\mathbf{Q}^*_{\mathcal{P}L} = \begin{bmatrix} A^*_L \\ (Au)^*_L \\ (A\phi)^*_L \end{bmatrix}, \quad \mathbf{Q}^*_{\mathcal{P}R} = \begin{bmatrix} A^*_R \\ (Au)^*_R \\ (A\phi)^*_R \end{bmatrix}. \tag{5.32}$$

Fig. 5.1 depicts the structure of the exact solution of the Riemann problem (5.30) for the pressure system (5.1). The waves related to the two real eigenvalues $\lambda_{\mathcal{P}1} = -c$, $\lambda_{\mathcal{P}3} = +c$ in case of arteries represent waves associated with genuinely non-linear fields that can be either shocks or rarefactions [80], while in case of veins this property is lost, allowing the formation of compound waves [49], the wave related to the eigenvalue $\lambda_{\mathcal{P}2} = 0$ is associated with a linearly degenerate field and is a contact discontinuity.

We are always in *subsonic regime*, because

$$\lambda_{\mathcal{P}1}(\mathbf{Q}) < 0 \quad \text{and} \quad \lambda_{\mathcal{P}3}(\mathbf{Q}) > 0, \quad \text{i.e. } c > 0, \quad \forall \mathbf{Q} \in \Omega. \tag{5.33}$$

Remark 5.2.1. *In this Thesis we do not focus our attention on proving the existence and uniqueness of the solution of the Riemann problem for the pressure system. Results have been obtained in case of 2×2 and $n \times n$ hyperbolic systems of conservation laws with a loss of genuine non-linearity in isolated (hyper)surfaces and under certain conditions of the related fluxes [49, 50]*

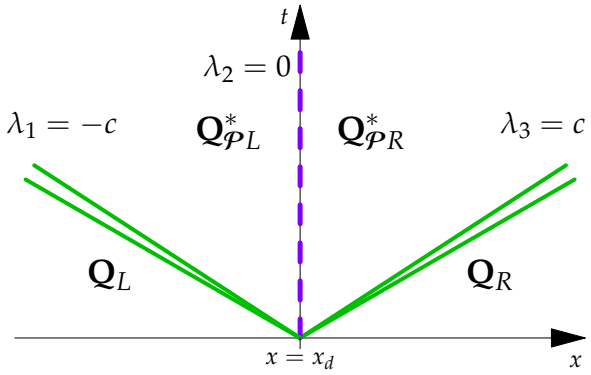

Figure 5.1: The configuration of the exact solution of the Riemann problem for the pressure system (5.30). The green solid lines in case of arteries represent waves associated with genuinely non-linear fields that can be either shocks or rarefactions, while in case of veins this property is lost, allowing the formation of compound waves. The purple dashed line represents the contact discontinuity for the passive scalar and is associated with a linearly degenerate field. In this Chapter the $\lambda_{\mathcal{P}1}$-wave will be sometimes called left wave, while the $\lambda_{\mathcal{P}3}$-one, right wave. It follows that the related wave patterns will be called *left rarefaction/shock/compound* or *right rarefaction/shock/compound*.

Proposition 5.2.1 (Generalized Riemann invariants for the $\lambda_{\mathcal{P}1}$ and $\lambda_{\mathcal{P}3}$- characteristic fields)**.** *The generalized Riemann invariants are given by*

$$q + \int c(A)dA = const, \quad A\phi = const, \tag{5.34}$$

for the $\lambda_{\mathcal{P}1}$ - characteristic field,

$$q - \int c(A)dA = const, \quad A\phi = const, \tag{5.35}$$

for the $\lambda_{\mathcal{P}3}$ - characteristic field.

Proof. The problem can be solved applying the generalized Riemann invariants method [90], i.e for a given hyperbolic system of n unknowns $[w_1, w_2, \dots, w_n]^T$, for any λ_k - characteristic field with right eigenvector $\mathbf{R}_k = [r_{1,k}, r_{2,k}, \dots, r_{n,k}]^T$ the generalized Riemann invariants are solutions of the following $n-1$ ordinary differential equations in phase-plane

$$\frac{dw_1}{r_{1,k}} = \frac{dw_2}{r_{2,k}} = \cdots = \frac{dw_n}{r_{n,k}}. \tag{5.36}$$

.

For the $\lambda_{\mathcal{P}1}$ - characteristic field we have

$$\frac{dA}{1} = \frac{dq}{-c} = \frac{d(A\phi)}{0}, \tag{5.37}$$

i.e. from the first and the second term

$$(-c)dA = dq, \tag{5.38}$$

and from the third

$$d(A\phi) = 0 \Longrightarrow A\phi = const. \tag{5.39}$$

For the $\lambda_{\mathcal{P}3}$ - characteristic field

$$\frac{dA}{1} = \frac{dq}{c} = \frac{d(A\phi)}{0}, \tag{5.40}$$

i.e. from the first and the second term

$$cdA = dq, \tag{5.41}$$

and from the third

$$d(A\phi) = 0 \Longrightarrow A\phi = const. \tag{5.42}$$

□

Proposition 5.2.2 (Generalized Riemann invariants for the $\lambda_{\mathcal{P}2}$- characteristic field)**.** *The generalized Riemann invariants for the $\lambda_{\mathcal{P}2}$ - characteristic field are*

$$A = const, \quad q = const, \quad \phi \neq const. \tag{5.43}$$

Proof. For the $\lambda_{\mathcal{P}2}$ - characteristic field

$$\frac{dA}{0} = \frac{dq}{0} = \frac{dA\phi}{1}, \tag{5.44}$$

that implies

$$A = const, \qquad q = const, \qquad \phi \neq const. \tag{5.45}$$

□

Proposition 5.2.2 states clearly that across the $\lambda_{\mathcal{P}2}$ - wave, only variable ϕ changes, so $\mathbf{Q}^*_{\mathcal{P}L}$ and $\mathbf{Q}^*_{\mathcal{P}R}$ in (5.32), become

$$\mathbf{Q}^*_{\mathcal{P}L} = \begin{bmatrix} A^* \\ A^*u^* = q^* \\ A^*\phi^*_L \end{bmatrix}, \quad \mathbf{Q}^*_{\mathcal{P}R} = \begin{bmatrix} A^* \\ A^*u^* = q^* \\ A^*\phi^*_R \end{bmatrix}. \tag{5.46}$$

Now we will treat separately the exact solution of the Riemann problem for the pressure system introduced in this Section, for the cases of arteries (Section 5.3) and veins (Section 5.4). In each of these Sections we refer to the model proposed in Section 5.1 and to the relations described in Section5.2 that are valid for both cases.

Remark 5.2.1. It is worth noting that, being $\lambda_{\mathcal{P}k}(\mathbf{Q}) = \pm c(A)$, $k = 1, 3$; in this Chapter we sometimes refer to the function $\lambda_{\mathcal{P}k}(\mathbf{Q})$ directly as $\lambda_{\mathcal{P}k}(A)$.

5.3 Exact solution of the Riemann problem for the pressure system in arteries

The model is that presented in Section 5.2, now we will describe how to calculate the exact solution of the Riemann problem in case of arteries.

5.3.1 Wave relations

The $\lambda_{\mathcal{P}2}$- wave relations are those in Proposition 5.2.2. Regarding the $\lambda_{\mathcal{P}1}$- and $\lambda_{\mathcal{P}3}$- waves, for arteries the related fields are genuinely non-linear, so they can be smooth waves (rarefactions) or

discontinuous waves (shocks) [80]. Now we will describe the relations in these different cases with a graphical insight into the rarefaction and shock curves in the phase plane (A, q) in a similar manner as in Chapter 2.

5.3.1.1 $\lambda_{\mathcal{P}1}$ AND $\lambda_{\mathcal{P}3}$- WAVE RELATIONS. CASE OF RAREFACTIONS

The generalized Riemann invariants in Proposition 5.2.1 clearly hold. The third equation in (5.1) is not affecting the others so variable ϕ can be treated separately. From Proposition 5.2.1, the generalized Riemann invariants for A and q defined from these ODEs with initial conditions

$$\left.\begin{aligned} \text{ODE:}\quad & \frac{dq}{dA} = -c, \\ \text{IC:}\quad & q(A_L) = q_L, \end{aligned}\right\} \quad \text{for the } \lambda_{\mathcal{P}1}\text{-wave,} \tag{5.47}$$

$$\left.\begin{aligned} \text{ODE:}\quad & \frac{dq}{dA} = c, \\ \text{IC:}\quad & q(A_R) = q_R, \end{aligned}\right\} \quad \text{for the } \lambda_{\mathcal{P}3}\text{-wave,} \tag{5.48}$$

where c is defined in (5.2). The solutions of (5.47) and (5.48) for $A \in \mathbb{R}^+$, are the two integral curves, one for each wave (the association of the $\lambda_{\mathcal{P}1}$-wave with $\mathbf{Q}_L$ in (5.47) is straightforward: this latter is the initial data that is connected with the unknown $\mathbf{Q}^*_{\mathcal{P}L}$ by the considered wave, the same for the right wave) that are actually functions of variable A (see Fig. 5.2a)

$$q_{rarL}(A) \quad \text{and} \quad q_{rarR}(A) \quad \text{with} \quad A \in \mathbb{R}^+. \tag{5.49}$$

The resulting curves are

$$\mathbf{Q}(A) = (A, q(A)). \tag{5.50}$$

Being q a function of A we will usually refer to these curves simply as $q(A)$. Additionally, with an abuse of notation, we sometimes refer to $\mathbf{Q}(A) = [A, q(A)]^T$ as a generic state belonging to that curve.

Proposition 5.3.1 (Physically admissible rarefaction curves)**.**
If the $\lambda_{\mathcal{P}1}$-wave, associated with a genuinely non-linear field, is a smooth wave (i.e. is a physically admissible rarefaction), the related admissible rarefaction curve is

$$q^a_{rarL}(A) = \{[A, q_{rarL}(A)]^T, \text{ s.t. } A \in \mathbb{R}^+ \text{ and } A \leq A_L\}, \tag{5.51}$$

with $q_{rarL}(A)$ in (5.49). In particular $A^* \leq A_L$.

If the $\lambda_{\mathcal{P}3}$-wave, associated with a genuinely non-linear field, is a smooth wave (i.e. is a physically admissible rarefaction), the related admissible rarefaction curve is

$$q^a_{rarR}(A) = \{[A, q_{rarR}(A)]^T, \text{ s.t. } A \in \mathbb{R}^+ \text{ and } A \leq A_R\}, \tag{5.52}$$

with $q_{rarR}(A)$ in (5.49). In particular $A^* \leq A_R$.

Proof. In a k-th genuinely non-linear characteristic field, $\lambda_k(A)$ is monotonically varying along the entire integral curve. Given the left state $\mathbf{Q}_{\hat{L}}$ belonging to the aforementioned integral curve $\mathbf{Q}_{rar}(A) = (A, q_{rar}(A))$, the admissible rarefaction curve is the part of the that integral curve s.t.

$$\lambda_k(\mathbf{Q}_{\hat{L}}) \leq \lambda_k(\mathbf{Q}_{rar}). \tag{5.53}$$

For the case of the $\lambda_{\mathcal{P}1}$-wave, having a physically admissible rarefaction with left value $\mathbf{Q}_L$, the admissible rarefaction curve is the set of generic states $\mathbf{Q}_{rarL}(A) = [A, q_{rarL}(A)]^T$ in the phase-plane (A, q), lying on the left integral curve $q_{rarL}(A)$ built in (5.47), for $A \in \mathbb{R}^+$, such that

$$\lambda_{\mathcal{P}1}(\mathbf{Q}_L) \leq \lambda_{\mathcal{P}1}(\mathbf{Q}_{rarL}(A)). \tag{5.54}$$

Considering now the curve $\mathbf{Q}_{rarL}(A) = (A, q_{rarL}(A))$ we want to calculate

$$\frac{d\lambda_{\mathcal{P}1}(\mathbf{Q}_{rarL}(A))}{dA} = \nabla\lambda_{\mathcal{P}1}(\mathbf{Q}_{rarL}(A)) \cdot \frac{d\mathbf{Q}_{rarL}(A)}{dA}. \tag{5.55}$$

We have that

$$\frac{d\mathbf{Q}_{rarL}(A)}{dA} = \begin{bmatrix} 1 \\ \dfrac{dq_{rarL}(A)}{dA} \end{bmatrix}, \tag{5.56}$$

but by construction of (5.47)

$$\frac{dq_{rarL}(A)}{dA} = -c(A), \tag{5.57}$$

consequently

$$\frac{d\mathbf{Q}_{rarL}(A)}{dA} = \begin{bmatrix} 1 \\ -c(A) \end{bmatrix} = \mathbf{R}_{\mathcal{P}1}(\mathbf{Q}_{rarL}(A)), \tag{5.58}$$

where $\mathbf{R}_{\mathcal{P}1}$ is the right eigenvector in (5.9). So

$$\frac{d\lambda_{\mathcal{P}1}(\mathbf{Q}_{rarL}(A))}{dA} = \nabla\lambda_{\mathcal{P}1}(\mathbf{Q}_{rarL}(A)) \cdot \mathbf{R}_{\mathcal{P}1}(\mathbf{Q}_{rarL}(A)) < 0, \tag{5.59}$$

for genuine non-linearity of the $\lambda_{\mathcal{P}1}$-field, as presented in Proposition 5.1.2. This means that $\lambda_{\mathcal{P}1}(\mathbf{Q}_{rarL}(A))$ is strictly decreasing in the domain $A \in \mathbb{R}^+$. In other words from (5.54)

$$\lambda_{\mathcal{P}1}(\mathbf{Q}_L) = \lambda_{\mathcal{P}1}(\mathbf{Q}_{rarL}(A_L)) \leq \lambda_{\mathcal{P}1}(\mathbf{Q}_{rarL}(A)) \qquad \Longrightarrow \qquad A \leq A_L, \tag{5.60}$$

thus we obtain the statement. In particular for a left rarefaction that has as left state $\mathbf{Q}_L$ and right state $\mathbf{Q}^*$, (5.54) becomes

$$\lambda_{\mathcal{P}1}(\mathbf{Q}_L) \leq \lambda_{\mathcal{P}1}(\mathbf{Q}^*_{\mathcal{P}L}), \tag{5.61}$$

from which

$$A^* \leq A_L. \tag{5.62}$$

The proof for the $\lambda_{\mathcal{P}3}$ - wave (sometimes called in this Chapter *right wave*) is similar, considering that for a right rarefaction

$$\lambda_{\mathcal{P}3}(\mathbf{Q}_{rarR}(A)) \leq \lambda_{\mathcal{P}3}(\mathbf{Q}_R) \quad \forall \mathbf{Q}, \tag{5.63}$$

must hold, furthermore

$$\frac{d\lambda_{\mathcal{P}3}(\mathbf{Q}_{rarR}(A))}{dA} = \nabla\lambda_{\mathcal{P}3}(\mathbf{Q}_{rarR}(A)) \cdot \mathbf{R}_{\mathcal{P}3}(\mathbf{Q}_{rarR}(A)) > 0, \tag{5.64}$$

for genuine non-linearity of the $\lambda_{\mathcal{P}3}$-field, as proved in Proposition 5.1.2. □

5.3.1.2 $\lambda_{\mathcal{P}1}$ and $\lambda_{\mathcal{P}3}$- wave relations. Case of shocks

In this Section we treat the relations across the $\lambda_{\mathcal{P}1}$ and $\lambda_{\mathcal{P}3}$-waves, in case they are shocks.

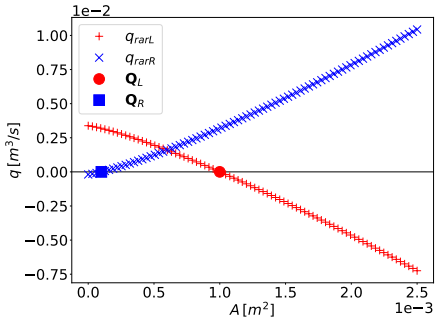

(a) The integral curves q_{rarL} and q_{rarR} defined in (5.49) for data of Test 2.

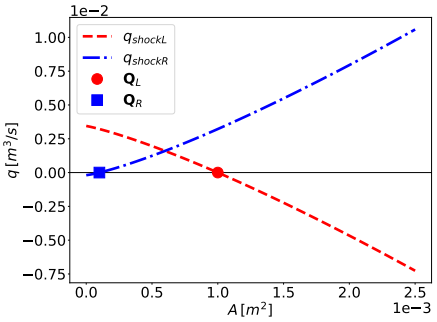

(b) The shock curves q_{shockL} and q_{shockR} defined in (5.66) and (5.90) for data of Test 2.

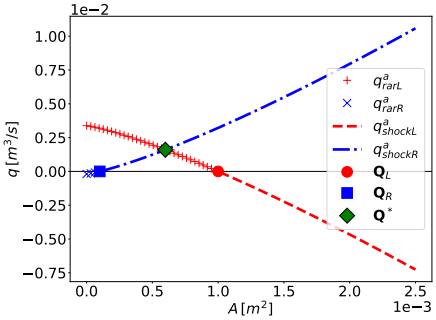

(c) The admissible rarefaction and shock curves for Test 2 as defined in Propositions 5.3.1, 5.3.2, 5.3.3.

Figure 5.2: Integral and shock curves for the Riemann problem in case of arteries with data of Test 2 in Tables 5.1, 5.2.

Proposition 5.3.2 (Entropy-satisfying left shock curves - case of arteries)**.**
If the $\lambda_{\mathcal{P}1}$ - wave, associated with a genuinely non-linear field, is an entropy satisfying shock, the related admissible shock curve is

$$q^a_{shockL}(A) = \{[A, q_{shockL}(A)]^T, \text{ s.t. } A \in \mathbb{R}^+ \text{ and } A > A_L\}, \tag{5.65}$$

where

$$q_{shockL}(A) = \begin{cases} q_L + f_L(A) & \text{for} \quad A \leq A_L, \\ q_L - f_L(A) & \text{for} \quad A > A_L. \end{cases} \quad \text{with} \quad f_L(A) = \sqrt{(A - A_L)\int_{A_L}^{A} c^2(\sigma)d\sigma}. \tag{5.66}$$

In particular $\mathbf{Q}^*_{\mathcal{P}L}$ is s.t.

$$\begin{cases} q^* = q_L - f_L(A^*), \\ \phi^*_L = \dfrac{A_L}{A^*}\phi_L, \end{cases} \tag{5.67}$$

with

$$A^* > A_L. \tag{5.68}$$

Proof. If a discontinuity propagating with speed S has constant values $\widehat{\mathbf{Q}}$, $\widetilde{\mathbf{Q}}$ on either side of it, then the Rankine-Hugoniot jump condition

$$\boldsymbol{\mathcal{P}}(\widetilde{\mathbf{Q}}) - \boldsymbol{\mathcal{P}}(\widehat{\mathbf{Q}}) = S(\widetilde{\mathbf{Q}} - \widehat{\mathbf{Q}}), \tag{5.69}$$

where $\mathcal{P}$ is defined in (5.6), must hold (see for example [44]). Now substituting $\widetilde{\mathbf{Q}} = \mathbf{Q}_{shockL}$, $\widehat{\mathbf{Q}} = \mathbf{Q}_L$ and $S = S_L$; attempting to determine the set of all states $\mathbf{Q}_{shockL}(A) = [A, q_{shockL}(A)]^T$ that can be connected to $\mathbf{Q}_L$ by a discontinuity satisfying (5.69) for some S_L, the so-called *Hugoniot Locus* of $\mathbf{Q}_L \in \mathbb{R}^3$, we obtain a system of 3 equations in $3+1$ unknowns: the 3 components of $\mathbf{Q}_{shockL}$ and S_L

$$\begin{cases} q_{shockL}(A) - q_L = S_L(A - A_L), \\ \int_{A_L}^{A} c^2(\sigma)d\sigma = S_L(q_{shockL}(A) - q_L), \\ 0 = S_L(A\phi_L(A) - A_L\phi_L), \end{cases} \tag{5.70}$$

with S_L the left shock speed.

We first analyze the first two variables A and q. With some calculations we obtain from the first and the second equation in (5.70)

$$(q_{shockL}(A) - q_L)^2 - (A - A_L)\int_{A_L}^{A} c^2(\sigma)d\sigma = 0, \tag{5.71}$$

so

$$q_{shockL}(A) - q_L = \pm\sqrt{(A - A_L)\int_{A_L}^{A} c^2(\sigma)d\sigma}. \tag{5.72}$$

As result

$$q_{shockL}(A) = q_L \pm f_L(A), \quad \text{with} \quad f_L(A) = \sqrt{(A - A_L)\int_{A_L}^{A} c^2(\sigma)d\sigma}. \tag{5.73}$$

To choose the correct sign we consider that for the first of (5.70)

$$S_L = \frac{q_{shockL}(A) - q_L}{A - A_L} = \frac{\pm f_L(A)}{A - A_L} = \frac{\pm\sqrt{(A - A_L)\int_{A_L}^{A} c^2(\sigma)d\sigma}}{A - A_L}, \tag{5.74}$$

a shock, to be entropy-satisfying, must fulfill the Lax-Entropy condition [42]

$$\lambda_{\mathcal{P}1}(\mathbf{Q}_L) > S_L > \lambda_{\mathcal{P}1}(\mathbf{Q}_{shockL}(A)) \Longrightarrow -c(A_L) > S_L > -c(A). \tag{5.75}$$

It follows that $S_L < 0$, being $c > 0$ by hypothesis in (5.2). This leads to two possibilities:

$$S_L = \begin{cases} \dfrac{+f_L(A)}{A - A_L} & \text{for} \quad A < A_L, \\ \dfrac{-f_L(A)}{A - A_L} & \text{for} \quad A > A_L, \end{cases} \tag{5.76}$$

i.e

$$q_{shockL}(A) = \begin{cases} q_L + f_L(A) & \text{for} \quad A \leq A_L, \\ q_L - f_L(A) & \text{for} \quad A > A_L, \end{cases} \tag{5.77}$$

extended to $A = A_L$ by continuity. This curve is locally at least C^1 in a neighbourhood of A_L as it is easy to prove, it belongs to the *Hugoniot Locus* of $\mathbf{Q}_L$ (please see [33]) and is shown in Fig. 5.2b. We proceed calculating

$$\frac{d\lambda_{\mathcal{P}1}(\mathbf{Q}_{shockL}(A))}{dA} = \nabla\lambda_{\mathcal{P}1}(\mathbf{Q}_{shockL}(A)) \cdot \frac{d\mathbf{Q}_{shockL}(A)}{dA}, \tag{5.78}$$

where

$$\mathbf{Q}_{shockL}(A) = \begin{bmatrix} A \\ q_{shockL}(A) \end{bmatrix}, \tag{5.79}$$

is the generic state belonging to the left shock curve, with

$$\frac{d\mathbf{Q}_{shockL}(A)}{dA} = \begin{bmatrix} 1 \\ \dfrac{dq_{shockL}(A)}{dA} \end{bmatrix} = \begin{bmatrix} 1 \\ \pm\dfrac{df_L(A)}{dA} \end{bmatrix}. \tag{5.80}$$

It is clear that

$$\frac{d\lambda_{\mathcal{P}1}(\mathbf{Q}_{shockL}(A))}{dA} = \nabla\lambda_{\mathcal{P}1}(\mathbf{Q}_{shockL}(A)) \cdot \frac{d\mathbf{Q}_{shockL}(A)}{dA} = -\frac{\partial c}{\partial A}, \tag{5.81}$$

i.e.

$$\frac{d\lambda_{\mathcal{P}1}(\mathbf{Q}_{shockL}(A))}{dA} = \frac{d\lambda_{\mathcal{P}1}(\mathbf{Q}_{rarL}(A))}{dA} < 0, \tag{5.82}$$

for genuine non-linearity of the left field in case of arteries (Proposition 5.1.2). The entropy satisfying part of the curve (5.77) considering the Lax-Entropy condition (5.75), is

$$\lambda_{\mathcal{P}1}(\mathbf{Q}_L) = \lambda_{\mathcal{P}1}(\mathbf{Q}_{shockL}(A_L)) > \lambda_{\mathcal{P}1}(\mathbf{Q}_{shockL}(A)) \Longrightarrow A > A_L. \tag{5.83}$$

In particular, considering $\mathbf{Q}^*_{\mathcal{P}L}$, which, when admissible, belongs by definition to the entropy-satisfying subset of the Hugoniot Locus of $\mathbf{Q}_L$, (5.83) becomes

$$\lambda_{\mathcal{P}1}(\mathbf{Q}_{shockL}(A_L)) > \lambda_{\mathcal{P}1}(\mathbf{Q}_{shockL}(A^*)) \Longrightarrow A^* > A_L. \tag{5.84}$$

$A^* > A_L$ is thus a *necessary* condition for an entropy-satisfying shock, and the correct formula from (5.77) is

$$q^* = q_L - f_L(A^*), \tag{5.85}$$

obtaining the statement.

Regarding the passive scalar ϕ, the third equation in (5.70) is verified for $S_L = 0$ trivial solution, or for

$$A^*\phi^*_L = A_L\phi_L \quad \Longleftrightarrow \quad \phi^*_L = \frac{A_L}{A^*}\phi_L, \tag{5.86}$$

this is clear also from the third of (5.1)

$$\partial_t(A\phi) = 0, \tag{5.87}$$

i.e.

$$A\phi = const \quad \forall t \in \mathbb{R}^+_0. \tag{5.88}$$

□

Proposition 5.3.3 (Entropy-satisfying right shock curves - case of arteries). *If the $\lambda_{\mathcal{P}1}$ - wave, associated with a genuinely non-linear field, is an entropy satisfying shock, the related admissible shock curve is*

$$q^a_{shockR}(A) = \{[A, q_{shockR}(A)]^T, \text{ s.t. } A \in \mathbb{R}^+ \text{ and } A > A_R\}, \tag{5.89}$$

where

$$q_{shockR}(A) = \begin{cases} q_R + f_R(A) & \text{for} \quad A \leq A_R, \\ q_R - f_R(A) & \text{for} \quad A > A_R. \end{cases} \quad \text{with} \quad f_R(A) = \sqrt{(A - A_R)\int_{A_R}^{A} c^2(\sigma)d\sigma}. \tag{5.90}$$

In particular $\mathbf{Q}^*_{\mathcal{P}R}$ *is s.t.*

$$\begin{cases} q^* = q_R + f_R(A^*), \\ \phi^*_R = \dfrac{A_R}{A^*}\phi_R, \end{cases} \tag{5.91}$$

with

$$A^* > A_R. \tag{5.92}$$

Proof. With a proof similar to that of Proposition 5.3.2 we obtain the result, considering that now the Lax-Entropy condition is

$$\lambda_{\mathcal{P}3}(\mathbf{Q}_{shockR}(A)) > S_R > \lambda_{\mathcal{P}3}(\mathbf{Q}_R) \Longrightarrow c(A) > S_R > c(A_R), \tag{5.93}$$

that leads to $S_R > 0$, the locally smooth right shock curve in the phase-plane (A, q) (please see Fig. 5.2b) is

$$q_{shockR}(A) = \begin{cases} q_R - f_R(A) & \text{for} \quad A \leq A_R, \\ q_R + f_R(A) & \text{for} \quad A > A_R, \end{cases} \tag{5.94}$$

and

$$\frac{d\lambda_{\mathcal{P}3}(\mathbf{Q}_{shockR}(A))}{dA} = \frac{d\lambda_{\mathcal{P}3}(\mathbf{Q}_{rarR}(A))}{dA} > 0, \tag{5.95}$$

for genuine non-linearity of the $\lambda_{\mathcal{P}3}$- field in case of arteries (Proposition 5.1.2). For the last variable ϕ the proof is similar. □

5.3.2 Solution in the Star Region for arteries

Defining the *Star Region* as the region in the half-plane (x, t) in Fig. 5.1 between the $\lambda_{\mathcal{P}1}$ and the $\lambda_{\mathcal{P}3}$ - wave, considering that a wave associated with a genuinely non-linear field can be either a shock or a rarefaction [80], we present these results

Theorem 5.3.1. *Given the Riemann problem* (5.30)*, the* $\lambda_{\mathcal{P}1}$*-wave is a physically admissible (left) rarefaction if and only if*

$$A^* \leq A_L. \tag{5.96}$$

The $\lambda_{\mathcal{P}3}$*-wave is a physically admissible (right) rarefaction if and only if*

$$A^* \leq A_R. \tag{5.97}$$

Proof.
($\Longrightarrow$)In Proposition 5.3.1 we have proved this part.
($\Longleftarrow$)In Propositions 5.3.2, 5.3.3 we have proved this part. □

Theorem 5.3.2. *Given the Riemann problem* (5.30)*, the* $\lambda_{\mathcal{P}1}$*-wave is an entropy-satisfying (left) shock if and only if*

$$A^* > A_L. \tag{5.98}$$

The $\lambda_{\mathcal{P}3}$*-wave is an entropy-satisfying (right) shock if and only if*

$$A^* > A_R. \tag{5.99}$$

Proof.
($\Longrightarrow$)In Propositions 5.3.2, 5.3.3 we have proved this part.
($\Longleftarrow$)In Proposition 5.3.1 we have proved this part. □

Proposition 5.3.4 (Graphic construction of $\mathbf{Q}^*_{\mathcal{P}}$). *Given the Riemann problem* (5.30), *the solution* $\mathbf{Q}^*_{\mathcal{P}} = [A^*, q^*]^T$ *is the unique intersection of the two curves in the phase-plane* (A, q)

$$q_{left}(A) = \begin{cases} q^a_{rarL}(A) & \text{for} \quad A \leq A_L, \\ q^a_{shockL}(A) & \text{for} \quad A > A_L, \end{cases} \tag{5.100}$$

$$q_{right}(A) = \begin{cases} q^a_{rarR}(A) & \text{for} \quad A \leq A_R, \\ q^a_{shockR}(A) & \text{for} \quad A > A_R. \end{cases} \tag{5.101}$$

The nature of the two curves at the intersection will show the wave pattern (Fig. 5.2c).

Proof. In Propositions 5.3.1, 5.3.2 and 5.3.3 we have proved that the physically admissible parts of the left and right rarefaction and shock curves are $q^a_{rarL}(A)$, $q^a_{rarR}(A)$, $q^a_{shockL}(A)$, $q^a_{shockR}(A)$ defined in the statements. The existence of these curves is a necessary condition for the physical admissibility of each type of wave, but not a sufficient one. We can find the unknown $\mathbf{Q}^*_{\mathcal{P}}$ graphically, without knowing a priori which type of wave is actually present: having constructed all these admissible curves, if the solution of our Riemann problem exists, it is unique (Remark 5.2.1), so by Propositions 5.3.1, 5.3.2 and 5.3.3 it must belong to respectively one between $q^a_{rarL}(A)$ and $q^a_{shockL}(A)$ curves and to one between $q^a_{rarR}(A)$ and $q^a_{shockR}(A)$ curves (considering that a wave associated with a genuinely non-linear field can be only a shock or a rarefaction and it is not possible to have both rarefactions and shocks together [80]). In other words the unknown $\mathbf{Q}^*_{\mathcal{P}}$ is the *unique* intersection of the $q_{left}(A)$ and $q_{right}(A)$ curves in (5.100) and (5.101) thus obtained.

Now we will prove that the intersection of the $q_{left}(A)$ and $q_{right}(A)$ curves (if it exists). This can be easily proved for any combination of waves. Considering only rarefaction waves, we define

$$h(A) = q_{rarL}(A) - q_{rarR}(A), \tag{5.102}$$

with $q_{rarL}(A)$ and $q_{rarR}(A)$ defined in (5.49). The solution of $h(A) = 0$ is clearly the sought A^*. We want to check

$$\frac{dh}{dA} = \frac{dq_{rarL}}{dA} - \frac{dq_{rarR}}{dA}, \tag{5.103}$$

considering (5.47) and (5.48) we obtain

$$\frac{dh}{dA} = -2c < 0, \quad \forall\, A \in \mathbb{R}^+, \tag{5.104}$$

so, in case of two rarefactions, function h in (5.102) is strictly monotonic in $\mathbb{R}^+$, so if a zero exists, it is unique. In case of shocks the discussion is the same, in fact recalling what stated in Propositions 5.3.2, 5.3.3, the behaviour of the two curves is the same. Thus we can conclude that for any admissible wave pattern the intersection of the two $q_{left}(A)$ and $q_{right}(A)$ curves is unique, provided it exists.

□

Following the approach presented in [87] and considering the relations across the waves presented in this Section, the exact solution of the Riemann problem for the pressure system in the Star Region, is found as follows:

Proposition 5.3.5 (Solution in the Star Region - Arteries). *The exact solution of the Riemann problem for the pressure system in the Star Region for arteries is* (5.46), *found as follows:* A^* *is the root* x *of the non-linear algebraic equation*

$$f_L(x) + f_R(x) + q_R - q_L = 0, \tag{5.105}$$

where

$$f_L(x) = \begin{cases} \int_{A_L}^{x} c(\sigma)d\sigma & \text{if } x \leq A_L \text{ (left rarefaction)}, \\ \sqrt{(x - A_L)\int_{A_L}^{x} c^2(\sigma)d\sigma} & \text{if } x > A_L \text{ (left shock)}, \end{cases} \tag{5.106}$$

$$f_R(x) = \begin{cases} \int_{A_R}^{x} c(\sigma)d\sigma & \text{if } x \leq A_R \text{ (right rarefaction)}, \\ \sqrt{(x - A_R)\int_{A_R}^{x} c^2(\sigma)d\sigma} & \text{if } x > A_R \text{ (right shock)}, \end{cases} \tag{5.107}$$

while c is the wave speed (5.2). Once A^* is known from (5.105) the solution $q^* = (Au)^*$ is

$$q^* = \frac{1}{2}(q_L + q_R) + \frac{1}{2}[f_R(A^*) - f_L(A^*)]. \tag{5.108}$$

Regarding the concentration of the passive scalar

$$\phi_L^* = \frac{A_L}{A^*\phi_L}, \qquad \phi_R^* = \frac{A_R}{A^*\phi_R}. \tag{5.109}$$

Proof. We put together the results stated in Section 5.3.1, and in Theorems 5.3.1, 5.3.2. The values of ϕ_L^* and ϕ_R^* are obtained thanks to the third of (5.1)

$$\partial_t(A\phi) = 0, \tag{5.110}$$

which gives the result. □

The integrals in case of arteries having $m = 0.5$ and $n = 0$ in (5.4), are explicitly calculated. Equation (5.105) is solved with a globally convergent Newton-Raphson method (see Appendix B.2).

5.3.3 Solution inside the rarefactions

Proposition 5.3.6 (Solution inside the left rarefaction). *The exact solution of the Riemann problem for the pressure system inside the left rarefaction is*

$$\mathbf{Q}_{irarL} = \begin{bmatrix} A_{irarL} \\ A_{irarL}u_{irarL} \\ A_{irarL}\phi_{irarL} \end{bmatrix}, \tag{5.111}$$

where A_{irarL} is obtained solving for the unknown x the following

$$\frac{\mathcal{X}}{t} + c(x) = 0, \tag{5.112}$$

being $\mathcal{X} = x - x_d$, where x is the specific place of the domain (vessel) in which we are calculating the desired values, x_d is the vessel spatial coordinate of the discontinuity, and t is the time. Afterwards the actual $q_{irarL} = A_{irarL}u_{irarL}$ corresponding to the found A_{irarL} is

$$q_{irarL}(A_{irarL}) = q_L - \int_{A_L}^{A_{irarL}} c(A)dA. \tag{5.113}$$

Regarding the last variable

$$\phi_{irarL} = \frac{A_L}{A_{irarL}}\phi_L. \tag{5.114}$$

Proof. We look for a similarity solution of the type

$$\mathbf{Q}(x,t) = v\left(\frac{\mathcal{X}}{t}\right). \tag{5.115}$$

Being

$$\partial_t \mathbf{Q} = -v'\left(\frac{\mathcal{X}}{t}\right)\frac{\mathcal{X}}{t^2}, \qquad \partial_x \mathbf{Q} = v'\left(\frac{\mathcal{X}}{t}\right)\frac{1}{t}, \tag{5.116}$$

so, considering system (5.1)

$$-v'\left(\frac{\mathcal{X}}{t}\right)\frac{\mathcal{X}}{t^2} + \mathcal{J}_{\mathcal{P}}(\mathbf{Q})v'\left(\frac{\mathcal{X}}{t}\right)\frac{1}{t} = 0, \tag{5.117}$$

with $\mathcal{J}_{\mathcal{P}}(\mathbf{Q})$ the Jacobian (5.7), then (5.117) becomes

$$\frac{1}{t}\left(\mathcal{J}_{\mathcal{P}}(\mathbf{Q}) - \frac{\mathcal{X}}{t}\mathbb{I}\right)v'\left(\frac{\mathcal{X}}{t}\right) = 0, \tag{5.118}$$

that is true if and only if

$$v'\left(\frac{\mathcal{X}}{t}\right) = 0, \tag{5.119}$$

trivial solution, or

$$\left(\mathcal{J}_{\mathcal{P}}(\mathbf{Q}) - \frac{\mathcal{X}}{t}\mathbb{I}\right)v'\left(\frac{\mathcal{X}}{t}\right) = 0, \tag{5.120}$$

i.e if and only if $v'\left(\frac{\mathcal{X}}{t}\right)$ is an eigenvector of $\mathcal{J}_{\mathcal{P}}(\mathbf{Q})$ and $\frac{\mathcal{X}}{t}$ is the corresponding eigenvalue, i.e.

$$\frac{\mathcal{X}}{t} = \lambda_{\mathcal{P}k}, \tag{5.121}$$

with λ_k in (5.8). This is possible only for eigenvalues and eigenvectors associated with genuinely non-linear fields [33]. Considering (5.121), we are looking for (5.111) s.t.

$$\frac{\mathcal{X}}{t} = \lambda_{\mathcal{P}1}(\mathbf{Q}_{irarL}) = -c(A_{irarL}), \tag{5.122}$$

with c in (5.2), A_{irarL} is the value of A inside the left rarefaction. We find the actual A_{irarL} corresponding to the given $\frac{\mathcal{X}}{t}$, solving (5.122), i.e. solving for the unknown x, equation (5.112). Regarding the last variable, the result is straightforward due to the third of (5.1). □

Please note that for (5.54) and (5.121), the actual boundaries of the left rarefaction in the half-plane (x,t) are the charateristics s.t.

$$\begin{aligned} \frac{\mathcal{X}}{t} &= \lambda_{\mathcal{P}1}(\mathbf{Q}_L), \quad \text{left border,} \\ \frac{\mathcal{X}}{t} &= \lambda_{\mathcal{P}1}(\mathbf{Q}^*_{\mathcal{P}L}), \quad \text{right border.} \end{aligned} \tag{5.123}$$

Proposition 5.3.7 (Solution inside the right rarefaction). *The exact solution of the Riemann problem for the pressure system inside the right rarefaction is*

$$\mathbf{Q}_{irarR} = \begin{bmatrix} A_{irarR} \\ A_{irarR} u_{irarR} \\ A_{irarR} \phi_{irarR} \end{bmatrix}, \tag{5.124}$$

where A_{irarR} is obtained solving for the unknown x the following

$$\frac{\mathcal{X}}{t} - c(x) = 0, \tag{5.125}$$

being $\mathcal{X} = x - x_d$, where x is the specific place of the domain (vessel) in which we are calculating the desired values, x_d is the vessel spatial coordinate of the discontinuity, and t is the time. Afterwards that the actual q_{irarR} corresponding to the found A_{irarR} is

$$q_{irarR}(A_{irarR}) = q_R + \int_{A_R}^{A_{irarR}} c(A) dA. \tag{5.126}$$

Regarding the last variable

$$\phi_{irarR} = \frac{A_R}{A_{irarR}} \phi_R. \tag{5.127}$$

Proof. As in the proof for the left part, looking for a similarity solution as in (5.115), and considering (5.121), we are looking for (5.124) s.t.

$$\frac{\mathcal{X}}{t} = \lambda_{\mathcal{P}3}(\mathbf{Q}_{irarR}) = c(A_{irarR}). \tag{5.128}$$

We find the actual A_{irarR} corresponding to the given $\frac{\mathcal{X}}{t}$, solving (5.128), i.e. solving for the unknown x, (5.125). Regarding the last variable, the result is straightforward due to the third of (5.1). □

Please note that for (5.63) and (5.121), the actual boudaries of the right rarefaction are in the half-plane (x, t)

$$\begin{aligned} \frac{\mathcal{X}}{t} &= \lambda_{\mathcal{P}3}(\mathbf{Q}^*_{\mathcal{P}R}), \quad \text{left border}, \\ \frac{\mathcal{X}}{t} &= \lambda_{\mathcal{P}3}(\mathbf{Q}_R), \quad \text{right border}. \end{aligned} \tag{5.129}$$

5.3.4 The complete exact solution of the Riemann problem for the pressure system in arteries

In this Section we present the sampling of the complete exact solution of the Riemann problem for the pressure system (5.1) in case of arteries. The initial data in this case are specified as follows

$$\mathbf{Q}_L = \begin{bmatrix} A_L \\ A_L u_L \\ A_L \phi_L \end{bmatrix}, \qquad \mathbf{Q}_R = \begin{bmatrix} A_R \\ A_R u_R \\ A_R \phi_R \end{bmatrix}. \tag{5.130}$$

Being as before $\mathcal{X} = x - x_d$, where x is the specific place of the domain (vessel) in which we are calculating the desired values, x_d is the vessel spatial coordinate of the discontinuity, and t is the time, thanks to Theorems 5.3.1, 5.3.2 the complete solution is

- if $A^* \leq A_L$ (left rarefaction):

$$\mathbf{Q}(x,t) = \begin{cases} \mathbf{Q}_L & \text{if} \quad \mathcal{X} < -c(A_L)t, \\ \mathbf{Q}_{irarL} & \text{if} \quad -c(A_L)t \leq \mathcal{X} \leq -c(A^*)t, \\ \mathbf{Q}^*_{\mathcal{P}L} & \text{if} \quad -c(A^*)t < \mathcal{X} \leq 0, \end{cases} \tag{5.131}$$

- if $A^* > A_L$ (left shock):

$$\mathbf{Q}(x,t) = \begin{cases} \mathbf{Q}_L & \text{if} \quad \mathcal{X} \leq S_L t, \\ \mathbf{Q}^*_{\mathcal{P}L} & \text{if} \quad S_L t < \mathcal{X} \leq 0. \end{cases} \tag{5.132}$$

Similarly on the right side the complete solution is

- if $A^* \leq A_R$ (right rarefaction):

$$\mathbf{Q}(x,t) = \begin{cases} \mathbf{Q}^*_{\mathcal{P}R} & \text{if} \quad 0 < \mathcal{X} < c(A^*)t, \\ \mathbf{Q}_{irarR} & \text{if} \quad c(A)^* t \leq \mathcal{X} \leq c(A_R)t, \\ \mathbf{Q}_R & \text{if} \quad \mathcal{X} > c(A_R)t, \end{cases} \tag{5.133}$$

- if $A^* > A_R$ (right shock):

$$\mathbf{Q}(x,t) = \begin{cases} \mathbf{Q}^*_{\mathcal{P}R} & \text{if} \quad 0 < \mathcal{X} \leq S_R t, \\ \mathbf{Q}_R & \text{if} \quad \mathcal{X} > S_R t. \end{cases} \tag{5.134}$$

$\mathbf{Q}^*_{\mathcal{P}L}$ and $\mathbf{Q}^*_{\mathcal{P}R}$ are defined in Proposition 5.3.5, $\mathbf{Q}_{irarL}$ is defined in Proposition 5.3.6, $\mathbf{Q}_{irarR}$ in Proposition 5.3.7, c is described in (5.2). S_L and S_R are the left and the right shock speeds and are defined according to the Rankine-Hugoniot condition, from Propositions 5.3.2, 5.3.3.

$$S_L = \frac{q_L - q^*}{A_L - A^*}, \qquad S_R = \frac{q_R - q^*}{A_R - A^*}. \tag{5.135}$$

5.3.5 RESULTS

Here we show and further validate the results of the exact solution of the Riemann problem for the pressure system presented in Section 5.3.4 by comparing them with numerical mesh-independent solutions obtained with a centred second order extension of FORCE numerical scheme, FORCEII (Appendix A.2), with a mesh of $I = 5000$ computational cells and a Courant–Friedrichs–Lewy number (C_{cfl}) of 0.9. We propose three tests in which we cover all the possibilities given by the genuinely non-linear fields, i.e. rarefactions and shocks. Initial data are reported in Tables 5.1, 5.2, results are depicted in Figs. 5.3, 5.4, 5.5. In Table 5.3 we present the values of the exact solution in the Star Region for the pressure system in arteries for the unknowns A, q, ϕ. It is worth noting Test 2 whose data lead to a transonic rarefaction in case of Riemann problem for the complete system of 1D blood flow, while in case of the pressure system reduces to a left subsonic rarefaction and a right shock. Overall a strong correspondence is observed between the exact solution and the one obtained through the numerical method. In addition we propose, for each test, the plots of the admissible rarefaction and shock curves presented in Section 5.3.

Table 5.1: Initial conditions for Tests from 1 to 3. The wave patterns are: R=rarefaction, C=contact discontinuity, S=shock. The units of measures used for this Thesis are: m, s, Kg, Pa.

Test	$A_L[m^2]$	$u_L[m/s]$	ϕ_L	$A_R[m^2]$	$u_R[m/s]$	ϕ_R	Wave pattern
1	$3.5 \cdot 10^{-4}$	0.00	1.00	$3.0 \cdot 10^{-4}$	0.00	0.50	RCS
2	$10.00 \cdot 10^{-4}$	0.00	1.00	$1.0 \cdot 10^{-4}$	0.00	0.50	RCS
3	$3.10 \cdot 10^{-4}$	-0.50	1.00	$3.14 \cdot 10^{-4}$	0.50	0.50	RCR

Table 5.2: Parameters used for Tests from 1 to 3: domain length ℓ, blood density ρ, vessel wall stiffness K, reference cross-sectional area A_0, external pressure p_e, location of the initial discontinuity x_d and output time t_{End}.

Test	Vessel	$\ell[m]$	ρ	$K[Pa]$	$A_0[m^2]$	$p_e[Pa]$	$x_d[m]$	$t_{End}[s]$
1	Artery	0.50	1000.00	20005.00	$3.14 \cdot 10^{-4}$	0.00	0.50ℓ	0.05
2	Artery	0.50	1000.00	20005.00	$3.14 \cdot 10^{-4}$	0.00	0.50ℓ	0.04
3	Artery	0.50	1000.00	20005.00	$3.14 \cdot 10^{-4}$	0.00	0.50ℓ	0.05

Table 5.3: Exact solution of the Riemann problem for the pressure system in the Star Region for arteries.

Test	$A^*[m^2]$	$q^*[m/s]$	ϕ_L^*	ϕ_R^*
1	$3.2524\ 10^{-4}$	7.973610^{-5}	1.0761	0.4611
2	$5.9862\ 10^{-4}$	1.6002410^{-3}	1.6704	0.0835
3	$2.6153\ 10^{-4}$	-5.315210^{-6}	1.1853	0.6003

5.4 Exact solution of the Riemann problem for the pressure system in veins

The model is that presented in Section 5.2, now we will describe how to calculate the exact solution of the Riemann problem in case of veins.

5.4.1 Wave relations

The $\lambda_{\mathcal{P}2}$- wave is associated with a linearly degenerate field and is a contact discontinuity, so the relations across this wave are those in Proposition 5.2.2. Regarding the $\lambda_{\mathcal{P}1}$- and $\lambda_{\mathcal{P}3}$- waves, in case of veins there is a loss of genuine non-linearity that leads to the formation of smooth waves (rarefactions), discontinuous waves (shocks) or compound (mixed) waves [49].

5.4.1.1 $\lambda_{\mathcal{P}1}$ and $\lambda_{\mathcal{P}3}$- wave relations. Case of rarefactions

The generalized Riemann invariants in Proposition 5.2.1, still hold $\forall A \neq A_c \in \mathbb{R}^+$. The third equation in (5.1) is not affecting the others so variable ϕ can be treated separately. (5.47) and (5.48) hold with c in (5.2) but with the parameters for veins in (5.3) and (5.4). Solving them for $A \in \mathbb{R}^+$, results in the construction of the two integral curves, one for each wave (see Fig. 5.6)

$$q_{rarL}(A) \quad \text{and} \quad q_{rarR}(A) \quad \text{with} \quad A \in \mathbb{R}^+. \tag{5.136}$$

Theorem 5.4.1. *If the $\lambda_{\mathcal{P}k}$-th, $k = 1$ or 3, field of system (5.1) is nongenuinely non-linear then $\lambda_{\mathcal{P}k}(\mathbf{Q}_{rarj}(A))$, with $\mathbf{Q}_{rarj}(A) = (A, q_{rarj}(A))$, $j = L$ or R, the corresponding integral curve and $A \in \mathbb{R}^+$, has a global maximum (minimum) in A_c defined in (5.12).*

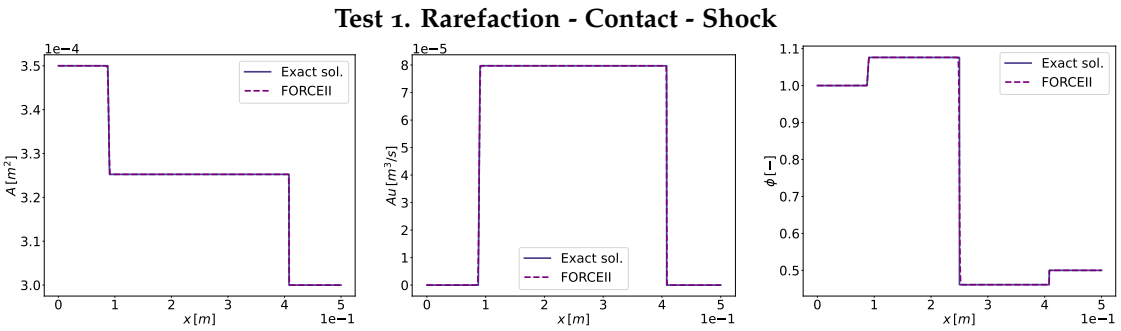

(a) Exact solution vs. FORCEII scheme.

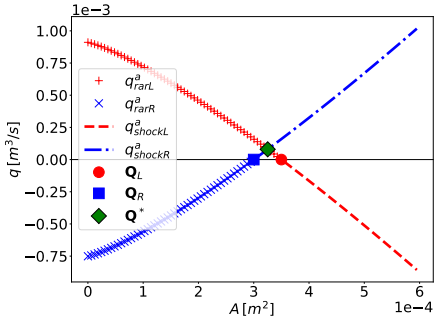

(b) The admissible rarefaction and shock curves in the phase-plane

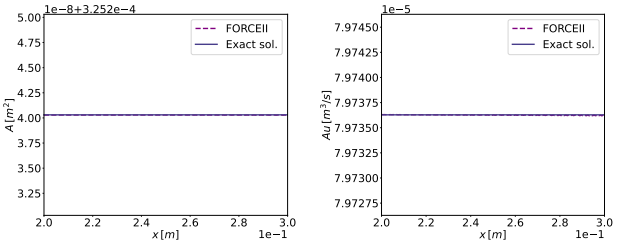

(c) A detail of A^* and q^*

Figure 5.3: Exact solution of the Riemann problem for the pressure system in an artery with data of Test 1 vs. FORCEII scheme. This Riemann problem shows a left rarefaction, a contact discontinuity for the passive scalar and a right shock. Initial data in Tables 5.1, 5.2.

Proof. From (5.47) (5.48)

$$\frac{d\mathbf{Q}_{rarj}}{dA}(A) = \begin{bmatrix} 1 \\ \dfrac{dq_{rarj}}{dA}(A) \end{bmatrix} = \mathbf{R}_k(\mathbf{Q}_{rarj}(A)), \tag{5.137}$$

so

$$\frac{d\lambda_k(\mathbf{Q}_{rarj}(A))}{dA} = \nabla\lambda_k(\mathbf{Q}_{rarj}(A)) \cdot \mathbf{R}_k(\mathbf{Q}_{rarj}(A)), \tag{5.138}$$

finally from Proposition 5.1.2

$$\begin{aligned} &\frac{d\lambda_{\mathcal{P}1}(\mathbf{Q}_{rarL}(A))}{dA} \quad \begin{cases} > 0 & \text{for} \quad A < A_c, \\ = 0 & \text{for} \quad A = A_c, \\ < 0 & \text{for} \quad A > A_c; \end{cases} \\ &\frac{d\lambda_{\mathcal{P}3}(\mathbf{Q}_{rarR}(A))}{dA} \quad \begin{cases} < 0 & \text{for} \quad A < A_c, \\ = 0 & \text{for} \quad A = A_c, \\ > 0 & \text{for} \quad A > A_c. \end{cases} \end{aligned} \tag{5.139}$$

□

We recall this definition

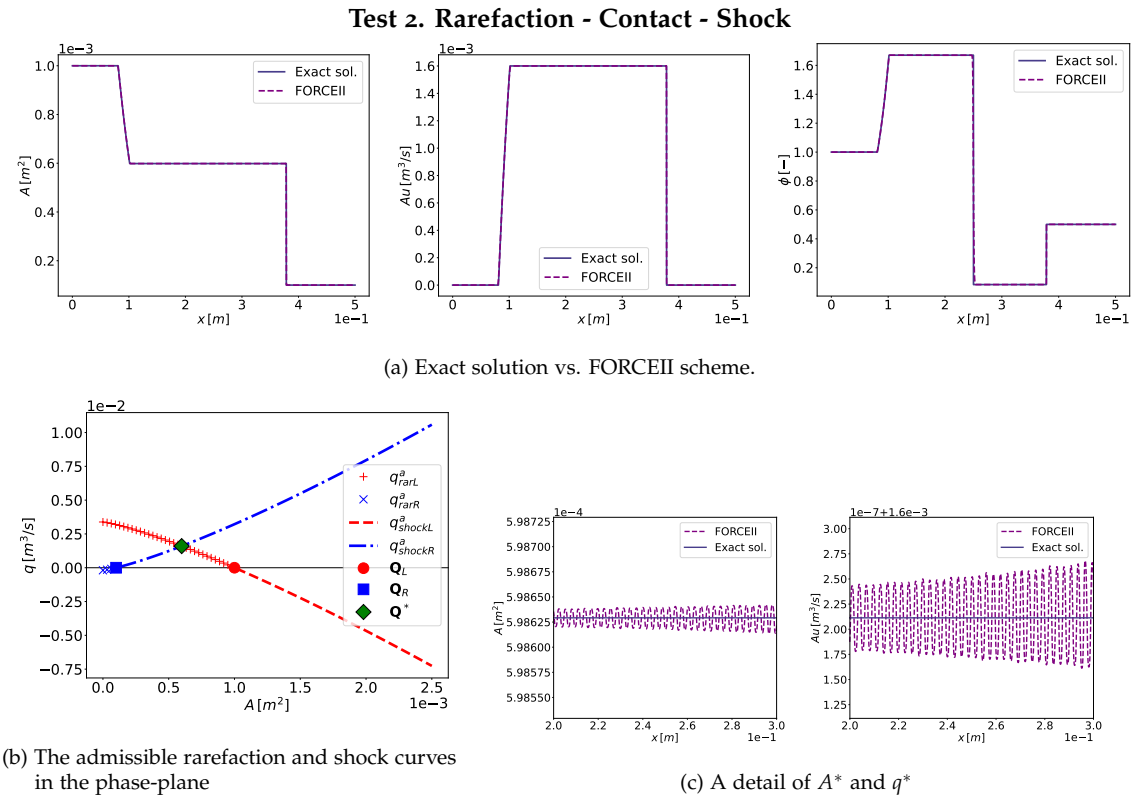

(a) Exact solution vs. FORCEII scheme.

(b) The admissible rarefaction and shock curves in the phase-plane

(c) A detail of A^* and q^*

Figure 5.4: Exact solution of the Riemann problem for the pressure system in an artery with data of Test 2 vs. FORCEII scheme. This Riemann problem shows a left rarefaction, a contact discontinuity for the passive scalar and a right shock. This test for the complete system of 1D blood flow equations leads to a left transonic rarefaction. Initial data in Tables 5.1, 5.2.

Definition 5.4.1 (Rarefaction in a wave associated with a nongenuinely non-linear field [17])**.** Having as initial state the left state $\mathbf{Q}_{\widehat{L}}$, the $\widehat{L}-$rarefaction curve $q_{rar\widehat{L}}(A)$ is the integral curve results of the ODEs (5.47), (5.48) and passing through $\mathbf{Q}_{\widehat{L}}$. Its admissible part denoted by $q^a_{rar\widehat{L}}(A)$ is the part such that

$$\lambda_k(A_{\widehat{L}}) \leq \lambda_k(A), \quad A \in \mathbb{R}^+, \tag{5.140}$$

with λ_k the related eigenvalue and the $\lambda_k(A)$ function monotonic in A.

Having as initial state a right state, the valid condition is clearly

$$\lambda_k(A) \leq \lambda_k(A_{\widehat{R}}), \quad A \in \mathbb{R}^+. \tag{5.141}$$

We now construct the admissible rarefaction curves in the same manner as in case of arteries.

Proposition 5.4.1 (Physically admissible rarefaction curves)**.**
If the $\lambda_{\mathcal{P}1}$-wave, associated with a nongenuinely non-linear field, is a smooth wave (i.e. is a physically admissible rarefaction), the related admissible rarefaction curve is

$$q^a_{rarL}(A) = \{[A, q_{rarL}(A)]^T, \text{ s.t. } c(A) \leq c(A_L), \quad A \in \mathbb{R}^+, A \in \mathcal{I}_L = [\min(A_L, A_c), \max(A_L, A_c)]\}, \tag{5.142}$$

with $q_{rarL}(A)$ in (5.136). In particular $c(A^*) \leq c(A_L)$.

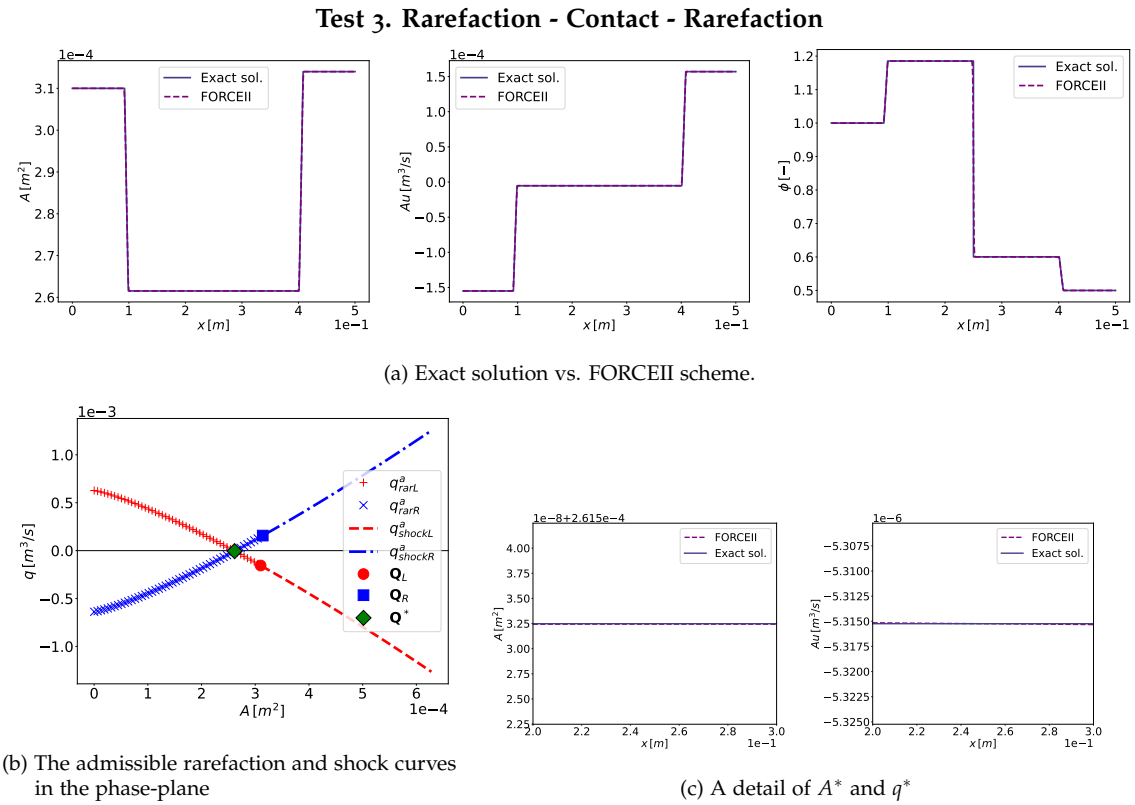

(a) Exact solution vs. FORCEII scheme.

(b) The admissible rarefaction and shock curves in the phase-plane

(c) A detail of A^* and q^*

Figure 5.5: Exact solution of the Riemann problem for the pressure system in an artery with data of Test 4 vs. FORCEII scheme. This Riemann problem shows a left rarefaction, a contact discontinuity for the passive scalar and a right rarefaction. Initial data in Tables 5.1, 5.2.

If the $\lambda_{\mathcal{P}3}$-wave associated with a nongenuinely non-linear field, is a smooth wave (i.e. is a physically admissible rarefaction), the related admissible rarefaction curve is

$$q^a_{rarR}(A) = \{[A, q_{rarR}(A)]^T, \text{ s.t. } c(A) \leq c(A_R), \quad A \in \mathbb{R}^+, A \in \mathcal{I}_R = [\min(A_R, A_c), \max(A_R, A_c)]\}, \tag{5.143}$$

with $q_{rarR}(A)$ in (5.136). In particular $c(A^*) \leq c(A_R)$.

Proof. The proof is similar to the case of arteries, in fact due to Def. 5.4.1 a rarefaction in a nongenuinely non-linear filed can occur in a part of the domain $\mathcal{I} \subset \mathbb{R}^+$ where the related $\lambda_{\mathcal{P}k}(A)$ function is monotonic. In other words, considering (5.139), the left admissible rarefaction curve having as initial (left) state, A_L, is bounded by A_c and the right one, having as initial (right) state A_R, by A_c indeed. This is the reason for the interval $\mathcal{I}_j = [\min(A_j, A_c), \max(A_j, A_c)]$ in the statement. It is worth noting that the boundary A_c should not be included in the interval, in fact the equation denoting a characteristic inside a rarefaction $\lambda_k = \dfrac{x}{t}$, already presented in Section 5.3.3, can not be derived if $\dfrac{d\lambda_k}{dA} = 0$ [33]. In addition it is worth noting that, differently from the case of arteries, the conditions of admissibility of the rarefaction curves in case of veins can not be related to the particular position of A with respect to A_j anymore, due to the curvature of the $\lambda_{\mathcal{P}k}$ function. □

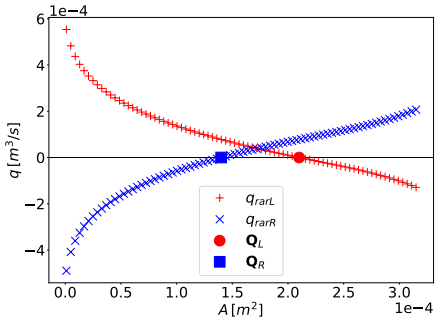

(a) The integral curves q_{rarL} and q_{rarR} defined in (5.136) for data of Test 4.

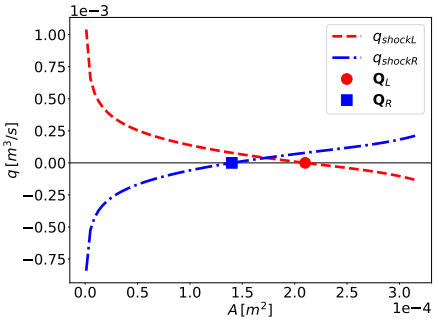

(b) The q_{shockL} and q_{shockR} shock curves defined in (5.148), (5.167) for data of Test 4.

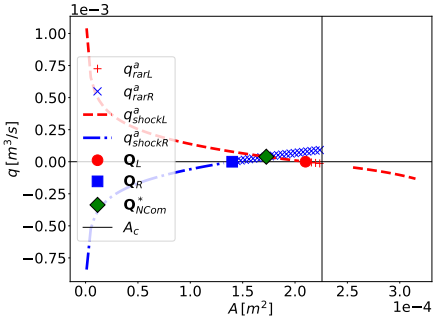

(c) The admissible rarefaction and shock curves for data of Test 4. It is worth noting that differently from the case of arteries the admissible curves are not longer continuous.

Figure 5.6: Integral and shock curves for the Riemann problem in case of veins with data of Test 4 in Tables 5.4, 5.5. This test does not present compound waves, for which more admissible shock curves have to be added, as explained in Section 5.4.6. It is worth noting that differently from the case of arteries the integral and shock curves are not convex or concave anymore and the admissible ones are not longer continuous.

5.4.1.2 $\lambda_{\mathcal{P}1}$ and $\lambda_{\mathcal{P}3}$- wave relations. Case of shocks

In nongenuinely non-linear fields if a discontinuity propagating with speed S has constant values $\mathbf{Q}_{\hat{L}}$ and $\mathbf{Q}_{\hat{R}}$ on either side of it, then the Rankine-Hugoniot jump condition

$$\boldsymbol{\mathcal{P}}(\mathbf{Q}_{\hat{R}}) - \boldsymbol{\mathcal{P}}(\mathbf{Q}_{\hat{L}}) = S(\mathbf{Q}_{\hat{R}} - \mathbf{Q}_{\hat{L}}), \tag{5.144}$$

where $\boldsymbol{\mathcal{P}}$ is deifined in (5.6) must hold [49]. A shock, to be entropy-satisfying must fulfill the so-called Oleinik-Liu condition [49]:

$$S(\mathbf{Q}_{\hat{L}}, \mathbf{Q}_{\hat{R}}) \leq S(\mathbf{Q}, \mathbf{Q}_{\hat{L}}) \quad \forall \mathbf{Q} \in q_{shock}(A) \quad s.t. \quad A \in \mathcal{I} = [\min(A_{\hat{L}}, A_{\hat{R}}), \max(A_{\hat{L}}, A_{\hat{R}})], \tag{5.145}$$

where S is the shock speed and $q_{shock}(A)$ is the related shock curve. The Oleinik-Liu condition (5.145) implies

$$\lambda_k(\mathbf{Q}_{\hat{L}}) \geq S(\mathbf{Q}_{\hat{L}}, \mathbf{Q}_{\hat{R}}) \geq \lambda_k(\mathbf{Q}_{\hat{R}}), \tag{5.146}$$

[49]. In case of genuinely non-linear fields (5.146) reduces to the Lax-Entropy condition [42]

$$\lambda_k(\mathbf{Q}_{\hat{L}}) > S(\mathbf{Q}_{\hat{L}}, \mathbf{Q}_{\hat{R}}) > \lambda_k(\mathbf{Q}_{\hat{R}}). \tag{5.147}$$

Proposition 5.4.2 (Admissibility of left shock curves - case of veins)**.**
If the $\lambda_{\mathcal{P}1}$ - wave, associated with a nongenuinely non-linear field, is an entropy satisfying shock, the admissible shock curve is

$$q^a_{shockL}(A) = \{[A, q_{shockL}(A)]^T, \text{ being } A \in \mathbb{R}^+ \text{ s.t. } S(\mathbf{Q}_L, \mathbf{Q}_{shockL}(A)) \leq S(\mathbf{Q}_{shockL}(\widetilde{A}), \mathbf{Q}_L), \\ \forall \widetilde{A} \in [\min(A, A_L), \max(A, A_L)], \tag{5.148}$$

where

$$q_{shockL}(A) = \begin{cases} q_L + f_L(A) & \text{for} \quad A \leq A_L, \\ q_L - f_L(A) & \text{for} \quad A > A_L \end{cases} \quad \text{with} \quad f_L(A) = \sqrt{(A - A_L)\int_{A_L}^{A} c^2(\sigma)d\sigma}. \tag{5.149}$$

In particular $\mathbf{Q}^*_{\mathcal{P}L}$ is s.t.

- *for $A^* > A_L$*

$$\begin{cases} q^* = q_L - f_L(A^*), \\ \phi^*_L = \dfrac{A_L}{A^*}\phi_L. \end{cases} \tag{5.150}$$

- *for $A^* \leq A_L$*

$$\begin{cases} q^* = q_L + f_L(A^*), \\ \phi^*_L = \dfrac{A_L}{A^*}\phi_L. \end{cases} \tag{5.151}$$

and

$$c(A^*) > c(A_L). \tag{5.152}$$

Proof. As in the case of arteries, if a discontinuity propagating with speed S has constant values $\widehat{\mathbf{Q}}$, $\widetilde{\mathbf{Q}}$ on either side of it, then the Rankine-Hugoniot jump condition

$$\boldsymbol{\mathcal{P}}(\widetilde{\mathbf{Q}}) - \boldsymbol{\mathcal{P}}(\widehat{\mathbf{Q}}) = S(\widetilde{\mathbf{Q}} - \widehat{\mathbf{Q}}), \tag{5.153}$$

where $\boldsymbol{\mathcal{P}}$ is defined in (5.6), must hold [49]. Now substituting $\widetilde{\mathbf{Q}} = \mathbf{Q}_{shockL}$, $\widehat{\mathbf{Q}} = \mathbf{Q}_L$ and $S = S_L$; attempting to determine the set of all states $\mathbf{Q}_{shockL}(A) = [A, q_{shockL}(A)]^T$ that can be connected to $\mathbf{Q}_L$ by a discontinuity satisfying (5.153) for some S_L, the so-called *Hugoniot Locus* of $\mathbf{Q}_L \in \mathbb{R}^3$, we obtain a system of 3 equations in $3+1$ unknowns: the 3 components of $\mathbf{Q}_{shockL}$ and S_L

$$\begin{cases} q_{shockL}(A) - q_L = S_L(A - A_L), \\ \displaystyle\int_{A_L}^{A} c^2(\sigma)d\sigma = S_L(q_{shockL}(A) - q_L), \\ 0 = S_L(A\phi_L(A) - A_L\phi_L), \end{cases} \tag{5.154}$$

with S_L the left shock speed.

We first analyze the first two variables A and q. With some calculations we obtain from the first and the second equation in (5.154)

$$(q_{shockL}(A) - q_L)^2 - (A - A_L)\int_{A_L}^{A} c^2(\sigma)d\sigma = 0, \tag{5.155}$$

so

$$q_{shockL}(A) - q_L = \pm\sqrt{(A - A_L)\int_{A_L}^{A} c^2(\sigma)d\sigma}. \tag{5.156}$$

As result

$$q_{shockL}(A) = q_L \pm f_L(A), \quad \text{with} \quad f_L(A) = \sqrt{(A - A_L)\int_{A_L}^{A} c^2(\sigma)d\sigma}. \tag{5.157}$$

To choose the correct sign we consider that for the first of (5.154)

$$S_L = \frac{q_{shockL}(A) - q_L}{A - A_L} = \frac{\pm f_L(A)}{A - A_L} = \frac{\pm\sqrt{(A - A_L)\int_{A_L}^{A} c^2(\sigma)d\sigma}}{A - A_L}, \tag{5.158}$$

a shock, to be entropy-satisfying, must fulfill the Oleinik-Liu condition (5.145) that implies (5.146), i.e.

$$\lambda_{\mathcal{P}1}(\mathbf{Q}_L) \geq S_L \geq \lambda_{\mathcal{P}1}(\mathbf{Q}_{shockL}(A)) \Longrightarrow -c(A_L) \geq S_L \geq -c(A). \tag{5.159}$$

It follows that $S_L < 0$, being $c > 0$ by hypothesis in (5.2). This leads to two possibilities:

$$S_L = \begin{cases} \dfrac{+f_L(A)}{A - A_L} & \text{for} \quad A < A_L, \\ \dfrac{-f_L(A)}{A - A_L} & \text{for} \quad A > A_L, \end{cases} \tag{5.160}$$

i.e

$$q_{shockL}(A) = \begin{cases} q_L + f_L(A) & \text{for} \quad A \leq A_L, \\ q_L - f_L(A) & \text{for} \quad A > A_L, \end{cases} \tag{5.161}$$

extended to $A = A_L$ by continuity. This curve is locally at least C^1 in a neighbourhood of A_L as it is easy to prove, and it belongs to the *Hugoniot Locus* of $\mathbf{Q}_L$ (please see [33]). We must notice that

$$\frac{d\lambda_{\mathcal{P}1}(\mathbf{Q}_{shockL}(A))}{dA} = \nabla\lambda_{\mathcal{P}1}(\mathbf{Q}_{shockL}(A)) \cdot \frac{d\mathbf{Q}_{shockL}(A)}{dA} = -\frac{\partial c}{\partial A}, \tag{5.162}$$

i.e.

$$\frac{d\lambda_{\mathcal{P}1}(\mathbf{Q}_{shockL}(A))}{dA} = \frac{d\lambda_{\mathcal{P}1}(\mathbf{Q}_{rarL}(A))}{dA}. \tag{5.163}$$

so the sign of $\dfrac{d\lambda_{\mathcal{P}1}(\mathbf{Q}_{shockL}(A))}{dA}$ changes from positive to negative, according to Proposition 5.1.2 i.e. the function $\lambda_{\mathcal{P}1}(\mathbf{Q}_{shockL}(A))$ is a concave function w.r.t. variable $A \in \mathbb{R}^+$. On the other hand the concavity of the $\lambda_{\mathcal{P}1}(A)$ function prevents us to choose one branck of the (5.161) function as we did in the case of arteries. In particular, considering $\mathbf{Q}^*_{\mathcal{P}L}$, which, when admissible, belongs by definition to the entropy-satisfying subset of the Hugoniot Locus of $\mathbf{Q}_L$, (5.161) becomes

$$q^* = \begin{cases} q_L + f_L(A^*) & \text{for} \quad A^* < A_L, \\ q_L - f_L(A^*) & \text{for} \quad A^* > A_L. \end{cases} \tag{5.164}$$

and from (5.159) we obtain

$$\lambda_{\mathcal{P}1}(\mathbf{Q}_L) = \lambda_{\mathcal{P}1}(\mathbf{Q}_{shockL}(A_L)) \geq S_L \geq \lambda_{\mathcal{P}1}(\mathbf{Q}_{shockL}(A^*)) \Longrightarrow -c(A_L) > -c(A^*), \tag{5.165}$$

in fact

$$\lambda_{\mathcal{P}1}(\mathbf{Q}_L) = S_L = \lambda_{\mathcal{P}1}(\mathbf{Q}_{shockL}(A^*)), \tag{5.166}$$

and consequently $c(A_L) = c(A^*)$, is not a possibility that we encounter.

The proof for the passive scalar is the same as in the case of arteries. □

Proposition 5.4.3 (Admissibility of right shock curves - case of veins).
If the $\lambda_{\mathcal{P}3}$ - wave, associated with a nongenuinely non-linear field, is an entropy satisfying shock, the admissible shock curve is

$$q^a_{shockR}(A) = \{[A, q_{shockR}(A)]^T, \text{ being } A \in \mathbb{R}^+ \; s.t. \; S(\mathbf{Q}_R, \mathbf{Q}_{shockR}(A)) \geq S(\mathbf{Q}_{shockR}(\widetilde{A}), \mathbf{Q}_R) \quad \forall \widetilde{A} \in [\min(A, A_R), \max(A, A_R)], \tag{5.167}$$

where

$$q_{shockR}(A) = \begin{cases} q_R - f_R(A) & \text{for} \quad A \leq A_R, \\ q_R + f_R(A) & \text{for} \quad A > A_R. \end{cases} \quad \text{with} \quad f_R(A) = \sqrt{(A - A_R)\int_{A_R}^{A} c^2(\sigma) d\sigma}. \tag{5.168}$$

In particular $\mathbf{Q}^*_{\mathcal{P}R}$ is s.t.

- *for $A^* > A_R$*

$$\begin{cases} q^* = q_R + f_R(A^*), \\ \phi^*_R = \dfrac{A_R}{A^*}\phi_R, \end{cases} \tag{5.169}$$

- *for $A^* < A_R$*

$$\begin{cases} q^* = q_R - f_R(A^*), \\ \phi^*_R = \dfrac{A_R}{A^*}\phi_R. \end{cases} \tag{5.170}$$

with

$$c(A^*) > c(A_R). \tag{5.171}$$

Proof. With a proof similar to that of Proposition 5.4.2 the statement is straightforward. □

5.4.2 Solution in the Star Region for veins in absence of compound waves

Differently from the case of arteries, a wave associated with a nongenuinely non-linear field can present shocks, rarefactions and also compound waves: these latter being composed by shocks and rarefactions together.

Nevertheless, as a first step, considering Propositions 5.4.1, 5.4.2, 5.4.3 in the following Theorems we calculate the exact solution of the Riemann problem for the pressure system in the Star Region, only in presence of rarefactions and shocks.

Theorem 5.4.2. *Given the Riemann problem (5.30), and ignoring the existence of the compound waves, the $\lambda_{\mathcal{P}1}$-wave is a physically admissible (left) rarefaction if and only if*

$$c(A^*) \leq \; c(A_L). \tag{5.172}$$

The $\lambda_{\mathcal{P}3}$-wave is a physically admissible (right) rarefaction if and only if

$$c(A^*) \leq \; c(A_R). \tag{5.173}$$

Proof.
($\Longrightarrow$)In Proposition 5.4.1 we have proved this part.
($\Longleftarrow$)In Propositions 5.4.2 5.4.3 we have proved this part. □

Theorem 5.4.3. *Given the Riemann problem (5.30), and ignoring the existence of the compound waves, the $\lambda_{\mathcal{P}1}$-wave is an entropy-satisfying (left) shock if and only if*

$$c(A^*) > c(A_L). \tag{5.174}$$

The $\lambda_{\mathcal{P}3}$-wave is an entropy-satisfying (right) shock if and only if

$$c(A^*) > c(A_R). \tag{5.175}$$

Proof.
($\Longrightarrow$)In Propositions 5.4.2 5.4.3 we have proved this part.
($\Longleftarrow$)In Proposition 5.4.1 we have proved this part. □

Theorem 5.4.4 (Solution in the Star Region - Veins - No compound waves)**.** *The exact solution of the Riemann problem for the pressure system in the Star Region for veins in absence of compound waves is*

$$\mathbf{Q}^*_{NComL} = \begin{bmatrix} A^*_{NCom} \\ A^*_{NCom}u^*_{NCom} = q^*_{NCom} \\ A^*_{NCom}\phi^*_{NComL} \end{bmatrix}, \quad \mathbf{Q}^*_{NComR} = \begin{bmatrix} A^*_{NCom} \\ A^*_{NCom}u^*_{NCom} = q^*_{NCom} \\ A^*_{NCom}\phi^*_{NComR} \end{bmatrix}, \tag{5.176}$$

found as follows: A^*_{NCom} is the root x of the non-linear algebraic equation

$$f_L(x) + f_R(x) + q_R - q_L = 0, \tag{5.177}$$

where

$$f_L(x) = \begin{cases} \displaystyle\int_{A_L}^{x} c(\sigma)d\sigma & \text{if } c(x) \le c(A_L) \text{ (left rarefaction)}, \\ \displaystyle\sqrt{(x-A_L)\int_{A_L}^{x} c^2(\sigma)d\sigma} & \text{if } \begin{cases} x > A_L \\ c(x) > c(A_L) \end{cases} \text{ (left shock)}, \\ \displaystyle-\sqrt{(x-A_L)\int_{A_L}^{x} c^2(\sigma)d\sigma} & \text{if } \begin{cases} x \le A_L \\ c(x) > c(A_L) \end{cases} \text{ (left shock)}, \end{cases} \tag{5.178}$$

$$f_R(x) = \begin{cases} \displaystyle\int_{A_R}^{x} c(\sigma)d\sigma & \text{if } c(x) \le c(A_R) \text{ (right rarefaction)}, \\ \displaystyle\sqrt{(x-A_R)\int_{A_R}^{x} c^2(\sigma)d\sigma} & \text{if } \begin{cases} x > A_R \\ c(x) > c(A_R) \end{cases} \text{ (right shock)}, \\ \displaystyle-\sqrt{(x-A_R)\int_{A_R}^{x} c^2(\sigma)d\sigma} & \text{if } \begin{cases} x \le A_R \\ c(x) > c(A_R) \end{cases} \text{ (right shock)}, \end{cases} \tag{5.179}$$

while c is the wave speed (5.2). Once A^*_{NCom} is known from (5.177) the solution $q^*_{NCom} = (Au)^*_{NCom}$ is

$$q^*_{NCom} = \frac{1}{2}(q_L + q_R) + \frac{1}{2}[f_R(A^*_{NCom}) - f_L(A^*_{NCom})]. \tag{5.180}$$

Regarding the concentration of the passive scalar

$$\phi^*_{NComL} = \frac{A_L}{A^*_{NCom}}\phi_L, \qquad \phi^*_{NComR} = \frac{A_R}{A^*_{NCom}}\phi_R. \tag{5.181}$$

Proof. We put together the relations stated in Propositions 5.4.1, 5.4.2, 5.4.3, and Theorems 5.4.2 and 5.4.3. □

The integrals in case of veins are calculated with a three-point Gauss quadrature rule. Equation (5.177) is solved with a globally convergent Newton-Raphson method (see Appendix B.2).

In other words Theorem 5.4.4 gives the exact solution of the Riemann problem for the pressure system in the Star Region in the following cases

Theorem 5.4.5 (Conditions for the absence of compound waves)**.** *The solution of Theorem 5.4.4 is the exact solution of the Riemann problem for the pressure system in veins in the Star Region, i.e.* $\mathbf{Q}^*_{NComL} = \mathbf{Q}^*_{\mathcal{P}L}$ *and* $\mathbf{Q}^*_{NComR} = \mathbf{Q}^*_{\mathcal{P}R}$*, if and only if in each left and right wave, associated with a nongenuinely non-linear field, being* $\mathcal{I}_{NC} = [\min(A_j, A^*_{NCom}), \max(A_j, A^*_{NCom})]$*, with* $j = L, R$ *according to the side of the wave, is verified one of the following:*

1. $A_c \notin \mathcal{I}_{NC}$ *(rarefactions or shocks),*
2. $A_c \in \mathcal{I}_{NC}$ and $\lambda_{\mathcal{P}k}(\mathbf{Q}_{\widehat{L}}) \geq S(\mathbf{Q}_{\widehat{L}}, \mathbf{Q}_{\widehat{R}}) \geq \lambda_{\mathcal{P}k}(\mathbf{Q}_{\widehat{R}})$ *(shocks).*

Proof. In Def. 5.4.1 we stated that a rarefaction in a wave associated with a nongenuinely non-linear field can occur only in a part of the domain where the $\lambda_{\mathcal{P}k}(A)$ function is locally monotonic in A, i.e. and in proof of Proposition 5.4.1 we have explained why A_c should be excluded from the rarefaction domain. On the other hand, being the rarefaction domain I_j defined in (5.142) and (5.143), for a rarefaction, the case $A_j = A_c$ is not admissible, due to the particular curvature of the $\lambda_{\mathcal{P}j}$ functions $j = L, R$ (Fig. 5.7 for example), instead the case $A^* = A_c$ is a limiting case that can be treated also as a compound wave (Section 5.4.3).

If $A_c \notin \mathcal{I}_{NC}$ and a rarefaction is not admissible, only a shock can occur, being, in that part of the domain, the related characteristic field *locally* genuinely non-linear.

If $A_c \in \mathcal{I}_{NC}$ a rarefaction is not admissible and a shock can occur only if (5.146) holds (Propositions 5.4.2 and 5.4.3).

□

5.4.3 Solution in the Star Region for veins in presence of compound waves

Theorem 5.4.6 (Necessary condition for a compound wave)**.** *The waves associated with the nongenuine non-linear fields of the Riemann problem for the pressure system in case of veins* (5.30)*, are compound waves* ***only if*** $A_c \in \mathcal{I} = [\min(A_j, A^*), \max(A_j, A^*)]$, $j = L, R$.

Proof. This statement means that if $A_c \notin \mathcal{I}$ *there are* ***no*** *compound waves*, in fact the function $\lambda_{\mathcal{P}k}(A)$ in $\mathcal{I}$ in this case is monotonic, so we can have rarefactions or shocks, while if $A_c \in \mathcal{I}$ there **may** be shocks (Theorem 5.4.5) or compound waves . In other words $A_c \in \mathcal{I}$ is a necessary condition for compound waves, but not a sufficient one. □

Compound waves are composed of the rarefactions and shock described in Sections 5.4.1.1, 5.4.1.2. In this section we will describe how we built them without extensively exploring the theoretical aspects.

We consider as example Test 8 in Tables 5.4, 5.5. The $\lambda_{\mathcal{P}1}$ and $\lambda_{\mathcal{P}3}$ waves related to these test data are depicted in Fig. 5.7. Regarding the left wave, $\lambda_{\mathcal{P}1}(A_L) > \lambda_{\mathcal{P}1}(A^*)$. Unfortunately none of the conditions of Theorem 5.4.5 holds. It follows that this can not be a rarefaction nor a shock wave. We must *proceed* from $\lambda_{\mathcal{P}1}(A_L)$ to $\lambda_{\mathcal{P}1}(A^*)$ in Fig. 5.7. We can notice that $\lambda_{\mathcal{P}1}(A_L) \leq \lambda_{\mathcal{P}1}(A)\ \forall\, A \in [A_c, A_L]$. Clearly with these conditions only a rarefaction can occur. The sought rarefaction can not *surpass* A_c (Def. 5.4.1). In particular it must end in $\widehat{A}_L$ belonging to its admissible rarefaction curve $q^a_{rarL}(A)$ built in (5.142), such that an entropy-satisfying shock can occur with left side $\widehat{\mathbf{Q}}_L = [\widehat{A}_L, \widehat{q}_L]^T$ and right side the sought $\mathbf{Q}^*_{\mathcal{P}L}$.

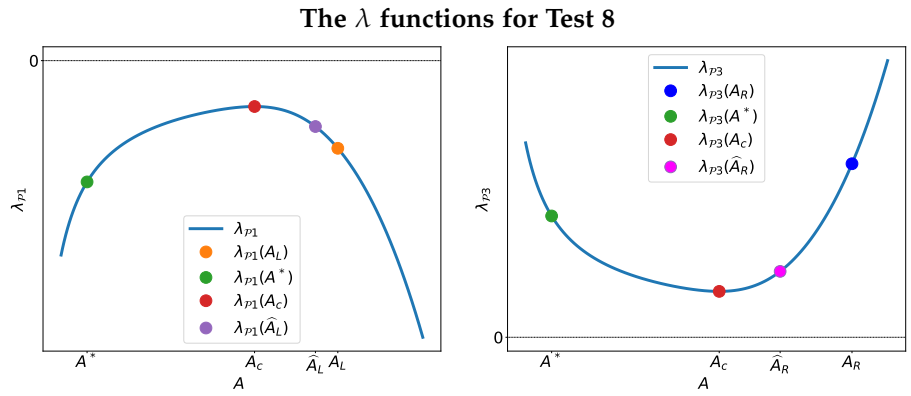

Figure 5.7: The λ functions for data of Test 8 in Tables 5.4, 5.5, with the positions of the principal states studied in the construction of the compound waves.

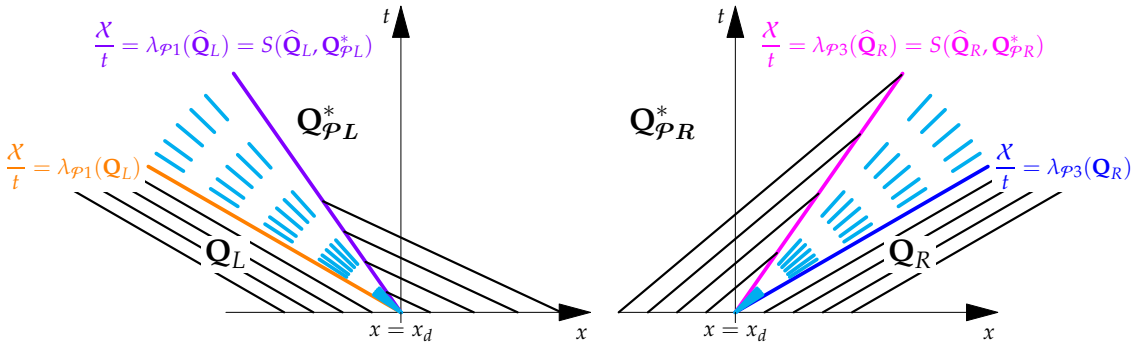

Figure 5.8: The characteristics of the left and right compound waves for data of Test 8 in Tables 5.4, 5.5. The colors used are the same as the related states in Fig. 5.7.

Drawing the characteristics (Fig. 5.8) it is straightforward to see that the only way to have a rarefaction with buondaries $\lambda_{\mathcal{P}1}(A_L)$ and $\lambda_{\mathcal{P}1}(\widehat{A}_L)$ followed by a shock with sides $\widehat{\mathbf{Q}}_L$ and $\mathbf{Q}^*_{\mathcal{P}L}$ avoiding superimpositions, is to have a semi-characteristic shock i.e. a shock such that

$$\lambda_{\mathcal{P}1}(\widehat{\mathbf{Q}}_L) = S(\widehat{\mathbf{Q}}_L, \mathbf{Q}^*_{\mathcal{P}L}) > \lambda_{\mathcal{P}1}(\mathbf{Q}^*_{\mathcal{P}L}), \tag{5.182}$$

[70, 98]. The shock speed clearly is

$$S = \frac{q^* - \widehat{q}_L}{A^* - \widehat{A}_L}. \tag{5.183}$$

being the sought shock built in the same manner as in Proposition 5.4.2, i.e. with Rankine-Hugoniot condition and the Oleinik-Liu condition.

The discussion concerning the right wave is similar, in this case $\lambda_{\mathcal{P}3}(A_R) > \lambda_{\mathcal{P}3}(A^*)$ (Fig. 5.7) but $A_c \in \mathcal{I}$, so again none of the conditions of Theorem 5.4.5 holds. It follows that this is again a compound wave. We must *proceed* from $\lambda_{\mathcal{P}3}(A_R)$ (the initial data) to $\lambda_{\mathcal{P}3}(A^*)$, following the same procedure described for the left wave. In particular the semi-characteristic shock in this case must satisfy

$$\lambda_{\mathcal{P}3}(\mathbf{Q}^*_{\mathcal{P}R}) > S(\widehat{\mathbf{Q}}_R, \mathbf{Q}^*_{\mathcal{P}R}) = \lambda_{\mathcal{P}3}(\widehat{\mathbf{Q}}_R). \tag{5.184}$$

In Fig. 5.8 there are the final results.

From (5.182) and (5.184) the fundamental equation to be solved for the numerical construction of a compound wave turns out to be

$$\lambda_{\mathcal{P}k}(\widehat{\mathbf{Q}}_j) = S(\widehat{\mathbf{Q}}_j, \mathbf{Q}^*). \tag{5.185}$$

Remark 5.4.1. Eq. (5.185) can be written as

$$\lambda_{\mathcal{P}k}(\widehat{A}) - S(\mathbf{Q}_{rarj}(\widehat{A}), \mathbf{Q}^*) = 0, \tag{5.186}$$

and in this form will be used in the next Sections.

5.4.4 Numerical procedure

Now we give a global overview of the numerical procedure to compute the exact solution in the Star Region in case of veins, starting from the beginning.

1. Calculate $\mathbf{Q}^*_{NComj}$, $j = L, R$, as described in Section 5.4.2.
2. Check if one of the conditions of Theorem 5.4.5 is satisfied in **both** nongenuinely non-linear waves. If this is the case, the sought solution is found. $\mathbf{Q}^*_{NComj} = \mathbf{Q}^*_{\mathcal{P}j}$, $j = L, R$. The Riemann problem is solved. Otherwise go to point 3.
3. If both conditions of Theorem 5.4.5 are **not** satisfied in **one or both** nongenuinely non-linear waves, we are in presence of one or both compound waves. In case of one compound wave check Section 5.4.4.1, otherwise check Section 5.4.4.2
4. Having obtained the required results ($\mathbf{Q}^*_{\mathcal{P}j}$, possible $\widehat{\mathbf{Q}}_j$, $j = L, R$) do the sampling in Section 5.4.5.

5.4.4.1 One compound wave

This is the case in which one of the two waves associated with the nongenuinely non-linear fields is a compound wave and the other is not. The found $\mathbf{Q}^*_{NComj}$, $j = L, R$ in Section 5.4.2, are not our sought solutions but can be used as initial guesses to find the correct solution that will be called $\mathbf{Q}^*_{Comj}$. This result is given as empirically valid and is not proved in this work.

To calculate the sought $\mathbf{Q}^*_{Comj}$, having executed steps 1 and 2 we apply the scheme reported in Fig. 5.9

5.4.4.2 Two compound waves

This is the case in which both of the two waves associated with the nongenuinely non-linear fields are compound waves. The found $\mathbf{Q}^*_{NComj}$, $j = L, R$ in Section 5.4.2, are not our sought solutions but again can be used as initial guess to find the correct $\mathbf{Q}^*_{Comj}$ one. To calculate the sought $\mathbf{Q}^*_{Comj}$, having executed steps 1 and 2 we executed the scheme reported in Fig. 5.10.

5.4.5 The complete exact solution of the Riemann problem for the pressure system in veins

In this Section we present the sampling of the complete exact solution of the Riemann problem for the pressure system for veins (5.1). Being as before $\mathcal{X} = x - x_d$, x is the specific place of the

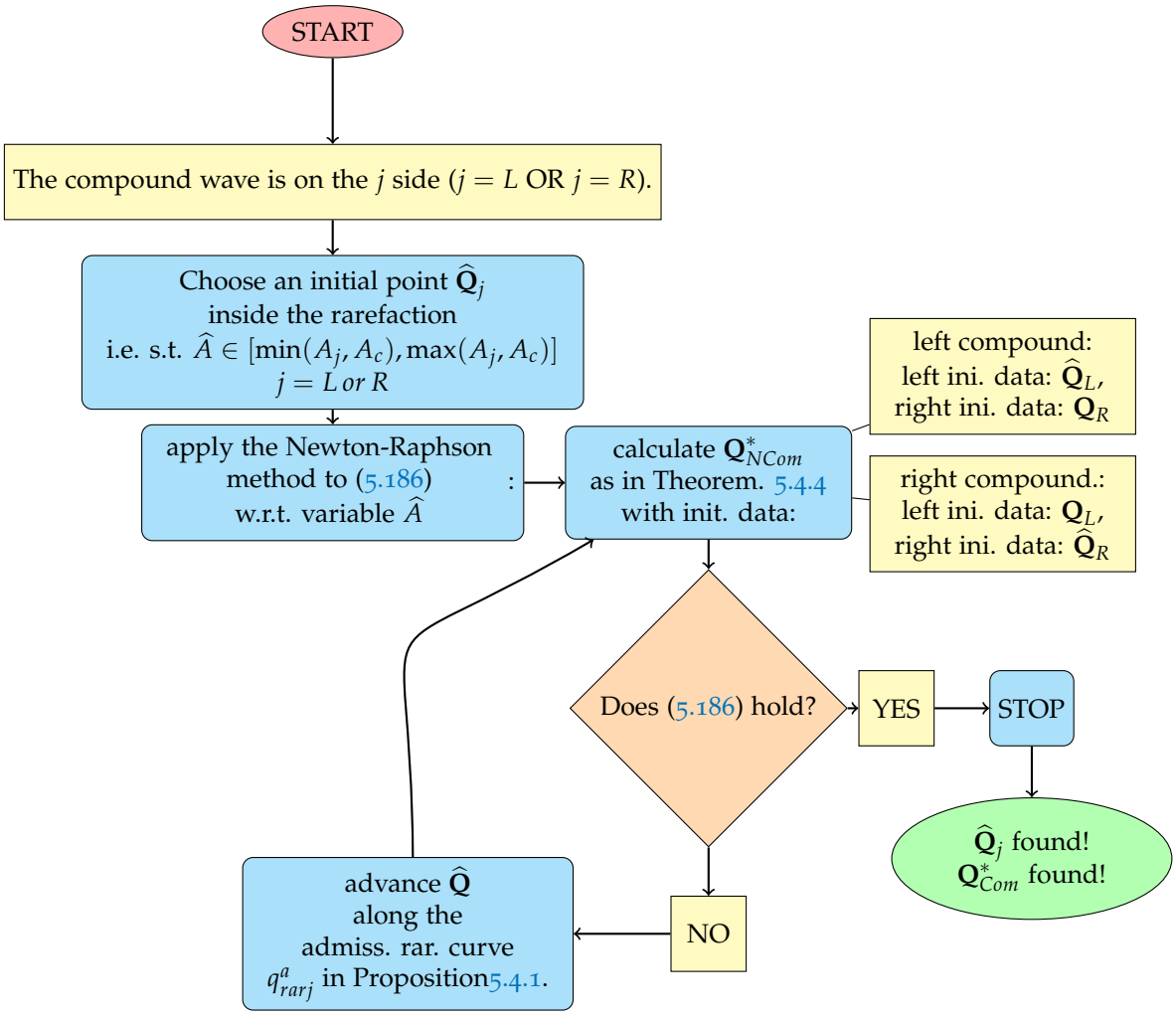

Figure 5.9: The method to calculate the exact $\mathbf{Q}^*$ in case of compound wave on *one* side. Please note that we focused on $\mathbf{Q}^*_{Com} = [A^*_{Com}, q^*_{Com}]$, being the passive scalar ϕ easy to calculate at the end of the process thanks to formulas $\phi^*_{ComL} = \dfrac{A_L}{A^*_{Com}}\phi_L$ and $\phi^*_{ComR} = \dfrac{A_R}{A^*_{Com}}\phi_R$

domain (vessel) in which we are calculating the desired values, x_d is the vessel spatial coordinate of the initial discontinuity, and t is the time, we put together all the relations proved in Section 5.4. Initial data

$$\mathbf{Q}_L = \begin{bmatrix} A_L \\ A_L u_L \\ A_L \phi_L \end{bmatrix}, \qquad \mathbf{Q}_R = \begin{bmatrix} A_R \\ A_R u_R \\ A_R \phi_R \end{bmatrix}. \tag{5.187}$$

The complete solution is

- if $c(A^*) \leq c(A_L)$ and $A_c \notin [\min(A_L, A_c), \max(A_L, A_c)]$ (left rarefaction):

$$\mathbf{Q}(x,t) = \begin{cases} \mathbf{Q}_L & \text{if} \quad \mathcal{X} < -c(A_L)t, \\ \mathbf{Q}_{irarL} & \text{if} \quad -c(A_L)t \leq \mathcal{X} \leq -c(A^*)t, \\ \mathbf{Q}^*_{\mathcal{P}L} & \text{if} \quad -c(A^*)t < \mathcal{X} \leq 0, \end{cases} \tag{5.188}$$

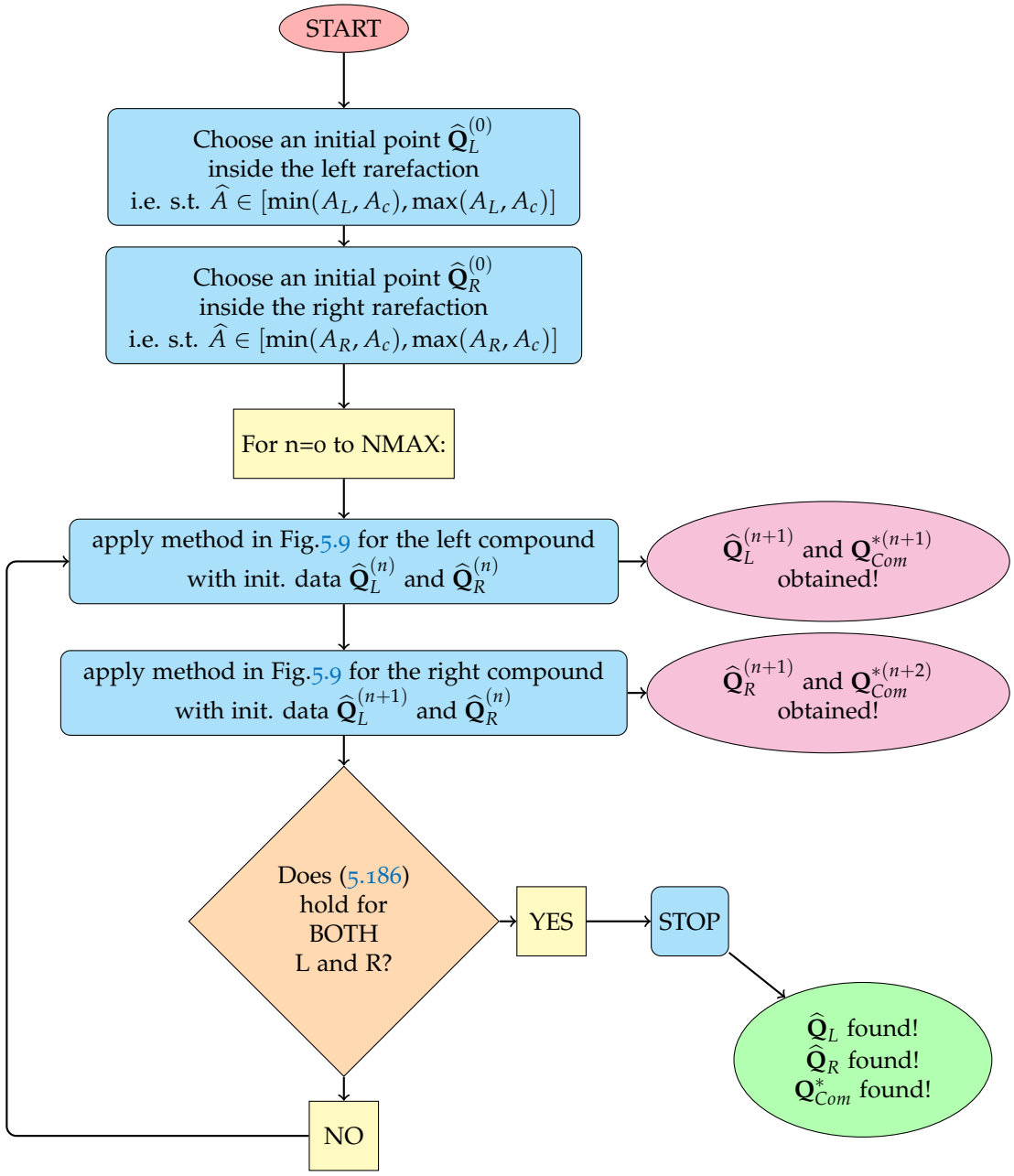

Figure 5.10: The method to calculate the exact $\mathbf{Q}^*$ in case of compound waves in *both sides*. Please note that we focused on $\mathbf{Q}^*_{Com} = [A^*_{Com}, q^*_{Com}]$, being the passive scalar ϕ easy to calculate at the end of the process thanks to formulas $\phi^*_{ComL} = \dfrac{A_L}{A^*_{Com}}\phi_L$ and $\phi^*_{ComR} = \dfrac{A_R}{A^*_{Com}}\phi_R$.

- if $c(A^*) > c(A_L)$ and $\lambda_{\mathcal{P}1}(\mathbf{Q}_L) \geq S(\mathbf{Q}_L, \mathbf{Q}^*_{\mathcal{P}L}) \geq \lambda_{\mathcal{P}1}(\mathbf{Q}^*_{\mathcal{P}L})$ (left shock):

$$\mathbf{Q}(x,t) = \begin{cases} \mathbf{Q}_L & \text{if} \quad \mathcal{X} \leq S_L t, \\ \mathbf{Q}^*_{\mathcal{P}L} & \text{if} \quad S_L t < \mathcal{X} \leq 0. \end{cases} \tag{5.189}$$

- if no one of the previous i.e.

$$\begin{cases} -c(A_L) \leq -c(A^*), \\ A_c \in [\min(A_L, A_c), \max(A_L, A_c)], \end{cases} \quad \text{OR} \quad \begin{cases} -c(A_L) > -c(A^*), \\ A_c \in [\min(A_L, A_c), \max(A_L, A_c)], \\ \text{NOT} \quad \lambda_{\mathcal{P}1}(\mathbf{Q}_L) \geq S(\mathbf{Q}_L, \mathbf{Q}^*_{\mathcal{P}L}) \geq \lambda_{\mathcal{P}1}(\mathbf{Q}^*_{\mathcal{P}L}) \end{cases} \tag{5.190}$$

(left compound wave):

$$\mathbf{Q}(x,t) = \begin{cases} \mathbf{Q}_L & \text{if} \quad \mathcal{X} < -c(A_L)t, \\ \mathbf{Q}_{irarL} & \text{if} \quad -c(A_L)t \leq \mathcal{X} \leq -c(\widehat{A}_L)t, \\ \mathbf{Q}^*_{\mathcal{P}L} & \text{if} \quad -c(\widehat{A}_L)t < \mathcal{X} \leq 0, \end{cases} \tag{5.191}$$

Similarly on the right side the complete solution is

- if $c(A^*) \leq c(A_R)$ and $A_c \notin [\min(A_R, A_c), \max(A_R, A_c)]$ (right rarefaction):

$$\mathbf{Q}(x,t) = \begin{cases} \mathbf{Q}^*_{\mathcal{P}R} & \text{if} \quad 0 < \mathcal{X} < c(A^*)t, \\ \mathbf{Q}_{irarR} & \text{if} \quad c(A)^* t \leq \mathcal{X} \leq c(A_R)t, \\ \mathbf{Q}_R & \text{if} \quad \mathcal{X} > c(A_R)t, \end{cases} \tag{5.192}$$

- if $c(A^*) > c(A_R)$ and $\lambda_{\mathcal{P}3}(\mathbf{Q}^*_{\mathcal{P}R}) \geq S(\mathbf{Q}^*_{\mathcal{P}R}, \mathbf{Q}_R) \geq \lambda_{\mathcal{P}3}(\mathbf{Q}_R)$ (right shock):

$$\mathbf{Q}(x,t) = \begin{cases} \mathbf{Q}^*_{\mathcal{P}R} & \text{if} \quad 0 < \mathcal{X} \leq S_R t, \\ \mathbf{Q}_R & \text{if} \quad \mathcal{X} > S_R t. \end{cases} \tag{5.193}$$

- if no one of the previous i.e.

$$\begin{cases} c(A^*) \leq c(A_R), \\ A_c \in [\min(A_R, A_c), \max(A_R, A_c)], \end{cases} \quad \text{OR} \quad \begin{cases} c(A^*) > c(A_R), \\ A_c \in [\min(A_L, A_c), \max(A_L, A_c)], \\ \text{NOT} \quad \lambda_{\mathcal{P}3}(\mathbf{Q}^*_{\mathcal{P}R}) \geq S(\mathbf{Q}^*_{\mathcal{P}R}, \mathbf{Q}_R) \geq \lambda_{\mathcal{P}3}(\mathbf{Q}_R) \end{cases} \tag{5.194}$$

(right compound wave):

$$\mathbf{Q}(x,t) = \begin{cases} \mathbf{Q}^*_{\mathcal{P}R} & \text{if} \quad 0 < \mathcal{X} < c(\widehat{A}_R)t, \\ \mathbf{Q}_{irarR} & \text{if} \quad c(\widehat{A}_R)t \leq \mathcal{X} \leq c(A_R)t, \\ \mathbf{Q}_R & \text{if} \quad \mathcal{X} > c(A_R)t, \end{cases} \tag{5.195}$$

$\mathbf{Q}_{irarL}$ is defined in Proposition 5.3.6, $\mathbf{Q}_{irarR}$ in Proposition 5.3.7, c is in (5.2). S_L and S_R are the left and the right shock speeds and are defined according to the Rankine-Hugoniot condition

$$S_L = \frac{q^* - q_L}{A^* - A_L}, \qquad S_R = \frac{q^* - q_R}{A^* - A_R}. \tag{5.196}$$

$\widehat{\mathbf{Q}}_j = [\widehat{A}_j, \widehat{q}_j, \widehat{A}_j\widehat{\phi}_j]^T$, $j = L, R$, are found in Sections 5.4.4.1, 5.4.4.2. $\mathbf{Q}^*_{\mathcal{P}L}$ and $\mathbf{Q}^*_{\mathcal{P}R}$ are defined in Theorem. 5.4.4 and Sections 5.4.4.1, 5.4.4.2, i.e.

$$\mathbf{Q}^*_{\mathcal{P}j}(x,t) = \begin{cases} \mathbf{Q}^*_{NComj} & \text{if there are no compound waves,} \\ \mathbf{Q}^*_{Comj} & \text{if there is at least a compound wave.} \end{cases} \tag{5.197}$$

Table 5.4: Initial conditions for Tests from 4 to 8. The wave patterns are: R=rarefaction, C=contact discontinuity, S=shock, CW=compound wave. The units of measures used for this Thesis are: m, s, Kg, Pa.

Test	$A_L[m^2]$	$u_L[m/s]$	ϕ_L	$A_R[m^2]$	$u_R[m/s]$	ϕ_R	Wave pattern
4	$2.1 \cdot 10^{-4}$	0.00	1.00	$1.4 \cdot 10^{-4}$	0.00	0.50	SCR
5	$2.30 \cdot 10^{-4}$	-0.80	1.00	$2.50 \cdot 10^{-4}$	-0.50	0.50	SCS
6	$1.00 \cdot 10^{-4}$	0.40	0.50	$3.70 \cdot 10^{-4}$	-0.50	1.00	CWCR
7	$2.10 \cdot 10^{-4}$	-1.50	1.00	$2.90 \cdot 10^{-4}$	0.00	0.50	SCCW
8	$3.10 \cdot 10^{-4}$	-1.00	1.00	$3.60 \cdot 10^{-4}$	1.50	0.50	CWCCW

Table 5.5: Parameters used for Tests from 4 to 8: domain length ℓ, blood density ρ, vessel wall stiffness K, reference cross-sectional area A_0, external pressure p_e, location of the initial discontinuity x_d and output time t_{End}.

Test	Vessel	$\ell[m]$	ρ	$K[Pa]$	$A_0[m^2]$	$p_e[Pa]$	$x_d[m]$	$t_{End}[s]$
4	Vein	0.50	1000.00	333.00	$3.14 \cdot 10^{-4}$	10.00	0.50ℓ	0.12
5	Vein	0.50	1000.00	33.00	$3.14 \cdot 10^{-4}$	0.00	0.50ℓ	0.2
6	Vein	0.50	1000.00	333.00	$3.14 \cdot 10^{-4}$	0.00	0.50ℓ	0.05
7	Vein	0.50	1000.00	333.00	$3.14 \cdot 10^{-4}$	0.00	0.50ℓ	0.07
8	Vein	0.50	1000.00	333.00	$3.14 \cdot 10^{-4}$	0.00	0.30ℓ	0.05

Table 5.6: Exact solution of the Riemann problem for the pressure system in the Star Region for veins.

Test	$A^*[m^2]$	$q^*[m/s]$	ϕ_L^*	ϕ_R^*
4	1.725510^{-4}	3.897710^{-5}	1.2169	0.4056
5	$1.5101\ 10^{-4}$	-1.576210^{-4}	1.5230	0.8277
6	$3.3813\ 10^{-4}$	-2.937110^{-4}	0.1478	1.0942
7	$1.1489\ 10^{-4}$	2.012110^{-4}	1.8277	1.2620
8	$5.6277\ 10^{-5}$	4.847010^{-5}	5.5084	3.1984

5.4.6 RESULTS

Here we show the results of the exact solution of the Riemann problem for the pressure system presented in Section 5.4.5. These solutions are compared against mesh-independent numerical ones obtained with a second order extension of FORCE centred numerical scheme: FORCEII (Appendix A.2), with a mesh of $I = 5000$ computational cells and a Courant–Friedrichs–Lewy number (C_{cfl}) of 0.9.

We propose five tests in which we cover all the possible waveforms arising in waves associated with nongenuinely non-linear fields, i.e. rarefactions, shocks, and compound waves. Plus a study of the admissible shocks and rarefaction curves is proposed for each test. Initial data are in Tables 5.4, 5.5, results in Figs. 5.11, 5.12, 5.13, 5.14, 5.15. In Table 5.6 the exact solution of the Riemann problem for the pressure system in case of veins is reported for the considered variables.

TEST 4: SHOCK - CONTACT - RAREFACTION This test presents a left shock, a central contact discontinuity, and a right rarefaction wave. A_c in (5.12) is not included in the range depicted by the test results, thus no compound waves are present (Theorem 5.4.5). From Fig. 5.11a we can observe the exact solutions plotted against FORCEII scheme, both for variable A and for variable q and for variable ϕ. In Fig. 5.11b we can appreciate the admissible entropy satisfying shock curves $q^a_{shockL}(A)$ and $q^a_{shockR}(A)$ defined in Propositions 5.4.2, 5.4.3, the Hugoniot Loci respectively of $\mathbf{Q}_L$ and $\mathbf{Q}_R$ and the admissible rarefaction curves q^a_{rarL} and q^a_{rarR} defined in Proposition 5.4.1. From A_L the left admissible rarefaction curve develops to A_c. From A_R the right admissible rarefaction curve develops to A_c. The sought $\mathbf{Q}^*_{NCom}$ is the actual intersection of the right broken

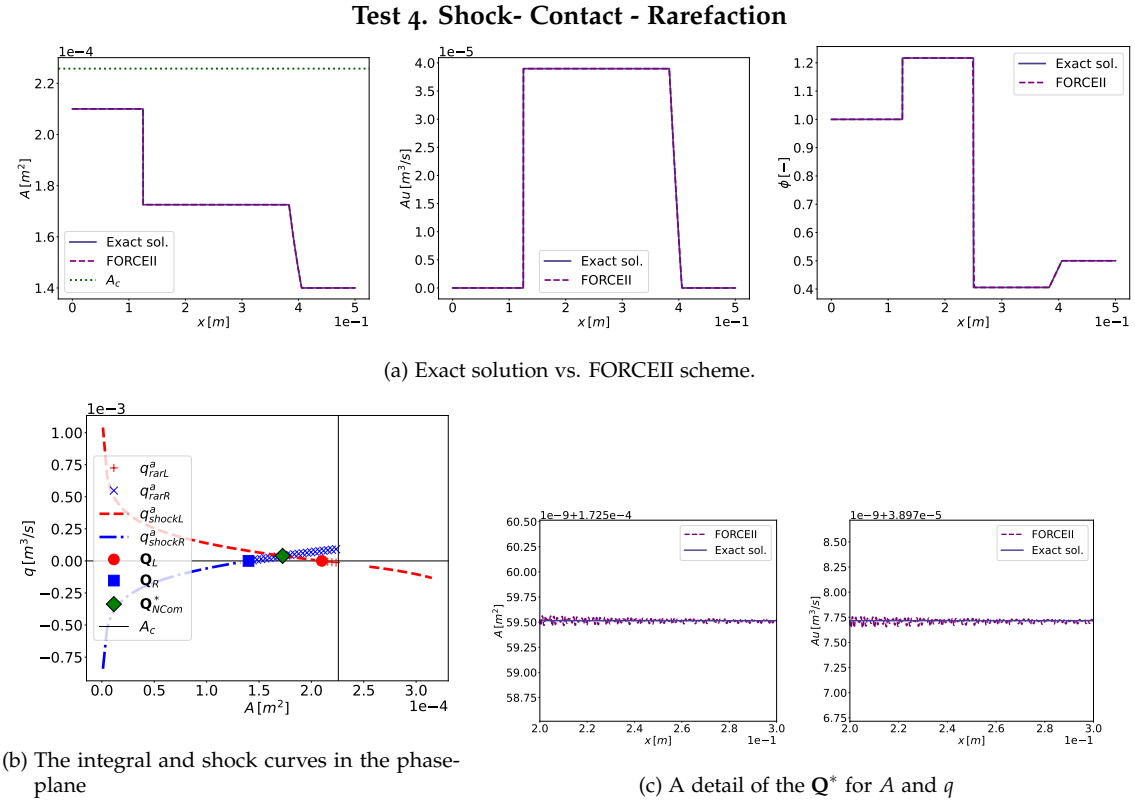

(a) Exact solution vs. FORCEII scheme.

(b) The integral and shock curves in the phase-plane

(c) A detail of the $\mathbf{Q}^*$ for A and q

Figure 5.11: Exact solution of the Riemann problem for the pressure system for Test 4 vs. FORCEII scheme. This Riemann problem shows a left shock, a contact discontinuity for the passive scalar and a right rarefaction. No compound waves are present here infact A_c in (5.12) is *above* the test results. Initial data are in Tables 5.4, 5.5.

line and the left broken line given by the admissible rarefaction and shock curves described before. Fig. 5.11c shows a detail of the $\mathbf{Q}^*$ region regarding variables A and q.

Test 5: Shock - Contact - Shock This test presents a left shock, a contact discontinuity and a right shock waves. A_c is included in the range described by the test results, neverthless no compound waves are depicted (Theorem 5.4.5). From Fig. 5.12a we can observe the exact solutions plotted against FORCEII scheme, both for variable A and for variable q and for variable ϕ. In Fig. 5.12b we can appreciate the admissible entropy satisfying shock curves $q^a_{shockL}(A)$ and $q^a_{shockR}(A)$ defined in Propositions 5.4.2, 5.4.3 the Hugoniot Loci respectively of $\mathbf{Q}_L$ and $\mathbf{Q}_R$ and the admissible rarefaction curves q^a_{rarL} and q^a_{rarR} as defined in Proposition 5.4.1. From A_L the left admissible rarefaction curve develops right before A_c (the left rarefaction curve is very short and is not clearly visible in the plot). From A_R the right admissible rarefaction curve develops right before A_c. The sought $\mathbf{Q}^*_{NCom}$ is the actual intersection of the right broken line and the left broken line given by the admissible rarefaction and shock curves described before. Fig. 5.12c shows a detail of the $\mathbf{Q}^*$ region regarding variables A and q.

Test 6: Compound - Contact - Rarefaction This test presents a left compound wave, a contact discontinuity and a right rarefaction wave. A_c is included in the results range described by the left wave and no one of the conditions of Theorem 5.4.5 is satisfied. From Fig. 5.13a we can observe from the left to the right of the left wave a rarefaction and then a shock both for variable A and for variable q and for variable ϕ. In Fig. 5.13b we can appreciate the admissible

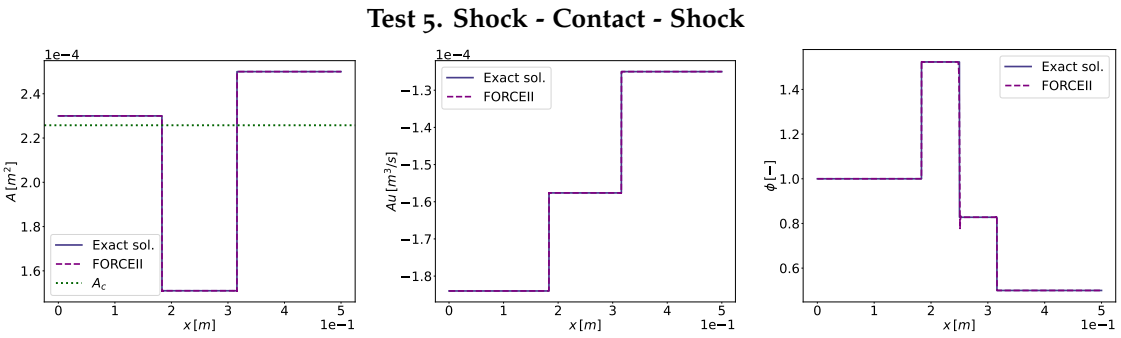

(a) Exact solution vs. FORCEII scheme.

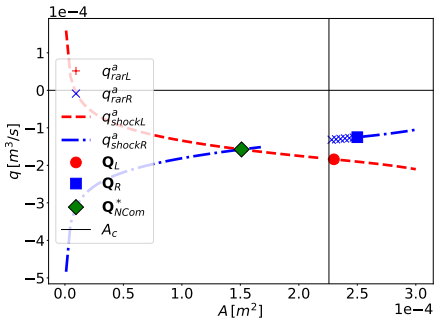

(b) The integral and shock curves in the phase-plane

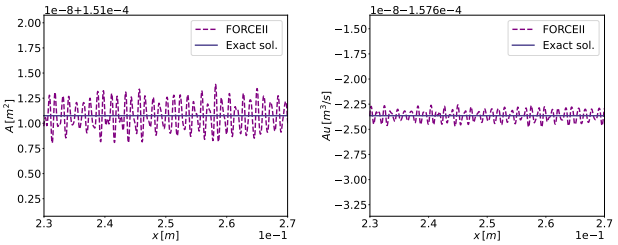

(c) A detail of the $\mathbf{Q}^*$ for A and q

Figure 5.12: Exact solution of the Riemann problem for the pressure system for Test 5 vs. FORCEII scheme. This Riemann problem shows a left shock, a contact discontinuity for the passive scalar and a right shock. No compound waves are present here. it is worth noting that A_c in (5.12) is *inside* both shocks. Initial data are in Tables 5.4, 5.5.

rarefaction curves $q^a_{rarL}(A)$ as defined in Proposition 5.4.1 starting from A_L and ending right before A_c. Before this latter $\widehat{\mathbf{Q}}_L$ belonging to the same rarefaction curve (i.e. to q^a_{rarL}) is found: this is the left side of the shock inside the left compound wave (the right side is $\mathbf{Q}^*_{Com}$). The entropy satisfying shock curve $q^a_{shock\widehat{L}}(A)$ that is the entropy-satisfying Hugoniot Locus of $\widehat{\mathbf{Q}}_L$ is shown. The admissible rarefaction curve $q^a_{rarR}(A)$ as defined in Proposition 5.4.1 is also depicted, starting from A_R and ending right before A_c. $\mathbf{Q}^*_{NCom}$ and $\mathbf{Q}^*_{Com}$ are both represented in the plot. They are *close but not superimposed*. The sought $\mathbf{Q}^*_{Com}$ is the actual intersection of the right broken line and the left broken line given by the admissible rarefaction and shock curves described before. Fig. 5.13c shows a detail of the $\mathbf{Q}^*$ region regarding variables A and q.

TEST 7: SHOCK - CONTACT - COMPOUND This test presents a left shock, a contact discontinuity and a right compound wave. A_c is included in the results depicted by the right wave and in that case no one of the conditions of Theorem 5.4.5 is satisfied. From Fig. 5.14a we can observe from the right to the left a small rarefaction and then a shock in the right compound, that are visible both for variable A and for variable q and for variable ϕ. in Fig. 5.14b we can appreciate the admissible rarefaction curves q^a_{rarL} and q^a_{rarR} as defined in Proposition 5.4.1 and the entropy satisfying shock curves q^a_{shockL} defined in Proposition 5.4.2 and $q^a_{shock\widehat{R}}$ the entropy-satisfying Hugoniot Locus of $\widehat{\mathbf{Q}}_R$. From $\mathbf{Q}_R$ the admissible rarefaction curve develops to A_c. Before this latter $\widehat{\mathbf{Q}}_R$ belonging to the same rarefaction curve (i.e. to q^a_{rarR}) is found: this is the right side of the shock inside the compound wave (the left side is $\mathbf{Q}^*_{Com}$). $\mathbf{Q}^*_{NCom}$ and $\mathbf{Q}^*_{Com}$ are both represented in the plot. They are *close but not superimposed*. The sought $\mathbf{Q}^*_{Com}$ is the actual intersection of the

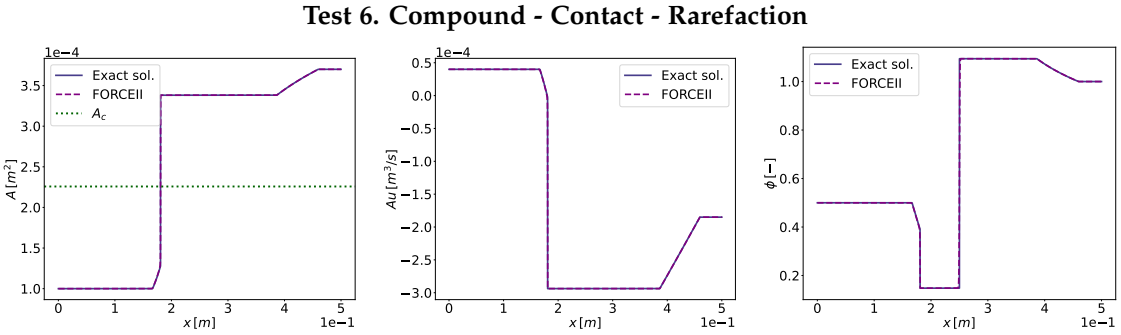

(a) Exact solution vs. FORCEII scheme.

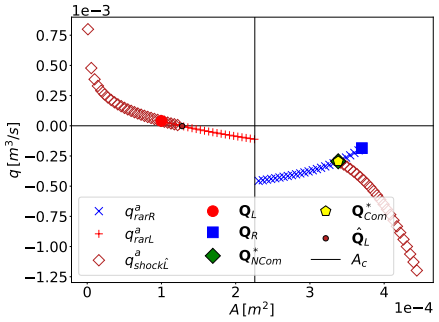

(b) The integral and shock curves in the phase-plane

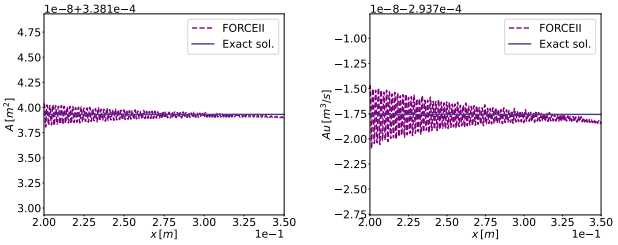

(c) A detail of the $\mathbf{Q}^*$ for A and q

Figure 5.13: Exact solution of the Riemann problem for the pressure system for Test 6 vs. FORCEII scheme. This Riemann problem shows a left compound, a contact discontinuity for the passive scalar and a right rarefaction. it is worth noting that A_c in (5.12) is *inside* the left compound. Initial data are in Tables 5.4, 5.5.

right broken line and the left broken line given by the admissible rarefaction and shock curves described before. Fig. 5.14c shows a detail of the $\mathbf{Q}^*$ region regarding variables A and q.

Test 8: Compound - Contact - Compound This test presents a left compound wave and a right compound wave. A_c is inside the results depicted by both waves and no one of the conditions of Theorem 5.4.5 is verified. From Fig. 5.15a we can observe from the outside to the inside a rarefaction and then a shock, that are visible both for variable A and for variable q and for variable ϕ, being the left rarefaction inside the compound wave remarkably smaller than the right one. In Fig. 5.15b we can appreciate the entropy satisfying shock curves $q^a_{shock\hat{L}}(A)$ and $q^a_{shock\hat{R}}(A)$, , i.e. the Hugoniot Loci of $\hat{\mathbf{Q}}_L$ and $\hat{\mathbf{Q}}_R$. In addition the admissible rarefaction curve $q^a_{rarL}(A)$ is represented as defined in Proposition 5.4.1 starting from A_L and ending right before A_c. Before this latter $\hat{\mathbf{Q}}_L$ belonging to the same rarefaction curve (i.e. to q^a_{rarL}) is found: this is the left side of the shock inside the left compound wave (the right side is $\mathbf{Q}^*_{Com}$). Is also shown the admissible rarefaction curve $q^a_{rarR}(A)$ as defined in Proposition 5.4.1 starting from A_R and ending right before A_c. Before this latter $\hat{\mathbf{Q}}_R$ belonging to the same rarefaction curve (i.e. to $q^a_{rarR}(A)$) is found: this is the right side of the shock inside the right compound wave (the left side is $\mathbf{Q}^*_{Com}$). $\mathbf{Q}^*_{NCom}$ and $\mathbf{Q}^*_{Com}$ are both represented in the plot. They are *close but not superimposed*. The sought $\mathbf{Q}^*_{Com}$ is the actual intersection of the right broken line and the left broken line given by the admissible rarefaction and shock curves described before. Fig. 5.15c shows a detail of the $\mathbf{Q}^*$ region regarding variables A and q.

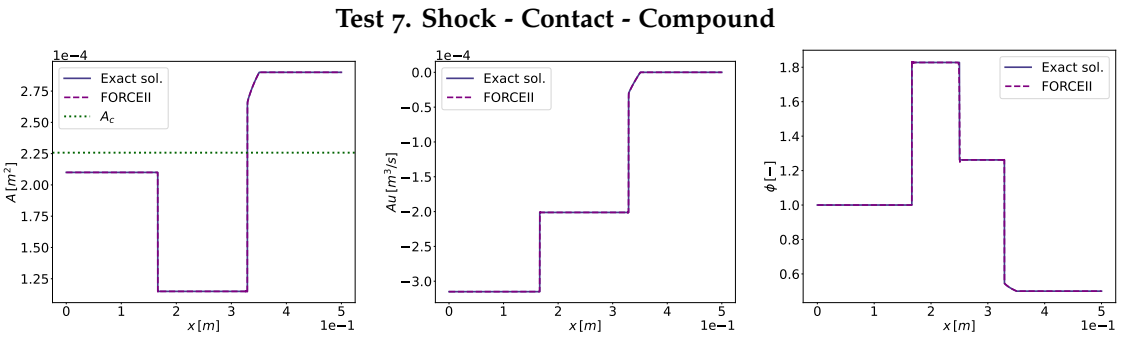

(a) Exact solution vs. FORCEII scheme.

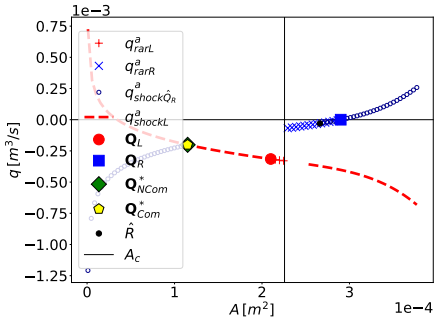

(b) The integral and shock curves in the phase-plane

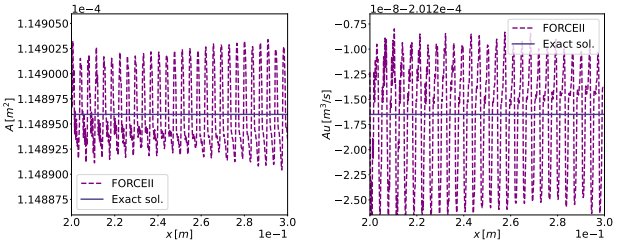

(c) A detail of the $\mathbf{Q}^*$ for A and q

Figure 5.14: Exact solution of the Riemann problem for the pressure system for Test 7 vs. FORCEII scheme. This Riemann problem shows a left shock, a contact discontinuity for the passive scalar and a right compound. it is worth noting that A_c in (5.12) is *inside* the right compound, Initial data are in Tables 5.4, 5.5.

In general the exact solution here proposed is well validated by the chosen second order numerical scheme.

5.4.7 Further remarks

In this section we further examine a few theoretical aspects covered in Section 5.4.

5.4.7.1 First remark

As described in Section 5.4.1.2. the Oleinik-Liu condition is

$$S(\mathbf{Q}_{\widehat{L}}, \mathbf{Q}_{\widehat{R}}) \leq S(\mathbf{Q}, \mathbf{Q}_{\widehat{L}}) \quad \forall \mathbf{Q} \in q_{shock}(A) \quad s.t. \quad A \in \mathcal{I} = [\min(A_{\widehat{L}}, A_{\widehat{R}}), \max(A_{\widehat{L}}, A_{\widehat{R}})]. \tag{5.198}$$

So for a left shock (5.198) is (5.148), i.e.

$$S(\mathbf{Q}_L, \mathbf{Q}_{shockL}(A)) \leq S(\mathbf{Q}_{shockL}(\widetilde{A}), \mathbf{Q}_L), \quad \forall \widetilde{A} \in [\min(A, A_L), \max(A, A_L)]. \tag{5.199}$$

For a right shock (5.198) should have been

$$S(\mathbf{Q}_{shockR}(A), \mathbf{Q}_R) \leq S(\mathbf{Q}_{shockR}(\widetilde{A}), \mathbf{Q}_{shockR}(A)) \quad \forall \widetilde{A} \in [\min(A, A_R), \max(A, A_R)]. \tag{5.200}$$

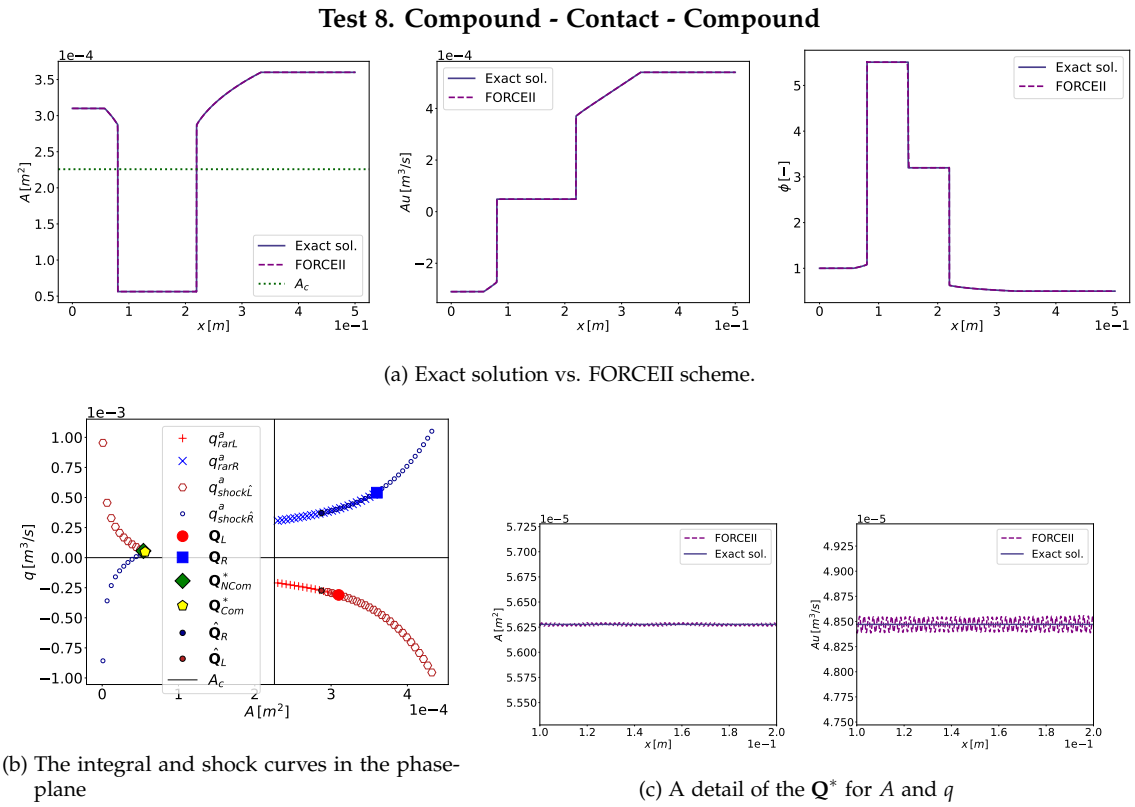

(a) Exact solution vs. FORCEII scheme.

(b) The integral and shock curves in the phase-plane

(c) A detail of the $\mathbf{Q}^*$ for A and q

Figure 5.15: Exact solution of the Riemann problem for the pressure system for Test 7 vs. FORCEII scheme. This Riemann problem shows a left compound, a contact discontinuity for the passive scalar and a right compound. it is worth noting that A_c in (5.12) is *inside* both compound. Initial data are in Tables 5.4, 5.5.

However to simplify the computations we instead proposed (5.167), i.e.

$$S(\mathbf{Q}_R, \mathbf{Q}_{shockR}(A)) \geq S(\mathbf{Q}_{shockR}(\widetilde{A}), \mathbf{Q}_R) \quad \forall \widetilde{A} \in [\min(A, A_R), \max(A, A_R)], \tag{5.201}$$

that is actually equivalent, due to the particular curvature of the shock curves. A detailed proof for this result is not provided.

5.4.7.2 Second remark

As described in Section 5.4.1.2, the Oleinik-Liu condition (5.145) implies (5.146) [49]. The contrary has not been stated. Despite that in Theor. 5.4.5 we use (5.146) instead of the Oleinik-Liu condition (5.145). This proves to be correct in our case. In this work we do not go further into this topic that needs to be developed properly. In general conditions (5.145) and (5.146), are not equivalent, in our case on the contrary, they prove to be.

5.5 Conclusions

In this Chapter we have presented the exact solution of the Riemann problem for the pressure system arising from the advection-pressure splitting for the conservative 1D blood flow model with transport for arteries and veins described in Chapter 3.1.

For the case of arteries the characteristic fields can be genuinely non-linear or linearly degenerate, leading to the formation of rarefactions, shocks, and contact discontinuities. A detailed mathematical analysis has been depicted with the description of the admissible rarefaction and shock curves and a numerical procedure to compute it is introduced.

For the case of veins the loss of genuine non-linearity can lead to the formation of compound waves. An accurate theoretical analysis of all the wave relations has been carried out also in this case, for all the possible waveforms, and a simple numerical procedure has been proposed to compute the exact solution also in this case.

Part II

UMERICAL SCHEMES

Chapter 6

Flux vector splitting schemes applied to a conservative 1D blood flow model with transport for arteries and veins

In this Chapter we present novel flux splitting-based numerical schemes for the conservative 1D blood flow equations with an advection equation for a passive scalar transport, considering tube laws that allow to model blood flow in arteries and veins (Chapter 2.1). Our schemes are inspired by the original flux vector splitting approach of Toro and Vázquez [92] and represent an extension of the work proposed by Toro et al. [91], which addressed tube laws suitable for describing blood flow in arteries. Our schemes separate advection terms and pressure terms, generating two different systems of PDEs: the advection system and the pressure system, both of which have a very simple eigenstructure compared to that of the full system (Chapters 3, 4, 5). We propose discretization schemes of the Godunov type that are simple and efficient. These qualities are evaluated on a suite of test problems with exact solution (Chapter 2.1). A detailed efficiency analysis is performed in order to illustrate situations in which the proposed methodology results advantageous with respect to standard approaches.

The Chapter is organized as follows: having presented the complete conservative 1D blood flow equations (Chapter 2.1), their splitting at the level of PDEs (Chapter 3.1), the pressure system resulting from it and its exact solution of the Riemann problem (Chapter 5), and acknowledging its computational complexity, in order to obtain efficient numerical methods in Section 6.1 we present two approximate Riemann solvers for the aforementioned pressure system. The numerical flux splitting schemes are presented in Section 6.2, the numerical results are given in Section 6.3, while in Section 6.3.2 the efficiency analysis is performed. The conclusions are drawn in Section 6.4.

This Chapter has been published in Spilimbergo et al. [83].

6.1 Approximate Riemann solvers for the pressure system

Having introduced the generalized Riemann invariants for the $\lambda_{\mathcal{P}1}$, $\lambda_{\mathcal{P}2}$ and $\lambda_{\mathcal{P}3}$-characteristic fields (Propositions 5.2.1, 5.2.2), we can introduce two approximate Riemann solvers for the pressure system (5.1). For the purposes of this work, we restrict ourselves to the presentation of the solution in the *Star Region* (i.e., the unknowns $\mathbf{Q}^*_{\mathcal{P}L}$ and $\mathbf{Q}^*_{\mathcal{P}R}$).

Remark 6.1.1. *Note that in this Chapter we refer to the flow rate as Au or $q = Au$, and also refer to c in (5.2) in this way: for example, we write c_L for $c(A_L)$, c_R for $c(A_R)$, c^* for $c(A^*)$, and so on.*

6.1.1 A two-rarefaction approximate Riemann solver for the pressure system

The two-rarefaction approximate Riemann solver operates under the assumption of two rarefaction waves, disregarding the shock wave relations. The solution in the Star Region in this case is

$$\mathbf{Q}^*_{TR,L} = \begin{bmatrix} A^*_{TR} \\ q^*_{TR} \\ A^*_{TR}\phi^*_{TR,L} \end{bmatrix}, \quad \mathbf{Q}^*_{TR,R} = \begin{bmatrix} A^*_{TR} \\ q^*_{TR} \\ A^*_{TR}\phi^*_{TR,R} \end{bmatrix}. \tag{6.1}$$

Given the wave relations described in Proposition 5.2.1

$$\begin{aligned} q^*_{TR} &= q_L - \int_{A_L}^{A^*_{TR}} c(A)dA, \\ q^*_{TR} &= q_R + \int_{A_R}^{A^*_{TR}} c(A)dA, \end{aligned} \tag{6.2}$$

with c the wave speed (5.2), in case of left and right rarefactions

$$q^*_{TR} = \frac{1}{2}(q_L + q_R) + \frac{1}{2}\left(\int_{A_R}^{A^*_{TR}} c(A)dA - \int_{A_L}^{A^*_{TR}} c(A)dA\right) = \frac{1}{2}(q_L + q_R) - \frac{1}{2}\int_{A_L}^{A_R} c(A)dA. \tag{6.3}$$

Having found q^*_{TR}, we obtain A^*_{TR} solving one of (6.2), for example

$$q^*_{TR} = q_L - \int_{A_L}^{A^*_{TR}} c(A)dA, \tag{6.4}$$

where the integrals in case of veins are calculated with a six-point Gauss quadrature rule thanks to the Python function *scipy.integrate.fixed_quad*, and equation (6.4) is solved with a globally convergent Newton-Raphson method (Appendix B.3) (for arteries with $m = 0.5$ and $n = 0$ in (5.4), the solution is explicit).

Regarding the last variable, considering Propositions 5.2.1 and 5.2.2

$$\phi^*_{TR,L} = \frac{A_L}{A^*_{TR}}\phi_L, \qquad \phi^*_{TR,R} = \frac{A_R}{A^*_{TR}}\phi_R. \tag{6.5}$$

6.1.2 A linearized two-rarefaction approximate Riemann solver for the pressure system

Now we proceed as in the case of the two-rarefaction Riemann solver and additionally approximate the relations (6.2). In this case, the solution in the *Star Region* is

$$\mathbf{Q}^*_{LTR,L} = \begin{bmatrix} A^*_{LTR} \\ q^*_{LTR} \\ A^*_{LTR}\phi^*_{LTR,L} \end{bmatrix}, \quad \mathbf{Q}^*_{LTR,R} = \begin{bmatrix} A^*_{LTR} \\ q^*_{LTR} \\ A^*_{LTR}\phi^*_{LTR,R} \end{bmatrix}. \tag{6.6}$$

Given the wave relations from Proposition 5.2.1 described in (6.2), we approximate the integrals in this way

$$\int_{A_L}^{A^*_{LTR}} c(A)dA \approx c_L(A^*_{LTR} - A_L), \tag{6.7}$$

$$\int_{A_R}^{A^*_{LTR}} c(A)dA \approx c_R(A^*_{LTR} - A_R). \tag{6.8}$$

Solving the system

$$\begin{cases} q^*_{LTR} = q_L - c_L(A^*_{LTR} - A_L), \\ q^*_{LTR} = q_R + c_R(A^*_{LTR} - A_R), \end{cases} \tag{6.9}$$

we obtain

$$\begin{aligned} q^*_{LTR} &= \frac{c_R(A_L c_L - A_R c_L + q_L) + c_L q_R}{c_L + c_R}, \\ A^*_{LTR} &= \frac{A_L c_L + A_R c_R + q_L - q_R}{c_L + c_R}. \end{aligned} \tag{6.10}$$

For the definition of c_L and c_R we refer again to Remark 6.1.1.

Regarding the last variable, as before

$$\phi^*_{LTR,L} = \frac{A_L}{A^*_{LTR}}\phi_L, \qquad \phi^*_{LTR,R} = \frac{A_R}{A^*_{LTR}}\phi_R. \tag{6.11}$$

6.2 Advection-pressure numerical splitting schemes for the complete conservative 1D blood flow model with transport

To numerically solve the complete system of conservative 1D blood flow equations (2.1), we employ a conservative method following the approach outlined in [92]. The numerical scheme is

$$\mathbf{Q}_i^{n+1} = \mathbf{Q}_i^n - \frac{\Delta t}{\Delta x}(\mathbf{F}_{i+\frac{1}{2}} - \mathbf{F}_{i-\frac{1}{2}}), \tag{6.12}$$

where

$$\mathbf{Q}_i^n \approx \frac{1}{\Delta x}\int_{x_{i-\frac{1}{2}}}^{x_{i+\frac{1}{2}}} \mathbf{Q}(x, t^n)dx, \tag{6.13}$$

with $\Delta x = x_{i+\frac{1}{2}} - x_{i-\frac{1}{2}}$, $\Delta t = t^{n+1} - t^n$. As anticipated in Section 3.1, the aim is to compute a numerical flux

$$\mathbf{F}_{i+\frac{1}{2}} = \mathcal{A}_{i+\frac{1}{2}} + \mathcal{P}_{i+\frac{1}{2}}, \tag{6.14}$$

where $\mathcal{A}_{i+\frac{1}{2}}$ and $\mathcal{P}_{i+\frac{1}{2}}$ are obtained from appropriate Cauchy problems for the advection (3.3) and pressure (3.4) systems, respectively.

We define

$$\mathcal{P}_{i+\frac{1}{2}} = \mathcal{P}(\mathbf{Q}_{i+\frac{1}{2}}(0)), \tag{6.15}$$

where $\mathcal{P}$ is in (3.5) and $\mathbf{Q}_{i+\frac{1}{2}}(0)$ denotes the Godunov state, i.e. the value $\mathbf{Q}_{i+\frac{1}{2}}\left(\frac{x-x_{i+\frac{1}{2}}}{t}\right)$ calculated at $\frac{x-x_{i+\frac{1}{2}}}{t}=0$, i.e. the solution of the following Riemann problem

$$\begin{cases}\partial_t\mathbf{Q}+\partial_x\mathcal{P}(\mathbf{Q})=\mathbf{0}, \quad x\in\mathbb{R}, \quad t>t^n,\\ \mathbf{Q}(x,t^n)=\begin{cases}\mathbf{Q}_L=\mathbf{Q}_i^n, & \text{if} \quad x<x_{i+\frac{1}{2}},\\ \mathbf{Q}_R=\mathbf{Q}_{i+1}^n, & \text{if} \quad x>x_{i+\frac{1}{2}},\end{cases}\end{cases} \tag{6.16}$$

evaluated at the interface $x_{i+\frac{1}{2}}$, for each cell i. Due to the fact that the wave configuration of the solution of the Riemann problem for the pressure system (6.16) will always result in two subsonic waves, $\mathbf{Q}_{i+\frac{1}{2}}(0)=\mathbf{Q}^*_{\text{PRESS},i+\frac{1}{2}}=[A^*_{\text{PRESS},i+\frac{1}{2}},q^*_{\text{PRESS},i+\frac{1}{2}},A^*_{\text{PRESS},i+\frac{1}{2}}\phi^*_{\text{PRESS},i+\frac{1}{2}}]^T$, the solution in the Star Region of the Riemann problem (6.16) for each cell i.

$\mathcal{A}_{i+\frac{1}{2}}$ is computed as proposed in [89], which represents a modification of the original splitting presented in [92] namely,

$$\mathcal{A}_{i+\frac{1}{2}}=\begin{bmatrix}0\\ q^*_{\text{PRESS},i+\frac{1}{2}}u_k\\ q^*_{\text{PRESS},i+\frac{1}{2}}\phi_k\end{bmatrix}, \tag{6.17}$$

where

$$u_k=\begin{cases}u_L & \text{if} \quad q^*_{\text{PRESS},i+\frac{1}{2}}>0,\\ u_R & \text{if} \quad q^*_{\text{PRESS},i+\frac{1}{2}}\leq 0,\end{cases} \qquad \phi_k=\begin{cases}\phi_L & \text{if} \quad q^*_{\text{PRESS},i+\frac{1}{2}}>0,\\ \phi_R & \text{if} \quad q^*_{\text{PRESS},i+\frac{1}{2}}\leq 0.\end{cases} \tag{6.18}$$

To compute $\mathbf{Q}^*_{\text{PRESS},i+\frac{1}{2}}$ we use two different methods

1. (TV+TR) $\mathbf{Q}^*_{\text{PRESS},i+\frac{1}{2}}=\mathbf{Q}^*_{TR,i+\frac{1}{2}}$, with $\mathbf{Q}^*_{TR,i+\frac{1}{2}}=[A^*_{TR,i+\frac{1}{2}},q^*_{TR,i+\frac{1}{2}},0]^T$ the (modified) approximate two rarefaction solution of the Riemann problem for the pressure system (6.16) in the Star Region presented in Section 6.1.1, for each cell i.

2. (TV+Lin.TR) $\mathbf{Q}^*_{\text{PRESS},i+\frac{1}{2}}=\mathbf{Q}^*_{LTR,i+\frac{1}{2}}$, with $\mathbf{Q}^*_{LTR,i+\frac{1}{2}}=[A^*_{LTR,i+\frac{1}{2}},q^*_{LTR,i+\frac{1}{2}},0]^T$ the (modified) approximate linearized two rarefaction solution of the Riemann problem for the pressure system (6.16) in the Star Region presented in Section 6.1.2, for each cell i.

It is worth remarking that the third component of any solution just presented is set equal to 0 because the variable ϕ has no value due to the contact discontinuity $\lambda_{\mathcal{P}2}$ at the interface. In fact, there are two values ϕ^*_L and ϕ^*_R for each solution type, one to the left and one to the right of the interface, but we do not actually need them because the pressure flux in (3.5) has 0 as its third component.

6.3 NUMERICAL RESULTS

In this Section, we design test problems and assess the performance of the numerical splitting methods of type TV presented in this Chapter.

We propose six test problems; these tests have been chosen to represent the different admissible solutions of the 1D blood flow equations in the case of arteries (Tests 1 and 2) and veins (Tests 3, 4, 5, 6), namely smooth solutions (rarefactions), elastic jumps (shocks), and contact discontinuities.

Table 6.1: Initial conditions for Tests from 1 to 6. The wave patterns are: R=rarefaction, C=contact discontinuity, S=shock. The units of measures used for this Thesis are: m, s, Kg, Pa.

Test	$A_L[m^2]$	$u_L[m/s]$	ϕ_L	$A_R[m^2]$	$u_R[m/s]$	ϕ_R	Wave pattern
1	$3.50 \cdot 10^{-4}$	0.00	1.00	$3.00 \cdot 10^{-4}$	0.00	0.00	RCS
2	$10.00 \cdot 10^{-4}$	0.00	1.00	$1.00 \cdot 10^{-4}$	0.00	0.00	R(sonic)CS
3	$2.80 \cdot 10^{-4}$	-0.50	1.00	$2.80 \cdot 10^{-4}$	0.50	0.00	RCR
4	$2.90 \cdot 10^{-4}$	0.00	1.00	$2.40 \cdot 10^{-4}$	0.00	0.00	RCS
5	$2.34 \cdot 10^{-4}$	0.10	0.00	$2.74 \cdot 10^{-4}$	0.20	1.00	SCR
6	$1.90 \cdot 10^{-4}$	1.00	1.00	$2.20 \cdot 10^{-4}$	0.50	0.00	SCS

Table 6.2: Parameters used for Tests from 1 to 6: domain length ℓ, blood density ρ, wessel wall stiffness K, reference cross-sectional area A_0, external pressure p_e, location of the initial discontinuity x_d and output time t_{End}.

Test	Vessel	$\ell[m]$	ρ	$K[Pa]$	$A_0[m^2]$	$p_e[Pa]$	$x_d[m]$	$t_{End}[s]$
1	Artery	0.50	1000.00	20005.00	$3.14 \cdot 10^{-4}$	0.00	0.50ℓ	0.05
2	Artery	0.50	1000.00	20005.00	$3.14 \cdot 10^{-4}$	0.00	0.50ℓ	0.04
3	Vein	0.50	1000.00	333.00	$3.14 \cdot 10^{-4}$	0.00	0.50ℓ	0.09
4	Vein	0.50	1000.00	333.00	$3.14 \cdot 10^{-4}$	0.00	0.50ℓ	0.10
5	Vein	0.50	1000.00	333.00	$3.14 \cdot 10^{-4}$	0.00	0.50ℓ	0.10
6	Vein	0.50	1000.00	333.00	$3.14 \cdot 10^{-4}$	0.00	0.30ℓ	0.15

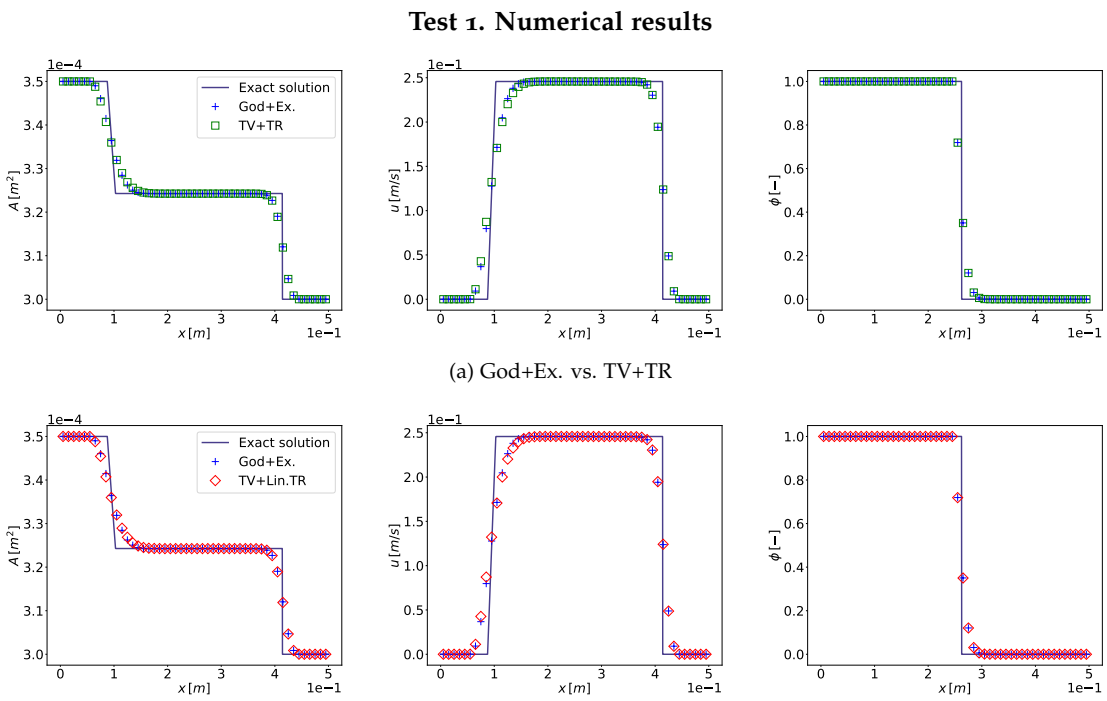

(a) God+Ex. vs. TV+TR

(b) God+Ex. vs. TV+Lin.TR

Figure 6.1: Test 1. Artery. RCS. Numerical results of methods 1, 2 vs. the classic Godunov method with $C_{cfl} = 0.9$, $I = 50$ cells, and the exact solution of the Riemann problem for the complete system presented in Chapter 2.1. Initial conditions and parameters are given in Tables 6.1, 6.2.

Of the three waves, the contact discontinuity is usually the one that presents a greater challenge, especially for linearized or incomplete solvers, since excessive numerical diffusion occurs in the form of smearing of the contact discontinuity. In the case of veins, the tests are constructed to explore different positions of A_c in (5.12) with respect to the tests data. This value is of critical

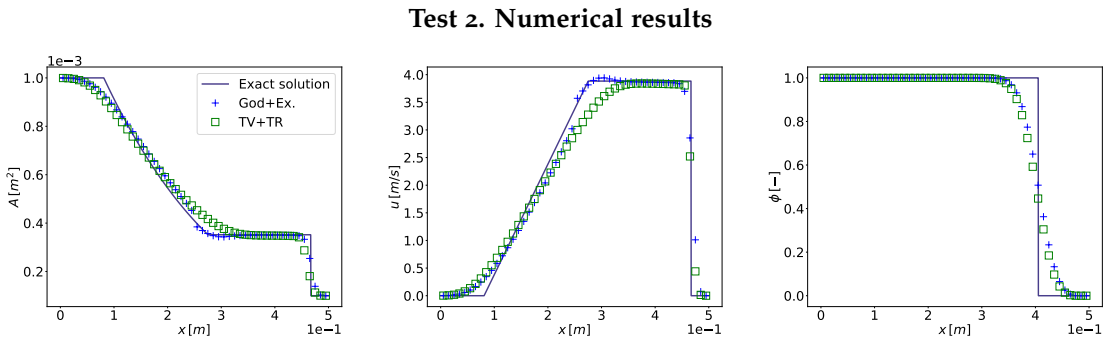

(a) God+Ex. vs. TV+TR

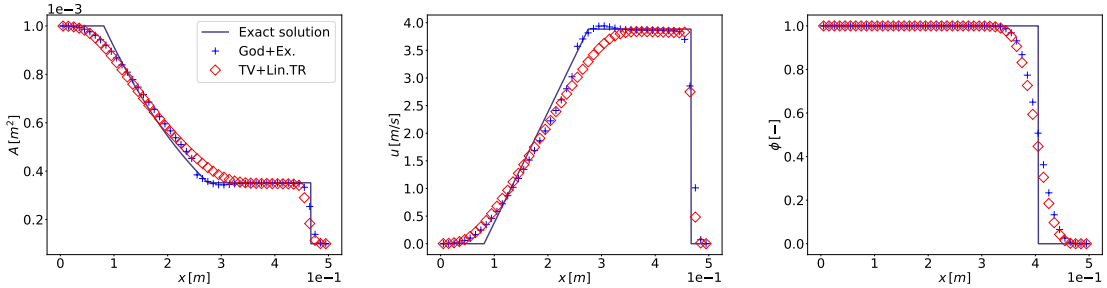

(b) God+Ex. vs. TV+Lin.TR

Figure 6.2: Test 2. Artery. R(sonic)CS. Numerical results of methods 1, 2 vs. the classic Godunov method with $C_{cfl} = 0.9$, $I = 50$ cells, and the exact solution of the Riemann problem for the complete system presented in Chapter 2.1. Initial conditions and parameters are given in Tables 6.1, 6.2.

importance for the wave pattern of the pressure system (see Chapter 5). In this Chapter we will restrict ourselves to showing that the presented schemes work properly even in cases when genuine non-linearity of the $\lambda_{\mathcal{P}1}$- and $\lambda_{\mathcal{P}3}$-characteristic fields of the pressure system is lost. The numerical results of the methods 1 and 2 are compared with the exact solution of the Riemann problem for the full 1D blood flow equations and some competing methods in the literature. The initial data, expressed in terms of the physical variables A, u, and ϕ, can be found in Table 6.1. Meanwhile, the model parameters are provided in Table 6.2. The discussion of the numerical results is covered in Section 6.3.1, while an efficiency test is performed in Section 6.3.2.

6.3.1 Results discussion

Numerical results for both methods 1 and 2 are shown and plotted against the exact solution of the Riemann problem for the full conservative 1D blood flow equations (2.1) presented in Chapter 2.1 and the results of the Godunov method [34] used in conjunction with the exact Riemann solver for the complete 1D system (fully described in [87]). For all tests, we use a Courant–Friedrichs–Lewy number $C_{cfl} = 0.9$ and a mesh of $I = 50$ computational cells (Figs. 6.1, 6.2, 6.3, 6.4, 6.5, 6.6). In this work the Courant–Friedrichs–Lewy number C_{cfl} is defined as follows

Definition 6.3.1.

$$C_{cfl} = \frac{\Delta t}{\Delta x} S^n_{max}, \tag{6.19}$$

where

$$S^n_{max} = max_i \left\{ max_k \left| \lambda^n_{k,i} \right| \right\}, \quad k = 1, ...N, \quad i = 1, ..., I; \tag{6.20}$$

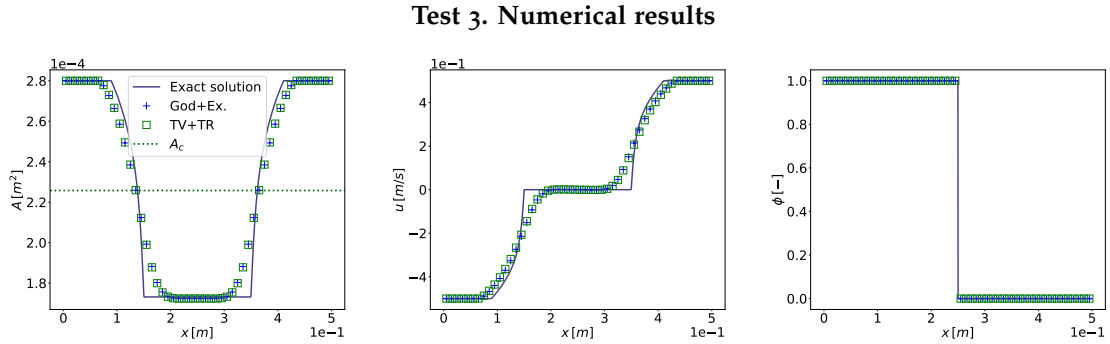

(a) God+Ex. vs. TV+TR

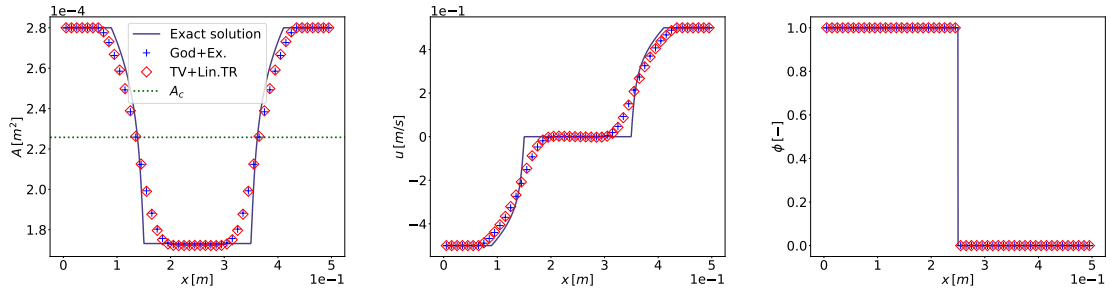

(b) God+Ex. vs. TV+Lin.TR

Figure 6.3: Test 3. Vein. RCR. Numerical results of methods 1, 2 vs. the classic Godunov method with $C_{cfl} = 0.9$, $I = 50$ cells, and the exact solution of the Riemann problem for the complete system presented in Chapter 2.1. Initial conditions and parameters are given in Tables 6.1, 6.2. A_c in (5.12) is located inside both rarefactions.

where $\lambda^n_{k,i}$ is the k-th eigenvalue of the complete system (2.1) evaluated in cell i at time t^n, and N is the number of eigenvalues of the considered system.

Test 1 (Artery): RCS The solution of Test 1 consists of three waves, namely a left-facing rarefaction wave, a middle contact discontinuity, visible for the tracer ϕ, and a right-facing elastic jump, or shock (RCS). The left rarefaction wave carries smooth transitions of cross-sectional area A and velocity u, while the right shock carries discontinuous jumps in these quantities. The numerical results of the two new methods presented are comparable to those of the Godunov scheme: all approximations are accurate and very similar among themselves for the rarefaction wave, the contact and the shock wave, we can appreciate monotone shocks, i.e. there are no spurious oscillations in the vicinity of shocks and also the contact discontinuity presents a minimal smearing and its speed of propagation is correct.

Test 2 (Artery): R(sonic)CS Test 2 contains the same wave pattern as Test 1, that is a left rarefaction, a middle contact and a right shock (RCS). However, there are two important differences. First, the strength of the waves; this may pose a challenge to the robustness of the methods. Second, the left rarefaction in Test 2 is transonic; i.e. the associated left eigenvalue $\lambda_1 = u - c$ transits monotonically from negative values to positive values, passing through a critical point at which $u = c$. Even though the wave is smooth, the correct approximation of the sonic point is challenging for all numerical methods. Some schemes will present a jump (shock) instead of a smooth transition across the sonic point; this is sometimes referred to as the *entropy glitch* and arises only in the presence of sonic rarefaction waves. Such a shock is entropy violating and therefore unphysical. This problem was overcome by the two new schemes, which

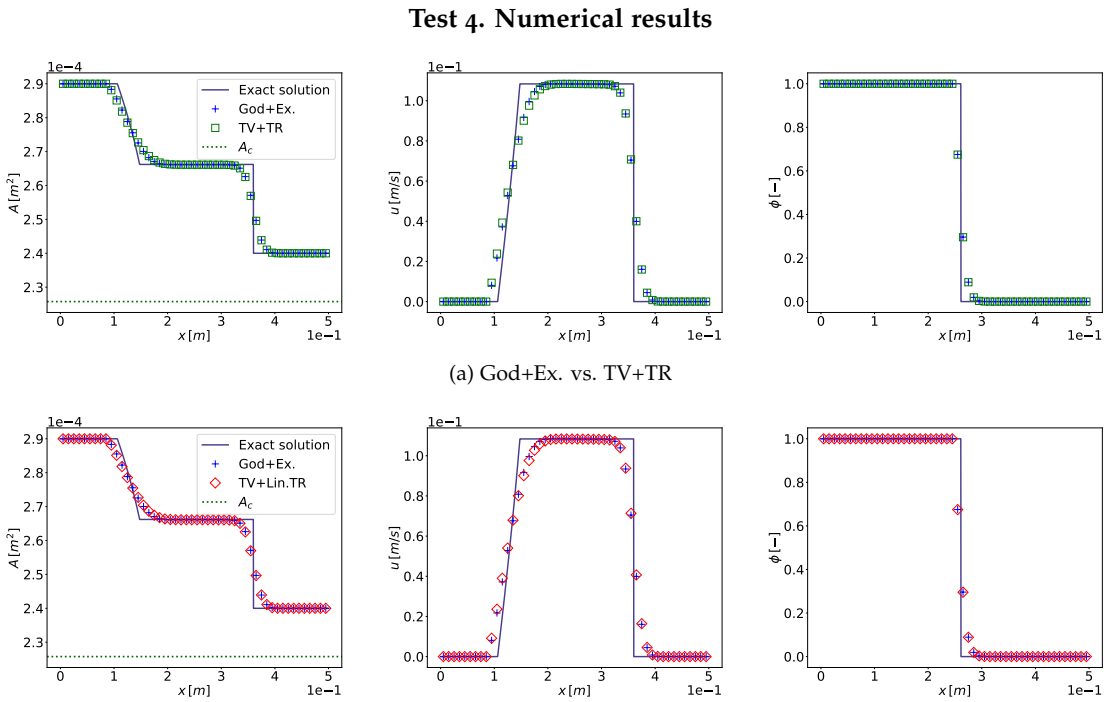

(a) God+Ex. vs. TV+TR

(b) God+Ex. vs. TV+Lin.TR

Figure 6.4: Test 4. Vein. RCS. Numerical results of methods 1, 2 vs. the classic Godunov method with $C_{cfl} = 0.9$, $I = 50$ cells, and the exact solution of the Riemann problem for the complete system presented in Chapter 2.1. Initial conditions and parameters are given in Tables 6.1, 6.2. A_c in (5.12) is located below the range covered by the Riemann problem results.

present smooth transitions for the area A and the velocity u. On the other hand, the results for both splitting schemes show a small overshoot for the velocity u in agreement with the shock front. The results for the contact discontinuity follow the path of the Godunov scheme and show a higher numerical diffusion. However, the propagation velocity and average position remain correct.

TEST 3 (VEIN): RCR The solution of Test 3 consists of a left rarefaction, a middle contact discontinuity for ϕ and a right rarefaction (RCR), in this problem A_c is located *inside* the rarefactions; we can appreciate that the accuracy of the methods is not affected by this particular position of A_c, and the results of the new schemes are comparable with those of the Godunov method: in particular, the contact discontinuity is well described without smearing.

TEST 4 (VEIN): RCS The solution of Test 4 consists of a left rarefaction, a middle contact discontinuity, and a right shock (RCS), A_c is outside the range covered by the exact solution and its numerical approximations. The comments are similar to those of Test 3, with minimal diffusion in the approximation of the contact discontinuity.

TEST 5 (VEIN): SCR With the same position of A_c as in Test 4, this test scenario features a left shock, a middle contact discontinuity, and a right rarefaction (SCR) problem. Once again, the results obtained from the two new methods are comparable to those of the Godunov scheme. Notably, the left shock exhibits some smoothing in all of these schemes, while the contact discontinuity experiences minimal diffusion.

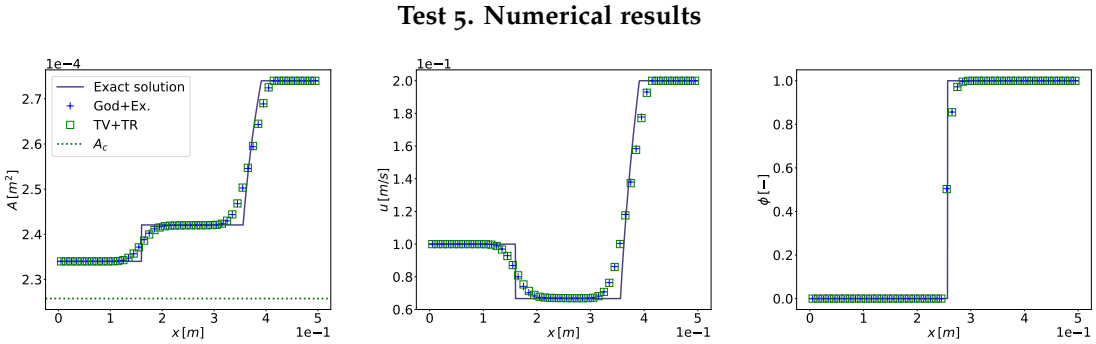

(a) God+Ex. vs. TV+TR

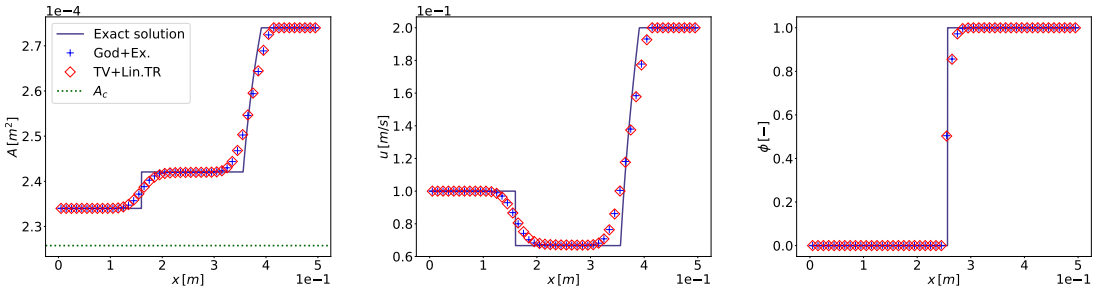

(b) God+Ex. vs. TV+Lin.TR

Figure 6.5: Test 5. Vein. SCR. Numerical results of methods 1, 2 vs. the classic Godunov method with $C_{cfl} = 0.9$, $I = 50$ cells, and the exact solution of the Riemann problem for the complete system presented in Chapter 2.1. Initial conditions and parameters are given in Tables 6.1, 6.2. A_c in (5.12) is located below the range covered by the Riemann problem results.

Test 6 (Vein): SCS Finally, the solution of Test 6 shows a left shock, a middle contact discontinuity, and a right shock (SCS) with A_c *inside* both shocks. While for the concentration of the passive scalar the results of the two new methods are comparable to those of the Godunov scheme, which describes the contact discontinuity with some diffusion, the left shock is smeared in the case of A and u, unlike in the Godunov scheme. We think that this difference could be due to the strength of the left shock and the non-linear behavior of the veins, and not to the particular position of A_c, because the latter is the same as that of the right shock.

6.3.2 Efficiency: error against CPU time

Efficiency is determined by the CPU time required by a method to achieve a specified error E. To assess the efficiency of the TV-type methods presented in this study (methods 1 and 2), we compare the results with those obtained with standard and well known numerical methods. We consider two non-linear and complete solvers: the Godunov method with the exact Riemann solver (Section 6.3.1), the DOT Riemann solver [23, 24] (Appendix A.5) and a centred, and thus incomplete, scheme: the FORCE scheme [88, 87] (Appendix A.1). Here we calculate the CPU cost and the L_1 error for each method cited above, for variables A, u and ϕ, with meshes $I = [50, 100, 200, 400]$ and a $C_{cfl} = 0.95$. L_1 error defined

$$L_1^{err}(t_{End}, \Delta x_j) = \Delta x_j \sum_{i=1}^{I_j} |q_{k,i}^{t_{End}} - q_{k,i}^{e}|, \quad k = 1, 2, 3; \tag{6.21}$$

Test 6. Numerical results

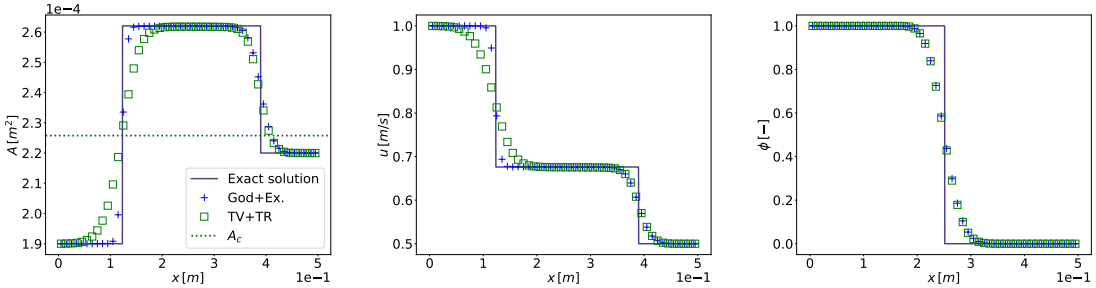

(a) God+Ex. vs. TV+TR

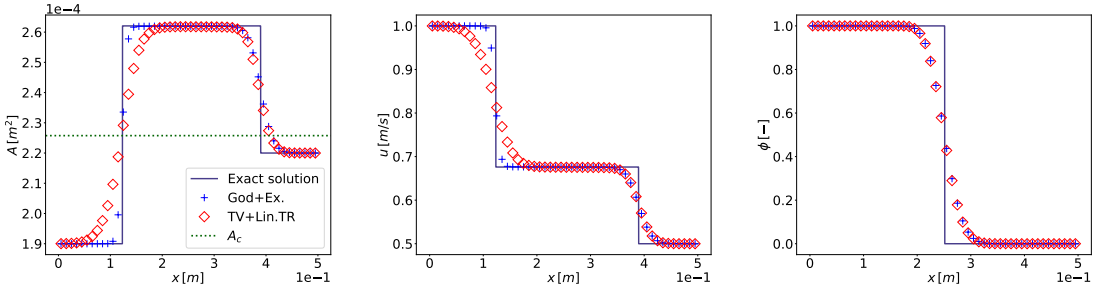

(b) God+Ex. vs. TV+Lin.TR

Figure 6.6: Test 6. Vein. SCS. Numerical results of methods 1, 2 vs. the classic Godunov method with $C_{cfl} = 0.9$, $I = 50$ cells, and the exact solution of the Riemann problem for the complete system presented in Chapter 2.1. Initial conditions and parameters are given in Tables 6.1, 6.2. A_c in (5.12) is located inside both shocks.

being t_{End} the output time, $q_{k,i}^{t_{End}}$ the *k-th* component of $\mathbf{Q}_i^n$ at time t_{End}, $q_{k,i}^e$ the corresponding exact solution and $\Delta x_j = \ell / I_j$, with ℓ the vessel length and I_j the actual mesh. The tests are carried out in Python language. Results are depicted in Figs. 6.7, 6.8, 6.9.

It is worth noting that for this efficiency test, the exact solution of the conservative complete 1D blood flow equations presented in Chapter 2.1, proved to be not adequate due to the numerical construction of the integral curves there performed. Being these tests carried out only for a momentum correction coefficient $\alpha = 1$, we use the *classic* exact Riemann solver presented for example in [90, 81], being the continuous parameters case here trated, a particular variant of the discontinuous parameters case there discussed.

In case of arteries, the two new methods prove to be the most efficient numerical methods (Figs. 6.7, 6.9). For the test in subsonic regime (Test 1) concerning the first two variables A and u, the new methods reach an accuracy comparable with that of the three classical numerical schemes (Godunov, FORCE, DOT) but with less computational effort. Regarding the concentration of the passive scalar, all methods reach the same level of accuracy with the exception of FORCE, due to its expected excessive numerical diffusion in the description of the intermediate wave (Fig. 6.7). In Test 2, where a left transonic rarefaction is depicted, the accuracy of the solution obtained with the new schemes is lower than the one of the solutions obtained with DOT and Godunov, regarding variables A and u (Fig. 6.7); however, the so-called *entropy glitch* must be taken into account. The two new methods in fact prove to reproduce this rarefaction in a smooth way.

As for veins, the method TV+Lin.TR proves to be the most efficient of the two new methods and for Tests 3, 4, 5 the most efficient of all the methods under analysis, achieving the same accuracy as the others, but in a lower CPU time. Also, the description of the concentration of the passive scalar ϕ is very accurate, a situation where instead FORCE usually fails, due to a high

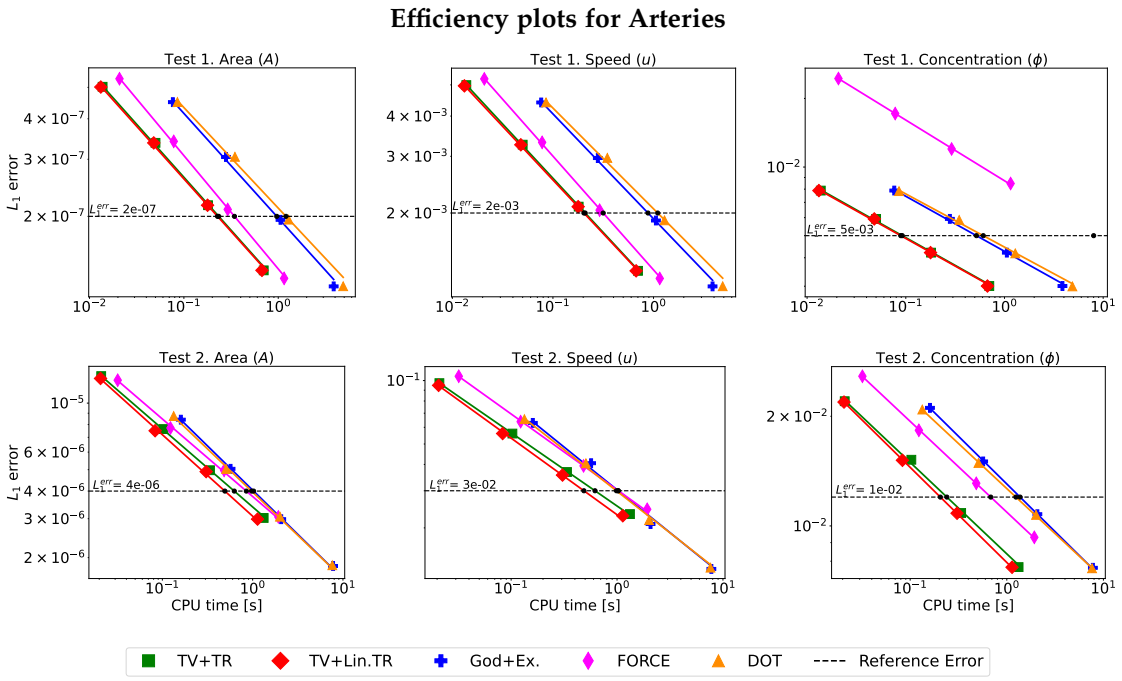

Figure 6.7: Efficiency plots for Tests 1, 2, in Tables 6.1, 6.2, calculated for meshes $I = [50, 100, 200, 400]$. The lines represent the least square approximation (where possible) of the data.

numerical diffusion (Figs. 6.8, 6.9). Test 6, on the other hand (left shock-middle contact-right shock in a vein), shows a remarkable decrease in accuracy for the two new methods, for variables A and u, with respect to the Godunov method and the DOT one, due to a higher diffusion in the description of the left shock (Fig. 6.8). In this case, the accuracy of the new methods is comparable to that of FORCE, on the contrary, the efficiency in describing the concentration ϕ is very good. In particular, the new methods exhibit a small diffusion in the description of ϕ, which, in contrast, is not present in Test 3. For this reason, the concentration plot for this test is the result of round-off errors and the results in Fig. 6.9 are omitted.

It is worth noting that the FORCE scheme for the passive scalar ϕ generally does not achieve the chosen reference error with the given meshes, but the CPU time is calculated using an extrapolation of the observed convergence pattern. Furthermore, regarding both arteries and veins, we can conclude that the two TV methods here proposed proved to be as accurate as Godunov's scheme in describing the contact discontinuity.

6.4 Conclusions

In this work, after having presented a flux splitting method at PDEs level for the original hyperbolic system of 1D blood flow equations with continuous parameters and an advection equation for a passive scalar transport, for both arteries and veins described in Chapter 3.1, separating the given system in advection system and pressure one, in this Chapter we have presented two approximated Riemann problem solvers for the obtained pressure system, and after, two final numerical flux splitting schemes for the complete conservative 1D blood flow model described in Chapter 2.1 have been built. These latter have been compared with the classic Godunov scheme and the exact solution of the Riemann problem for the complete system, in various test problems for arteries and veins, both in subsonic and transonic regime, proving

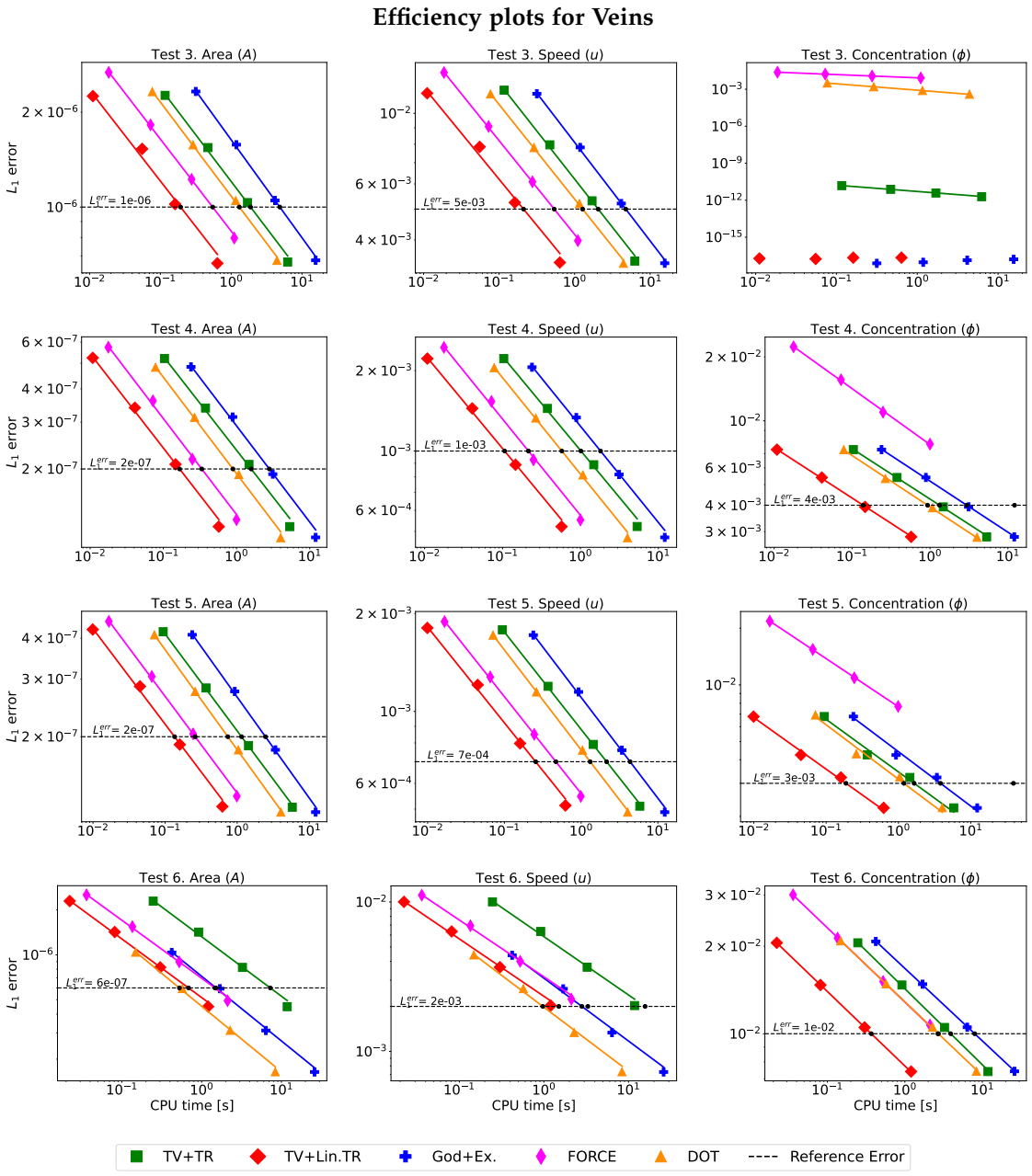

Figure 6.8: Efficiency plots for Tests 3, 4, 5, 6 in Tables 6.1, 6.2, calculated for meshes $I = [50, 100, 200, 400]$. The lines represent the least square approximation (where possible) of the data.

that the issues faced with the lack of genuine non-linearity of two characteristic fields of the pressure system do not prevent the final splitting schemes from working properly. Finally an efficiency analysis has been carried out. The two proposed methods have proved to be in general considerably more efficient than the original Godunov method, the FORCE centred numerical scheme and the DOT Riemann solver, and can be considered as competitive methods to solve the Riemann problems under study. In the forthcoming research, the proposed techniques will be implemented to solve networks of 1D blood flow models.

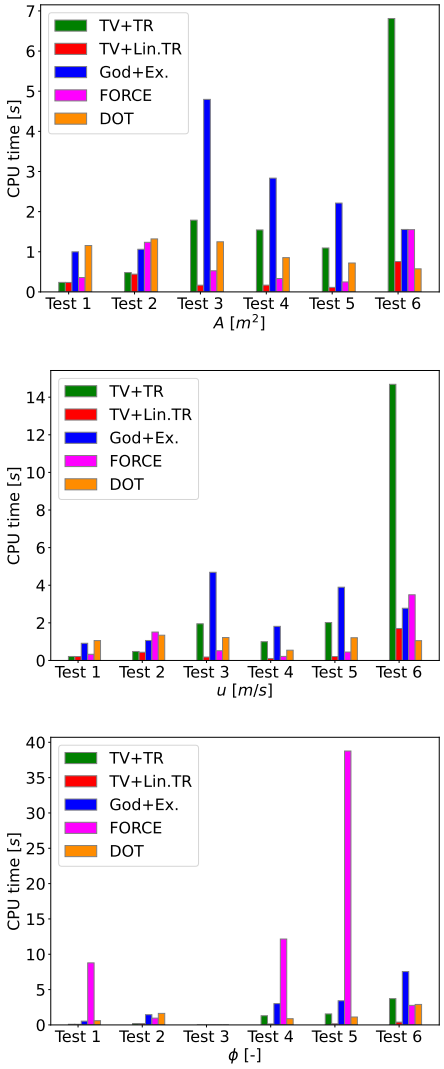

Figure 6.9: Efficiency bar plots for Tests 1, 2, 3, 4, 5, 6 in Tables 6.1, 6.2 representing the actual time each method takes to reach errors given in Figs. 6.7, 6.8, for each variable.

Chapter 7

Advection-pressure splitting schemes applied to a non-conservative 1D blood flow model with transport for arteries and veins

In this Chapter we introduce innovative, splitting-based, numerical schemes for the non-conservative one-dimensional (1D) blood flow equations that incorporate an advection equation for a passive scalar transport, are designed to model blood flow in arteries and veins and take into account a general constant momentum correction coefficient (Chapter 2.2).

Our schemes are inspired by the original flux vector splitting approach of Toro and Vázquez-Cendón [92] designed for the Euler equations, and represent an improvement of the work proposed by Toro et al. [91] regarding non-conservative systems, which considered a tube law describing only arteries, a momentum correction coefficient equal to one, no passive scalar transport equation and involves a minor number of discontinuous mechanical and geometrical parameters. Our schemes separate advection terms and pressure terms, generating two different systems of PDEs: the advection system in conservative form, and the pressure system in non-conservative form, both of which have a very simple eigenstructure compared to that of the full system (Chapter 3.2). The splitting schemes of this Chapter are systematically assessed on a carefully designed suite of test problems with exact solution and compared with several existing mainstream methods. A detailed efficiency analysis is performed in order to showcase the advantages of the proposed methodology in comparison to standard approaches.

The Chapter is organized as follows: having presented the complete non-conservative 1D blood flow equations (Chapter 2.2) their splitting at the level of PDEs (Chapter 3.2), we briefly present some theoretical aspects of the pressure system resulting from the aforementioned splitting (Section 7.1), introducing the associated Riemann problem (Section 7.1.1), and two approximate Riemann solvers for the aforementioned system (Section 7.1.2). Finally, the numerical splitting schemes are presented in Section 7.2, the numerical results are given in Section 7.3, with an efficiency analysis performed in Section 7.3.2. The conclusions are drawn in Section 7.4.

This research work is in preparation.

7.1 THE NON-CONSERVATIVE PRESSURE SYSTEM

7.1.1 THEORETICAL NOTIONS

The pressure system resulting from the splitting of the non-conservative 1D blood flow equations is presented in Chapter 3.2, and will be here briefly recalled. The pressure system is

$$\partial_t \mathbf{Q} + \boldsymbol{\mathcal{P}}(\mathbf{Q})\partial_x \mathbf{Q} = \mathbf{0}, \tag{7.1}$$

where

$$\mathbf{Q} = \begin{bmatrix} A \\ Au \\ K \\ A_0 \\ p_e \\ A\phi \end{bmatrix}, \quad \boldsymbol{\mathcal{P}}(\mathbf{Q}) = \begin{bmatrix} 0 & 1 & 0 & 0 & 0 & 0 \\ c^2 & 0 & \frac{A}{\rho}\psi_K & \frac{A}{\rho}\psi_{A_0} & \frac{A}{\rho} & 0 \\ 0 & 0 & 0 & 0 & 0 & 0 \\ 0 & 0 & 0 & 0 & 0 & 0 \\ 0 & 0 & 0 & 0 & 0 & 0 \\ 0 & 0 & 0 & 0 & 0 & 0 \end{bmatrix}. \tag{7.2}$$

where c is the *wave speed* (2.183) and ρ, ψ_K, ψ_{A_0} are defined in Chapter 2.2. The eigenvalues of matrix $\boldsymbol{\mathcal{P}}(\mathbf{Q})$ in (7.2) are all real for parameters in (2.177), and given by

$$\lambda_{\mathcal{P}1} = -c, \qquad \lambda_{\mathcal{P}2} = \lambda_{\mathcal{P}3} = \lambda_{\mathcal{P}4} = \lambda_{\mathcal{P}5} = 0, \qquad \lambda_{\mathcal{P}6} = c, \tag{7.3}$$

and a possible choice of right eigenvectors corresponding to eigenvalues (7.3) is

$$\begin{aligned} \mathbf{R}_{\mathcal{P}1} &= \begin{bmatrix} 1 \\ -c \\ 0 \\ 0 \\ 0 \\ 0 \end{bmatrix}, \quad \mathbf{R}_{\mathcal{P}2} = \begin{bmatrix} 0 \\ 0 \\ 1 \\ 0 \\ -\psi_k \\ 0 \end{bmatrix}, \quad \mathbf{R}_{\mathcal{P}3} = \begin{bmatrix} 0 \\ 0 \\ 0 \\ 1 \\ -\psi_{A_0} \\ 0 \end{bmatrix}, \quad \mathbf{R}_{\mathcal{P}4} = \begin{bmatrix} 1 \\ 0 \\ 0 \\ 0 \\ -\frac{\rho}{A}c^2 \\ 0 \end{bmatrix}, \\ \mathbf{R}_{\mathcal{P}5} &= \begin{bmatrix} 0 \\ 0 \\ 0 \\ 0 \\ 0 \\ 1 \end{bmatrix}, \quad \mathbf{R}_{\mathcal{P}6} = \begin{bmatrix} 1 \\ c \\ 0 \\ 0 \\ 0 \\ 0 \end{bmatrix}, \end{aligned} \tag{7.4}$$

where c is the wave speed (2.183).

Proposition 7.1.1 (Hyperbolicity). *System (7.1) is hyperbolic under the following hypotheses:*

1. *the set of admissible solutions is restricted to* $\mathbf{Q} \in \Omega = [\mathbb{R}^+ \times \mathbb{R} \times \Omega_P \times \mathbb{R}_0^+] \subset \mathbb{R}^6$;
2. *the tube law is a monotonically increasing function of the cross-sectional area* A, *i.e.* $\dfrac{\partial p}{\partial A} > 0$.

Proof. This can be clearly seen from the definition of wave speed given in (2.183). Under the conditions considered in this proposition $c \in \mathbb{R}^+ \; \forall \mathbf{Q} \in \Omega$, which results in $\lambda_{\mathcal{P}1} \in \mathbb{R}^-$, $\lambda_{\mathcal{P}6} \in \mathbb{R}^+$, $\forall \mathbf{Q} \in \Omega$. In particular this is true for the parameters given in (2.176), (2.177). □

Proposition 7.1.2 (Nature of the $\lambda_{\mathcal{P}1}$- and $\lambda_{\mathcal{P}6}$-characteristic fields)**.** *Under the hypotheses of Proposition 7.1.1, in case of arteries (parameters are given in (2.176),(2.177)) the $\lambda_{\mathcal{P}1}$- and $\lambda_{\mathcal{P}6}$-characteristic fields are genuinely non-linear with*

$$\begin{aligned} \nabla\lambda_{\mathcal{P}1}(\mathbf{Q})\cdot\mathbf{R}_{\mathcal{P}1}(\mathbf{Q}) < 0, \quad \forall \mathbf{Q}\in\Omega, \\ \nabla\lambda_{\mathcal{P}6}(\mathbf{Q})\cdot\mathbf{R}_{\mathcal{P}6}(\mathbf{Q}) > 0, \quad \forall \mathbf{Q}\in\Omega, \end{aligned} \tag{7.5}$$

instead in case of veins, they are not. In fact

$$\begin{aligned} \nabla\lambda_{\mathcal{P}1}(\mathbf{Q})\cdot\mathbf{R}_{\mathcal{P}1}(\mathbf{Q}) \quad & \begin{cases} > 0 & \text{for} \quad A < A_{cL}, \\ = 0 & \text{for} \quad A = A_{cL}, \\ < 0 & \text{for} \quad A > A_{cL}, \end{cases} \\ \nabla\lambda_{\mathcal{P}6}(\mathbf{Q})\cdot\mathbf{R}_{\mathcal{P}6}(\mathbf{Q}) \quad & \begin{cases} < 0 & \text{for} \quad A < A_{cR}, \\ = 0 & \text{for} \quad A = A_{cR}, \\ > 0 & \text{for} \quad A > A_{cR}, \end{cases} \end{aligned} \tag{7.6}$$

where A_{cL}, A_{cR}, for parameters in (2.177), are

$$A_{cL} \approx 0.7190\, A_{0L}, \qquad A_{cR} \approx 0.7190\, A_{0R}. \tag{7.7}$$

Proof. Omitted.The proof is analogous to the corresponding one presented in Chapter 5. □

Proposition 7.1.3 (Nature of the $\lambda_{\mathcal{P}2,\mathcal{P}3,\mathcal{P}4,\mathcal{P}5}$-characteristic fields)**.** *Under the hypotheses of Proposition 7.1.1, the $\lambda_{\mathcal{P}2,\mathcal{P}3,\mathcal{P}4,\mathcal{P}5}$-characteristic fields are linearly degenerate.*

Proof. It can be easily verified that

$$\nabla\lambda_{\mathcal{P}k}(\mathbf{Q})\cdot\mathbf{R}_{\mathcal{P}k}(\mathbf{Q}) = 0, \qquad k = 2,3,4,5, \quad \forall \mathbf{Q}\in\Omega. \tag{7.8}$$

□

Proposition 7.1.4 (Generalized Riemann invariants for the $\lambda_{\mathcal{P}1}$- and $\lambda_{\mathcal{P}6}$-characteristic fields)**.** *The Riemann invariants are given by*

$$q + \int c(A)dA = const, \quad K = const, \quad A_0 = const, \quad p_e = const, \quad A\phi = const, \tag{7.9}$$

for the $\lambda_{\mathcal{P}1}$-characteristic field,

$$q - \int c(A)dA = const, \quad K = const, \quad A_0 = const, \quad p_e = const, \quad A\phi = const, \tag{7.10}$$

for the $\lambda_{\mathcal{P}6}$-characteristic field.

Proof. The problem can be solved applying the generalized Riemann invariants method (for example see [90]), i.e for a given hyperbolic system of n unknowns $[w_1, w_2, \ldots, w_n]^T$, for any $\lambda_{\mathcal{P}k}$-characteristic field with right eigenvector $\mathbf{R}_{\mathcal{P}k} = [r_{1,k}, r_{2,k}, \ldots, r_{n,k}]^T$ the generalized Riemann invariants are solutions of the following $n-1$ ordinary differential equations in phase-plane

$$\frac{dw_1}{r_{1,k}} = \frac{dw_2}{r_{2,k}} = \cdots = \frac{dw_n}{r_{n,k}}. \tag{7.11}$$

For the $\lambda_{\mathcal{P}1}$-characteristic field we have

$$\frac{dA}{1} = \frac{dq}{-c} = \frac{dK}{0} = \frac{dA_0}{0} = \frac{dp_e}{0} = \frac{d(A\phi)}{0}, \tag{7.12}$$

i.e. from the first and the second term

$$(-c)dA = dq, \tag{7.13}$$

from which integrating we obtain the statement. From the others

$$K = const, \qquad A_0 = const, \qquad p_e = const, \qquad A\phi = const. \tag{7.14}$$

An analougue proof for the $\lambda_{\mathcal{P}6}$-characteristic field. □

Proposition 7.1.5 (Jump conditions across the stationary contact discontinuities associated with eigenvalues $\lambda_{\mathcal{P}2} = \lambda_{\mathcal{P}3} = \lambda_{\mathcal{P}4} = \lambda_{\mathcal{P}5} = 0$)**.** *Across the four superimposed contact discontinuities the following relations hold*

$$q = Au = const, \qquad \psi + p_e = const. \tag{7.15}$$

Proof. Following the method presented in [81], we consider matrix $\boldsymbol{\mathcal{P}}(\mathbf{Q})$ in (7.2) i.e

$$\boldsymbol{\mathcal{P}}(\mathbf{Q}) = \begin{bmatrix} 0 & 1 & 0 & 0 & 0 & 0 \\ c^2 & 0 & \frac{A}{\rho}\psi_K & \frac{A}{\rho}\psi_{A_0} & \frac{A}{\rho} & 0 \\ 0 & 0 & 0 & 0 & 0 & 0 \\ 0 & 0 & 0 & 0 & 0 & 0 \\ 0 & 0 & 0 & 0 & 0 & 0 \\ 0 & 0 & 0 & 0 & 0 & 0 \end{bmatrix}. \tag{7.16}$$

For an arbitrary eigenvector $\mathbf{R} = [r_1, r_2, r_3, r_4, r_5, r_6]^T$ we have

$$\boldsymbol{\mathcal{P}}\mathbf{R} = \lambda\mathbf{R}, \tag{7.17}$$

which gives the algebraic system

$$\begin{cases} r_2 = \lambda r_1, \\ c^2 r_1 + \frac{A}{\rho}\psi_K r_3 + \frac{A}{\rho}\psi_{A_0} r_4 + \frac{A}{\rho} r_5 = \lambda r_2, \\ 0 = \lambda r_3, \\ 0 = \lambda r_4, \\ 0 = \lambda r_5, \\ 0 = \lambda r_6, \end{cases} \tag{7.18}$$

Putting $\lambda = 0$ in (7.18) we notice that from the first of (7.18) $r_2 = 0$. Posing $r_1 = \beta$, $r_3 = \gamma$, $r_4 = \epsilon$, $r_6 = \delta$, for $\beta, \gamma, \epsilon, \delta \in \mathbb{R}$, arbitrary constants, we obtain

$$\mathbf{R}_0 = \begin{bmatrix} \beta \\ 0 \\ \gamma \\ \epsilon \\ \left[-c^2\beta - \frac{A}{\rho}\psi_K\gamma - \frac{A}{\rho}\psi_{A_0}\epsilon\right]\frac{\rho}{A} \\ \delta \end{bmatrix}. \tag{7.19}$$

This is a general form of a vector belonging to the subspace associated with $\lambda_{\mathcal{P}} = 0$ for every choice of $\beta, \gamma, \epsilon, \delta, \in \mathbb{R}$. We then apply the generalized Riemann invariants method to this vector

$$\frac{dA}{\beta} = \frac{dq}{0} = \frac{dK}{\gamma} = \frac{dA_0}{\epsilon} = \frac{dp_e}{\left[-c^2\beta - \frac{A}{\rho}\psi_K\gamma - \frac{A}{\rho}\psi_{A_0}\epsilon\right]\frac{\rho}{A}} = \frac{d(A\phi)}{\delta}; \tag{7.20}$$

from the second of (7.20) we have

$$q = const, \tag{7.21}$$

from the first and the fifth of (7.20) we have

$$\frac{dA}{\beta} = \frac{dp_e}{\left[-c^2\beta - \frac{A}{\rho}\psi_K\gamma - \frac{A}{\rho}\psi_{A_0}\epsilon\right]\frac{\rho}{A}} \rightarrow -c^2\frac{\rho}{A}dA - \psi_K\frac{\gamma}{\beta}dA - \psi_{A_0}\frac{\epsilon}{\beta}dA = dp_e, \tag{7.22}$$

considering the first and the third of (7.20) coupled together and then the first and the fourth of (7.20), we have that

$$\gamma dA = \beta dK, \quad \epsilon dA = \beta dA_0. \tag{7.23}$$

Being c defined in (2.183), we have

$$-c^2\frac{\rho}{A}dA = -\psi_A dA, \tag{7.24}$$

so (7.22) becomes

$$-\psi_A dA - \psi_K dK - \psi_{A_0} dA_0 - dp_e = 0. \tag{7.25}$$

Considering that

$$d\psi = \psi_A dA + \psi_K dK + \psi_{A_0} dA_0, \tag{7.26}$$

we have that (7.25) becomes

$$-d\psi - dp_e = 0, \tag{7.27}$$

from that, integrating, we obtain the second of (7.15). From the first and the sixth of (7.20) we have

$$\frac{dA}{\beta} = \frac{d(A\phi)}{\delta}, \tag{7.28}$$

that leads to

$$\frac{dA}{A} = \left(\frac{\beta}{\delta - \beta\phi}\right)d\phi. \tag{7.29}$$

Unfortunately β and δ are arbitrary, so from (7.28) and (7.29) the only thing we can say is that

$$A\phi \neq const, \qquad \phi \neq const. \tag{7.30}$$

□

The Riemann problem for system (7.1) is

$$\begin{cases} \partial_t \mathbf{Q} + \boldsymbol{\mathcal{P}}(\mathbf{Q})\partial_x(\mathbf{Q}) = 0, \quad x \in \mathbb{R}, \quad t > 0, \\ \mathbf{Q}(x,0) = \begin{cases} \mathbf{Q}_L, & \text{if} \quad x < x_d, \\ \mathbf{Q}_R & \text{if} \quad x > x_d, \end{cases} \end{cases} \tag{7.31}$$

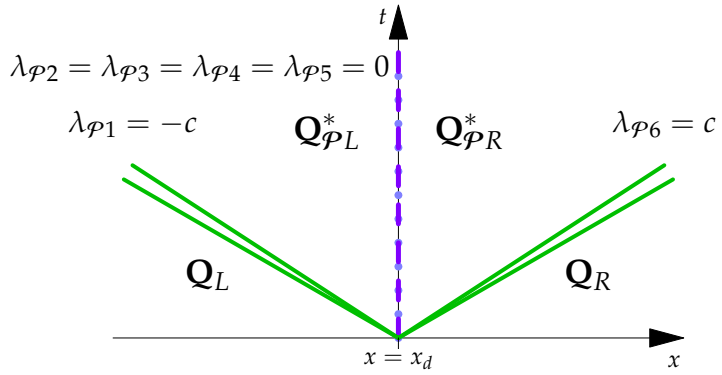

Figure 7.1: The configuration of the exact solution of the Riemann problem for the pressure system (7.31). The green solid lines, in case of arteries, represent waves associated with genuinely non-linear fields, while in case of veins this property is lost. The purple dashed line represents the contact discontinuity for the passive scalar and is associated with a linearly degenerate field, the indigo dotted line represents the three superimposed contact discontinuities for the parameters and is associated with linearly degenerate fields.

where $x_d \in \mathbb{R}$ is the spatial location of the discontinuity at $t = 0$. The initial data are $\mathbf{Q}_L$ and $\mathbf{Q}_R$. The unknowns are $\mathbf{Q}^*_{\mathcal{P}L}$ and $\mathbf{Q}^*_{\mathcal{P}R}$ defined as

$$\mathbf{Q}^*_{\mathcal{P}L} = \begin{bmatrix} A^*_L \\ q^*_L \\ K_L \\ A_{0L} \\ p_{eL} \\ A^*_L \phi^*_L \end{bmatrix}, \qquad \mathbf{Q}^*_{\mathcal{P}R} = \begin{bmatrix} A^*_R \\ q^*_R \\ K_R \\ A_{0R} \\ p_{eR} \\ A^*_R \phi^*_R \end{bmatrix}, \tag{7.32}$$

thanks to Propositions (7.1.4), (7.1.5) explaining that the $\lambda_{\mathcal{P}2} = \lambda_{\mathcal{P}3} = \lambda_{\mathcal{P}4}$-contact discontinuities are the only discontinuities for parameters K, A_0 and p_e that are only space-dependent.

Fig. 7.1 depicts the structure of the exact solution of the Riemann problem (7.31) for the pressure system (7.1): the waves related to the $\lambda_{\mathcal{P}2} = \lambda_{\mathcal{P}3} = \lambda_{\mathcal{P}4} = \lambda_{\mathcal{P}5}$-characteristic fields are associated with linearly degenerate fields and are contact discontinuities, while the waves related to the $\lambda_{\mathcal{P}1}$- and $\lambda_{\mathcal{P}6}$-characteristic fields, in case of arteries, are associated with genuine non-linear fields (Proposition 7.1.2) and can be either shocks (elastic jumps) or rarefactions [80]; in case of veins, the loss of genuine non-linearity can lead to a formation of compound waves [49].

Remark 7.1.1. In is worth noting that for the pressure system, the waves associated with the $\lambda_{\mathcal{P}1}$- and $\lambda_{\mathcal{P}6}$-characteristic fields will always be *subsonic*, since

$$\lambda_{\mathcal{P}1}(\mathbf{Q}) < 0 \quad \text{and} \quad \lambda_{\mathcal{P}6}(\mathbf{Q}) > 0, \quad \text{i.e. } c > 0, \quad \forall \mathbf{Q} \in \Omega. \tag{7.33}$$

Remark 7.1.2. The purpose of this Chapter is not to provide a comprehensive account of the exact solution of the Riemann problem for the pressure system (7.31). A complete analysis of the analogous exact solution for the conservative case was presented in Chapter 5, the related discussion regarding the non-conservative counterpart is in progress. Our assumption, for this research, is that the waves associated with the $\lambda_{\mathcal{P}1}$- and $\lambda_{\mathcal{P}6}$-characteristic fields are always rarefaction waves, while still recognizing the existence of the contact discontinuities associated with the $\lambda_{\mathcal{P}2} = \lambda_{\mathcal{P}3} = \lambda_{\mathcal{P}4} = \lambda_{\mathcal{P}5}$-characteristic fields. This decision is based on the proposed numerical schemes and the complexity of the mathematical analysis of the solution in case of veins, due to the loss of genuine non-linearity of the $\lambda_{\mathcal{P}1}$- and $\lambda_{\mathcal{P}6}$-characteristic fields (Proposition 7.1.2). The current work solely focuses on observing the behavior of the splitting schemes in

scenarios where the genuine non-linearity is lost for the $\lambda_{\mathcal{P}1}$- and $\lambda_{\mathcal{P}6}$-characteristic fields of the pressure system.

7.1.2 Approximate Riemann solvers for the pressure system

Having introduced the relations across the waves (Propositions 7.1.4, 7.1.5), we can introduce two approximate Riemann solvers for the pressure system (7.1). For the purposes of this Thesis, we restrict ourselves to the presentation of the solution in the *Star Region*, that is the region in the (x,t) plane in Fig. 7.1 included between the waves associated with the two nongenuine non-linear fields (i.e., the unknowns $\mathbf{Q}^*_{\mathcal{P}L}$ and $\mathbf{Q}^*_{\mathcal{P}R}$).

7.1.2.1 A two-rarefaction approximate Riemann solver for the pressure system

The two-rarefaction approximate Riemann solver operates under the assumption that the wave associated with the $\lambda_{\mathcal{P}1}$ and $\lambda_{\mathcal{P}5}$-characteristic fields, are rarefaction waves, disregarding the shock waves relations (and also the compound waves relations). The solution in the Star Region in this case is

$$\mathbf{Q}^*_{TR,L} = \begin{bmatrix} A^*_{TR,L} \\ q^*_{TR} \\ K_L \\ A_{0L} \\ p_{eL} \\ A^*_{TR,L}\phi^*_{TR,L} \end{bmatrix}, \qquad \mathbf{Q}^*_{TR,R} = \begin{bmatrix} A^*_{TR,R} \\ q^*_{TR} \\ K_R \\ A_{0R} \\ p_{eR} \\ A^*_{TR,R}\phi^*_{TR,R} \end{bmatrix}. \tag{7.34}$$

To calculate (7.34) we must solve the system of the relations across the waves obtained in Section 7.1.1 (see [90, 81, 82]):

$$\begin{cases} f_1(x_1,x_2) = x_2 - q_L + f_L(x_1) = 0, \\ f_2(x_3,x_4) = x_4 - q_R - f_R(x_3) = 0, \\ f_3(x_2,x_4) = x_2 - x_4 = 0, \\ f_4(x_1,x_3) = K_L\left[\left(\frac{x_1}{A_{0L}}\right)^m - \left(\frac{x_1}{A_{0L}}\right)^n\right] - K_R\left[\left(\frac{x_3}{A_{0R}}\right)^m - \left(\frac{x_3}{A_{0R}}\right)^n\right] + (p_{eL} - p_{eR}) = 0, \end{cases} \tag{7.35}$$

where

$$f_L(x_1) = \int_{A_L}^{x_1} c(\sigma, K_L, A_{0L})d\sigma \quad \text{(left rarefaction)}, \tag{7.36}$$

$$f_R(x_3) = \int_{A_R}^{x_3} c(\sigma, K_R, A_{0R})d\sigma \quad \text{(right rarefaction)}, \tag{7.37}$$

while c is the wave speed (2.183) and

$$\boldsymbol{X} = \begin{bmatrix} x_1 \\ x_2 \\ x_3 \\ x_4 \end{bmatrix} = \begin{bmatrix} A^*_{TR,L} \\ q^*_{TR,L} \\ A^*_{TR,R} \\ q^*_{TR,R}, \end{bmatrix}. \tag{7.38}$$

K_L and K_R are evaluated on data from (2.176). System (7.35) is solved with a globally convergent Newton-Raphson method with initial guesses A_L, q_L, A_R, q_R (see Appendix B.4). Moreover,

integrals in (7.36) and (7.37) in case of veins are calculated with a three-points Gauss quadrature rule, while in case of arteries (with $m = 0.5$ and $n = 0$ in (2.177)) the solution is explicit.

$\phi^*_{TR,L}$ and $\phi^*_{TR,R}$ are calculated from Proposition 7.1.4, i.e.

$$\phi^*_{TR,L} = \frac{A_L}{A^*_{TR,L}}\phi_L, \qquad \phi^*_{TR,R} = \frac{A_R}{A^*_{TR,R}}\phi_R. \tag{7.39}$$

7.1.2.2 A linearized two-rarefaction approximate Riemann solver for the pressure system

We proceed as in the case of the two-rarefaction Riemann solver and additionally approximate the relations (7.36), (7.37). The solution in the Star Region in this case is

$$\mathbf{Q}^*_{LTR,L} = \begin{bmatrix} A^*_{LTR,L} \\ q^*_{LTR} \\ K_L \\ A_{0L} \\ p_{eL} \\ A^*_{LTR,L}\phi^*_{LTR,L} \end{bmatrix}, \qquad \mathbf{Q}^*_{LTR,R} = \begin{bmatrix} A^*_{LTR,R} \\ q^*_{LTR} \\ K_R \\ A_{0R} \\ p_{eR} \\ A^*_{LTR,R}\phi^*_{LTR,R} \end{bmatrix}. \tag{7.40}$$

To obtain (7.40) we must solve

$$\begin{cases} f_1(x_1, x_2) = x_2 - q_L + f_L(x_1) = 0, \\ f_2(x_3, x_4) = x_4 - q_R - f_R(x_3) = 0, \\ f_3(x_2, x_4) = x_2 - x_4 = 0, \\ f_4(x_1, x_3) = K_L\left[\left(\frac{x_1}{A_{0L}}\right)^m - \left(\frac{x_1}{A_{0L}}\right)^n\right] - K_R\left[\left(\frac{x_3}{A_{0R}}\right)^m - \left(\frac{x_3}{A_{0R}}\right)^n\right] + (p_{eL} - p_{eR}) = 0, \end{cases} \tag{7.41}$$

where we approximate (7.36), (7.37) with

$$f_L(x_1) = \int_{A_L}^{x_1} c(\sigma, K_L, A_{0L})d\sigma \approx c_L(x_1 - A_L) \quad \text{(left rarefaction)}, \tag{7.42}$$

$$f_R(x_3) = \int_{A_R}^{x_3} c(\sigma, K_R, A_{0R})d\sigma \approx c_R(x_3 - A_R) \quad \text{(right rarefaction)}, \tag{7.43}$$

while $c_L = c(A_L, K_L, A_{0L})$ and $c_R = c(A_R, K_R, A_{0R})$ are the wave speeds (2.183) and

$$\boldsymbol{X} = \begin{bmatrix} x_1 \\ x_2 \\ x_3 \\ x_4 \end{bmatrix} = \begin{bmatrix} A^*_{LTR,L} \\ q^*_{LTR,L} \\ A^*_{LTR,R} \\ q^*_{LTR,R}, \end{bmatrix}. \tag{7.44}$$

K_L and K_R are evaluated on the data from (2.176). System (7.41) reduces to

$$\begin{cases} f_5(x_1, x_3) = -q_L + c_L(x_1 - A_L) + q_R + c_R(x_3 - A_R) = 0, \\ f_4(x_1, x_3) = K_L\left[\left(\frac{x_1}{A_{0L}}\right)^m - \left(\frac{x_1}{A_{0L}}\right)^n\right] - K_R\left[\left(\frac{x_3}{A_{0R}}\right)^m - \left(\frac{x_3}{A_{0R}}\right)^n\right] + (p_{eL} - p_{eR}) = 0, \end{cases} \tag{7.45}$$

from the first of (7.45) we obtain

$$x_1 = \frac{q_L - q_R - c_R x_3 + c_R A_R + c_L A_L}{c_L}, \tag{7.46}$$

so the second becomes

$$f_4(x_3) = K_L \left[\left(\frac{q_L - q_R - c_R x_3 + c_R A_R + c_L A_L}{c_L A_{0L}} \right)^m - \left(\frac{q_L - q_R - c_R x_3 + c_R A_R + c_L A_L}{c_L A_{0L}} \right)^n \right] - \\ - K_R \left[\left(\frac{x_3}{A_{0R}} \right)^m - \left(\frac{x_3}{A_{0R}} \right)^n \right] + (p_{eL} - p_{eR}) = 0, \tag{7.47}$$

(7.47) is solved with a globally convergent Newton-Raphson method of initial point A_R. Having found $x_3 = A^*_{LTR,R}$ from (7.47), we calculate $x_1 = A^*_{LTR,L}$ from (7.46) and after that, we calculate $x_2 = x_4 = q^*_{LTR,L} = q^*_{LTR,R}$ from the first or the second of (7.41).

$\phi^*_{LTR,L}$ and $\phi^*_{LTR,R}$ are calculated from Proposition 7.1.4, i.e.

$$\phi^*_{LTR,L} = \frac{A_L}{A^*_{LTR,L}} \phi_L, \qquad \phi^*_{LTR,R} = \frac{A_R}{A^*_{LTR,R}} \phi_R. \tag{7.48}$$

7.2 Advection-pressure numerical splitting schemes for the complete non-conservative 1D blood flow model with transport

To solve numerically system (7.1), we employ a path-conservative method [64]

$$\mathbf{Q}_i^{n+1} = \mathbf{Q}_i^n - \frac{\Delta t}{\Delta x} (\mathbf{D}^+_{i-\frac{1}{2}} + \mathbf{D}^-_{i+\frac{1}{2}}), \tag{7.49}$$

where

$$\mathbf{Q}_i^n \approx \frac{1}{\Delta x} \int_{x_{i-\frac{1}{2}}}^{x_{i+\frac{1}{2}}} \mathbf{Q}(x, t^n) dx, \tag{7.50}$$

with $\Delta x = x_{i+\frac{1}{2}} - x_{i-\frac{1}{2}}$, $\Delta t = t^{n+1} - t^n$. The aim is to compute the fluctuations

$$\mathbf{D}^{\pm}_{i+\frac{1}{2}} = \mathcal{A}^{\pm}_{i+\frac{1}{2}} + \mathcal{P}^{\pm}_{i+\frac{1}{2}}, \tag{7.51}$$

where $\mathcal{A}^{\pm}_{i+\frac{1}{2}}$ are the fluctuations related to the advection system and $\mathcal{P}^{\pm}_{i+\frac{1}{2}}$ are the fluctuations related to the pressure system. From [64, 23], we know that in case of a conservative system, we have

$$\mathbf{D}^+_{i-\frac{1}{2}} = \mathbf{F}(\mathbf{Q}^+_{i-\frac{1}{2}}) - \mathbf{F}_{i-\frac{1}{2}}, \qquad \mathbf{D}^-_{i+\frac{1}{2}} = \mathbf{F}_{i+\frac{1}{2}} - \mathbf{F}(\mathbf{Q}^-_{i+\frac{1}{2}}), \tag{7.52}$$

where $\mathbf{F}$ is the physical conservative flux and $\mathbf{F}_{i+\frac{1}{2}}$ is the numerical conservative flux of the model.

For a first order method, regarding the pressure system, (7.52) is adapted into

$$\mathcal{P}^+_{i-\frac{1}{2}} = \mathbf{F}_{\mathcal{P}}(\mathbf{Q}_i) - \mathbf{F}_{\mathcal{P}}(\mathbf{Q}^*_{\text{Press}R,i-\frac{1}{2}}), \qquad \mathcal{P}^-_{i+\frac{1}{2}} = \mathbf{F}_{\mathcal{P}}(\mathbf{Q}^*_{\text{Press}L,i+\frac{1}{2}}) - \mathbf{F}_{\mathcal{P}}(\mathbf{Q}_i), \tag{7.53}$$

where $\mathbf{F}_{\mathcal{P}}(\mathbf{Q})$ is the physical conservative flux of the pressure system, found acting as if system (7.1) could be written in conservative form (i.e. if it had constant parameters), i.e.

$$\mathbf{F}_{\mathcal{P}}(\mathbf{Q}) = \begin{bmatrix} Au \\ \int c(A)^2\, dA \\ 0 \\ 0 \\ 0 \\ 0 \end{bmatrix} = \begin{bmatrix} Au \\ \frac{KA}{\rho}\left(\frac{m}{m+1}\left(\frac{A}{A_0}\right)^m - \frac{n}{n+1}\left(\frac{A}{A_0}\right)^n\right) \\ 0 \\ 0 \\ 0 \\ 0 \end{bmatrix}, \tag{7.54}$$

and

$$\mathbf{Q}^*_{\text{PRESS}L,i+\frac{1}{2}} = \begin{bmatrix} A^*_{\text{PRESS}L,i+\frac{1}{2}} \\ q^*_{\text{PRESS}L,i+\frac{1}{2}} \\ K_{L,i+\frac{1}{2}} \\ A_{0L,i+\frac{1}{2}} \\ p_{eL,i+\frac{1}{2}} \\ A^*_{\text{PRESS}L,i+\frac{1}{2}}\phi^*_{\text{PRESS}L,i+\frac{1}{2}} \end{bmatrix}, \qquad \mathbf{Q}^*_{\text{PRESS}R,i+\frac{1}{2}} = \begin{bmatrix} A^*_{\text{PRESS}R,i+\frac{1}{2}} \\ q^*_{\text{PRESS}R,i+\frac{1}{2}} \\ K_{R,i+\frac{1}{2}} \\ A_{0R,i+\frac{1}{2}} \\ p_{eR,i+\frac{1}{2}} \\ A^*_{\text{PRESS}R,i+\frac{1}{2}}\phi^*_{\text{PRESS}R,i+\frac{1}{2}} \end{bmatrix}, \tag{7.55}$$

are the solutions in the Star Region of the Riemann problem for the pressure system

$$\begin{cases} \partial_t \mathbf{Q} + \boldsymbol{\mathcal{P}}(\mathbf{Q})\partial_x \mathbf{Q} = 0, \quad x \in \mathbb{R}, \quad t > t^n, \\ \mathbf{Q}(x, t^n) = \begin{cases} \mathbf{Q}_L = \mathbf{Q}^n_i \quad \text{if} \quad x < x_{i+\frac{1}{2}}, \\ \mathbf{Q}_R = \mathbf{Q}^n_{i+1} \quad \text{if} \quad x > x_{i+\frac{1}{2}}, \end{cases} \end{cases} \tag{7.56}$$

for each cell i, with $\boldsymbol{\mathcal{P}}(\mathbf{Q})$ defined in (7.2). The motivation for (7.53) is straightforward: the pressure system can be written in conservative form if the parameters K, A_0 and p_e are actually constants, i.e. the unknowns of the system are only A, Au and $A\phi$. We can notice that for each cell i, $\mathbf{Q}_i$, $\mathbf{Q}^*_{\text{PRESS}L,i+\frac{1}{2}}$ and $\mathbf{Q}^*_{\text{PRESS}R,i-\frac{1}{2}}$ share the same values of the parameters K, A_0 and p_e, thus the pressure system (7.1) is locally conservative. The motivation for (7.54) is indeed thus clear: in case of conservative 1D blood flow, and consequently a conservative pressure system (Chapters 3.1, 5, 6), the pressure term of the second equation in (7.1) becomes

$$\frac{A}{\rho}\partial_x p = \frac{A}{\rho}\frac{\partial p}{\partial A}\partial_x A = c(A)^2\partial_x A = \partial_x \int c(A)^2 dA, \tag{7.57}$$

being c the wave speed in (2.183).

Similarly, for the advection system, for a first order method, (7.52) is adapted into

$$\boldsymbol{\mathcal{A}}^+_{i-\frac{1}{2}} = \mathbf{F}_{\boldsymbol{\mathcal{A}}}(\mathbf{Q}_i) - \boldsymbol{\mathcal{A}}_{i-\frac{1}{2}}, \qquad \boldsymbol{\mathcal{A}}^-_{i+\frac{1}{2}} = \boldsymbol{\mathcal{A}}_{i+\frac{1}{2}} - \mathbf{F}_{\boldsymbol{\mathcal{A}}}(\mathbf{Q}_i). \tag{7.58}$$

It is worth noting that the advection system (3.9) is actually conservative, i.e it can be written as

$$\partial_t \mathbf{Q} + \partial_x \mathbf{F}_{\boldsymbol{\mathcal{A}}}(\mathbf{Q}) = 0, \tag{7.59}$$

with the physical flux

$$\mathbf{F}_{\mathcal{A}}(\mathbf{Q}) = \begin{bmatrix} 0 \\ \alpha A u^2 \\ 0 \\ 0 \\ 0 \\ Au\phi \end{bmatrix}. \tag{7.60}$$

The numerical flux $\mathcal{A}_{i+\frac{1}{2}}$ is a modification of the TV-advection flux defined in Chapter 6 for the conservative blood flow model and is defined as

$$\mathcal{A}_{i+\frac{1}{2}} = \begin{bmatrix} 0 \\ \alpha q^*_{\text{Press},i+\frac{1}{2}} u_{i+\frac{1}{2}} \\ 0 \\ 0 \\ 0 \\ q^*_{\text{Press},i+\frac{1}{2}} \phi_{i+\frac{1}{2}} \end{bmatrix}, \tag{7.61}$$

where, recalling Proposition 7.1.5

$$q^*_{\text{Press},i+\frac{1}{2}} = q^*_{\text{Press}L,i+\frac{1}{2}} = q^*_{\text{Press}R,i+\frac{1}{2}}. \tag{7.62}$$

It is worth noting that although the advection system is conservative, and thus the Godunov state calculated at $x_{i+\frac{1}{2}}$, for each cell i, does exist, in our case we are using the solution of the Riemann problem for the pressure system, this latter lacking this particular state; thus (7.62) is defined *by continuity* (Proposition 7.1.5). Also $u_{i+\frac{1}{2}}$ and $\phi_{i+\frac{1}{2}}$ are defined by approximation. The ones that yield the best results are

$$u_{i+\frac{1}{2}} = \begin{cases} u_L & \text{if} \quad q^*_{\text{Press},i+\frac{1}{2}} > 0 \quad \text{and} \quad \begin{cases} K_{L,i+\frac{1}{2}} = K_{R,i+\frac{1}{2}}, \\ A_{0L,i+\frac{1}{2}} = A_{0R,i+\frac{1}{2}}, \\ p_{eL,i+\frac{1}{2}} = p_{eR,i+\frac{1}{2}}, \end{cases} \\ u_R & \text{if} \quad q^*_{\text{Press},i+\frac{1}{2}} \leq 0 \quad \text{and} \quad \begin{cases} K_{L,i+\frac{1}{2}} = K_{R,i+\frac{1}{2}}, \\ A_{0L,i+\frac{1}{2}} = A_{0R,i+\frac{1}{2}}, \\ p_{eL,i+\frac{1}{2}} = p_{eR,i+\frac{1}{2}}, \end{cases} \\ \dfrac{u^*_{\text{Press}L,i+\frac{1}{2}} + u^*_{\text{Press}R,i+\frac{1}{2}}}{2} & \text{if} \quad \begin{cases} K_{L,i+\frac{1}{2}} \neq K_{R,i+\frac{1}{2}}, \\ A_{0L,i+\frac{1}{2}} \neq A_{0R,i+\frac{1}{2}}, \\ p_{eL,i+\frac{1}{2}} \neq p_{eR,i+\frac{1}{2}}, \end{cases} \end{cases} \tag{7.63}$$

$$\phi_{i+\frac{1}{2}} = \begin{cases} \phi_L & \text{if} \quad q^*_{\text{Press},i+\frac{1}{2}} > 0, \\ \phi_R & \text{if} \quad q^*_{\text{Press},i+\frac{1}{2}} \leq 0. \end{cases} \tag{7.64}$$

Finally scheme (7.49) results

$$\mathbf{Q}_i^{n+1} = \mathbf{Q}_i^n - \frac{\Delta t}{\Delta x}(\mathcal{A}^+_{i-\frac{1}{2}} + \mathcal{A}^-_{i+\frac{1}{2}}) - \frac{\Delta t}{\Delta x}(\mathcal{P}^+_{i-\frac{1}{2}} + \mathcal{P}^-_{i+\frac{1}{2}}), \tag{7.65}$$

that with some calculations becomes

$$\begin{aligned}\mathbf{Q}_i^{n+1} =& \mathbf{Q}_i^n - \frac{\Delta t}{\Delta x}(\mathbf{F}_{\mathcal{A}}(\mathbf{Q}_i) - \mathcal{A}_{i-\frac{1}{2}} + \mathcal{A}_{i+\frac{1}{2}} - \mathbf{F}_{\mathcal{A}}(\mathbf{Q}_i)) - \\ & \frac{\Delta t}{\Delta x}(\mathbf{F}_{\mathcal{P}}(\mathbf{Q}_i) - \mathbf{F}_{\mathcal{P}}(\mathbf{Q}^*_{\text{PRESS}R,i-\frac{1}{2}}) + \mathbf{F}_{\mathcal{P}}(\mathbf{Q}^*_{\text{PRESS}L,i+\frac{1}{2}}) - \mathbf{F}_{\mathcal{P}}(\mathbf{Q}_i)),\end{aligned} \tag{7.66}$$

that reduces to

$$\mathbf{Q}_i^{n+1} = \mathbf{Q}_i^n - \frac{\Delta t}{\Delta x}(\mathcal{A}_{i+\frac{1}{2}} - \mathcal{A}_{i-\frac{1}{2}}) - \frac{\Delta t}{\Delta x}(\mathbf{F}_{\mathcal{P}}(\mathbf{Q}^*_{\text{PRESS}L,i+\frac{1}{2}}) - \mathbf{F}_{\mathcal{P}}(\mathbf{Q}^*_{\text{PRESS}R,i-\frac{1}{2}})). \tag{7.67}$$

Considering (7.67) we present two possibilities for $\mathbf{Q}^*_{\text{PRESS}J,i+\frac{1}{2}}$, $J = L, R$; that consequently lead to two different final numerical schemes

1. (TVM+TR) in which $\mathbf{Q}^*_{\text{PRESS}L,i+\frac{1}{2}} = \mathbf{Q}^*_{TR,L,i+\frac{1}{2}}$ and $\mathbf{Q}^*_{\text{PRESS}R,i+\frac{1}{2}} = \mathbf{Q}^*_{TR,R,i+\frac{1}{2}}$, the approximate two rarefaction solution of the Riemann problem for the pressure system (7.31) in the Star Region presented in Section 7.1.2.1, for each cell i,
2. (TVM+Lin.TR) in which $\mathbf{Q}^*_{\text{PRESS}L,i+\frac{1}{2}} = \mathbf{Q}^*_{LTR,L,i+\frac{1}{2}}$ and $\mathbf{Q}^*_{\text{PRESS}R,i+\frac{1}{2}} = \mathbf{Q}_{LTR,R,i+\frac{1}{2}}$, the approximate linearized two rarefaction solution of the Riemann problem for the pressure system (7.31) in the Star Region presented in Section 7.1.2.2, for each cell i,

where TVM stands for *Toro-Vázquez Modified*.

Method (7.67) circumvents the necessity to use any path, reducing effectively the computational cost as it will be shown in Section 7.3.

7.3 NUMERICAL RESULTS

Within this section, we present test problems and evaluate the effectiveness of the numerical splitting methods of type TV introduced in this Chapter. We propose seven test problems; these tests have been chosen to represent the different admissible solutions of the 1D blood flow equations in the case of arteries (Tests 1, 2, 3) and veins (Tests 4, 5, 6, 7), namely smooth solutions (rarefactions), elastic jumps (shocks), and contact discontinuities. The contact discontinuity, out of the three waves, typically proves to be the most challenging. This is particularly true for linearized or incomplete solvers, as they encounter excessive numerical diffusion resulting in the smearing of the contact discontinuity. The two new methods will prove to be able to depict also these waves.

Tests are constructed to provide an explanation of the necessity to modify the TV-advection flux already presented in Chapter 6 for the conservative 1D blood flow, to handle non-conservative systems. Recalling the original TV-advection flux

$$\boldsymbol{A}_{TV,i+\frac{1}{2}} = \begin{bmatrix} 0 \\ \alpha q^*_{\text{PRESS},i+\frac{1}{2}} u_{TV,i+\frac{1}{2}} \\ 0 \\ 0 \\ 0 \\ q^*_{\text{PRESS},i+\frac{1}{2}} \phi_{i+\frac{1}{2}} \end{bmatrix}, \tag{7.68}$$

where

$$u_{TV,i+\frac{1}{2}} = \begin{cases} u_L & \text{if} \quad q^*_{\text{PRESS},i+\frac{1}{2}} > 0, \\ u_R & \text{if} \quad q^*_{\text{PRESS},i+\frac{1}{2}} \leq 0, \end{cases} \tag{7.69}$$

Table 7.1: Left and right initial conditions for Tests from 1 to 7. The units of measures used for this Thesis are: m, s, kg, Pa.

	Test	$A_L[m^2]$	$u_L[m/s]$	$K_L[Pa]$	$A_{0L}[m^2]$	$p_{eL}[Pa]$	ϕ_L
Left data	1	$1.0228A_{0L}$	0.0	K_{ref}	$2.0A_{0,ref}$	9999.15	1.0
	2	$1.6A_{0L}$	1.0	K_{ref}	$0.5A_{0,ref}$	3999.66	1.0
	3	$1.1A_{0L}$	1.0	K_{ref}	$0.5A_{0,ref}$	3999.66	0.5
	4	$1.8 \cdot 10^{-5}$	0.5	K_{ref}	$A_{0,ref}$	60.0	0.5
	5	A_{0L}	0.1	$60.0K_{ref}$	$A_{0,ref}$	100.0	0.5
	6	$1.3 \cdot 10^{-5}$	0.0	K_{ref}	$1.5A_{0,ref}$	40.0	0.5
	7	$1.5 \cdot 10^{-5}$	-0.3	$8.0K_{ref}$	$A_{0,ref}$	0.0	0.5
	Test	$A_R[m^2]$	$u_R[m/s]$	$K_R[Pa]$	$A_{0R}[m^2]$	$p_{eR}[Pa]$	ϕ_R
Right data	1	$0.9977A_{0R}$	0.0	$10.0K_{ref}$	$A_{0,ref}$	11340.56820743433	0.5
	2	$1.05A_{0R}$	0.0	$10.0K_{ref}$	$A_{0,ref}$	0.0	0.5
	3	$0.7A_{0R}$	-0.5	$10.0K_{ref}$	$0.2A_{0,ref}$	0.0	1.0
	4	$1.8 \cdot 10^{-5}$	-0.2	$0.7K_{ref}$	$1.2A_{0,ref}$	10.0	1.0
	5	A_{0R}	0.2	K_{ref}	$1.1A_{0,ref}$	60.0	1.0
	6	$1.9 \cdot 10^{-5}$	0.0	$10.0K_{ref}$	$A_{0,ref}$	0.0	1.0
	7	$2.0 \cdot 10^{-5}$	0.6	K_{ref}	$1.5A_{0,ref}$	10.0	1.0

Table 7.2: Parameters used for Tests 1 to 7: blood density ρ; reference vessel wall stiffness K_{ref}; reference cross-sectional area $A_{0,ref}$; domain length ℓ; location of the initial discontinuity x_d and output time t_{End}. Regarding the resulting wave pattern, *R=rarefaction*, *S=shock*, C_u=*contact discontinuity associated with* $\lambda = u$, C_0=*contact discontinuity associated with* $\lambda = 0$.

Test	Vessel	Wave pattern	$\rho[kg/m^3]$	$K_{ref}[Pa]$	$A_{0,ref}[m^2]$	$\ell[m]$	$x_d[m]$	$t_{End}[s]$
1	Artery	Stationary	1000.0	58725.0	$3.1353 \cdot 10^{-4}$	0.2	0.5ℓ	0.007
2	Artery	SC_0C_uS	1000.0	58725.0	$3.1353 \cdot 10^{-4}$	0.2	0.3ℓ	0.007
3	Artery	RC_0C_uS	1050.0	50000.0	$3.1353 \cdot 10^{-4}$	0.2	0.3ℓ	0.007
4	Vein	SC_0C_uS	1050.0	300.0	$2.8274 \cdot 10^{-5}$	0.5	0.5ℓ	0.2
5	Vein	RC_0C_uR	1000.0	33.0	$2.8274 \cdot 10^{-5}$	1.1	0.75ℓ	0.11
6	Vein	RC_0C_uS	1050.0	30.0	$2.8274 \cdot 10^{-5}$	0.5	0.4ℓ	0.25
7	Vein	SC_uC_0R	1050.0	300.0	$2.8274 \cdot 10^{-5}$	0.8	0.6ℓ	0.12

while $\phi_{i+\frac{1}{2}}$ is as in (7.64). This option has been discarded due to its lack of accuracy in the results of certain tests as it will be shown in the next Sections. In addition, in case of veins, the tests are designed to explore different placements of A_{cL} and A_{cR} in (7.7) with respect to the range depicted by the test results. These values are of crucial importance in determining the wave pattern of the pressure system, however, it is worth noting that this specific matter will not be addressed in this Thesis (for the related issue in the conservative case, see Chapter 5), instead, the focus is on demonstrating the effectiveness of the presented schemes, even in cases where the genuine non-linearity of the $\lambda_{\mathcal{P}1}$- and $\lambda_{\mathcal{P}6}$-characteristic fields of the pressure system is lost.

The numerical results of methods 1 and 2 are compared with the exact solution of the Riemann problem for the full non-conservative 1D blood flow equations and some classic methods in literature. The initial data, expressed in terms of the physical variables A, u, and ϕ, can be found in Table 7.1. Meanwhile, the model parameters are provided in Table 7.2. The discussion of the numerical results is covered in Section 7.3.1, while an efficiency test is performed in Section 7.3.2.

7.3.1 Results discussion

Numerical results for both methods 1 and 2 are shown and plotted against the exact solution of the Riemann problem for the full 1D blood flow equations (Chapter 2.2) and the results of the following numerical methods

1. DOT+WB: the well-balanced version of DOT solver that combines the DOT solver for the full system presented in [23] with the path described in [56], modified for a generic momentum correction coefficient (see Appendix A.5) for a detailed presentation);

2. TV+PMG+TR: combines the TV-splitting at the level of PDE presented in this Chapter, the Parés-Muñoz-Godunov scheme [66] applied to the pressure system and described in Appendix A.4, in conjunction with the approximate two-rarefaction Riemann solver for the pressure system described in Section 7.1.2.1, and the original TV-advection flux (7.68). This scheme is a generalization of the TV+PMG+Ex.RS scheme depicted in [91] for non conservative systems: in fact this latter is presented for a single discontinuous parameter without transport added and includes an exact Riemann solver for the pressure system, considered only for the case of arteries. We extend the method to three discontinuous parameters and a passive scalar transport equation added, using the original TV-advection flux reported in (7.68) and substituting the exact Riemann solver with the approximate two-rarefaction one. This latter choice is necessary as we extend the discussion to veins, being the exact solution of the Riemann problem for the pressure system in case of veins not trivial, due to the loss of genuine non-linearity.

All results are finally proposed for two different values of the momentum correction coefficient α in (2.3), i.e. $\alpha = 1$ corresponding to a flat velocity profile, regards an inviscid fluid and $\alpha = 4/3$ that concerns a parabolic velocity profile; and are calculated with a mesh of $I = 50$ computational cells (Figs. 7.2, 7.3, 7.4,7.5, 7.6, 7.7, 7.8) and a Courant–Friedrichs–Lewy number $C_{cfl} = 0.9$ defined as follows

Definition 7.3.1.

$$C_{cfl} = \frac{\Delta t}{\Delta x} S^n_{max}, \tag{7.70}$$

where

$$S^n_{max} = max_i \left\{ max_k \left| \lambda^n_{k,i} \right| \right\}, \quad k = 1, ...N, \quad i = 1, ..., I; \tag{7.71}$$

with $\lambda^n_{k,i}$ the k-th eigenvalue of the complete system (2.180) evaluated in cell i at time t^n, and N is the number of eigenvalues of the considered system.

Test 1 (Artery): Stationary The solution of Test 1 consists of a stationary solution. The results of the two new splitting method proposed in this Chapter perfectly describe the type of problem and in particular the contact discontinuity for the passive scalar is flawlessly portrayed as shown in Fig. 7.2.

Test 2 (Artery): SC_0C_uS The solution of Test 2 contains a left shock, a middle stationary contact discontinuity associated with the eigenvalue $\lambda = 0$, a contact discontinuity associated with the eigenvalue $\lambda = u$ and a right shock (SC_0C_uS). This test does not present any particular trouble, and all the three methods give similar outcomes. We can appreciate monotone shocks, i.e. there are no spurious oscillantions in the vicinity of shocks and also the contact discontinuity for the passive scalar presents a minimal smearing and its speed of propagation is correct (Fig. 7.3).

Test 3 (Artery): RC_0C_uS The solution of Test 3 shows a left rarefaction, a middle stationary contact discontinuity associated with the eigenvalue $\lambda = 0$, a contact discontinuity associated with the eigenvalue $\lambda = u$ and a right shock (RC_0C_uS). The TVM-methods and the DOT+PM one result to be more accurate than the TV+PMG+TR scheme on reaching the exact value of the solution in the Star Region regarding variables A and u. On the contrary the computation of the passive scalar ϕ is unchanged in all the three TV-type methods, presents a little diffusion but is analogous to that of DOT+WB method (Fig. 7.4).

Test 4 (Vein): SC_0C_uS The Test 4 scenario features a left shock, a middle stationary contact discontinuity associated with the eigenvalue $\lambda = 0$, a contact discontinuity associated with the eigenvalue $\lambda = u$ and a right shock (SC_0C_uS). The test was formulated and designed in order to evaluate the effectiveness of the TVM-methods when A_{cL} and A_{cR} in (7.7) are located *inside* the range depicted by the test results. Reported results suggest that the TVM-methods are not affected by the loss of genuine non-linearity that occurs for the pressure system, with minimal diffusion in the approximation of the contact discontinuity for the passive scalar (Fig. 7.5).

Test 5 (Vein): RC_0C_uR The solution of Test 5 consists of a left rarefaction, a middle stationary contact discontinuity associated with the eigenvalue $\lambda = 0$, a contact discontinuity associated with the eigenvalue $\lambda = u$ and a right rarefaction (RC_0C_uR). In this case A_{cL} and A_{cR} in (7.7) are located *below* the range depicted by the test results. Reported results suggest that the TVM-methods act in an appropriate manner also for this particular position of the critical area values. Finally the contact discontinuity for the passive scalar is depicted with minimal diffusion. (Fig. 7.6).

Test 6 (Vein): RC_0C_uS The solution of Test 6 contains a left rarefaction, a middle stationary contact discontinuity associated with the eigenvalue $\lambda = 0$, a contact discontinuity associated with the eigenvalue $\lambda = u$ and a right shock (RC_0C_uS). The TVM-methods prove to be more accurate than the TV+PMG+TR and also DOT+WB method fails on reaching the exact value of the solution in the Star Region regarding variables A and u. On the contrary the computation of the passive scalar ϕ is unchanged in all the three TV-type methods. In this test A_{cL} is located *above* the test results and A_{cR} is located *inside* the results range depicted by the right wave (Fig. 7.7).

Test 7 (Vein): SC_uC_0R The solution of Test 6 shows a left shock, a middle stationary contact discontinuity associated with the eigenvalue $\lambda = u$, a contact discontinuity associated with the eigenvalue $\lambda = 0$ and a right rarefaction (SC_uC_0R). Similarly to Test 6, we face a lack of accuracy of the TV+PMG+TR method and the DOT+WB one with respect to the TVM-schemes. As usual the computation of the passive scalar ϕ is comparable and presents a little diffusion. In this test A_{cL} and A_{cR} in (7.7) are located *above* the test results (Fig. 7.8).

Remark 7.3.1. It is worth noting that although the flow rate q is costant across the initial discontinuity of the parameters as described in Propositions 2.2.4, 2.2.6 in some cases (in this Chapter in Tests 3, 6, 7) the numerical schemes 1, 2 can present a jump describing this variable, while facing the initial discontinuity x_d of the parameters. This issue is due to the particular approximation of the advection flux. In other words considering only the pressure system approximation in scheme (7.67), the final numerical scheme does not present any jump.

7.3.2 Efficiency: error against CPU time

Efficiency is determined by the CPU time required by a method to provide a numerical solution with a specified error E. In order to evaluate the efficiency of the TVM-methods 1 and 2 discussed in this research, we compare their results to those obtained from well-known numerical methods in literature. We consider the DOT+WB solver already treated, the TV+PMG+TR solver discussed in Section 7.3.1, and the TV+TR solver constructed applying the original TV-advection flux in (7.68) to the numerical method presented in (7.67). This choice is made to prove that the increase of accuracy of the TVM-methods here presented is actually due to the modification applied to the original TV-advection flux in (7.68) that leads to the TVM-advection flux in (7.61). Here we

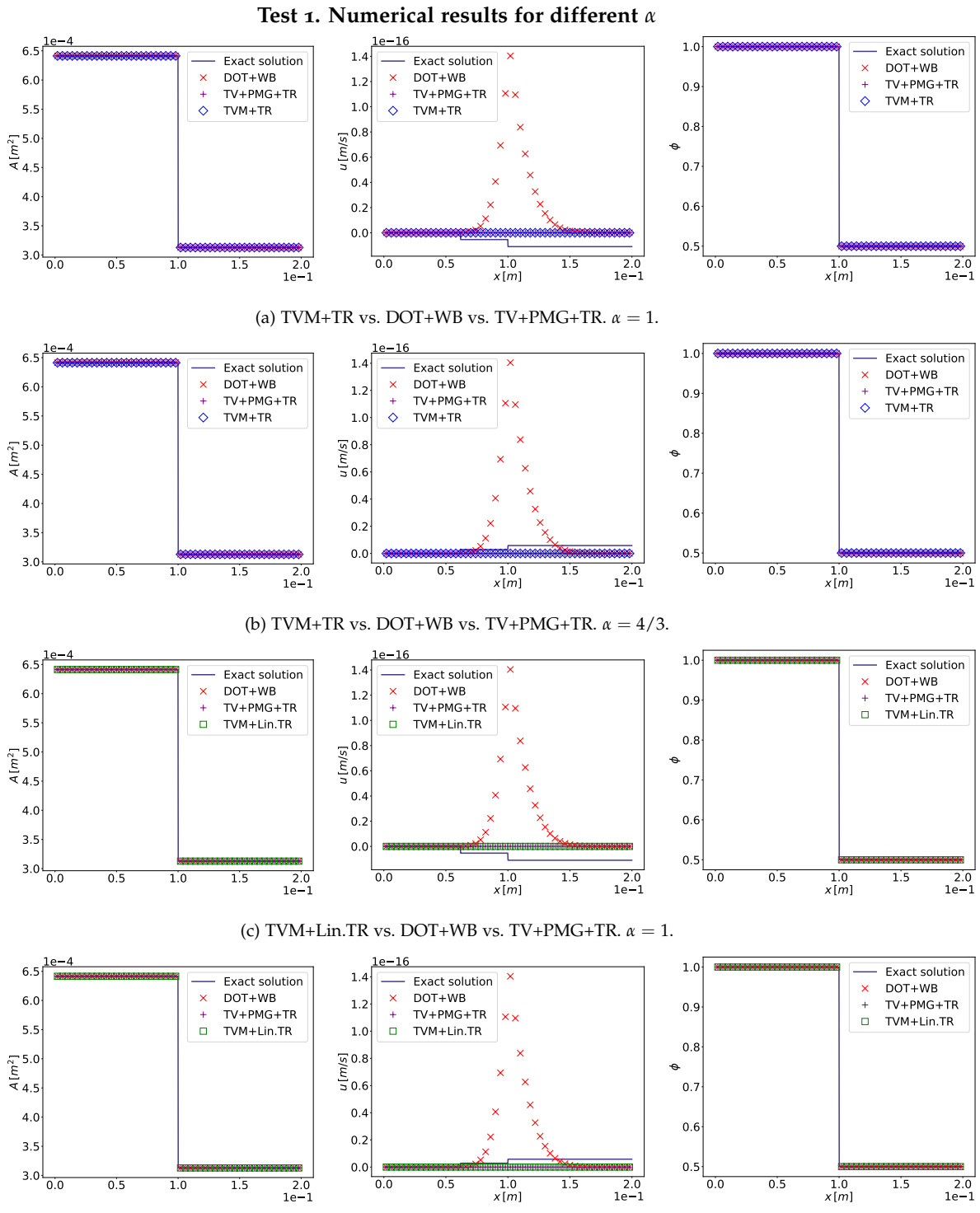

(a) TVM+TR vs. DOT+WB vs. TV+PMG+TR. $\alpha = 1$.

(b) TVM+TR vs. DOT+WB vs. TV+PMG+TR. $\alpha = 4/3$.

(c) TVM+Lin.TR vs. DOT+WB vs. TV+PMG+TR. $\alpha = 1$.

(d) TVM+Lin.TR vs. DOT+WB vs. TV+PMG+TR. $\alpha = 4/3$.

Figure 7.2: Test 1. Artery. Stationary. Numerical results of methods 1, 2 vs. the DOT+WB solver, the TV+PMG+TR solver with $C_{cfl} = 0.9$, $I = 50$ cells, and the exact solution of the Riemann problem for the complete 1D non-conservative blood flow equations with momentum correction coefficient $\alpha = 1, 4/3$. Initial conditions and parameters are given in Tables 7.1, 7.2.

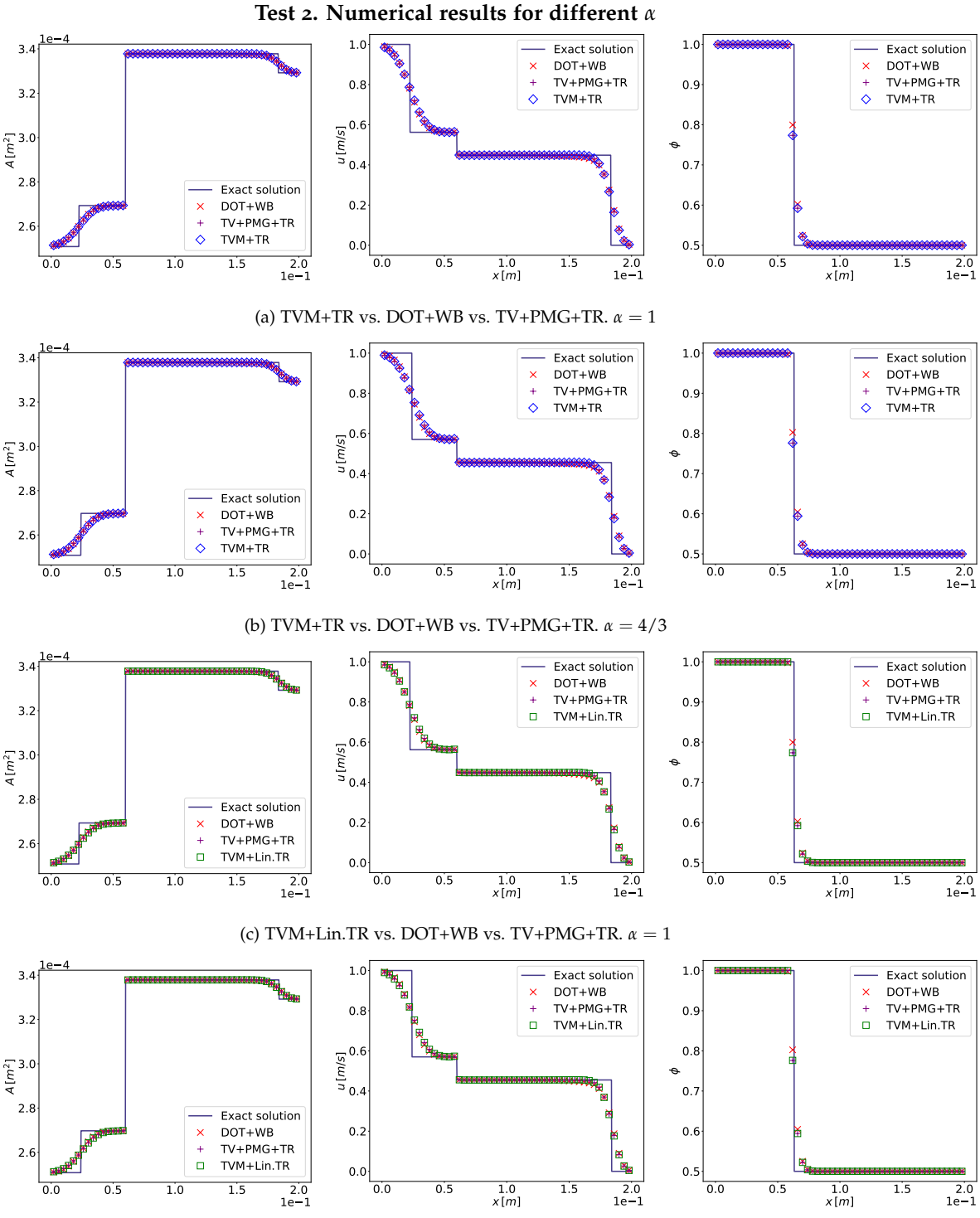

(a) TVM+TR vs. DOT+WB vs. TV+PMG+TR. $\alpha = 1$

(b) TVM+TR vs. DOT+WB vs. TV+PMG+TR. $\alpha = 4/3$

(c) TVM+Lin.TR vs. DOT+WB vs. TV+PMG+TR. $\alpha = 1$

(d) TVM+Lin.TR vs. DOT+WB vs. TV+PMG+TR. $\alpha = 4/3$

Figure 7.3: Test 2. Artery. SC_0C_uS. Numerical results of methods 1, 2 vs. the DOT+WB solver, the TV+PMG+TR solver with $C_{cfl} = 0.9$, $I = 50$ cells, and the exact solution of the Riemann problem for the complete 1D non-conservative blood flow equations with momentum correction coefficient $\alpha = 1, 4/3$. Initial conditions and parameters are given in Tables 7.1, 7.2.

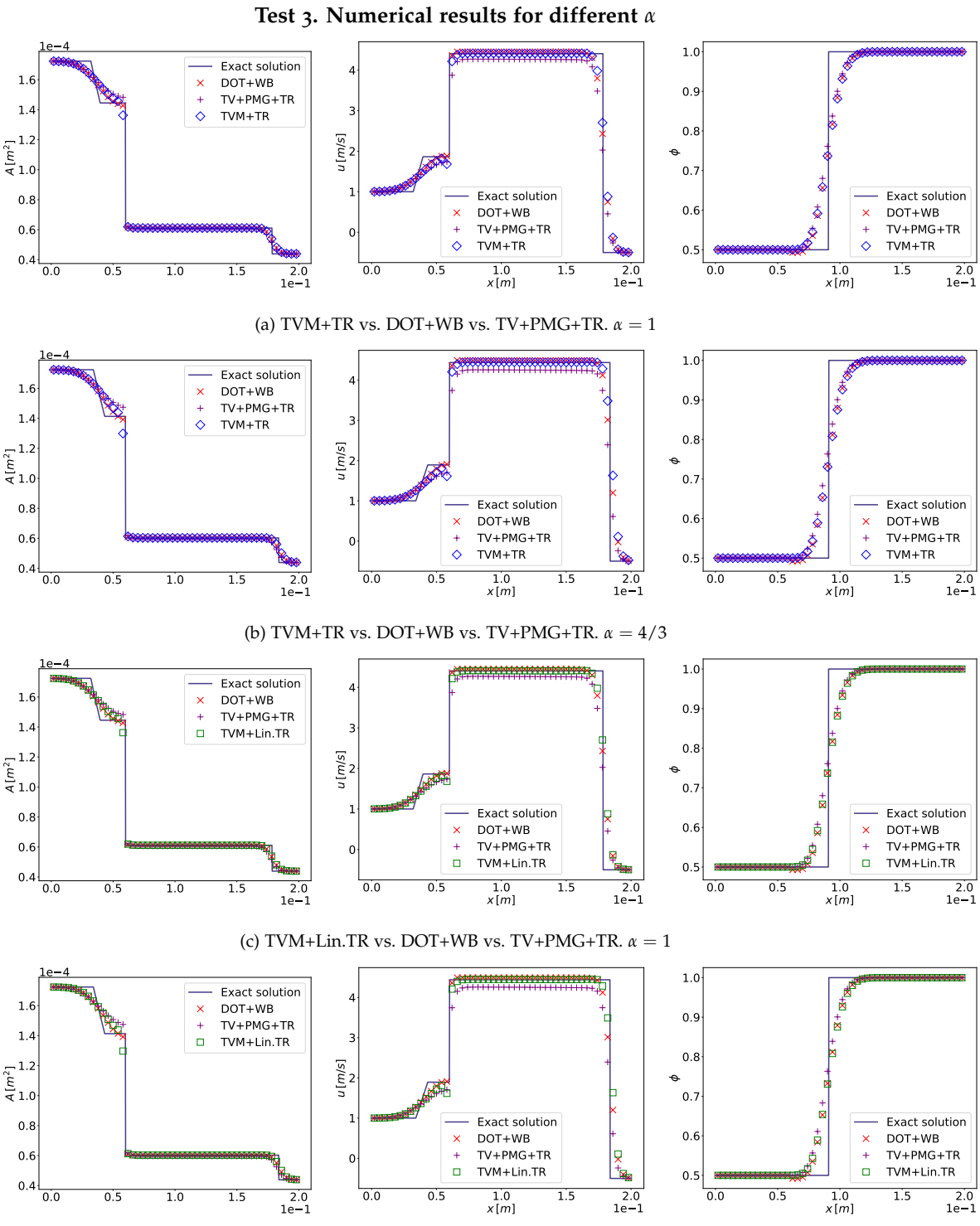

(a) TVM+TR vs. DOT+WB vs. TV+PMG+TR. $\alpha = 1$

(b) TVM+TR vs. DOT+WB vs. TV+PMG+TR. $\alpha = 4/3$

(c) TVM+Lin.TR vs. DOT+WB vs. TV+PMG+TR. $\alpha = 1$

(d) TVM+Lin.TR vs. DOT+WB vs. TV+PMG+TR. $\alpha = 4/3$

Figure 7.4: Test 3. Artery. RC_0C_uS. Numerical results of methods 1, 2 vs. the DOT+WB solver, the TV+PMG+TR solver with $C_{cfl} = 0.9$, $I = 50$ cells, and the exact solution of the Riemann problem for the complete 1D non-conservative blood flow equations with momentum correction coefficient $\alpha = 1, 4/3$. Initial conditions and parameters are given in Tables 7.1, 7.2.

Test 4. Numerical results for different α

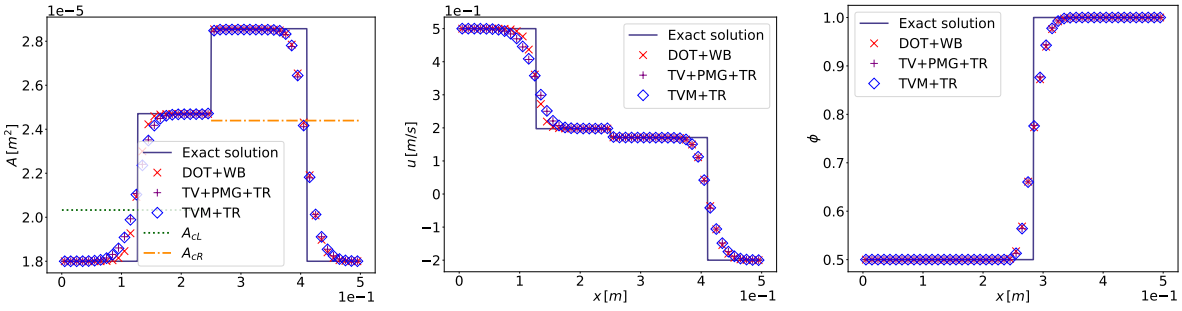

(a) TVM+TR vs. DOT+WB vs. TV+PMG+TR. $\alpha = 1$

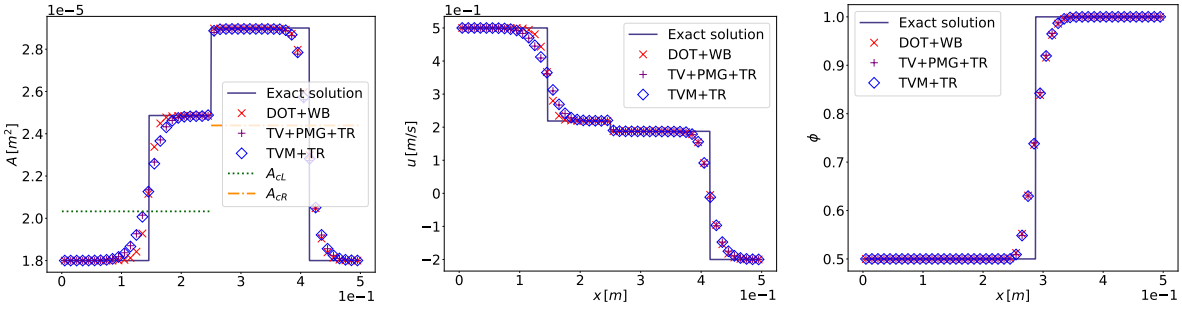

(b) TVM+TR vs. DOT+WB vs. TV+PMG+TR. $\alpha = 4/3$

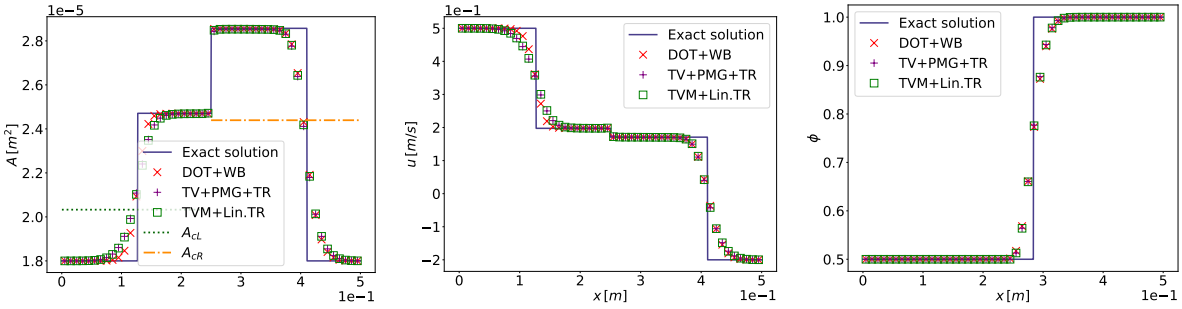

(c) TVM+Lin.TR vs. DOT+WB vs. TV+PMG+TR. $\alpha = 1$

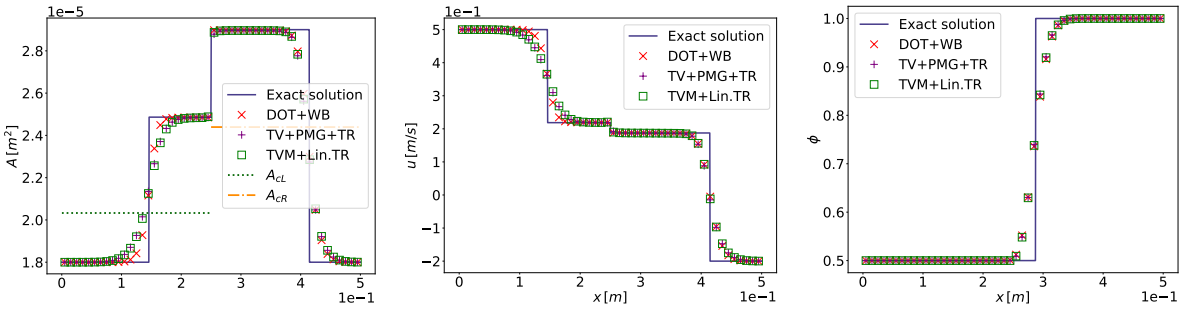

(d) TVM+Lin.TR vs. DOT+WB vs. TV+PMG+TR. $\alpha = 4/3$

Figure 7.5: Test 4. Vein. SC_0C_uS. Numerical results of methods 1, 2 vs. the DOT+WB solver, the TV+PMG+TR solver with $C_{cfl} = 0.9$, $I = 50$ cells, and the exact solution of the Riemann problem for the complete 1D non-conservative blood flow equations with momentum correction coefficient $\alpha = 1, 4/3$. Initial conditions and parameters are given in Tables 7.1, 7.2.

Test 5. Numerical results for different α

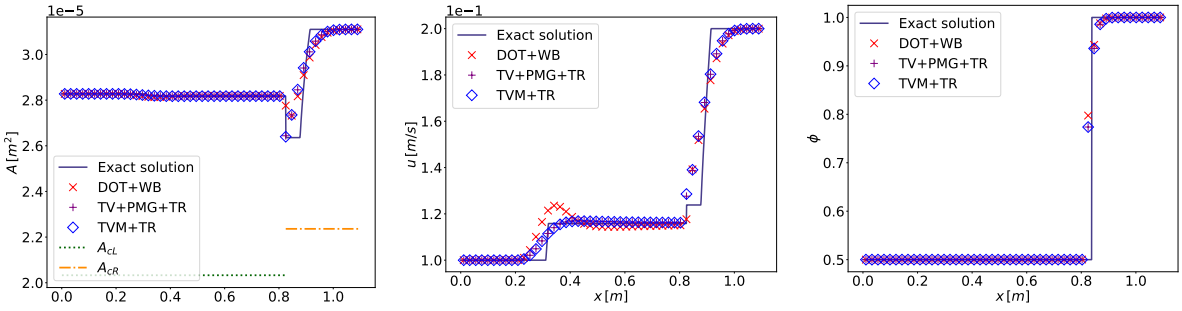

(a) TVM+TR vs. DOT+WB vs. TV+PMG+TR. $\alpha = 1$

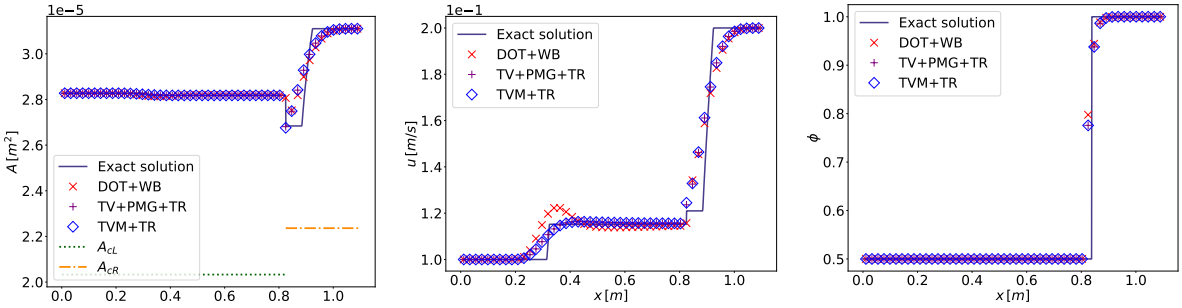

(b) TVM+TR vs. DOT+WB vs. TV+PMG+TR. $\alpha = 4/3$

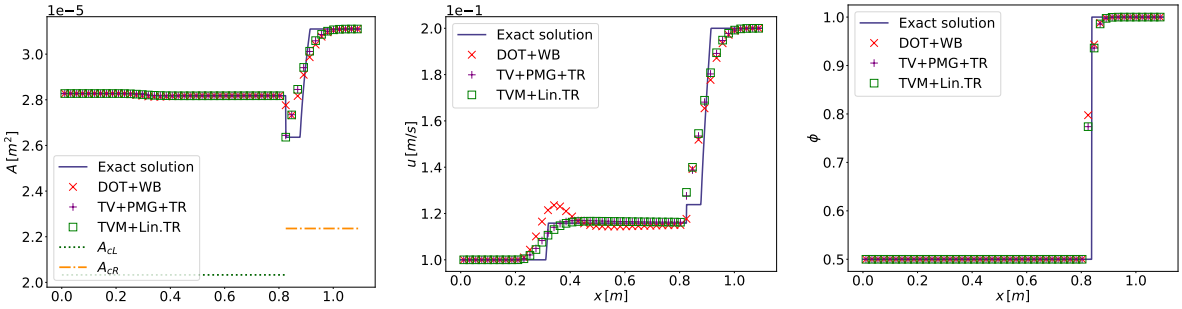

(c) TVM+Lin.TR vs. DOT+WB vs. TV+PMG+TR. $\alpha = 1$

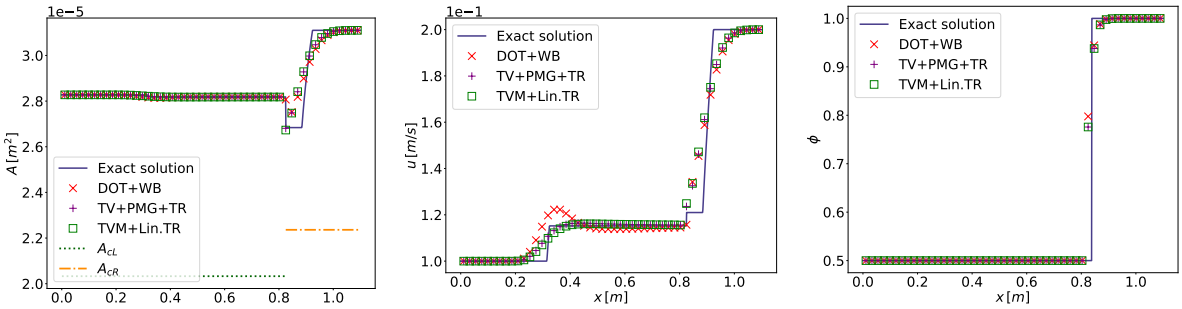

(d) TVM+Lin.TR vs. DOT+WB vs. TV+PMG+TR. $\alpha = 4/3$

Figure 7.6: Test 5. Vein. RC_0C_uR. Numerical results of methods 1, 2 vs. the DOT+WB solver, the TV+PMG+TR solver with $C_{cfl} = 0.9$, $I = 50$ cells, and the exact solution of the Riemann problem for the complete 1D non-conservative blood flow equations with momentum correction coefficient $\alpha = 1, 4/3$. Initial conditions and parameters are given in Tables 7.1, 7.2.

Test 6. Numerical results for different α

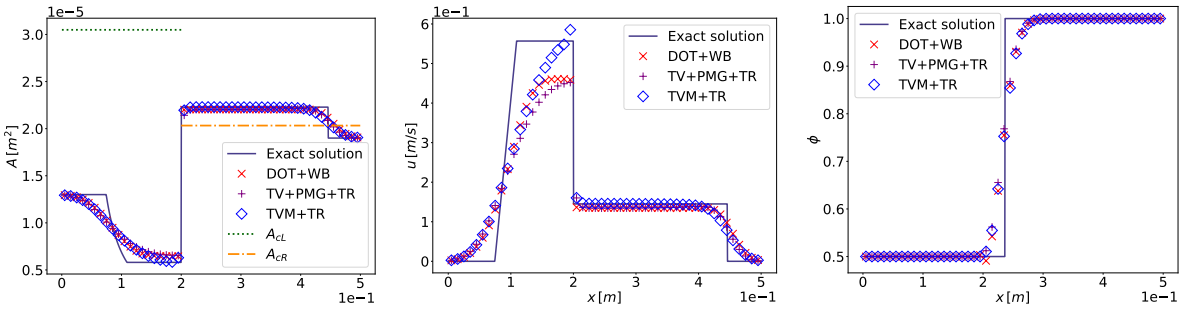

(a) TVM+TR vs. DOT+WB vs. TV+PMG+TR. $\alpha = 1$

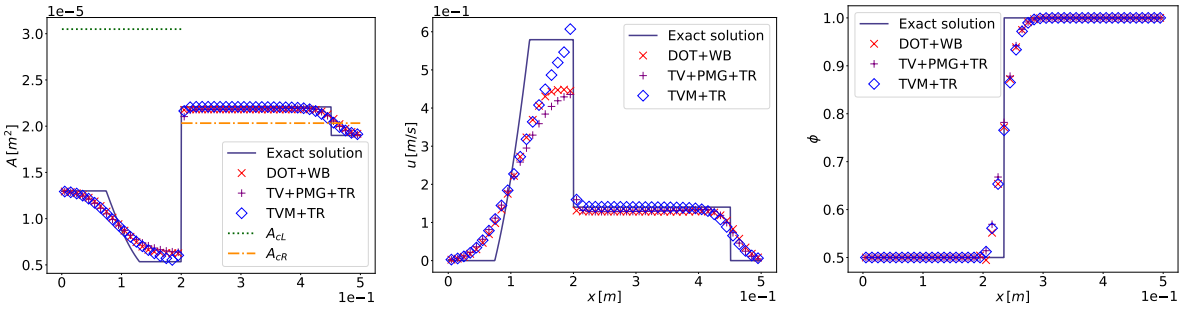

(b) TVM+TR vs. DOT+WB vs. TV+PMG+TR. $\alpha = 4/3$

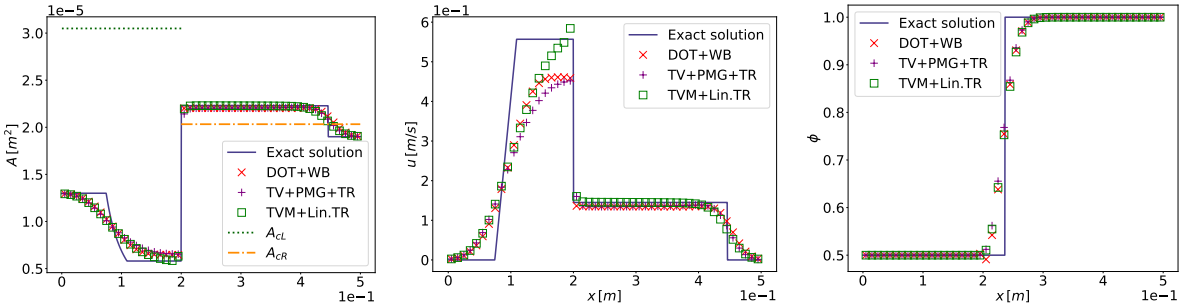

(c) TVM+Lin.TR vs. DOT+WB vs. TV+PMG+TR. $\alpha = 1$

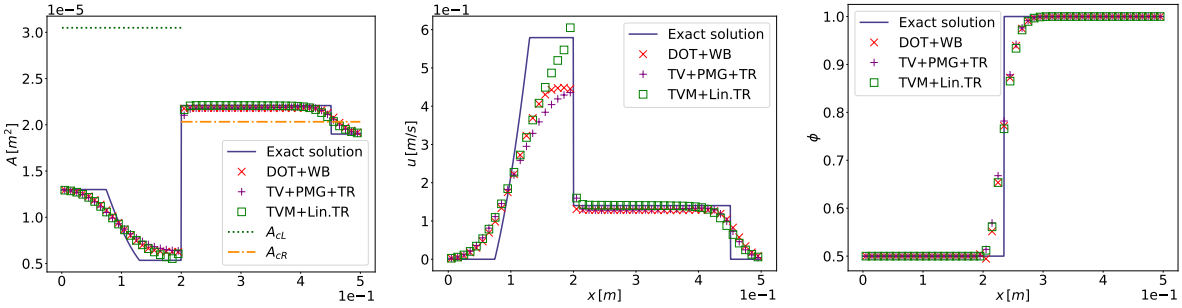

(d) TVM+Lin.TR vs. DOT+WB vs. TV+PMG+TR. $\alpha = 4/3$

Figure 7.7: Test 6. Vein- RC_0C_uS. Numerical results of methods 1, 2 vs. the DOT+WB solver, the TV+PMG+TR solver with $C_{cfl} = 0.9$, $I = 50$ cells, and the exact solution of the Riemann problem for the complete 1D non-conservative blood flow equations with momentum correction coefficient $\alpha = 1, 4/3$. Initial conditions and parameters are given in Tables 7.1, 7.2.

Test 7. Numerical results for different α

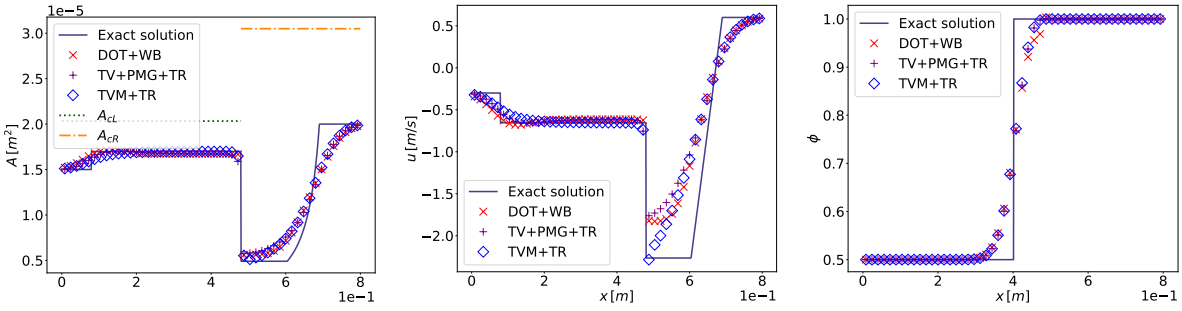

(a) TVM+TR vs. DOT+WB vs. TV+PMG+TR. $\alpha = 1$

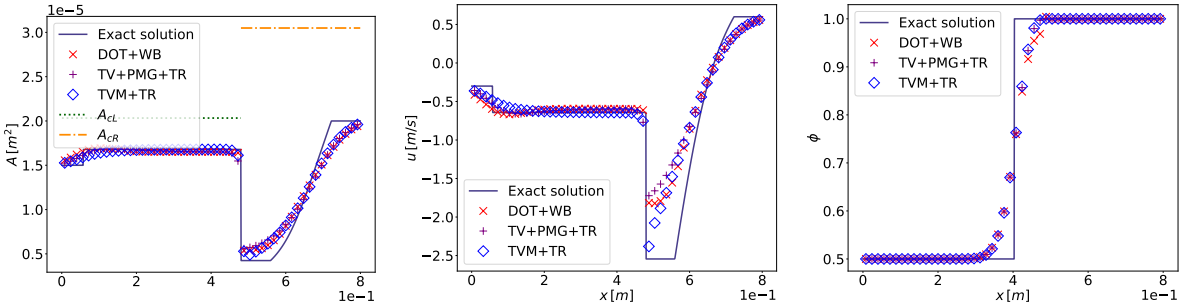

(b) TVM+TR vs. DOT+WB vs. TV+PMG+TR. $\alpha = 4/3$

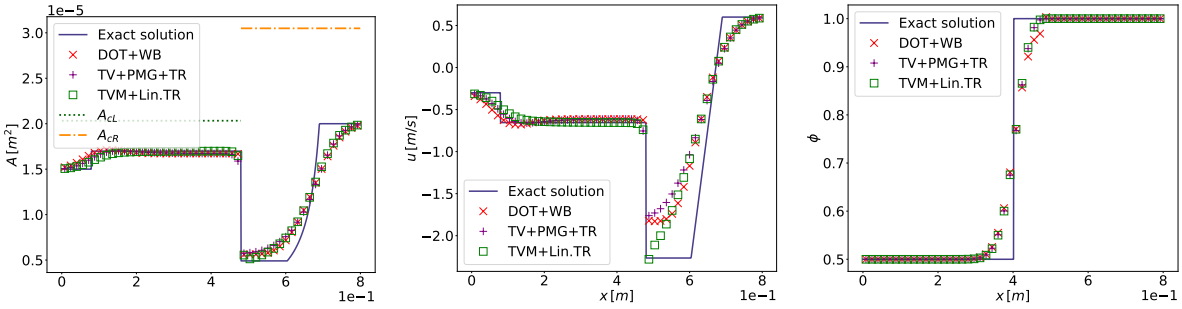

(c) TVM+Lin.TR vs. DOT+WB vs. TV+PMG+TR. $\alpha = 1$

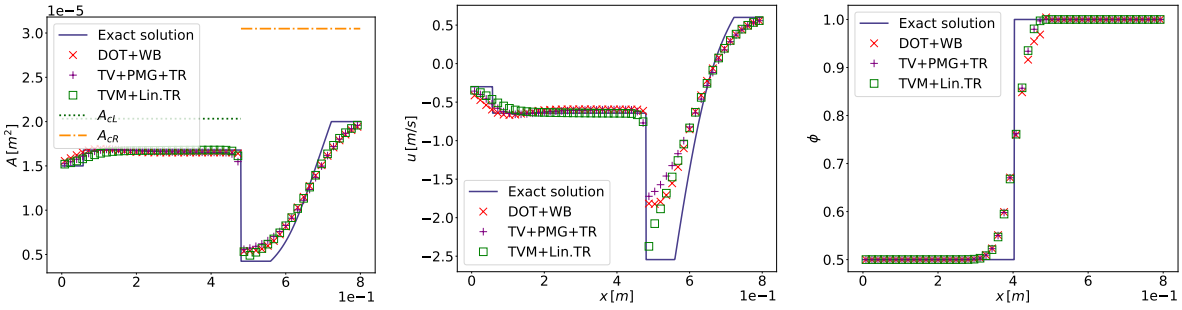

(d) TVM+Lin.TR vs. DOT+WB vs. TV+PMG+TR. $\alpha = 4/3$

Figure 7.8: Test 7. Vein. SC_uC_0R. Numerical results of methods 1, 2 vs. the DOT+WB solver, the TV+PMG+TR solver with $C_{cfl} = 0.9$, $I = 50$ cells, and the exact solution of the Riemann problem for the complete 1D non-conservative blood flow equations with momentum correction coefficient $\alpha = 1, 4/3$. Initial conditions and parameters are given in Tables 7.1, 7.2.

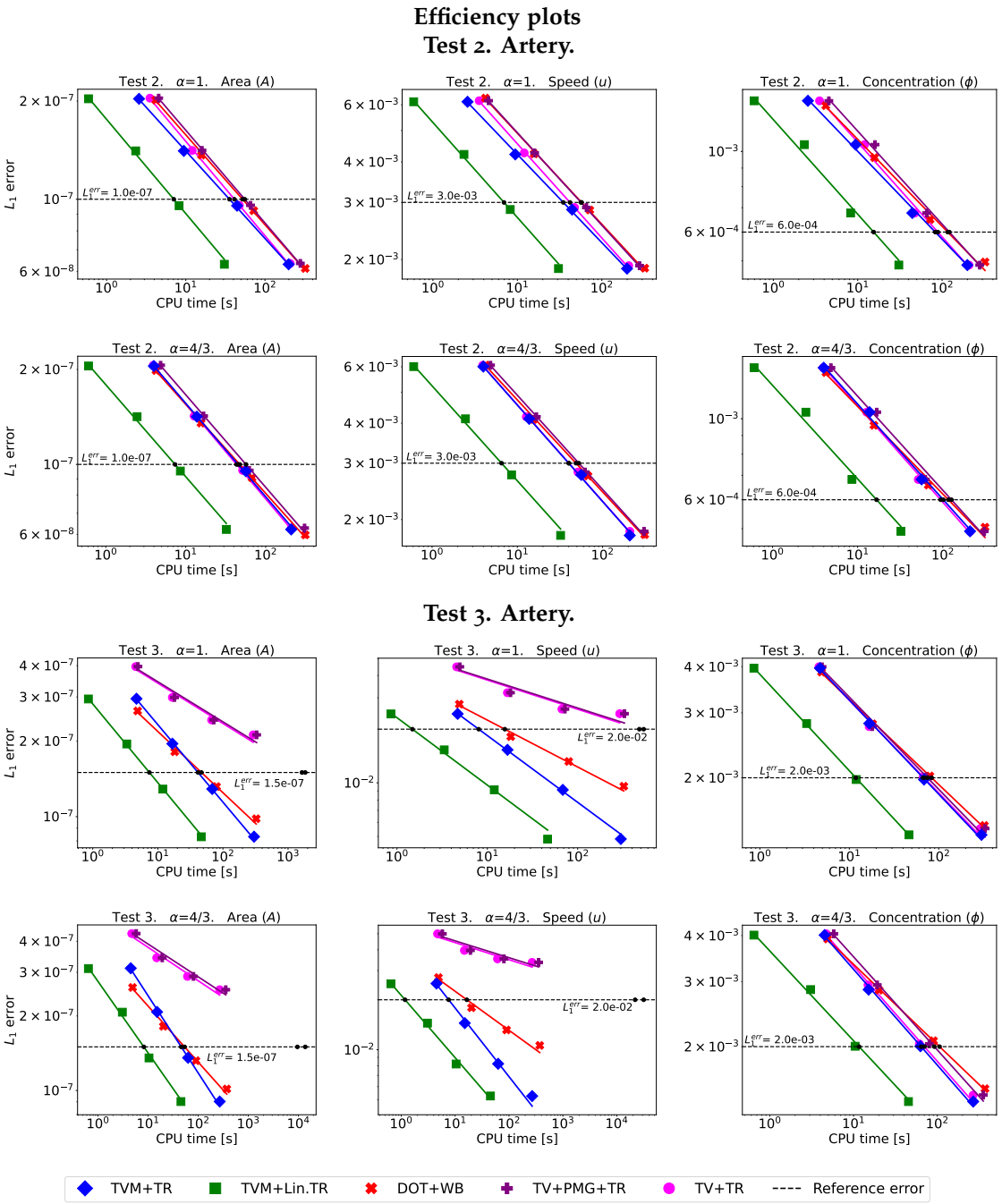

Figure 7.9: Efficiency plots for Tests 2, 3 in Tables 7.1, 7.2, calculated for meshes $I = [50, 100, 200, 400]$ and for momentum correction coefficient $\alpha = 1, 4/3$. The lines represent the least square approximation (where possible) of the data.

calculate the CPU cost and the L_1 error for each method cited above, for variables A, u and ϕ, with meshes $I = [50, 100, 200, 400]$ and a $C_{cfl} = 0.9$. L_1 error defined

$$L_1^{err}(t_{End}, \Delta x_j) = \Delta x_j \sum_{i=1}^{I_j} |q_{k,i}^{t_{End}} - q_{k,i}^{e}|, \quad k = 1, 2, 3; \tag{7.72}$$

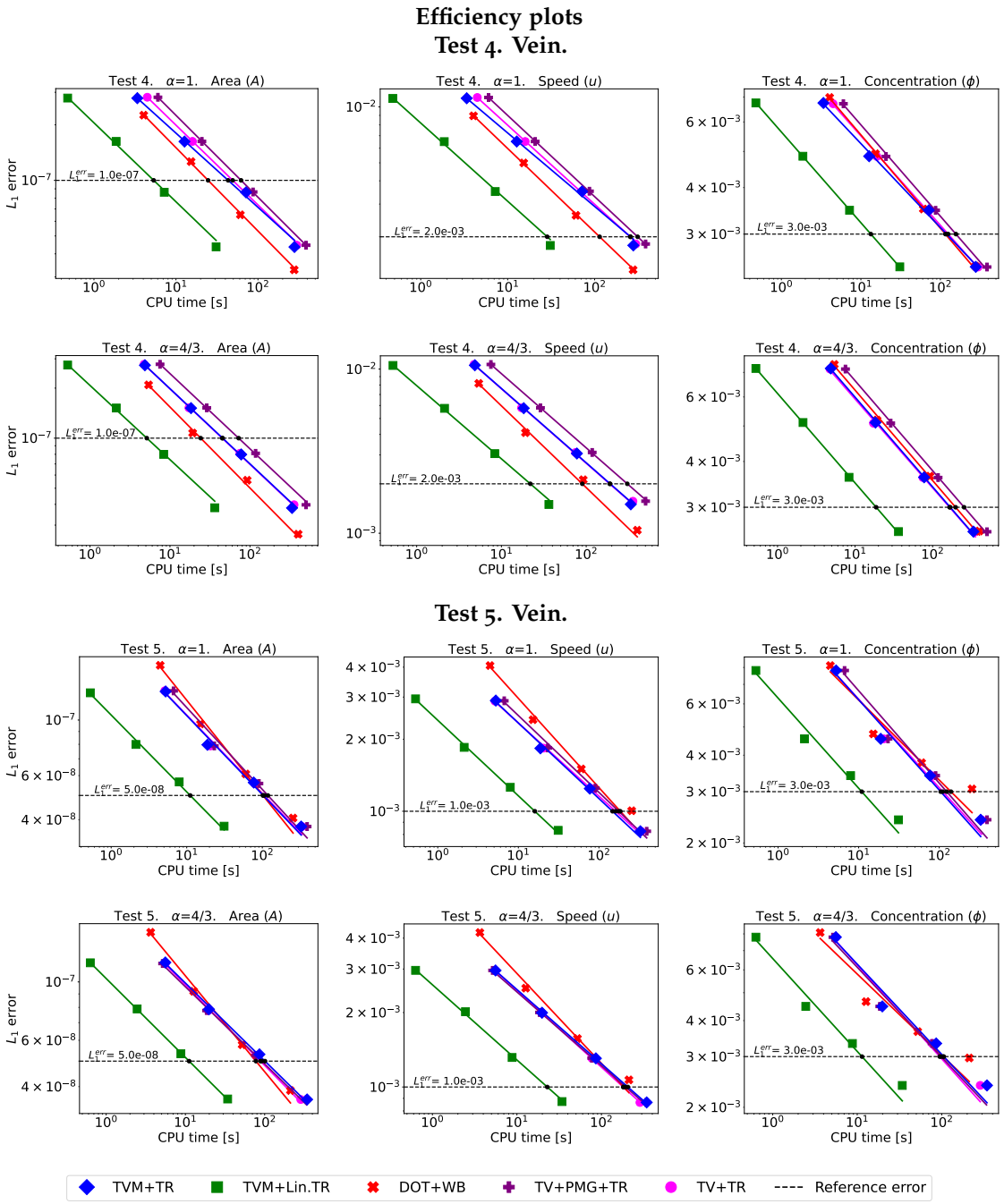

Figure 7.10: Efficiency plots for Tests 4, 5 in Tables 7.1, 7.2, calculated for meshes $I = [50, 100, 200, 400]$ and for momentum correction coefficient $\alpha = 1, 4/3$. The lines represent the least square approximation (where possible) of the data.

being t_{End} the output time, $q_{k,i}^{t_{End}}$ the *k-th* component of $\mathbf{Q}_i^n$ at time t_{End}, $q_{k,i}^e$ the corresponding exact solution and $\Delta x_j = \ell / I_j$, with ℓ the vessel length and I_j the actual mesh. The tests are carried out in Python language. Results are depicted in Figs. 7.9, 7.10, 7.11, 7.12.

In case of arteries, the two new methods prove to be the most efficient numerical methods (Figs. 7.9, 7.12). Test 1 depicts a stationary solution and the efficiency test was not performed. Regarding Test 2 all methods reach the same accuracy but in a different CPU times, among them

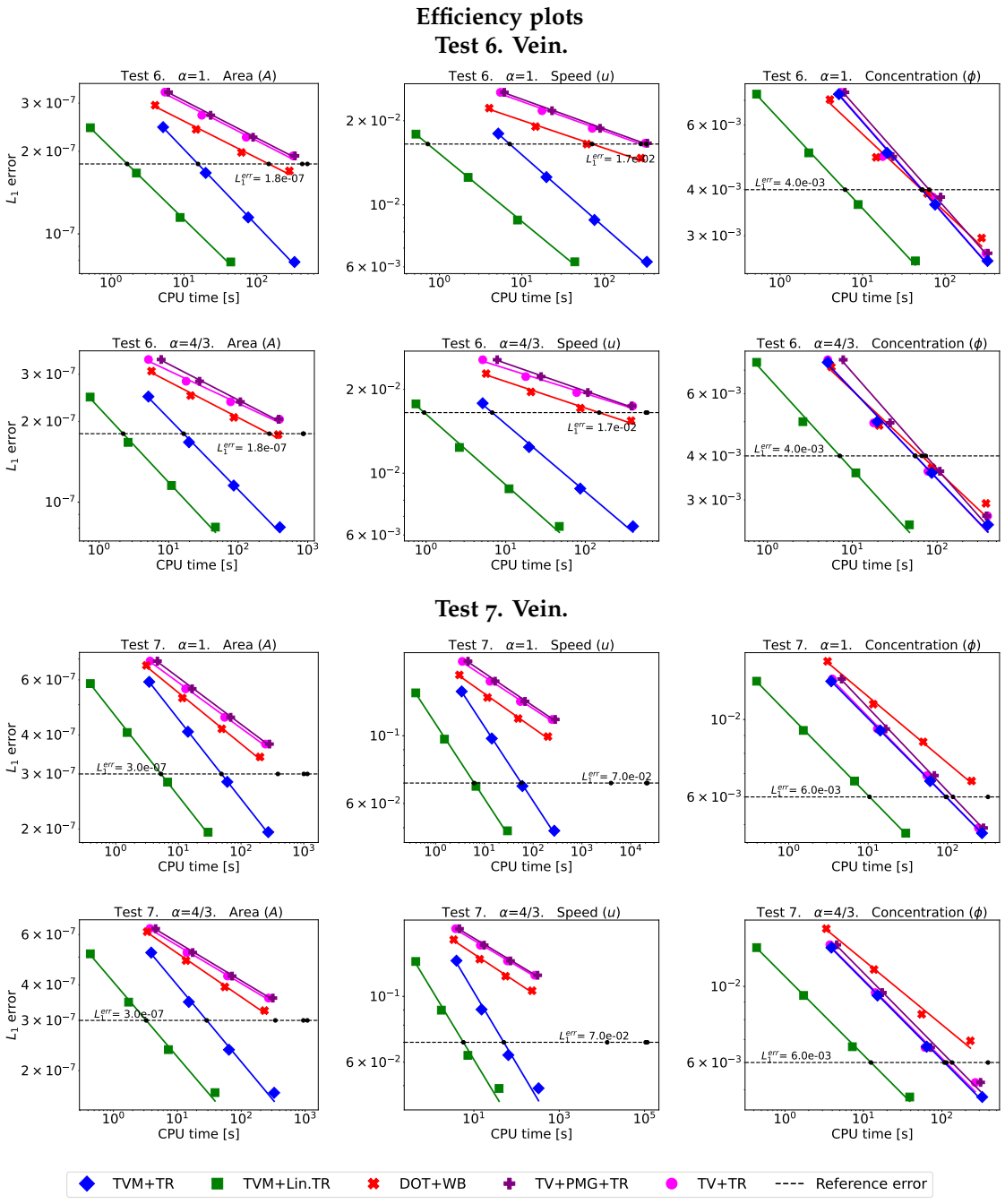

Figure 7.11: Efficiency plots for Tests 6, 7 in Tables 7.1, 7.2, calculated for meshes $I = [50, 100, 200, 400]$ and for momentum correction coefficient $\alpha = 1, 4/3$. The lines represent the least square approximation (where possible) of the data.

the new TVM-methods prove to be the more efficient, expecially the TVM+Lin.TR solver for both the values of the momentum correction coefficient analysed. Test 3 on the other hand shows a remarkable improvement of the accuracy in the two TVM-methods in describing variables A and u for both values of the momentum correction coefficient, with respect to the other considered methods. In describing the concentration ϕ the accuracy is comparable but the CPU time prove to be minor in the TVM+Lin.TR method.

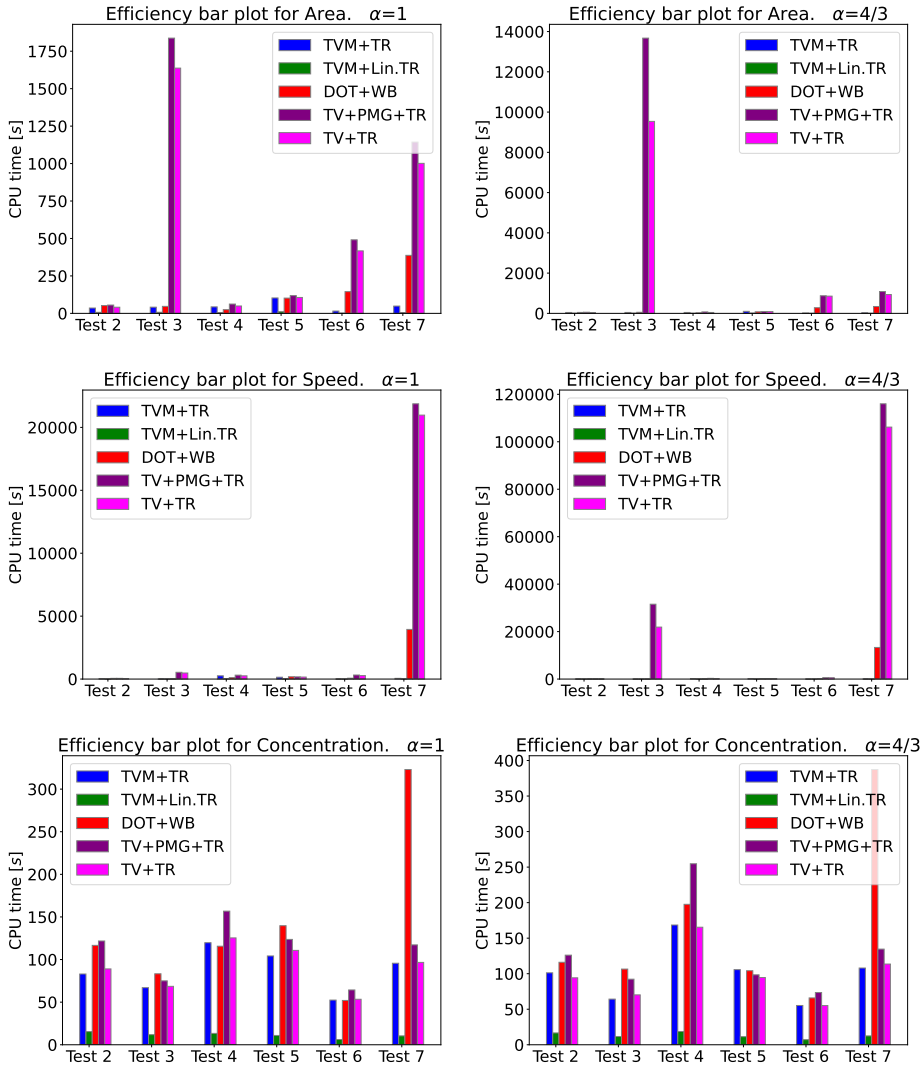

Figure 7.12: Efficiency bar plots for Tests 2, 3, 4, 5, 6, 7 in Tables 7.1, 7.2 representing the actual time each method takes to reach errors given in Figs. 7.9, 7.10, 7.11 for each variable.

Regarding veins, Test 4 shows the remarkable saving of CPU time of TVM+Lin.TR that reaches however the same accuracy of the other TV-type methods, the DOT+WB solver proves to be the most accurate but with higher CPU time with respect to the new TVM-solver. This is revealed for both the values of the momentum correction coefficient (Figs.7.10, 7.12). Test 5 depicts again the higher efficiency of the two new TVM-methods in describing the three unknowns A, u and ϕ, with respect to all the methods considered, that however reaches a comparable accuracy, for both values of α, as already described in Test 2 (Figs.7.10 7.12). A similar scenario of Test 3 instead, is faced in Tests 6 and 7 where the level of both accuracy and CPU time saving is really improved by the two new TVM-methods with respect to the others, for variables A and u. Regarding the concentration ϕ, the efficiency of the two TVM-methods is still the best one, however the accuracy attained is comparable with the one of the other methods (Figs.7.11, 7.12).

Furthermore it is worth noting that for particular Riemann problems (here Tests, 3, 6, 7) the jump in the vicinity of the intitial discontinuity of the parameters does not affect the overall accuracy of the two new methods. In addition it is of utmost significance to recognize the CPU

time saving that characterizes the TV,TVM-methods using (7.67) with respect to the TV+PMG ones, circumventing the computations of path and matrices (Fig. 7.12). Finally it can be observed that in general the particular position of A_{cL} and A_{cR} in (7.7), with respect to the problem outcomes, does not affect the accuracy of the results of the new TVM-splitting methods presented in this Chapter, however it should be kept in mind that the TVM+Lin.TR method, although being really efficient, is build from a linearized solver that is not a robust method, in fact it may lead the TVM+Lin.TR scheme to crush due to the heavy approximation applied to the wave relations (Section 7.1.2.2). However, when possibile, it proves to be a very efficient alternative to the robust TVM+TR solver.

7.4 Conclusions

In this Chapter we have presented an advection-pressure splitting method at PDEs level for the complete hyperbolic system of 1D blood flow equations with discontinuous parameters and an advection equation for a passive scalar transport, for both arteries and veins, separating the given system in advection system and pressure one. Consequently we have presented two approximated Riemann problem solvers for the obtained pressure system, and after, two final simple, finite volume, first order, numerical advection-pressure splitting schemes for the complete 1D blood flow model have been built. They have been derived from a conservative form of the path-conservative schemes for the pressure system, obviating the use of any path and the implementation of the matrices necessary for the path-conservative methods. Regarding the advection numerical flux a modification with respect to the one described in [83, 91] is presented, to adequately address a greater number of discontinuous parameters. These schemes have been compared with the classic DOT well-balanced Riemann solver, the TV+PMG+TR scheme, a splitting scheme obtained from the Parés-Muñoz-Godunov scheme for the pressure system and the original TV-advection flux for the advection system and the exact solution of the Riemann problem for the complete system, in various test problems for arteries and veins, in subsonic regime, proving that the final splitting schemes continue to operate effectively despite the lack of genuine non-linearity in two characteristic fields of the pressure system. Finally an efficiency analysis has been carried out. The two proposed methods, built from a modification of the original TV-advection flux, have proved to be in general considerably more efficient than the considered reference methods and can be contemplated as competitive methods to solve the Riemann problems under study.

The upcoming study will utilise the methods presented in this work to address 1D blood flow model networks. Furthermore, a thorough examination of the entire solution to the Riemann problem for the pressure system will be carried out, with emphasis on inspecting the consequences of the absence of genuine non-linearity.

Conclusions

This Thesis has focuses on investigating splitting techniques for the 1D blood flow equations with a passive scalar transport equation added, both from a theoretical and a numerical point of view.

Our analysis has adopted a two-step framework that encompasses splitting at the level of partial differential equations (PDEs) and numerical methods for discretizing the ensuing problems. We have extended the principles of the flux splitting approach introduced by Toro and Vázquez [92], referred to, hereafter, as TV splitting. Initially designed for the conservative Euler equations governing compressible gas dynamics, this approach involves the division of the flux vector into advection and pressure terms. Consequently, two distinct systems of partial differential equations emerge: the advection system and the pressure one. In this framework, the wave relations that must be enforced when employing a Riemann solver are simplified. This simplification not only positively impacts the numerical method employed to solve blood flow equations within vessels but also influences the determination of coupling conditions between one-dimensional domains [27, 73].

The dissertation has been divided into two parts: in the first part we have introduced the systems of PDEs and theoretically studied the exact solutions of the Riemann problems associated with them. In the second part we have developed first-order, finite volume-type, numerical methods to numerically solve the aforementioned problems.

In this Chapter we discuss the achievements reached through the results presented in this Thesis. Furthermore, we suggest possible topics to be considered in a future work.

I Part 1

I.I Exact solution of the Riemann problem for the complete 1D blood flow equations with general constant momentum correction coefficient and transport

The mathematical model presented in this Thesis is well known and widely treated in literature ([40, 28, 90, 84, 71, 81] and others), in particular its derivation has been presented in [28].

The momentum correction coefficient in the 1D blood flow equations is related to the assumed velocity profile. The derivation of this term has been presented in [28] and in this Thesis we consider the velocity profile function proposed in [77].

The exact solution of the Riemann problem has been widely treated in literature, but only for a momentum correction coefficient equal to one [90, 38, 39, 71, 81] corresponding to a flat velocity profile, i.e. an inviscid fluid. In addition, there is still a significant amount of research that remains to be carried out on veins, these latter presenting a highly non-linear behaviour.

In this Thesis we have presented the complete exact solution of the Riemann problem for the 1D blood flow equations with an advection equation for a passive scalar transport and a

general constant momentum correction coefficient $\alpha \in [1, 2]$. This latter includes velocity profiles as the *parabolic* and *blunt* ones, widely treated in literature (for example see [41]). For tube laws describing arteries and veins with continuous mechanical and geometrical parameters we have explored both the subcritical and the supercritical cases. For tube laws describing arteries and veins with discontinuous parameters we have explored only the subcritical case. The exact solution, presented with a complete mathematical analysis and a simple procedure to compute it, has been also compared with a numerical mesh-independent solution obtained with first order classical numerical schemes.

This research study, without considering the passive scalar transport equation, has been published in [82].

Future work The exact solution of the Riemann problem in supersonic regime in case of veins with discontinuous mechanical and geometrical properties remains to be studied, as well as the entire exact solution for the 1D blood flow equations with a momentum correction coefficient not constant. Furthermore the exact solution of the Riemann problem for the 1D blood flow equations in case of junctions of three and more vessels represents a critical issue to describe coupling conditions in case of junctions and can be an interesting challenge for a future research.

I.II Exact solution of the Riemann problem for the 1D advection system with general constant momentum correction coefficient and without transport

In this Thesis we have presented the exact solution of the Riemann problem for the advection system arising from the splitting at the level of PDEs of the complete 1D blood flow equations with general constant momentum correction coefficient. This splitting is a modification of the TV splitting presented in Toro and Vázquez [92] for the 1D Euler equations and has been used as a building technique for new computationally efficient numerical schemes. The resulting system can be incorporated to the so-called *pressureless* systems of PDEs, generally developed for the Euler equations. A complete mathematical analysis has been carried out and the exact solution has been finally further validated by the comparison with numerical, mesh-independent, solutions, obtained with a second order, centred, extension of FORCE scheme.

Future work The advection system analyzed in this Thesis does not include the passive scalar transport equation. Further work is necessary to complete the analysis.

I.III Exact solution of the Riemann problem for the conservative 1D pressure system with transport

In this Thesis we have solved exactly the Riemann problem for the 1D pressure system arising from the aforementioned splitting at the level of PDEs of the complete conservative 1D blood flow equations with an advection equation for a passive scalar transport. A complete mathematical analysis has been carried out for both arteries and veins. In the latter case the loss of genuine non-linearity of the characteristic fields has been discussed, introducing a particular waveform not presented in the models already treated in this Thesis, the compound wave. A simple procedure to compute the resulting exact solution has been proposed and the latter has been also compared with numerical mesh-independent solutions obtained with a second order, centred, extension of FORCE numerical scheme.

Future work The exact solution of the Riemann problem for the pressure system here depicted, regards only the system arising from the splitting of the conservative 1D blood flow equations. The solution concerning the non-conservative counterpart remains to be developed. These exact solutions of the Riemann problem are significant not only to validate advection-pressure numerical schemes, but also to create coupling conditions between vessels in large networks, being these latter exact solutions simpler to implement with respect to the one of the complete 1D blood flow equations, expecially for momentum correction coefficient different from one.

II Part 2

II.I Flux vector splitting schemes applied to a conservative 1D blood flow model with transport for arteries and veins

In this study, two finite volume, first order, flux splitting, numerical schemes have been introduced for the original hyperbolic system of 1D blood flow equations with continuous parameters and an advection equation for a passive scalar transport. The methods have been applied to both arteries and veins. By separating the given system into an advection system and a pressure system, two approximated Riemann problem solvers have been developed for the pressure system.

To evaluate the performance of these schemes, they have been compared with the classic Godunov scheme and the exact solution of the Riemann problem for the complete system. Various test problems for arteries and veins, including subsonic and transonic regimes, have been considered. The results have demonstrated that despite the lack of genuine non-linearity in two characteristic fields of the pressure system in case of veins, the final splitting schemes have performed effectively. Furthermore, an efficiency analysis has been conducted to assess the performance of the proposed methods. The findings have revealed that the two proposed methods have been generally more efficient than the original Godunov method, the FORCE centred numerical scheme, and the DOT Riemann solver. Therefore, these methods can be considered as competitive alternatives for solving the Riemann problems under investigation.

Future work In a future research, the proposed techniques will be implemented to solve networks of 1D blood flow models. This will further enhance our understanding and ability to analyze complex blood flow phenomena. Furthermore extending this topic to viscoelastic vessels, for both arteries and veins with a passive scalar transport equation added, and after, to networks, would be of paramount importance for simulations more consistent with the reality of the human body.

II.II Advection-pressure splitting schemes applied to a non-conservative 1D blood flow model with transport for arteries and veins

In this study, we have introduced a novel advection-pressure splitting technique for the complete hyperbolic system of 1D blood flow equations. This method is specifically designed to handle discontinuous parameters and a passive scalar transport equation in both arteries and veins. By separating the given system into an advection system and a pressure system, we have

developed two approximate solvers for the pressure system. Subsequently, we have constructed two numerical advection-pressure splitting schemes for the complete 1D blood flow model.

To evaluate the performance of these schemes, we have compared them with some classic first order numerical schemes suitable for handling non-conservative models. Additionally, we have considered the exact solution of the Riemann problem for the complete system. These comparisons have been conducted in various test problems for arteries and veins under subsonic conditions. Remarkably, our findings demonstrate that the final splitting schemes continue to operate effectively despite the absence of genuine non-linearity in two characteristic fields of the pressure system in case of veins. Furthermore, we have performed an efficiency analysis to assess the computational performance of the proposed methods. Our results indicate that the modified TV-advection flux-based methods are generally more efficient than the reference methods considered in this study. Therefore, these methods can be regarded as competitive alternatives for solving the Riemann problems under investigation.

Future work In a forthcoming study, the suggested methods will be applied to address 1D blood flow model networks, and also viscoelastic vessels, as in the conservative counterpart.

Chapter A

REFERENCE METHODS

In this Appendix we describe the numerical schemes applied in this Thesis as reference numerical solutions to compare and validate our new presented schemes or exact solutions.

A.1 FORCE NUMERICAL SCHEME

The centred, monotone, finite volume, FORCE scheme [88], was originally derived [86] as a deterministic version of the stochastic Random Choice Method [32]. The resulting FORCE flux turns out to be the arithmetic mean of the Lax-Friedrichs and Lax-Wendroff ones. Given the conservative hyperbolic system

$$\partial_t \mathbf{Q} + \partial_x \mathbf{F}(\mathbf{Q}) = \mathbf{0}, \tag{A.1}$$

a finite volume scheme may be constructed by integrating (A.1) in space and time in the control volume $[x_{i-\frac{1}{2}}, x_{i+\frac{1}{2}}] \times [t^n, t^{n+1}]$, leading to

$$\mathbf{Q}_i^{n+1} = \mathbf{Q}_i^n - \frac{\Delta t}{\Delta x}(\mathbf{F}_{i+\frac{1}{2}} - \mathbf{F}_{i-\frac{1}{2}}); \tag{A.2}$$

where

$$\mathbf{Q}_i^n \approx \frac{1}{\Delta x}\int_{x_{i-\frac{1}{2}}}^{x_{i+\frac{1}{2}}} \mathbf{Q}(x, t^n)dx, \tag{A.3}$$

and

$$\mathbf{F}_{i+\frac{1}{2}} = \mathbf{F}_{i+\frac{1}{2}}^{FORCE}, \tag{A.4}$$

with

$$\mathbf{F}_{i+\frac{1}{2}}^{FORCE} = \frac{1}{2}(\mathbf{F}_{i+\frac{1}{2}}^{LW} + \mathbf{F}_{i+\frac{1}{2}}^{LF}). \tag{A.5}$$

We recall

$$\mathbf{F}_{i+\frac{1}{2}}^{LW} = \mathbf{F}(\mathbf{Q}_{i+\frac{1}{2}}^{LW}), \tag{A.6}$$

with

$$\mathbf{Q}_{i+\frac{1}{2}}^{LW} = \frac{1}{2}(\mathbf{Q}_i^n + \mathbf{Q}_{i+1}^n) - \frac{1}{2}\frac{\Delta t}{\Delta x}(\mathbf{F}(\mathbf{Q}_{i+1}^n) - \mathbf{F}(\mathbf{Q}_i^n)), \tag{A.7}$$

and

$$\mathbf{F}_{i+\frac{1}{2}}^{LF} = \frac{1}{2}(\mathbf{F}(\mathbf{Q}_i^n) + \mathbf{F}(\mathbf{Q}_{i+1}^n)) - \frac{1}{2}\frac{\Delta x}{\Delta t}(\mathbf{Q}_{i+1}^n - \mathbf{Q}_i^n). \tag{A.8}$$

Here $\Delta x = x_{i+\frac{1}{2}} - x_{i-\frac{1}{2}}$, $\Delta t = t^{n+1} - t^n$, $\mathbf{Q}_{i+\frac{1}{2}}$ are the states at cell interface $x_{i+\frac{1}{2}}$ and $\mathbf{F}$ is the physical flux of the system. Please note that *LW* stands for *Lax-Wendroff*, while *LF* stands for *Lax-Friedrichs*.

A.2 A SECOND ORDER EXTENSION OF FORCE

A second order, finite volume, extension of FORCE scheme presented in Appendix A.1 can be obtained in the following manner (for further details see [87]). Given the conservative hyperbolic system

$$\partial_t \mathbf{Q} + \partial_x \mathbf{F}(\mathbf{Q}) = \mathbf{0}, \tag{A.9}$$

integrating (A.9) in space and time in the control volume $[x_{i-\frac{1}{2}}, x_{i+\frac{1}{2}}] \times [t^n, t^{n+1}]$, leads to

$$\mathbf{Q}_i^{n+1} = \mathbf{Q}_i^n - \frac{\Delta t}{\Delta x}(\mathbf{F}_{i+\frac{1}{2}} - \mathbf{F}_{i-\frac{1}{2}}); \tag{A.10}$$

where

$$\mathbf{Q}_i^n \approx \frac{1}{\Delta x}\int_{x_{i-\frac{1}{2}}}^{x_{i+\frac{1}{2}}} \mathbf{Q}(x, t^n)dx, \tag{A.11}$$

and

$$\mathbf{F}_{i+\frac{1}{2}} = \frac{1}{\Delta t}\int_{t^n}^{t^{n+1}} \mathbf{F}(\mathbf{Q}(x_{i+\frac{1}{2}}, t))dt. \tag{A.12}$$

We define

$$\mathbf{F}_{i+\frac{1}{2}} = \mathbf{F}_{i+\frac{1}{2}}^{FORCE}, \tag{A.13}$$

with

$$\mathbf{F}_{i+\frac{1}{2}}^{FORCE} = \frac{1}{2}(\mathbf{F}_{i+\frac{1}{2}}^{LW} + \mathbf{F}_{i+\frac{1}{2}}^{LF}). \tag{A.14}$$

Now

$$\mathbf{F}_{i+\frac{1}{2}}^{LW} = \mathbf{F}(\mathbf{Q}_{i+\frac{1}{2}}^{LW}), \tag{A.15}$$

with

$$\mathbf{Q}_{i+\frac{1}{2}}^{LW} = \frac{1}{2}(\overline{\mathbf{Q}}_i^R + \overline{\mathbf{Q}}_{i+1}^L) - \frac{1}{2}\frac{\Delta t}{\Delta x}(\mathbf{F}(\overline{\mathbf{Q}}_{i+1}^L) - \mathbf{F}(\overline{\mathbf{Q}}_i^R)), \tag{A.16}$$

and

$$\mathbf{F}_{i+\frac{1}{2}}^{LF} = \frac{1}{2}(\mathbf{F}(\overline{\mathbf{Q}}_i^R) + \mathbf{F}(\overline{\mathbf{Q}}_{i+1}^L)) - \frac{1}{2}\frac{\Delta x}{\Delta t}(\overline{\mathbf{Q}}_{i+1}^L - \overline{\mathbf{Q}}_i^R). \tag{A.17}$$

Here $\Delta x = x_{i+\frac{1}{2}} - x_{i-\frac{1}{2}}$, $\Delta t = t^{n+1} - t^n$, $\mathbf{Q}_{i+\frac{1}{2}}$ are the states at cell interface $x_{i+\frac{1}{2}}$ and $\mathbf{F}$ is the physical flux of the system. Please note that *LW* stands for *Lax-Wendroff*, while *LF* stands for *Lax-Friedrichs*.

To compute $\overline{\mathbf{Q}}_i^L$ and $\overline{\mathbf{Q}}_i^R$ we perform the following steps

1. *Data reconstruction and boundary extrapolated values*
   From the polynomial vector

   $$\mathbf{P}_i(x) = \mathbf{Q}_i^n + (x - x_i)\Delta VA_i, \tag{A.18}$$

   where: Δ_i is the associated slope of its reconstruction polynomial $\mathbf{P}_i(x)$. To choose these slopes we use VASLIC criterion.

   Definition A.2.1. *VASLIC (Van-Albada Slope Limiter Centred) criterion reads as follows: considering*

   $$q_{k,i} - q_{k,i-1} = \begin{cases} tol * sgn(q_{k,i} - q_{k,i-1}) & if \quad |q_{k,i} - q_{k,i-1}| \leq tol \quad and \quad sgn(q_{k,i} - q_{k,i-1}) \neq 0 \\ tol & if \quad |q_{k,i} - q_{k,i-1}| \leq tol \quad and \quad sgn(q_{k,i} - q_{k,i-1}) = 0 \end{cases} \tag{A.19}$$

$$q_{k,i+1} - q_{k,i} = \begin{cases} tol * sgn(q_{k,i+1} - q_{k,i}) & if \quad |q_{k,i+1} - q_{k,i}| \leq tol \quad and \quad sgn(q_{k,i+1} - q_{k,i}) \neq 0 \\ tol & if \quad |q_{k,i+1} - q_{k,i}| \leq tol \quad and \quad sgn(q_{k,i+1} - q_{k,i}) = 0 \end{cases} \tag{A.20}$$

we define

$$\Delta_{k,i} = 0.5(q_{k,i} - q_{k,i-1}) + 0.5(q_{k,i+1} - q_{k,i}), \tag{A.21}$$

$$r_{k,i} = \frac{q_{k,i} - q_{k,i-1}}{q_{k,i+1} - q_{k,i}}, \tag{A.22}$$

$$d_{k,i} = 1 + r_{k,i}, \tag{A.23}$$

then

$$\Delta VA_{k,i} = \frac{\min\left(\frac{2}{d_{k,i}}, r_{k,i}\frac{1+r_{k,i}}{1+r_{k,i}r_{k,i}}\right)\Delta_{k,i}}{\Delta x} \quad \text{if} \quad r_{k,i} \geq 0. \tag{A.24}$$

In each cell i we obtain two boundary extrapolated values

$$\mathbf{Q}_i^L = \mathbf{P}_i(x_{i-\frac{1}{2}}); \quad \mathbf{Q}_i^R = \mathbf{P}_i(x_{i+\frac{1}{2}}). \tag{A.25}$$

2. *Evolution*
For each cell i, the boundary extrapolated values $\mathbf{Q}_i^L$ and $\mathbf{Q}_i^R$ are evolved by a time $\frac{\Delta t}{2}$

$$\begin{aligned} \overline{\mathbf{Q}}_i^L &= \mathbf{Q}_i^L - \frac{1}{2}\frac{\Delta t}{\Delta x}\mathbf{F}(\mathbf{Q}_i^R) - \mathbf{F}(\mathbf{Q}_i^L)], \\ \overline{\mathbf{Q}}_i^R &= \mathbf{Q}_i^R - \frac{1}{2}\frac{\Delta t}{\Delta x}[\mathbf{F}(\mathbf{Q}_i^R) - \mathbf{F}(\mathbf{Q}_i^L)]. \end{aligned} \tag{A.26}$$

In this scheme the boundary conditions are set as *transmissive*.

A.3 A BRIEF OVERVIEW OF THE PATH-CONSERVATIVE APPROACH

A.3.1 PATH-CONSERVATIVE NUMERICAL SCHEMES

We consider a general $N \times N$ quasi-linear hyperbolic system

$$\partial_t \mathbf{Q} + \mathbf{M}(\mathbf{Q})\partial_x \mathbf{Q} = 0, \tag{A.27}$$

with the vectors of variables denoted as

$$\mathbf{Q} = [q_1, q_2, ..., q_N]^T \in \Omega_q. \tag{A.28}$$

Here, Ω_q is the so-called domain of definition of PDE (A.27) and is supposed to be a convex set.

Definition A.3.1 (Path). *$\Psi(\mathbf{Q}_L, \mathbf{Q}_R, s)$ with $0 \leq s \leq 1$, is a Lipschitz continuous function that connects the left state $\mathbf{Q}_L$ to the right state $\mathbf{Q}_R$ in phase space, satisfying*

$$\Psi(\mathbf{Q}_L, \mathbf{Q}_R, 0) = \mathbf{Q}_L, \qquad \Psi(\mathbf{Q}_L, \mathbf{Q}_R, 1) = \mathbf{Q}_R. \tag{A.29}$$

Parés [64] proposed a simple straight-line segment path

$$\boldsymbol{\Psi}(\mathbf{Q}_L, \mathbf{Q}_R, s) = \mathbf{Q}_L + s(\mathbf{Q}_R - \mathbf{Q}_L), \quad \text{with with } 0 \leq s \leq 1, \tag{A.30}$$

to connect the two states.

Definition A.3.2 (Path-conservative scheme [64]). *Given a family of paths $\boldsymbol{\Psi}$, a numerical scheme is said to be $\boldsymbol{\Psi}$-conservative (path-conservative) if it can be written under the form*

$$\mathbf{Q}_i^{n+1} = \mathbf{Q}_i^n - \frac{\Delta t}{\Delta x}(\mathbf{D}^+_{i-\frac{1}{2}} + \mathbf{D}^-_{i+\frac{1}{2}}), \tag{A.31}$$

with

$$\mathbf{D}^{\pm}_{i+\frac{1}{2}} = \mathbf{D}^{\pm}(\mathbf{Q}_L, \mathbf{Q}_R), \tag{A.32}$$

where $\mathbf{Q}_L$ and $\mathbf{Q}_R$ are the left and right state with respect to $x_{i+\frac{1}{2}}$, $\mathbf{D}^-$ and $\mathbf{D}^+$ are two continuous functions satisfying

$$\mathbf{D}^{\pm}(\mathbf{Q}, \mathbf{Q}) = 0, \quad \forall \mathbf{Q} \in \Omega_q, \tag{A.33}$$

and

$$\mathbf{D}^-(\mathbf{Q}_L, \mathbf{Q}_R) + \mathbf{D}^+(\mathbf{Q}_L, \mathbf{Q}_R) = \mathbf{D}^-_{i+\frac{1}{2}} + \mathbf{D}^+_{i+\frac{1}{2}} = \int_0^1 \mathbf{M}(\boldsymbol{\Psi}(\mathbf{Q}_L, \mathbf{Q}_R, s))\frac{\partial \boldsymbol{\Psi}}{\partial s}(\mathbf{Q}_L, \mathbf{Q}_R, s)ds, \tag{A.34}$$

for every $\mathbf{Q}_L, \mathbf{Q}_R \in \Omega_q$.

See [64] to gain more information concerning the characteristics of a *path-conservative* scheme.

A.3.2 Well-balanced numerical schemes

Well-balanced schemes were originally motivated by the need to find numerical approximations to hyperbolic equations with source terms, to achieve equilibrium between flux spatial gradient and geometric source terms near the steady state. The present work is concerned with a numerical scheme in a class of methods in which the source term is considered by reformulating the original system into an augmented hyperbolic system with a modified eigenstructure (see Chapter 2.2).

Definition A.3.3 (Integral curve). *Let $\gamma_p(s)$ be a curve in phase space parametrized by a scalar parameter s. We define this curve to be an integral curve of the vector field $\mathbf{R}_p$ of system*

$$\partial_t \mathbf{Q} + \mathbf{M}(\mathbf{Q})\partial_x \mathbf{Q} = 0, \tag{A.35}$$

if at each point $\gamma_p(s)$, the tangent vector $\gamma_p'(s)$ to the curve is an eigenvector of $\mathbf{M}(\gamma_p(s))$ corresponding to the eigenvalue $\lambda_p(\gamma_p(s))$.

Furthermore, the expression for the integral curve gives rise to generalized Riemann invariants, which are functions of $\mathbf{Q}$ whose values are invariant along the integral curve $\gamma_p(s)$; see [44] for background.

Considering system (A.35), we have that steady state solutions are related to linearly degenerate fields marked with "$\lambda = 0$": as explained in [64], let in fact $\mathbf{Q}^{st}(x)$ be a regular steady state solution, we have that (A.35) becomes

$$\mathbf{A}(\mathbf{Q}^{st}(x)) \cdot \partial_x \mathbf{Q}^{st}(x) = 0 \quad \forall x \in \mathbb{R}. \tag{A.36}$$

If $\partial_x \mathbf{Q}^{st}(x) \neq 0$, then 0 is an eigenvalue of $\mathbf{A}(\mathbf{Q}^{st}(x))$ (i.e eigenvalues are λ such that $\mathbf{AR} = \lambda \mathbf{R}$, with $\mathbf{A}$ a $N \times N$ matrix and $\mathbf{R}$ an arbitrary right eigenvector) and $\partial_x \mathbf{Q}^{st}(x)$ is an associated

eigenvector. Therefore, $x \to \mathbf{Q}^{st}(x)$ can be interpreted as a parametrization of an integral curve of a linearly degenerate characteristic field whose corresponding eigenvalue takes the value 0 through the curve.

Let us also introduce the set Υ_{LD} of all integral curves γ_{LD}, associated with the LD field of $\mathbf{A}$ marked with "$\lambda = 0$".

Definition A.3.4 (Well-balanced numerical scheme [65]). *A numerical scheme of the form (A.31) for system (A.27) is said to be exactly well-balanced for $\gamma_{LD} \in \Upsilon_{LD}$ if, given any steady solution $\mathbf{Q}^{st}(x) \in \gamma_{LD}\ \forall x \in (x_l, x_r) \subset \mathbb{R}$ and initial conditions such that $\mathbf{Q}_i^n \in \gamma_{LD}\ \forall i \in [1, ..., I]$, where I is the number of cells used to discretize the spatial domain (x_l, x_r), then*

$$\mathbf{D}^-_{i+\frac{1}{2}} + \mathbf{D}^+_{i-\frac{1}{2}} = 0, \qquad \forall i \in [1, ..., I]. \tag{A.37}$$

The well-balanced property is also necessary for the correct numerical solution of unsteady problems.

A.4 The Parés-Muñoz-Godunov scheme

This method is presented in [66] and applied to non-conservative systems.

A.4.1 Path-conservative approach

This is a path-conservative scheme [64]. The path-conservative approach is already described in Appendix A.3 and is here briefly recalled.

The finite volume-type scheme for the non-conservative hyperbolic system

$$\partial_t \mathbf{Q} + \mathbf{M}(\mathbf{Q})\partial_x \mathbf{Q} = \mathbf{0}, \tag{A.38}$$

is

$$\mathbf{Q}_i^{n+1} = \mathbf{Q}_i^n - \frac{\Delta t}{\Delta x}(\mathbf{D}^+_{i-\frac{1}{2}} + \mathbf{D}^-_{i+\frac{1}{2}}); \tag{A.39}$$

where

$$\mathbf{Q}_i^n \approx \frac{1}{\Delta x}\int_{x_{i-\frac{1}{2}}}^{x_{i+\frac{1}{2}}} \mathbf{Q}(x, t^n)dx, \tag{A.40}$$

and

$$\mathbf{D}^{\pm}_{i+\frac{1}{2}} = \frac{1}{\Delta t}\int_{t^n}^{t^{n+1}} \mathbf{D}^{\pm}\left(\mathbf{Q}^-_{i+\frac{1}{2}}(t), \mathbf{Q}^+_{i+\frac{1}{2}}(t)\right) dt. \tag{A.41}$$

Here $\Delta x = x_{i+\frac{1}{2}} - x_{i-\frac{1}{2}}$, $\Delta t = t^{n+1} - t^n$, $\mathbf{Q}^{\pm}_{i+\frac{1}{2}}$ are limiting data states from left and right at cell interface $x_{i+\frac{1}{2}}$.

The fluctuations $\mathbf{D}^-_{i+\frac{1}{2}}$ and $\mathbf{D}^+_{i+\frac{1}{2}}$ are expected to satisfy the consistency condition

$$\mathbf{D}^-_{i+\frac{1}{2}}(\mathbf{Q}, \ldots, \mathbf{Q}) = \mathbf{0}\,, \quad \mathbf{D}^+_{i+\frac{1}{2}}(\mathbf{Q}, \ldots, \mathbf{Q}) = \mathbf{0} \tag{A.42}$$

and the compatibility condition

$$\mathbf{D}^-_{i+\frac{1}{2}} + \mathbf{D}^+_{i+\frac{1}{2}} = \int_0^1 \mathbf{M}(\mathbf{Q}(\mathbf{\Psi}(s; \mathbf{Q}_i^n, \mathbf{Q}_{i+1}^n))\frac{\partial}{\partial s}\mathbf{\Psi}(s; \mathbf{Q}_i^n, \mathbf{Q}_{i+1}^n)ds\,. \tag{A.43}$$

The path function $\boldsymbol{\Psi}(s;\mathbf{Q}_i^n,\mathbf{Q}_{i+1}^n)$, with $s\in[0,1]$, joins $\mathbf{Q}_i^n$ to $\mathbf{Q}_{i+1}^n$ and

$$\boldsymbol{\Psi}(0;\mathbf{Q}_i^n,\mathbf{Q}_{i+1}^n)=\mathbf{Q}_i^n\ ,\quad \boldsymbol{\Psi}(1;\mathbf{Q}_i^n,\mathbf{Q}_{i+1}^n)=\mathbf{Q}_{i+1}^n\ . \tag{A.44}$$

While many choices for the path $\boldsymbol{\Psi}(s;\mathbf{Q}_i^n,\mathbf{Q}_{i+1}^n)$ are available, here we assume the canonical path

$$\boldsymbol{\Psi}(s;\mathbf{Q}_i^n,\mathbf{Q}_{i+1}^n)=\mathbf{Q}_i^n+s(\mathbf{Q}_{i+1}^n-\mathbf{Q}_i^n)\ . \tag{A.45}$$

In analogy to conservative methods, which require an intercell numerical flux $\mathbf{F}_{i+\frac{1}{2}}$ to be determined, path-conservative methods are defined once the path $\boldsymbol{\Psi}(s;\mathbf{Q}_i^n,\mathbf{Q}_{i+1}^n)$ is specified and the fluctuations $\mathbf{D}^-_{i+\frac{1}{2}}$, $\mathbf{D}^+_{i+\frac{1}{2}}$ are determined.

A.4.2 The scheme

Parés and Muñoz [66] proposed a Godunov-type, path-conservative method that results from the following definitions for the fluctuations

$$\left.\begin{aligned}\mathbf{D}^-_{i+\frac{1}{2}}&=\int_0^1\mathbf{M}(\boldsymbol{\Psi}(s;\mathbf{Q}_i^n,\mathbf{Q}_{i+\frac{1}{2}}(0)))\frac{\partial}{\partial s}\boldsymbol{\Psi}(s,\mathbf{Q}_i^n,\mathbf{Q}_{i+\frac{1}{2}}(0))ds\ ,\\ \mathbf{D}^+_{i+\frac{1}{2}}&=\int_0^1\mathbf{M}(\boldsymbol{\Psi}(s;\mathbf{Q}_{i+\frac{1}{2}}(0),\mathbf{Q}_{i+1}^n))\frac{\partial}{\partial s}\boldsymbol{\Psi}(s,\mathbf{Q}_{i+\frac{1}{2}}(0),\mathbf{Q}_{i+1}^n)ds\ .\end{aligned}\right\} \tag{A.46}$$

Here $\mathbf{Q}_{i+\frac{1}{2}}(x/t)$ denotes the solution of the local Riemann problem

$$\left.\begin{aligned}&\partial_t\mathbf{Q}+\mathbf{M}(\mathbf{Q})\partial_x\mathbf{Q}=\mathbf{0}\ ,\\ &\mathbf{Q}(x,0)=\begin{cases}\mathbf{Q}_i^n & \text{if}\quad x<0\ ,\\ \mathbf{Q}_{i+1}^n & \text{if}\quad x<0\ .\end{cases}\end{aligned}\right\} \tag{A.47}$$

$\mathbf{Q}_{i+\frac{1}{2}}(0)$ is the Godunov state, the determination of which requires solving the Riemann problem (A.47) to determine $\mathbf{Q}_{i+\frac{1}{2}}(x/t)$ and a solution sampling procedure to find $\mathbf{Q}_{i+\frac{1}{2}}(0)$.

A Riemann solver for (A.47) is now required. The scheme just described will be denoted as the PMG scheme, for Parés, Muñoz and Godunov.

Implementing the PMG scheme. On the assumption that the Godunov state $\mathbf{Q}_{i+\frac{1}{2}}(0)$ is known, the implementation of the scheme proceeds as follows. Assuming the canonical paths (A.45) in (A.46) we have

$$\left.\begin{aligned}\boldsymbol{\Psi}(s;\mathbf{Q}_i^n,\mathbf{Q}_{i+\frac{1}{2}}(0))&=\mathbf{Q}_i^n+s[\mathbf{Q}_{i+\frac{1}{2}}(0)-\mathbf{Q}_i^n]\ ,\\ \boldsymbol{\Psi}(s;\mathbf{Q}_{i+\frac{1}{2}}(0),\mathbf{Q}_{i+1}^n)&=\mathbf{Q}_{i+\frac{1}{2}}(0)+s[\mathbf{Q}_{i+1}^n-\mathbf{Q}_{i+\frac{1}{2}}(0)]\ .\end{aligned}\right\} \tag{A.48}$$

Then, from (A.46) and (A.48) we have

$$\mathbf{D}^-_{i+\frac{1}{2}}=\widehat{\mathbf{M}}^-_{i+\frac{1}{2}}[\mathbf{Q}_{i+\frac{1}{2}}(0)-\mathbf{Q}_i^n]\ ;\quad \mathbf{D}^+_{i+\frac{1}{2}}=\widehat{\mathbf{M}}^+_{i+\frac{1}{2}}[\mathbf{Q}_{i+1}^n-\mathbf{Q}_{i+\frac{1}{2}}(0)]\ . \tag{A.49}$$

Here $\widehat{\mathbf{M}}^{-}_{i+\frac{1}{2}}$ and $\widehat{\mathbf{M}}^{+}_{i+\frac{1}{2}}$ are numerical approximations to respective integrals in (A.46), that is

$$\left.\begin{aligned}\widehat{\mathbf{M}}^{-}_{i+\frac{1}{2}} &\approx \int_0^1 \mathbf{M}(\mathbf{\Psi}(s;\mathbf{Q}^n_i,\mathbf{Q}_{i+\frac{1}{2}}(0)))ds\,,\\ \widehat{\mathbf{M}}^{+}_{i+\frac{1}{2}} &\approx \int_0^1 \mathbf{M}(\mathbf{\Psi}(s;\mathbf{Q}_{i+\frac{1}{2}}(0),\mathbf{Q}^n_{i+1}))ds\,.\end{aligned}\right\} \tag{A.50}$$

Using a Gaussian-Legendre rule to evaluate the integrals in (A.50) numerically we obtain

$$\left.\begin{aligned}\widehat{\mathbf{M}}^{-}_{i+\frac{1}{2}} &= \sum_{j=1}^{G}\omega_j\mathbf{M}\left(\mathbf{\Psi}(s_j;\mathbf{Q}^n_i,\mathbf{Q}_{i+\frac{1}{2}}(0))\right)\,,\\ \widehat{\mathbf{M}}^{+}_{i+\frac{1}{2}} &= \sum_{j=1}^{G}\omega_j\mathbf{M}\left(\mathbf{\Psi}(s_j;\mathbf{Q}_{i+\frac{1}{2}}(0),\mathbf{Q}^n_{i+1})\right)\,.\end{aligned}\right\} \tag{A.51}$$

For the integration points and weights, recommended choices are

$$s_1=\frac{1}{2}-\frac{\sqrt{15}}{10}\,,s_2=\frac{1}{2}\,,s_3=\frac{1}{2}+\frac{\sqrt{15}}{10}\,,\omega_1=\frac{5}{18}\,,\omega_2=\frac{8}{18}\,,\omega_3=\frac{5}{18}\,. \tag{A.52}$$

The scheme, as formulated, is rather general. The specificity of the problem of interest will enter in resolving the pending task, namely finding a Riemann solver to determine the Godunov state $\mathbf{Q}_{i+\frac{1}{2}}(0)$ for use in (A.49) and (A.51). In particular, we use the two-rarefaction and the linearized two-rarefaction solvers presented in Section 7.1.2.

A.5 Well balanced path-conservative DOT Riemann solver

The DOT Riemann solver was put forward in [24] as a modified version of the Osher–Solomon Riemann solver [63] for a conservative hyperbolic system. The DOT scheme has also been extended in [23] to deal with non-conservative hyperbolic systems. Here we recall the finite volume, path-conservative, DOT solver for non-conservative systems presented in [56, 81], adapted for a general constant momentum correction coefficient as presented in [82]. The path-conservative approach is already described in Appendix A.3.

The scheme for the non-conservative hyperbolic system

$$\partial_t\mathbf{Q}+\mathbf{M}(\mathbf{Q})\partial_x\mathbf{Q}=\mathbf{0}, \tag{A.53}$$

is

$$\mathbf{Q}^{n+1}_i=\mathbf{Q}^n_i-\frac{\Delta t}{\Delta x}(\mathbf{D}^{+}_{i-\frac{1}{2}}+\mathbf{D}^{-}_{i+\frac{1}{2}}); \tag{A.54}$$

where

$$\mathbf{Q}^n_i\approx\frac{1}{\Delta x}\int_{x_{i-\frac{1}{2}}}^{x_{i+\frac{1}{2}}}\mathbf{Q}(x,t^n)dx, \tag{A.55}$$

and

$$\mathbf{D}^{\pm}_{i+\frac{1}{2}}=\frac{1}{\Delta t}\int_{t^n}^{t^{n+1}}\mathbf{D}^{\pm}\left(\mathbf{Q}^{-}_{i+\frac{1}{2}}(t),\mathbf{Q}^{+}_{i+\frac{1}{2}}(t)\right)dt. \tag{A.56}$$

Here $\Delta x = x_{i+\frac{1}{2}} - x_{i-\frac{1}{2}}$, $\Delta t = t^{n+1} - t^n$, $\mathbf{Q}^{\pm}_{i+\frac{1}{2}}$ are limiting data states from left and right at cell interface $x_{i+\frac{1}{2}}$.

NUMERICAL FLUCTUATIONS

Fluctuations in the DOT scheme, as proposed in [23] are computed as

$$\begin{aligned}\mathbf{D}^{\pm}\left(\mathbf{Q}^{-}_{i+\frac{1}{2}}(t), \mathbf{Q}^{+}_{i+\frac{1}{2}}(t)\right) = \\ = \frac{1}{2}\int_0^1 \left[\mathbf{M}(\mathbf{\Psi}(\mathbf{Q}^{-}_{i+\frac{1}{2}}(t), \mathbf{Q}^{+}_{i+\frac{1}{2}}(t), s)) \pm \left|\mathbf{M}(\mathbf{\Psi}(\mathbf{Q}^{-}_{i+\frac{1}{2}}(t), \mathbf{Q}^{+}_{i+\frac{1}{2}}(t), s))\right|\right] \frac{\partial \mathbf{\Psi}}{\partial s} ds,\end{aligned} \tag{A.57}$$

with the absolute value of a matrix defined as

$$|\mathbf{M}| = \mathbf{R}|\mathbf{\Lambda}|\mathbf{R}^{-1}, \qquad |\mathbf{\Lambda}| = diag(|\lambda_1|, |\lambda_2|, ...|\lambda_N|), \tag{A.58}$$

where $\mathbf{R}$ is the matrix of right eigenvectors of $\mathbf{M}$, and $\mathbf{R}^{-1}$ is its inverse.
Fluctuations in the DOT solver using the 3-points Gauss quadrature rule proposed in [23] are

$$\begin{aligned}\mathbf{D}^{\pm}\left(\mathbf{Q}^{-}_{i+\frac{1}{2}}(t), \mathbf{Q}^{+}_{i+\frac{1}{2}}(t)\right) = \\ = \frac{1}{2}\left(\sum_{j=1}^{3} \omega_j \left\{\mathbf{M}(\mathbf{\Psi}(\mathbf{Q}^{-}_{i+\frac{1}{2}}(t), \mathbf{Q}^{+}_{i+\frac{1}{2}}(t), s_j)) \pm \mid \mathbf{M}(\mathbf{\Psi}(\mathbf{Q}^{-}_{i+\frac{1}{2}}(t), \mathbf{Q}^{+}_{i+\frac{1}{2}}(t), s_j)) \mid \left.\frac{\partial \mathbf{\Psi}}{\partial s}\right|_{s_j}\right\}\right),\end{aligned} \tag{A.59}$$

in which w_j and s_j are the *j-th* weight and Gaussian point coordinate of a quadrature rule with 3 points.

INTEGRATION PATH IN PHASE-PLANE

The segment path

$$\mathbf{\Psi}(\mathbf{Q}_L, \mathbf{Q}_R, s) = \mathbf{Q}_L + s(\mathbf{Q}_R - \mathbf{Q}_L), \quad \text{with } 0 \leq s \leq 1, \tag{A.60}$$

proposed in [64], has been widely used in the numerical solution of several physical problems involving both conservative and non-conservative hyperbolic systems. Early numerical experiments on the application of the DOT scheme to system (A.53) using the segment path (A.60), showed the inability of the scheme to preserve stationary solutions, that is, solutions for which $u(x,t) = 0$. The reason can be deduced from the analysis of the Riemann invariants associated with the linearly degenerate (LD) characteristic field marked with "$\lambda = 0$" in case of $u(x,t) = 0$, $\forall x \in \mathbb{R}$, $\forall t > 0$ [56, 81].

Proposition A.5.1 (Jump conditions across the stationary contact discontinuity associated with eigenvalues $\lambda_2 = \lambda_3 = \lambda_4 = 0$, in case of stationary solutions ($u = 0$))**.** *Across the stationary contact discontinuity the following relations hold*

$$Au = 0, \qquad \psi + p_e = constant. \tag{A.61}$$

Proof. Following the method presented in [81], we consider matrix $\mathbf{M}$ in (2.182) for the case $u(x,t) = 0$, i.e

$$\mathbf{M} = \begin{bmatrix} 0 & 1 & 0 & 0 & 0 & 0 \\ c^2 & 0 & \frac{A}{\rho}\psi_K & \frac{A}{\rho}\psi_{A_0} & \frac{A}{\rho} & 0 \\ 0 & 0 & 0 & 0 & 0 & 0 \\ 0 & 0 & 0 & 0 & 0 & 0 \\ 0 & 0 & 0 & 0 & 0 & 0 \\ 0 & \phi & 0 & 0 & 0 & 0 \end{bmatrix}. \tag{A.62}$$

The proof from now on is the same as that of Proposition 2.2.6. □

As just presented, through the linearly degenerate (LD) field associated with "$\lambda = 0$" eigenvalue of $\mathbf{M}$ in (2.182), in case of stationary solutions $u(x,t) = 0$, $\forall\, x \in \mathbb{R}$, $\forall t > 0$, we have

$$p = \psi + p_e = \bar{\Gamma}_1^{LD}, \quad 0 = q = \bar{\Gamma}_2^{LD}, \tag{A.63}$$

where $\bar{\Gamma}_{1,2}^{LD}$ are constant values of total pressure and volumetric flow rate ($q = Au$). There is a non-linear dependence between K and A. In order to accommodate changes in K, A_0 or p_e, while preserving constancy of the right-hand side in the first equation of (A.63), the cross-sectional area A will have to change non-linearly. In other words, the use of the segment path (A.60) is not adequate for the first variable A. In this Chapter, we adopt the path proposed by Müller and Toro [56]. Such path only preserves stationary solutions exactly. This choice is justified by the fact that exact well-balanced schemes for stationary solutions solve unsteady problems in a satisfactory manner.

$$\mathbf{\Psi}(\mathbf{Q}^-_{i+\frac{1}{2}}(t), \mathbf{Q}^+_{i+\frac{1}{2}}(t), s) = \begin{bmatrix} \overline{A}(s) \\ \overline{q}(s) \\ \overline{K}(s) \\ \overline{A_0}(s) \\ \overline{p_e}(s) \\ \overline{A\phi}(s) \end{bmatrix} = \begin{bmatrix} \overline{\psi}_K(s)^{-1} \\ q^-_{i+\frac{1}{2}} + s(q^+_{i+\frac{1}{2}} - q^-_{i+\frac{1}{2}}) \\ K^-_{i+\frac{1}{2}} + s(K^+_{i+\frac{1}{2}} - K^-_{i+\frac{1}{2}}) \\ A^-_{0,i+\frac{1}{2}} + s(A^+_{0,i+\frac{1}{2}} - A^-_{0,i+\frac{1}{2}}) \\ p^-_{e,i+\frac{1}{2}} + s(p^+_{e,i+\frac{1}{2}} - p^-_{e,i+\frac{1}{2}}) \\ A\phi^-_{i+\frac{1}{2}} + s(A\phi^+_{i+\frac{1}{2}} - A\phi^-_{i+\frac{1}{2}}) \end{bmatrix}, \tag{A.64}$$

where $\overline{\psi}_K$ is defined as

$$\overline{\psi}_K(s) = \frac{\overline{\Gamma}(s) - \overline{p_e}(s)}{\overline{K}(s)}, \tag{A.65}$$

and $\overline{\Gamma}(s)$ is

$$\overline{\Gamma}(s) = \overline{\Gamma}^{1,-}_{LD,i+\frac{1}{2}} + s\left(\overline{\Gamma}^{1,+}_{LD,i+\frac{1}{2}} - \overline{\Gamma}^{1,-}_{LD,i+\frac{1}{2}}\right). \tag{A.66}$$

Once that $\overline{\psi}_K(s)$ is known, we compute $\overline{A}(s)$ from the second of (2.179) using a globally convergent Newton-Raphson method for $n \neq 0$. It is possible to verify that a solution always exists for $A > 0$ and is unique. When $n = 0$ the solution is explicit.

Regarding $\dfrac{\partial \mathbf{\Psi}}{\partial s}$, derivatives for most variables are easily computed, besides that for $\bar{A}(s)$ is computed as

$$\frac{\partial \overline{A}}{\partial s}(s_j) = \left(\frac{\partial \bar{\psi}_K}{\partial s}(s_j) - \frac{\partial \psi_K}{\partial \bar{A}_0}\bigg|_{s=s_j} \frac{\partial \bar{A}_0}{\partial s}(s_j)\right)\left(\frac{\partial \psi_K}{\partial \bar{A}}\bigg|_{s=s_j}\right)^{-1}. \tag{A.67}$$

WELL-BALANCED PROPERTIES

Well-balanced schemes were originally motivated by the need to find numerical approximations to hyperbolic equations with source terms, to achieve equilibrium between flux spatial gradient and geometric source terms near the steady state.

Definition A.5.1 (Well-balanced numerical scheme [65]). *Being Υ_{LD} the set of all integral curves γ_{LD}, associated with the linearly degenerate (LD) field of matrix $\boldsymbol{M}$ marked with "$\lambda = 0$" (see [81] for further explanations), a numerical scheme of the form (A.54) for system (A.53) is said to be exactly well-balanced for $\gamma_{LD} \in \Upsilon_{LD}$ if, given any steady solution $\mathbf{Q}^{st}(x) \in \gamma_{LD}$ $\forall x \in (x_l, x_r) \subset \mathbb{R}$ and initial conditions such that $\mathbf{Q}_i^n \in \gamma_{LD}$ $\forall i \in [1, ..., I]$, where I is the number of cells used to discretize the spatial domain (x_l, x_r), then*

$$\mathbf{D}^-_{i+\frac{1}{2}} + \mathbf{D}^+_{i-\frac{1}{2}} = \mathbf{0}, \qquad \forall i \in [1, ..., I]. \tag{A.68}$$

The well-balanced property is also necessary for the correct numerical solution of unsteady problems.

Proposition A.5.2. *The numerical scheme (A.54) with fluctuations (A.59) and path (A.64) fulfils well-balanced property (A.68) for stationary solutions, i.e. when $u(x,t) = 0$.*

Proof. The proof is similar to the analogue in [81] considering that now, matrix $\mathbf{M}(\mathbf{\Psi})$ is a 5×5 matrix. □

For a first order method we have that

$$\mathbf{D}^{\pm}_{i+\frac{1}{2}} = \mathbf{D}^{\pm}\left(\mathbf{Q}_i^n, \mathbf{Q}_{i+1}^n\right). \tag{A.69}$$

A.6 A CONSERVATIVE VERSION OF PATH-CONSERVATIVE DOT RIEMANN SOLVER

This scheme was presented in [24] and will be here briefly recalled. The path-conservative approach is already described in Appendix A.3.

Given the conservative hyperbolic system

$$\partial_t \mathbf{Q} + \partial_x \mathbf{F}(\mathbf{Q}) = \mathbf{0}, \tag{A.70}$$

integrating (A.70) in space and time in the control volume $[x_{i-\frac{1}{2}}, x_{i+\frac{1}{2}}] \times [t^n, t^{n+1}]$, leads to

$$\mathbf{Q}_i^{n+1} = \mathbf{Q}_i^n - \frac{\Delta t}{\Delta x}(\mathbf{F}_{i+\frac{1}{2}} - \mathbf{F}_{i-\frac{1}{2}}); \tag{A.71}$$

where

$$\mathbf{Q}_i^n \approx \frac{1}{\Delta x}\int_{x_{i-\frac{1}{2}}}^{x_{i+\frac{1}{2}}} \mathbf{Q}(x, t^n)dx, \tag{A.72}$$

and

$$\mathbf{F}_{i+\frac{1}{2}} = \frac{1}{\Delta t}\int_{t^n}^{t^{n+1}} \mathbf{F}(\mathbf{Q}(x_{i+\frac{1}{2}}, t))dt. \tag{A.73}$$

In our case (A.73) is

$$\mathbf{F}_{i+\frac{1}{2}} = \frac{1}{2}\left(\mathbf{F}(\mathbf{Q}_i) + \mathbf{F}(\mathbf{Q}_{i+1})\right) - \frac{1}{2}\int_0^1 |\mathbf{J}(\mathbf{\Psi}(\mathbf{Q}_i(t), \mathbf{Q}_{i+1}(t), s))|\,\frac{\partial \mathbf{\Psi}}{\partial s}ds, \tag{A.74}$$

with the absolute value of a matrix defined as

$$|\mathbf{J}| = \mathbf{R}|\boldsymbol{\Lambda}|\mathbf{R}^{-1}, \qquad |\boldsymbol{\Lambda}| = diag(|\lambda_1|, |\lambda_2|, ...|\lambda_N|), \tag{A.75}$$

where $\mathbf{J}$ is the Jacobian of the system, $\mathbf{R}$ is the matrix of right eigenvectors of $\mathbf{J}$, and $\mathbf{R}^{-1}$ is its inverse, while λ_k are the eigenvalues of $\mathbf{J}$.

(A.74) with the segment path

$$\boldsymbol{\Psi}(\mathbf{Q}_L, \mathbf{Q}_R, s) = \mathbf{Q}_L + s(\mathbf{Q}_R - \mathbf{Q}_L), \quad \text{with } 0 \leq s \leq 1, \tag{A.76}$$

becomes

$$\mathbf{F}_{i+\frac{1}{2}} = \frac{1}{2}\left(\mathbf{F}(\mathbf{Q}_i) + \mathbf{F}(\mathbf{Q}_{i+1})\right) - \frac{1}{2}\left(\int_0^1 |\mathbf{J}(\boldsymbol{\Psi}(\mathbf{Q}_i(t), \mathbf{Q}_{i+1}(t), s))|\, ds\right)(\mathbf{Q}_{i+1} - \mathbf{Q}_i), \tag{A.77}$$

in which w_j and s_j are the *j-th* weight and Gaussian point coordinate of a quadrature rule with 3 points.

Chapter B

Newton-Raphson methods

In this Appendix we report the Newton-Raphson schemes applied in this Thesis to compute both the numerical schemes and the exact solutions here presented.

B.1 Newton-Raphson method for the numerical computation of the exact solution of the Riemann problem for the non-conservative 1D blood flow equations

Here we present the Newton-Raphson method used to solve (2.254). The others are similar in structure, with the same tolerances. This method is written in Python language.

```
# ######################################################################
# Newton-Raphson method
# ######################################################################

#initial value for Xstar:
AsL=AL
uSL=0
AsR=AR
uSR=0
Xstar=np.array([AsL,uSL,AsR,uSR])
for i in range(50):
        # calculate fun=np.array([f1,f2.f3,f4]) and the jacobian of fun
        fun=self.funct(Xstar,QL,QR)
        jac=self.jacfunct(Xstar,QL,QR)
        epsi = 1.
        for i2 in range(50):
                XstarA =  Xstar- epsi*scipy.linalg.solve(jac,fun)
                if XstarA[0]>0 and XstarA[2]>0:
                        fAux=self.funct(XstarA,QL,QR)
                        if np.linalg.norm(fAux,np.inf)<=np.linalg.norm(fun,np.inf):
                                break
                        else:
                                epsi *= 0.8
                else:
                        epsi *= 0.8
        XstarOld=np.copy(Xstar)
        Xstar = Xstar - epsi*scipy.linalg.solve(jac,fun)
        if (np.abs(Xstar[0]-XstarOld[0])/((Xstar[0]+XstarOld[0])/2.))<1e-8 and
        (np.abs(Xstar[2]-XstarOld[2])/((Xstar[2]+XstarOld[2])/2.))<1e-8:
                break
        if i==(50-1):
                print('no convergence')
                exit(-1)

return Xstar
```

B.2 Newton-Raphson method for the numerical computation of the exact solution of the Riemann problem for the pressure system

Here we present the Newton-Raphson method used to solve (5.105) and (5.177). This method is written in Python language.

```
# ######################################################################
# Newton-Raphson method
# ######################################################################

#c is the wave speed (2.14)
cL=c(AL)
cR=c(AR)
epsi = 1.e-13

#choose an initial point for As between the two-rar and the mean
aS0=(AL*cL + AR*cR + qL - qR)/(cL + cR)
if aS0>0:
        aS=aS0
else:
        aS=(aL+aR)/2.


fun=100.
for i in range(50):
        fun = self.ExactRPpressFunction(aS, aL, aR, qL, qR)
        fp = self.ExactRPpressFunction(aS+epsi, aL, aR, qL, qR)
        fm = self.ExactRPpressFunction(aS-epsi, aL, aR, qL, qR)
        df = (fp-fm)/(2.*self.epsi)
        alpha = 1.
        for i2 in range(50):
                aAux = aS - alpha*fun/df
                if aAux > 0.:
                        fAux = self.ExactRPpressFunction(aAux, aL, aR, qL, qR)
                        if np.abs(fAux) <= np.abs(fun):
                                break
                        else:
                                alpha *= 0.8
                else:
                        alpha *= 0.8
        aSOld=aS
        aS = aS - alpha*fun/df
        if np.abs(np.abs(aS-aSOld)/((aS+aSOld)/2.))<1e-7:
                break
# computing fL and fR
fL = self.fK(aS, aL, x)
fR = self.fK(aS, aR, x)
qS = (qL+qR+fR-fL)/2.

return [aS,qS]
```

B.3 Newton-Raphson method for the splitting schemes for the conservative 1D blood flow model

Here we present the Newton-Raphson method used to solve (6.4). The others are similar in structure, with the same tolerances. This method is written in the Python language.

```
# ################################################
# Newton-Raphson method
# ################################################

#initial value for As:
```

```
As=AL
for i in range(50):
        #functTR is described in (6.4)
        #c is the wave speed (2.14)
        fun=self.functTR(As, AL, qS, qL)
        df=self.c(As)
        alpha = 1.
        for i2 in range(50):
                aAux = As - alpha*fun/df
                if aAux > 0.:
                        fAux=self.functTR(aAux, AL, qS, qL)
                        if np.abs(fAux) <= np.abs(fun):
                                break
                        else:
                                alpha *= 0.8
                else:
                        alpha *= 0.8
        AsOld=As
        As = As - alpha*fun/df
        if np.abs(np.abs(As-AsOld)/((As+AsOld)/2.))<1e-7:
                break
        if i==(50-1):
                print('No_convergence')
                exit(-1)
return[As,qS]
```

B.4 Newton-Raphson method for the splitting schemes for the non-conservative 1D blood flow model

Here we present the Newton–Raphson method used to solve (7.35). The others are similar in structure, with the same tolerances. This method is written in the Python language.

```
# ################################################
# Newton-Raphson method
# ################################################
#initial values
Xstar=np.zeros(4)
Xstar[0]=aL
Xstar[1]=qL
Xstar[2]=aR
Xstar[3]=qR

for i in range(50):
        #fun=np.array([f1,f2,f3,f4]) is described in (7.35)
        fun=self.FuncStar(Xstar[0], Xstar[1], Xstar[2], Xstar[3],QL,QR)
        #jf is the jacobian of f
        jf=self.JacobFuncStar(Xstar[0], Xstar[1], Xstar[2], Xstar[3],QL,QR)

        alpha = 1.
        for i2 in range(50):
                XstarA= Xstar - alpha*(scipy.linalg.solve(jf,fun))
                if XstarA[0]>0 and XstarA[2]>0:
                        fAux=self.FuncStar(XstarA[0], XstarA[1], XstarA[2], XstarA[3],QL,QR)
                        if  (np.linalg.norm(fAux,np.inf)<np.linalg.norm(fun,np.inf)):
                                break
                        else:
                                alpha *= 0.8
                else:
                        alpha *= 0.8
        XstarOld= np.copy(Xstar)
        Xstar= Xstar  - alpha*(scipy.linalg.solve(jf,fun))
        if (np.abs(Xstar[0]-XstarOld[0])/((Xstar[0]+XstarOld[0])/2.))<1e-6 and
        (np.abs(Xstar[2]-XstarOld[2])/((Xstar[2]+XstarOld[2])/2.))<1e-6:
                break
        if i==(49):
                print('Newton does not converge')
                exit(-1)
aSL=Xstar[0]
qSL=Xstar[1]
```

```
aSR=Xstar[2]
qSR=Xstar[3]
```

BIBLIOGRAPHY

[1] J. Alastruey, K.H. Parker, J. Peiró, and S.J. Sherwin. "Lumped Parameter Outflow Models for 1-D Blood Flow Simulations: Effect on Pulse Waves and Parameter Estimation". In: *Commun. Comput. Phys.* 4.2 (2008), pp. 317–336.

[2] D.C. Alpini, P.M. Bavera, A. Hahn, and V. Mattei. "Chronic cerebrospinal venous insufficiency (CCSVI) in Ménière's disease, case or cause?" In: *Science Med.* 4 (2013), pp. 9–15.

[3] A. Bermudez and M.E. Vázquez. "Upwind methods for hyperbolic conservation laws with source terms". In: *Comput. Fluids* 23.8 (1994), pp. 1049–1071. DOI: 10.1016/0045-7930(94)90004-3.

[4] A.L. Bernard, W. Hunt, W. Timlake, and E. Varley. "A Theory of Fluid Flow in Compliant Tubes". In: *Biophys. J.* 6.6 (1966), pp. 717–724. DOI: 10.1016/S0006-3495(66)86690-0.

[5] D. Bessems, C.G. Giannopapa, M.C.M. Rutten, and F.N. van de Vosse. "Experimental validation of a time-domain-based wave propagation model of blood flow in viscoelastic vessels". In: *J. Biomech.* 41.2 (2008), pp. 284–291. DOI: 10.1016/j.jbiomech.2007.09.014.

[6] D. Bessems, M. Rutten, and F. van de Vosse. "A wave propagation model of blood flow in large vessels using an approximate velocity profile function". In: *J. Fluid Mech.* 580 (2007), pp. 145–168. DOI: 10.1017/S0022112007005344.

[7] P.J. Blanco and R.A. Feijóo. "A dimensionally-heterogeneous closed-loop model for the cardiovascular system and its applications". In: *Med. Eng. Phys.* 35.5 (2013), pp. 652–667. DOI: 10.1016/j.medengphy.2012.07.011.

[8] P.J. Blanco, S.M. Watanabe, and R.A. Feijóo. "Identification of vascular territory resistances in one-dimensional hemodynamics simulations". In: *J. Biomech.* 45(12) (2012), pp. 2066–2073. DOI: 10.1016/j.jbiomech.2012.06.002.

[9] P.J. Blanco, S.M. Watanabe, M.A.R.F. Passos, P.A. Lemos, and R.A. Feijóo. "An Anatomically Detailed Arterial Network Model for One-Dimensional Computational Hemodynamics". In: *IEEE Trans. Biomed. Eng.* 62.2 (2015), pp. 736–753. DOI: 10.1109/TBME.2014.2364522.

[10] E. Boileau, P. Nithiarasu, P.J. Blanco, L.O. Müller, F. Fossan, L.R. Hellevik, W.P. Donders, W. Huberts, M. Willemet, and J. Alastruey. "A Benchmark Study of Numerical Schemes for One-Dimensional Arterial Blood Flow Modelling". In: *Int. J. Numer. Method Biomed. Eng.* 31.10 (2015). DOI: 10.1002/cnm.2732.

[11] R. Borsche and J. Kall. "ADER schemes and high order coupling on networks of hyperbolic conservation laws". In: *J. Comput. Phys.* 273 (2014), pp. 658–670. DOI: 10.1016/j.jcp.2014.05.042.

[12] A. Bressan. *Hyperbolic systems of conservation laws*. ISBN: 9780198507000. Oxford university press, 2000.

[13] B.S. Brook, S.A.E.G. Falle, and T.J. Pedley. "Numerical solutions for unsteady gravity-driven flows in collapsible tubes: evolution and roll-wave instability of a steady state". In: *J. Fluid Mech.* 396 (1999), pp. 223–256. DOI: 10.1017/S0022112099006084.

[14] A. Bruno, L. Califano, D. Mastrangelo, M. De Vizia, B. Benedetto, and F. Salafia. "Chronic cerebrospinal venous insufficiency in Ménière's Disease: diagnosis and treatment". In: *Veins and Lymphatics* 3.3 (2014). DOI: 10.4081/vl.2014.3854.

[15] S. Čanić and E.H. Kim. "Mathematical analysis of the quasilinear effects in a hyperbolic model blood flow through compliant axi-symmetric vessels". In: *Math. Methods Appl. Sci.* 26.14 (2003), pp. 1161–1186. DOI: 10.1002/mma.407.

[16] M. J. Castro, A.P. Milanés, and C. Parés. "Well-balanced numerical schemes based on a Generalized Hydrostatic Reconstruction technique". In: *Math. Models Methods Appl. Sci.* 17.12 (2007), pp. 2055–2113. DOI: 10.1142/S021820250700256X.

[17] I-L. Chern. "Local and Global Interaction for Nongenuinely Nonlinear Hyperbolic Conservation Laws". In: *Indiana Univ. Math. J.* 49.3 (2000), pp. 1199–1227.

[18] C. Contarino, E.F. Toro, G.I. Montecinos, R. Borsche, and J. Kall. "Junction-Generalized Riemann Problem for stiff hyperbolic balance laws in networks: An implicit solver and ADER schemes". In: *J. Comput. Phys.* 315 (2016), pp. 409–433. DOI: 10.1016/j.jcp.2016.03.049.

[19] P. Crosetto, P. Reymond, S. Deparis, D. Kontaxakis, N. Stergiopulos, and A. Quarteroni. "Fluid–structure interaction simulation of aortic blood flow". In: *Comput. Fluids* 43.1 (2011), pp. 46–57. DOI: 10.1016/j.compfluid.2010.11.032.

[20] C.M. Dafermos. *Hyperbolic conservation laws in continuum physics-Third edition*. Springer, 2010. DOI: 10.1007/978-3-642-04048-1.

[21] G. Dal Maso, P.H. LeFloch, and F. Murat. "Definition and weak stability of nonconservative products". In: *J. Math. Pures Appl.* 74 (1995), pp. 483–548.

[22] O. Delestre and P.Y. Lagree. "A well-balanced finite volume scheme for blood flow simulation". In: *Int. J. Numer. Methods Fluids* 72 (2012), pp. 177–205. DOI: 10.1002/fld.3736.

[23] M. Dumbser and E.F. Toro. "A simple extension of the Osher Riemann solver to non-conservative hyperbolic systems". In: *J Sci Comput* 48 (2011), pp. 70–88. DOI: 10.1007/s10915-010-9400-3.

[24] M. Dumbser and E.F. Toro. "On Universal Osher-Type Schemes for General Nonlinear Hyperbolic Conservation Laws". In: *Commun. Comput. Phys.* 10.3 (2011), pp. 635–671. DOI: 10.4208/cicp.170610.021210a.

[25] R. Filipo, F. Ciciarello, G. Attanasio, P. Mancini, E. Covelli, L. Agati, F. Fedele, and M. Viccaro. "Chronic cerebrospinal venous insufficiency in patients with Ménière's disease". In: *Eur. Arch. Otorhinolaryngol.* 272.1 (2015), pp. 77–82. DOI: 10.1007/s00405-013-2841-1.

[26] L. Formaggia, J.F. Gerbeau, F. Nobile, and A. Quarteroni. "On the coupling of 3D and 1D Navier–Stokes equations for flow problems in compliant vessels". In: *Comput. Methods Appl. Mech. Eng.* 191.6-7 (2001), pp. 561–582. DOI: 10.1016/S0045-7825(01)00302-4.

[27] L. Formaggia, D. Lamponi, and A. Quarteroni. "One-dimensional models for blood flow in arteries". In: *J. Eng. Math.* 47 (2003), pp. 251–276. DOI: 10.1023/B:ENGI.0000007980.01347.29.

[28] L. Formaggia, A. Quarteroni, and A. Veneziani. *Cardiovascular Mathematics. Modeling and simulation of the circulatory system*. Springer, 2009. DOI: 10.1007/978-88-470-1152-6.

[29] L. Formaggia, A. Quarteroni, and C. Vergara. "On the physical consistency between three-dimensional and one-dimensional models in haemodynamics". In: *J. Comput. Phys.* 244 (2013), pp. 97–112. DOI: 10.1016/j.jcp.2012.08.001.

[30] A.R. Ghigo, O. Delestre, J.M. Fullana, and P.Y. Lagrée. "Low-Shapiro Hydrostatic Reconstruction Technique for Blood Flow Simulation in Large Arteries with Varying Geometrical and Mechanical Properties". In: *J. Comput. Phys.* 331 (2017), pp. 108–136. DOI: 10.1016/j.jcp.2016.11.032.

[31] B. Ghitti, E.F. Toro, and L.O. Müller. "Nonlinear lumped-parameter models for blood flow simulations in networks of vessels". In: *ESAIM. M2AN* 56.5 (2022), pp. 1579–1627. DOI: 10.1051/m2an/2022052.

[32] J. Glimm. "Solution in the large for nonlinear hyperbolic systems of equations". In: *Comm. Pure. Appl. Math.* 18 (1965), pp. 697–715. DOI: 10.1002/cpa.3160180408.

[33] E. Godlewski and P.A. Raviart. *Numerical Approximation of Hyperbolic Systems of Conservation Laws*. Springer, 2021. DOI: 10.1007/978-1-0716-1344-3.

[34] S.K. Godunov. "Finite difference method for numerical computation of discontinuous solutions of the equations of fluid dynamics". In: *Mat. Sb.* 47 (1959), pp. 271–306.

[35] J.M. Greenberg, A.Y. LeRoux, R. Baraille, and A. Noussair. "Analysis and Approximation of Conservation Laws with Source Terms". In: *SIAM J. Numer. Anal.* 34.5 (1997), pp. 1980–2007. DOI: 10.1137/S0036142995286751.

[36] L. Grinberg, E. Cheever, T. Anor, J.R. Madsen, and G.E. Karniadakis. "Modeling Blood Flow Circulation in Intracranial Arterial Networks: A Comparative 3D/1D Simulation Study". In: *Ann Biomed Eng* 39 (2011), pp. 297–309. DOI: 10.1007/s10439-010-0132-1.

[37] E.M. Haacke, W. Feng, D. Utriainen, G. Trifan, Z. Wu, Z. Latif, Y. Katkuri, J. Hewett, and D. Hubbard. "Patients with Multiple Sclerosis with Structural Venous Abnormalities on MR Imaging Exhibit an Abnormal Flow Distribution of the Internal Jugular Veins". In: *J. Vasc. Interv. Radiol.* 23.1 (2012), pp. 60–68. DOI: 10.1016/j.jvir.2011.09.027.

[38] E. Han, G. Warnecke, E. F. Toro, and A. Siviglia. *On Riemann Solutions to Weakly Hyperbolic Systems: Part 2. Modelling Supercritical Flows in Arteries*. Technical Report NI15004NPA. Isaac Newton Institute for Mathematical Sciences, University of Cambridge, 2015.

[39] E. Han, G. Warnecke, E.F. Toro, and A. Siviglia. *On Riemann Solutions to Weakly Hyperbolic Systems: Part 1. Modelling Subcritical Flows in Arteries*. Technical Report NI15003NPA. Isaac Newton Institute for Mathematical Sciences, University of Cambridge, 2015.

[40] T. Hughes and J. Lubliner. "On the one-dimensional theory of blood flow in the larger vessels". In: *Math. Biosci.* 18 (1973), pp. 161–170. DOI: 10.1016/0025-5564(73)90027-8.

[41] P.J. Hunter. *Numerical simulation of arterial blood flow, Master's thesis*. The University of Auckland, Auckland, 1972.

[42] P.D. Lax. *Hyperbolic Systems of Conservation Laws and the Mathematical Theory of Shock Waves*. SIAM, Society for Industrial and Applied Mathematics, 1973. DOI: 10.1137/1.9781611970562.

[43] B. van Leer. *Flux Vector splitting for the Euler equations*. Tech. rep. ICASE, 1982.

[44] R.J. Leveque. *Numerical Methods for Conservation Laws*. Birkhäuser Verlag, 1999. DOI: 10.1007/978-3-0348-5116-9.

[45] G. Li, O. Delestre, and L. Yuan. "Well-Balanced Discontinuous Galerkin Method and Finite Volume WENO Scheme Based on Hydrostatic Reconstruction for Blood Flow Model in Arteries". In: *Int. J. Numer. Methods Fluids* 86.7 (2018), pp. 491–508. DOI: 10.1002/fld.4463.

[46] F.Y. Liang, S. Takagi, R. Himeno, and H. Liu. "Biomechanical characterization of ventricular–arterial coupling during aging: A multi-scale model study". In: *J. Biomech.* 42.6 (2009), pp. 692–704. DOI: 10.1016/j.jbiomech.2009.01.010.

[47] M.S. Liou and C.J. Steffen. "A New Flux Splitting Scheme". In: *J. Comput. Phys.* 107.1 (1993), pp. 23–39. DOI: 10.1006/jcph.1993.1122.

[48] M. Liu, H. Xu, Y. Wang, Y. Zhong, S. Xia, D. Utriainen, T. Wang, and E. M. Haacke. "Patterns of Chronic Venous Insufficiency in the Dural Sinuses and Extracranial Draining Veins and their Relationship with White Matter Hyperintensities for Patients with Parkinson's Disease". In: *J. Vasc. Surg.* 61.16 (2015), pp. 1511–1520. DOI: 10.1016/j.jvs.2014.02.021.

[49] T.P. Liu. "The Riemann Problem for General 2 × 2 Conservation Laws". In: *Trans. Am. Math. Soc.* 199 (1974), pp. 89–112. DOI: 10.2307/1996875.

[50] T.P. Liu. "The Riemann Problem for General systems of Conservation Laws". In: *J. Differ. Equations* 18 (1975), pp. 218–234. DOI: 10.1016/0022-0396(75)90091-1.

[51] K. Low, R. van Loon, I. Sazonov, R.L.T. Bevan, and P. Nithiarasu. "An improved baseline model for a human arterial network to study the impact of aneurysms on pressure-flow waveforms". In: *Int. J. Numer. Methods Biomed. Eng.* 28.12 (2012), pp. 1224–1246. DOI: 10.1002/cnm.2533.

[52] K.S. Matthys, J. Alastruey, J. Peiró, A.W. Khir, P. Segers, P.R. Verdonck, K.H. Parker, and S.J. Sherwin. "Pulse wave propagation in a model human arterial network: Assessment of 1D numerical simulations against in vitro measurements". In: *J. Biomech.* 40.15 (2007), pp. 3476–3486. DOI: 10.1016/j.jbiomech.2007.05.027.

[53] L.O. Müller and P.J. Blanco. "A high order approximation of hyperbolic conservation laws in networks: Application to one-dimensional blood flow". In: *J. Comput. Phys.* 300 (2015), pp. 423–437. DOI: 10.1016/j.jcp.2015.07.056.

[54] L.O. Müller, G. Leugering, and P.J. Blanco. "Consistent treatment of viscoelastic effects at junctions in one-dimensional blood flow models". In: *J. Comput. Phys.* 314 (2016), pp. 167–193. DOI: 10.1016/j.jcp.2016.03.012.

[55] L.O. Müller, C. Parés, and E.F. Toro. "Well-Balanced High-Order Numerical Schemes for One-Dimensional Blood Flow in Vessels with Varying Mechanical Properties". In: *J. Comput. Phys.* 242 (2013), pp. 53–85. DOI: 10.1016/j.jcp.2013.01.050.

[56] L.O. Müller and E.F. Toro. "Well-balanced high-order solver for blood flow in networks of vessels with variable properties". In: *Int. J.Numer. Methods Biomed. Eng.* 29 (2013), pp. 1388–1411. DOI: 10.1002/cnm.2580.

[57] L.O. Müller and E.F. Toro. "A global multi-scale model for the human circulation with emphasis on the venous system". In: *Int. J. Numer. Method Biomed. Eng.* 30.7 (2014), pp. 681–725. DOI: 10.1002/cnm.2622.

[58] L.O. Müller and E.F. Toro. "Enhanced global mathematical model for studying cerebral venous blood flow". In: *J. Biomech.* 47.13 (2014), pp. 3361–3372. DOI: 10.1016/j.jbiomech.2014.08.005.

[59] J. Murillo and P. García-Navarro. "A Roe Type Energy Balanced Solver for 1D Arterial Blood Flow and Transport". In: *Comput. Fluids* 117 (2015), pp. 149–167. DOI: 10.1016/j.compfluid.2015.05.003.

[60] J.P. Mynard and P. Nithiarasu. "A 1D arterial blood flow model incorporating ventricular pressure, aortic valve and regional coronary flow using the locally conservative Galerkin (LCG) method". In: *Commun. Numer. Methods Eng.* 24.5 (2008), pp. 367–417. DOI: 10.1002/cnm.1117.

[61] J.P. Mynard and J.J. Smolich. "One-Dimensional Haemodynamic Modeling and Wave Dynamics in the Entire Adult Circulation". In: *Ann Biomed Eng* 43 (2015), pp. 1443–1460. DOI: 10.1007/s10439-015-1313-8.

[62] M.S. Olufsen, C.S. Peskin, W.Y. Kim, E.M. Pedersen, A. Nadim, and J. Larsen. "Numerical Simulation and Experimental Validation of Blood Flow in Arteries with Structured-Tree Outflow Conditions". In: *Ann. Biomed. Eng.* 28 (2000), pp. 1281–1299. DOI: 10.1114/1.1326031.

[63] S. Osher and F. Solomon. "Upwind difference schemes for hyperbolic systems of conservation laws". In: *Math. Comput.* 38.158 (1982), pp. 339–374. DOI: 10.2307/2007275.

[64] C. Parés. "Numerical Methods for nonconservative hyperbolic systems: a theoretical framework". In: *SIAM J. Numer. Anal.* 44 (2006), pp. 300–321. DOI: 10.1137/050628052.

[65] C. Parés and M. Castro. "On the well-balance property of Roe's method for nonconservative hyperbolic systems. Applications to shallow-water systems". In: *ESAIM. M2AN* 38.5 (2004), pp. 821–852. DOI: 10.1051/m2an:2004041.

[66] C. Parés and M.L. Muñoz-Ruiz. "On some difficulties of the numerical approximation of nonconservative hyperbolic systems". In: *Bol. Soc. Esp. Mat. Apl.* 47 (2009), pp. 19–48.

[67] E. Pimentel-García, L.O. Müller, E.F. Toro, and C. Parés. "High-order fully well-balanced numerical methods for one-dimensional blood flow with discontinuous properties". In: *J. Comput. Phys.* 475 (2023), p. 111869. DOI: 10.1016/j.jcp.2022.111869.

[68] A. Quarteroni, A. Manzoni, and C. Vergara. "The cardiovascular system: Mathematical modelling, numerical algorithms and clinical applications". In: *Acta Numer.* 26 (2017), pp. 365–590. DOI: 10.1017/S0962492917000046.

[69] P. Reymond, F. Merenda, F. Perren, D. Rüfenacht, and N. Stergiopulos. "Validation of a one-dimensional model of the systemic arterial tree". In: *Am. J. Physiol. Heart Circ. Physiol.* 297.1 (2009), H208–H222. DOI: 10.1152/ajpheart.00037.2009.

[70] D.V. Sharma. *Quasilinear hyperbolic systems, compressible flows, and waves*. CRC press, 2010. DOI: 10.1201/9781439836910.

[71] W. Sheng, Q. Zhang, and Y. Zheng. "The Riemann Problem for a Blood Flow Model in Arteries". In: *Commun. Comput. Phys.* 27.1 (2019), pp. 227–250. DOI: 10.4208/cicp.OA-2018-0220.

[72] S.J. Sherwin, L. Formaggia, J. Peiró, and V. Franke. "Computational modelling of 1D blood flow with variable mechanical properties and its application to the simulation of wave propagation in the human arterial system". In: *Int. J. Numer. Methods Fluids* 43.6-7 (2003), pp. 673–700. DOI: 10.1002/fld.543.

[73] S.J. Sherwin, V. Franke, J. Peiró, and K. Parker. "One-dimensional modelling of a vascular network in space-time variables". In: *J. Eng. Math.* 47 (2003), pp. 217–250. DOI: 10.1023/B:ENGI.0000007979.32871.e2.

[74] A.V. Singh and P. Zamboni. "Anomalous venous blood flow and iron deposition in multiple sclerosis". In: *J Cereb Blood Flow Metab.* 29.12 (2009), pp. 1867–1878. DOI: 10.1038/jcbfm.2009.180.

[75] A. Siviglia and M. Toffolon. "Steady analysis of transcritical flows in collapsible tubes with discontinuous mechanical properties: implications for arteries and veins". In: *J. Fluid Mech.* 736 (2013), pp. 195–215. DOI: 10.1017/jfm.2013.542.

[76] A. Siviglia, D. Vanzo, and E.F. Toro. "A splitting scheme for the coupled Saint-Venant-Exner model". In: *Adv. Water Resour.* 159 (2022). DOI: 10.1016/j.advwatres.2021.104062.

[77] N.P. Smith, A.J. Pullan, and P.J. Hunter. "An anatomically based model of transient coronary blood flow in the heart". In: *SIAM J. Appl. Math.* 62.3 (2002), pp. 990–1018. DOI: 10.1137/S0036139999355199.

[78] J. Smoller. "A uniqueness theorem for Riemann problems". In: *Arch. Rational Mech. Anal.* 33 (1969), pp. 110–115. DOI: 10.1007/BF00247755.

[79] J. Smoller. "On the solution of the Riemann problem with general step data for an extended class of hyperbolic systems". In: *Michigan Math. J.* 16.3 (1969), pp. 201–210. DOI: 10.1307/mmj/1029000262.

[80] J. Smoller. *Shock Waves and Reaction-Diffusion Equations*. Second. Springer New York, NY, 1994. DOI: 10.1007/978-1-4612-0873-0.

[81] A. Spilimbergo, E.F. Toro, and L.O. Müller. "One-Dimensional Blood Flow with Discontinuous Properties and Transport: Mathematical Analysis and Numerical Schemes". In: *Commun. Comput. Phys.* 29.03 (2021), pp. 649–697. DOI: 10.4208/cicp.OA-2020-0132.

[82] A. Spilimbergo, E.F. Toro, and L.O. Müller. "Exact solution of the Riemann problem for the one-dimensional blood flow equations with general constant momentum correction coefficient". In: *Commun. Comput. Phys.* (2024). In press.

[83] A. Spilimbergo, E.F. Toro, A. Siviglia, and L.O. Müller. "Flux Vector Splitting schemes applied to a conservative 1D blood flow model with transport for arteries and veins". In: *Comput. Fluids* 271 (2024). DOI: 10.1016/j.compfluid.2023.106165.

[84] E. Spiller, E.F. Toro, M.E. Vázquez Cendón, and C. Contarino. "On the exact solution of the Riemann problem for blood flow in human veins, including collapse". In: *Appl. Math. Comput.* 303 (2017), pp. 178–189. DOI: 10.1016/j.amc.2017.01.024.

[85] J.L. Steger and R.F. Warming. "Flux vector splitting of the inviscid gasdynamic equations with application to finite-difference methods". In: *J. Comput. Phys.* 40.2 (1981), pp. 263–293. DOI: 10.1016/0021-9991(81)90210-2.

[86] E.F. Toro. *On Glimm-Related schemes for conservation laws*. Technical Report MMU-9602. Department of Mathematics and Physics, Manchester Metropolitan University, UK, 1996.

[87] E.F. Toro. *Riemann Solvers and Numerical Methods for Fluid Dynamics: A Practical Introduction*. Third. Springer-Verlag Berlin Heidelberg, 2009. DOI: 10.1007/b79761.

[88] E.F. Toro and S.J. Billett. "Centred TVD schemes for hyperbolic conservation laws". In: *IMA J. Numer. Anal.* 20.1 (2000), pp. 47–79. DOI: 10.1093/imanum/20.1.47.

[89] E.F. Toro, C.E. Castro, D. Vanzo, and A. Siviglia. "A flux-vector splitting scheme for the shallow water equations extended to high-order on unstructured meshes". In: *Int J Numer Meth Fluids* (2022), pp. 1–27. DOI: 10.1002/fld.5099.

[90] E.F. Toro and A. Siviglia. "Flow in collapsible tubes with discontinuous mechanical properties: mathematical model and exact solutions". In: *Commun. Comput. Phys.* 13.2 (2013), pp. 361–385. DOI: 10.4208/cicp.210611.240212a.

[91] E.F. Toro, A. Siviglia, A. Spilimbergo, and L.O. Müller. "Advection-Pressure Splitting Schemes for the Equations of Blood Flow. Conservative and Non-Conservative Forms". In: *East Asian J. Appl. Math.* 14.2 (2024), pp. 223–259. DOI: 10.4208/eajam.2023-045.090523.

[92] E.F. Toro and M.E. Vázquez-Cendón. "Flux splitting schemes for the Euler equations". In: *Comput. Fluids* 70 (2012), pp. 1–12. DOI: 10.1016/j.compfluid.2012.08.023.

[93] Z. Wang, G. Li, and O. Delestre. "Well-Balanced Finite Difference Weighted Essentially Non-Oscillatory Schemes for the Blood Flow Model". In: *Int. J. Numer. Methods Fluids* 82.9 (2016), pp. 607–622. DOI: 10.1002/fld.4232.

[94] N. Xiao, J. Alastruey, and A.C. Figueroa. "A systematic comparison between 1-D and 3-D hemodynamics in compliant arterial models". In: *Int. J. Numer. Method Biomed. Eng.* 30(2) (2014), pp. 204–231. DOI: 10.1002/cnm.2598.

[95] P. Zamboni, R. Galeotti, E. Menegatti, A.M. Malagoni, G. Tacconi, S. Dall'Ara, I. Bartolomei, and F. Salvi. "Chronic cerebrospinal venous insufficiency in patients with multiple sclerosis". In: *J. Neurol. Neurosurg. Psychiatry* 80.4 (2009), pp. 392–399. DOI: 10.1136/jnnp.2008.157164.

[96] Y.B. Zeldovich. "Gravitational instability: an approximate theory for large density perturbations". In: *Astron. Astrophys.* 5 (1970), pp. 84–89.

[97] G. Zha and E. Bilgen. "Numerical solutions of Euler equations by using a new flux vector splitting scheme". In: *Int. J. Numer. Methods Fluids* 17.2 (1993), pp. 115–144. DOI: 10.1002/fld.1650170203.

[98] F. Zhu and N. Dodd. "Riemann solution for a class of morphodynamic shallow water dam-break problems". In: *J. Fluid Mech.* 835 (2018), pp. 1022–1047. DOI: 10.1017/jfm.2017.794.

[99] R. Zivadinov, G.U. Poloni, K. Marr, C.V. Schirda, C.R. Magnano, E. Carl, N. Bergsland, D. Hojnacki, C. Kennedy, C.B. Beggs, M.G. Dwyer, and B. Weinstock-Guttman. "Decreased brain venous vasculature visibility on susceptibility-weighted imaging venography in patients with multiple sclerosis is related to chronic cerebrospinal venous insufficiency". In: *BMC Neurology* 11.128 (2011). DOI: 10.1186/1471-2377-11-128.

List of Figures

List of Tables